Dismantling the Deep Earth: Geochemical Constraints from Hotspot Lavas for the Origin and Lengthscales of Mantle Heterogeneity

by

Matthew G. Jackson

B.S., Yale University, 2001

Submitted in partial fulfillment of the requirements for the degree of
Doctor of Philosophy

at the

MASSACHUSETTS INSTITUTE OF TECHNOLOGY

and the

WOODS HOLE OCEANOGRAPHIC INSTITUTION

February 2008

Signature of Author . . . . . .

Joint Program in Oceanography
Massachusetts Institute of Technology
and Woods Hole Oceanographic Institution
November 2007

Certified by . . . . . .

Dr. Stanley R. Hart, Thesis Supervisor

Accepted by . . . . . .

Prof. Bradford H. Hager
Co-Chair, Joint Committee for Marine Geology and Geophysics

Tileinkað Önnu Maríu

Acknowledgements

First off, I want to thank my advisor, Stan Hart, for being so generous, with his time, his resources, and his thoughts. Stan sent me to the edges of the earth to collect rocks on islands and by sea ("a happy student is a traveling student"). And the fishing trips didn't end when I got back to the lab. When I went to him for answers, I often just ended up with more questions, we'd dream up a dozen projects, and he'd send me off with more projects and questions (back in my office, I'd realize that the meeting didn't go as *I'd* planned)! But the questions were more important than the answers: the questions will keep me employed after I graduate! It's only now that I'm realizing that without so much independence to explore (though frightening at times), I may have never understood that I was capable of generating some fun ideas!

I can't express my gratitude to Nobu Shimizu and Mark Kurz for their "open door" policy. They are always ready to give me time, sit down, and hash out new ideas. Their offices are idea factories. I don't know how I would have written this thesis without their constant input.

My deepest appreciation to J. Collins for sweating it out with me in the field in Samoa, and to the rest of my committee, P. Kelemen, Erik Hauri and Fred Frey for their stimulating input and for traveling so far to attend the general exam, thesis defense, and committee meetings.

J. Blusztajn has always been so optimistic and helpful, and has given me so much of his time and advice. J. Curtice and T. Atwood have also given me dollops of help, and without them I could not have accomplished much of the thesis work.

I am so thankful for the friendship of my dear friends, S. Hoffmann, D. Stuebe and J. Blythe, Heidi Marcella, Carolyn Walker, Lauge Sokol-Hessner and Hannah Cole. They kept me going when the times were rough, and we shared many of the best times as well.

I am also thankful for the friendship and advice that I received from the "old guard" of JP students, who left the WHOI "nest" before me. J. Warren, C. Williams, A. Michal, M. Cook, M. Boettcher, J. Standish, A. Kvasness, C. Santelli and D. Lund. I especially thank R. Workman for the early "coaching" in the black arts of mantle geochemistry.

I thank H. Oates for providing sustenance in the form of gourmet meals, and E. Rolland and C. Saenger for delicious lasagna these last few trying weeks. P. Craddock, W. Krey, C. Petrik, C. Wood, Christine Mingione, C. Miller and E. Banning for late night visits to our local community center, The Captain Kidd.

My office mates Michael "Wacky" Holcomb and Zhengrong "The General" Wang provided endless late-night weirdness and, more importantly, helped me realize that I could work even harder than I had thought possible.

Andrew ("MacGyver") and Peggy Daly have been great friends, and I highly recommend Andrew in the field!

Thanks to C. Waters, E. Rolland and C. Walker, I will graduate much thinner than predicted. The runs and conversation kept me sane!

Sheila Clifford and her generosity have always managed to save me when I had something technical and urgent.

I thank Pam Foster for her delicious tomatoes and all her help.

My sincerest gratitude goes to all everyone in the Academic Programs office: J. Westwater, M. Gomes, S. Vitelli, C. Charette, V. Caron, J. Price, J. Yoder, and J. Farrington. They "shield" students from the perils of MIT beauracracy, and help make graduate student life as good as possible.

Rose. We all know who she is. Bless her heart for being so cheerful and keeping us company on the late nights.

Last, and by no means least, I want to thank my whole family for being an inspiration to me. My mother, who did the impossible, and showed her children that they could do it too. My grandpa, for showing me the satisfaction of a hard-day's work and a job well done. My grandma, for introducing me to the world of books. My father, who gave me physics and astronomy lessons when I was a child and convinced me that science could answer the "important" questions. My stepfather, for being there when I needed his help, for paying for my college education, teaching me how to change the oil, sparkplugs, fix flats, fill out tax forms, and the list goes on. To Auntie Sara, for being an awesome older "sibling", and Uncle Larry, for being so generous with me. And to my brother and sister, I love you both.

I also am grateful for the various sources of funding that made my graduate education possible. Funding was provided by a National Science Foundation Graduate Research Fellowship, the National Science Foundation grants EAR- 0509891 and EAR-0652707 to Stanley R. Hart, the Woods Hole Oceanographic Institution Academic Programs Office, the Woods Hole Oceanographic Institution Deep Ocean Exploration Institute, the Woods Hole Oceanographic Institution Coastal Ocean Institute, and the Ocean Ventures Fund. Noble gas measurements at WHOI were supported by OCE-05825864 to Mark D. Kurz.

Table of Contents

Dismantling the Deep Earth: Geochemical Constraints from Hotspot Lavas for the Origin and Lengthscales of Mantle Heterogeneity

by
Matthew G. Jackson

Submitted to the Department of Marine Geology and Geophysics,
Massachusetts Institute of Technology-Woods Hole Oceanographic Insitution
in partial fulfillment of the requirements for the degree of Doctor of Philosophy

Abstract

Chapter 1 presents the first published measurements of Sr-isotope variability in olivine-hosted melt inclusions. Melt inclusions in just two Samoan basalt hand samples exhibit most of the total Sr-isotope variability observed in Samoan lavas. Chapter 3 deals with the largest possible scales of mantle heterogeneity, and presents the highest magmatic $^{3}He/^{4}He$ (33.8 times atmospheric) discovered in Samoa and the southern hemisphere. Along with Samoa, the highest $^{3}He/^{4}He$ sample from each southern hemisphere high $^{3}He/^{4}He$ hotspot exhibits lower $^{143}Nd/^{144}Nd$ ratios than their counterparts in the northern hemisphere. Chapter 2 presents geochemical data for a suite of unusually enriched Samoan lavas. These highly enriched Samoan lavas have the highest $^{87}Sr/^{86}Sr$ values (0.72163) measured in oceanic hotspot lavas to date, and along with trace element ratios (low Ce/Pb and Nb/U ratios), provide a strong case for ancient recycled sediment in the Samoan mantle. Chapter 4 explores whether the eclogitic and peridotitic portions of ancient subducted oceanic plates can explain the anomalous titanium, tantalum and niobium (TITAN) enrichment in high $^{3}He/^{4}He$ ocean island basalts (OIBs). The peridotitic portion of ancient subducted plates can contribute high $^{3}He/^{4}He$ and, after processing in subduction zones, a refractory, rutile-bearing eclogite may contribute the positive TITAN anomalies.

Introduction

Unlike the earth's crust, it is difficult to sample the mantle directly. However, there are a few isolated (and geographically limited) instances where we can observe the uppermost regions of the mantle. Ophiolites—portions of oceanic plates that have been uplifted and emplaced (obducted) onto the edge of continents—expose the uppermost regions of the mantle on the surface (Dick, 1976). Similarly, at certain, ultra-slow spreading mid-ocean ridges, mantle peridotites are emplaced on the surface (Dick et al., 2003), where they can be recovered with deep submersibles or dredging operations. Additionally, ultramafic xenoliths, which are pieces of the upper mantle entrained in upwelling magmas, allow direct inspection of the composition of the upper mantle (but unlike ophiolites and abyssal peridotites recovered by submersibles, ultramafic xenoliths provide little spatial context for study of the mantle). Thus, except for these few rare instances, we cannot examine the composition of the mantle directly: The deepest hole ever drilled, only ~12.3 km deep, took 22 years and untold Soviet resources to complete--and got no where near mantle depths (unfortunately, the drill site was atop thick continental crust). While robots rove the surface of a planet, Mars, that is > 56,000,000 km distant, we have not directly observed our own planet at depths >12 km!

Nonetheless, there are indirect methods for evaluating the composition of the deeper earth. Mantle geochemists often use lavas erupted on the surface as "windows" to the composition of the mantle below. Hotspot lavas erupted in oceanic settings, or oceanic island basalts (OIBs), are formed by partially melting and upwelling, solid mantle. During melting, several radiogenic isotope systems and a number of trace element ratios remain unfractionated (or little fractionated, in the case of trace elements with similar compatibilities, at least when the partition coefficients are much less than the degree of melting) from the original, unmelted mantle. OIBs exhibit a great deal of isotopic and trace element heterogeneity, indicating that the mantle from which they were derived is also quite heterogeneous (Zindler and Hart, 1986). This fundamental observation leads to some of the most important questions in the field of mantle

geochemistry: How did the mantle become heterogeneous? At what scale lengths do the heterogeneities exist? How long do the heterogeneities survive?

One common paradigm in mantle geochemistry assumes that oceanic plates, which form by melting and depleting the upper mantle at mid-ocean ridges, are subducted back into the mantle from which they formed. Covered with a veneer of oceanic/continental sediment, subducted oceanic plates inject sediment, oceanic crust and depleted peridotitic mantle lithosphere into the mantle (Hofmann and White, 1982; White and Hofmann, 1982). In this way, mantle heterogeneities are born. Following storage in the mantle, subducted plates and sediment are thought to be sampled by upwelling plumes that melt and erupt lavas on the surface. However, a counteracting mechanism—chaotic mantle convection—stretches, thins, mixes and stirs, and thus homogenizes (or at least greatly attenuates) mantle heterogeneities on long timescales.

In Chapter 1, isotopic heterogeneities are explored at very short lengthscales in olivine-hosted melt inclusions in oceanic OIBs. Using a laser ablation system coupled to a MC-ICPMS (multi-collector inductively coupled plasma mass spectrometer), $^{87}Sr/^{86}Sr$ was measured in olivine-hosted melt inclusions recovered from Samoan basalts. Complementing the pioneering work on Pb-isotopes in olivine-hosted melt inclusions from two Polynesian hotspots (Saal et al., 1998), significant Sr-isotope heterogeneity was also observed in the melt inclusions from individual Samoan basalt hand samples. Melt inclusions in one Samoan lava exhibit a range of $^{87}Sr/^{86}Sr$ from 0.70686 to 0.70926. The isotopic diversity hosted in the melt inclusions from a single lava indicate that the size of the melting zone beneath a Samoan volcano can be larger than the lengthscales of mantle heterogeneities in the mantle upwelling beneath the hotspot. Furthermore, none of the 41 melt inclusions analyzed exhibit $^{87}Sr/^{86}Sr$ ratios lower than the least radiogenic whole-rock basalts in Samoa ($^{87}Sr/^{86}Sr$ =0.7044). This $^{87}Sr/^{86}Sr$ data, combined with trace element data on the same melt inclusions, provide strong evidence against assimilation of oceanic crust as the source of the isotopic diversity in the melt inclusions.

Chapter 3 also deals with lengthscales of mantle heterogeneity, but by comparison to Chapter 1, Chapter 3 considers the largest possible lengthscales of heterogeneity in the Earth's mantle. The high $^{3}He/^{4}He$ (or FOZO, Focus Zone; Hart et al., 1992) mantle

reservoir, a domain that is considered to be one of the oldest (and deepest?) reservoirs in the mantle, is the focus of chapter 3. In this chapter, the highest magmatic $^{3}He/^{4}He$ ratios ever recorded in a southern hemisphere lava (33.8 times atmospheric) are reported in samples from the Samoan island of Ofu. These new measurements from Ofu Island place Samoa in the same category of high $^{3}He/^{4}He$ hotspots as Hawaii, Iceland and the Galapagos. Along with Samoa, the highest $^{3}He/^{4}He$ sample from each southern hemisphere high $^{3}He/^{4}He$ hotspot exhibits lower $^{143}Nd/^{144}Nd$ ratios than their counterparts in the northern hemisphere (excluding lavas erupted in continental, back-arc, and submarine ridge environments). The observation of a large-scale isotopic enrichment in the FOZO-A (austral) high $^{3}He/^{4}He$ mantle compared to the FOZO-B (boreal) high $^{3}He/^{4}He$ mantle is similar to the DUPAL anomaly, a globe-encircling feature of isotopic enrichment observed primarily in southern hemisphere ocean island basalts. The possible existence of hemispheric-scale heterogeneity in one of the oldest reservoirs in the mantle has important implications for mantle dynamics. It suggests that regions of the (lower?) mantle have escaped the rapid convection motions that dominate the upper mantle. However, the origin of the hemispheric-scale heterogeneity in the FOZO (and DUPAL) reservoir is unknown.

Nonetheless, having defined the variability that exists in the high $^{3}He/^{4}He$ mantle, Chapter 3 also explores whether or not the FOZO reservoirs are truly depleted, as is commonly suggested (Hart et al., 1992), or whether they have been re-enriched. The recent discovery of superchondritic $^{142}Nd/^{144}Nd$ ratios in terrestrial (Boyet and Carlson, 2005), martian and lunar (Caro et al., 2007) suggests that bulk silicate earth (BSE) may have superchondritic Sm/Nd ratios ($^{147}Sm/^{144}Nd>0.209$, the minimum ratio necessary to generate the terrestrial mantle $^{142}Nd/^{144}Nd$ anomaly relative to chondrites), and that the earth has a minimum $^{143}Nd/^{144}Nd$ of 0.51304. If this is true, then the FOZO reservoirs are actually enriched relative to BSE.

Chapter 2 explores a common paradigm in mantle geochemistry, that subduction of marine/continental sediments can generate geochemically enriched mantle domains that can be sampled by mantle upwellings. In this chapter, remarkably high $^{87}Sr/^{86}Sr$ ratios are reported in submarine lavas recovered from the flanks of the Samoan island of

Savai'i. These Savai'i lavas exhibit the highest $^{87}Sr/^{86}Sr$ ratios reported for ocean island basalts to date. The isotope and trace element data are consistent with the presence of a recycled sediment component (with a composition similar to the upper continental crust) in the Samoan mantle. Importantly, Pb-isotopes in the most enriched Samoan lavas preclude contamination by modern-marine sediment. The ultra-enriched Samoan lavas have most certainly been "contaminated" by sediment, but the sediment is of an ancient (>> 200 Ma) origin and has been recycled into the Samoan mantle source. In summary, Chapter 3 provides the strongest evidence yet that the sediment that goes down in subduction zones does come back up in OIBs. However, given the large mass of sediment that has been subducted into the mantle over geologic history, it is still a mystery why clear signatures of sediment recycling are so rare in OIBs (Hofmann, 1997).

Chapter 4 reports evidence for radiogenic $^{187}Os/^{188}Os$ and enrichment in Titanium, Tantalum and Niobium (TITAN) in high $^{3}He/^{4}He$ lavas globally. To explain these observations, the dominant paradigm for the formation of mantle heterogeneity is applied to the high $^{3}He/^{4}He$ reservoir: Can the subduction of oceanic plates (crust and peridotite) generate the geochemical signatures associated with the high $^{3}He/^{4}He$ reservoir? Radiogenic $^{187}Os/^{188}Os$ and TITAN enrichment are both geochemical signatures that are associated with recycled eclogite, suggesting that the high $^{3}He/^{4}He$ lavas were derived from a mantle source hosting a recycled slab component However, eclogites are quantitatively degassed in subduction zones and do not have intrinsically high $^{3}He/^{4}He$. None-the-less, the peridotitic portion of recycled slabs has been suggested to preserve high $^{3}He/^{4}He$ over time (e.g., Parman et al., 2005). The eclogitic and peridotitic portions of subducted plates are intimately associated in space and time, a geometry that is conducive to later mixing in the mantle. Thus, together, the two lithologies can provide the "raw materials" for the formation of the high $^{3}He/^{4}He$ mantle.

Importantly, the TITAN enrichment in high $^{3}He/^{4}He$ mantle sampled by oceanic hotspot lavas may provide a clue about the location of the "missing" TITAN in the earth. Shallow geochemical reservoirs in the earth—continental crust and the depleted mid-ocean ridge basalt mantle (DMM)—have a shortage of the element Ti, Ta and Nb (TITAN) (McDonough, 1991; Rudnick et al., 2000). The observation of TITAN

enrichment in high $^{3}He/^{4}He$ OIB lavas suggests that the mantle domain hosting the Earth's "missing" TITAN is sampled by deep, high $^{3}He/^{4}He$ mantle plumes.

References

Boyet, M., and R. W. Carlson, ^{142}Nd evidence for early (>4.53 Ga) global differentiation of the silicate earth, *Science, 309*, 576–581, 2005

Caro, G., B. Bourdon, A. N. Halliday, and G. Quitte, Super-chondritic Sm/Nd in Mars, Earth, and the Moon. *EOS* (Transaction of AGU), *88*, 2007 *submitted.*

Dick, H.J.B., Origin and Emplacement of the Josephine Peridotite of Southwestern Oregon. PhD Thesis, Yale University, Univ. Microfilms, Ann Arbor, Michigan, 409 pp., 1976.

Dick, H. J. B., J. Lin, and H. Schouten, An ultraslow-spreading class of ocean ridge, *Nature, 426*, 405-412, 2003.

Hart, S. R., E. H. Hauri, L. Oschmann, and J. A. Whitehead, Mantle plumes and entrainment: isotopic evidence, *Science, 256*, 517–520, 1992.

Hofmann, A. W., Mantle geochemistry, the message from oceanic volcanism, *Nature, 385,* 219-229, 1997.

Hofmann, A. W., and W. M. White, Mantle plumes from ancient oceanic crust, *Earth Planet. Sci. Lett., 57*, 421–436, 1982.

McDonough, W.F., Partial melting of subducted oceanic crust and isolation of its residual eclogitic lithology, *Philos. Trans. R. Soc. London, Ser. A, 335*, 407-418, 1991.

Parman, S. W., M. D. Kurz, S. R. Hart, and T. L. Grove, Helium solubility in olivine and implications for high 3He/4He in ocean island basalts, *Nature, 437*, 1,140-1,143, 2005.

Rudnick, R.L., M. Barth, I. Horn, and W. F. McDonough, Rutile-bearing refractory eclogites: the missing link between continents and depeted mantle. *Science,* 287, 278-281, 2000.

Saal, A. E., S. R. Hart, N. Shimizu, E. H. Hauri, and G. D. Layne, Pb isotopic variability in melt inclusions from oceanic island basalts, Polynesia, *Science, 282*, 1,481-1,484, 1998.

White, W. M., and A. W. Hofmann, Sr and Nd isotope geochemistry of oceanic basalts and mantle evolution, *Nature, 296*, 821–825, 1982.

Zindler, A., and S. R. Hart, Chemical Geodynamics, *Annu. Rev. Earth Planet. Sci., 14,* 493–571, 1986

Chapter 1

Strontium isotopes in melt inclusions from Samoan basalts: Implications for heterogeneity in the Samoan plume*

Abstract

We measured $^{87}Sr/^{86}Sr$ ratios on 41 olivine-hosted melt inclusions from nine Samoan basalts using laser ablation multi-collector (LA-MC) ICPMS. $^{87}Sr/^{86}Sr$ ratios are corrected for mass bias after eliminating major isobaric interferences from Rb and Kr. The external precision averages ±320 ppm (2σ) for the $^{87}Sr/^{86}Sr$ ratios on natural Samoan basalt glass standards of a similar composition to the melt inclusions.

All of the Sr-isotope ratios measured by LA-MC-ICPMS on Samoan melt inclusions fall within the range measured on whole rocks using conventional methods. However, melt inclusions from two Samoan basalt bulk rock samples are extremely heterogeneous in $^{87}Sr/^{86}Sr$ (0.70459–0.70926), covering 70% of the variability observed in ocean island basalts worldwide and nearly all of the variability observed in the Samoan island chain (0.7044–0.7089). Seven melt inclusions from a third high $^{3}He/^{4}He$ Samoan basalt are isotopically homogeneous and exhibit $^{87}Sr/^{86}Sr$ values from 0.70434 to 0.70469.

Several melt inclusions yield $^{87}Sr/^{86}Sr$ ratios higher than their host rock, indicating that assimilation of oceanic crust and lithosphere is not the likely mechanism contributing to the isotopic variability in these melt inclusions. Additionally, none of the 41 melt inclusions analyzed exhibit $^{87}Sr/^{86}Sr$ ratios lower than the least radiogenic basalts in Samoa ($^{87}Sr/^{86}Sr$=0.7044), within the quoted external precision. This provides an additional argument against assimilation of oceanic crust and lithosphere as the source of the isotopic diversity in the melt inclusions.

The trace element and isotopic diversity in Samoan melt inclusions can be modeled by aggregated fractional melting of two sources: A high $^{3}He/^{4}He$ source and an EM2 (enriched mantle 2) source. Melts of these two sources mix to generate the isotopic diversity in the Samoan melt inclusions. However, the melt inclusions from a basalt with the highest $^{3}He/^{4}He$ ratios in Samoa exhibit no evidence of an enriched component, but can be modeled as melts of a pure high $^{3}He/^{4}He$ mantle source.

*Published as: M. G. Jackson and S. R. Hart, Strontium isotopes in melt inclusions from Samoan basalts: Implications for heterogeneity in the Samoan plume, *Earth. Planet. Sci. Lett., v. 245*, pp. 260-277, 2006, doi:10.1016/j.epsl.2006.02.040.

Available online at www.sciencedirect.com
SCIENCE DIRECT
ELSEVIER
Earth and Planetary Science Letters 245 (2006) 260–277
EPSL
www.elsevier.com/locate/epsl

Strontium isotopes in melt inclusions from Samoan basalts: Implications for heterogeneity in the Samoan plume

Matthew G. Jackson [a,*], Stanley R. Hart [b]

[a] *Massachusetts Institute of Technology–Woods Hole Oceanographic Institution Joint Program, Woods Hole, Massachusetts, 02543, USA*
[b] *Department of Geology and Geophysics, Woods Hole Oceanographic Institution, Woods Hole, Massachusetts, 02543, USA*

Received 25 October 2005; received in revised form 22 February 2006; accepted 26 February 2006
Available online 19 April 2006
Editor: R.W. Carlson

Abstract

We measured $^{87}Sr/^{86}Sr$ ratios on 41 olivine-hosted melt inclusions from nine Samoan basalts using laser ablation multi-collector (LA-MC) ICPMS. $^{87}Sr/^{86}Sr$ ratios are corrected for mass bias after eliminating major isobaric interferences from Rb and Kr. The external precision averages ±320 ppm (2σ) for the $^{87}Sr/^{86}Sr$ ratios on natural Samoan basalt glass standards of a similar composition to the melt inclusions.

All of the Sr-isotope ratios measured by LA-MC-ICPMS on Samoan melt inclusions fall within the range measured on whole-rocks using conventional methods. However, melt inclusions from two Samoan basalt bulk rock samples are extremely heterogeneous in $^{87}Sr/^{86}Sr$ (0.70459–0.70926), covering 70% of the variability observed in ocean island basalts worldwide and nearly all of the variability observed in the Samoan island chain (0.7044–0.7089). Seven melt inclusions from a third high $^{3}He/^{4}He$ Samoan basalt are isotopically homogeneous and exhibit $^{87}Sr/^{86}Sr$ values from 0.70434 to 0.70469.

Several melt inclusions yield $^{87}Sr/^{86}Sr$ ratios higher than their host rock, indicating that assimilation of oceanic crust and lithosphere is not the likely mechanism contributing to the isotopic variability in these melt inclusions. Additionally, none of the 41 melt inclusions analyzed exhibit $^{87}Sr/^{86}Sr$ ratios lower than the least radiogenic basalts in Samoa ($^{87}Sr/^{86}Sr=0.7044$), within the quoted external precision. This provides an additional argument against assimilation of oceanic crust and lithosphere as the source of the isotopic diversity in the melt inclusions.

The trace element and isotopic diversity in Samoan melt inclusions can be modeled by aggregated fractional melting of two sources: A high $^{3}He/^{4}He$ source and an EM2 (enriched mantle 2) source. Melts of these two sources mix to generate the isotopic diversity in the Samoan melt inclusions. However, the melt inclusions from a basalt with the highest $^{3}He/^{4}He$ ratios in Samoa exhibit no evidence of an enriched component, but can be modeled as melts of a pure high $^{3}He/^{4}He$ mantle source.

Keywords: $^{87}Sr/^{86}Sr$; laser ablation; MC-ICPMS; melt inclusion; Samoa; EM2; PHEM; FOZO

1. Introduction

Ocean island basalts (OIBs) erupted at hotspots are thought to be the surface expression of buoyantly upwelling mantle plumes that sample the mantle's compositional heterogeneities at various depths and times

* Corresponding author. Tel.: +1 508 289 3490; fax: +1 508 457 2175.
E-mail address: mjackson@whoi.edu (M.G. Jackson).

0012-821X/$ - see front matter © 2006 Elsevier B.V. All rights reserved.
doi:10.1016/j.epsl.2006.02.040

[1,2]. The Samoan islands and seamounts, formed by a mantle plume impinging on the Pacific plate just north of the Tonga Trench, form a time-progressive hotspot track [3,4] which conforms reasonably well to Morgan's hotspot model [5]. Samoan lavas exhibit the highest $^{87}Sr/^{86}Sr$ ratios and the largest $^{87}Sr/^{86}Sr$ variation (0.7044–0.7089) measured in fresh OIBs [4,6], making them ideal for prospecting for diverse Sr-isotope compositions in melt inclusions.

Olivine-hosted melt inclusions in Samoan lavas provide snapshots of diverse magma chemistry before complete melt aggregation, providing an opportunity to see more of the isotopic heterogeneity which exists in the melt source but that is not detectable in whole rocks. However, the chemical variability in melt inclusions may be generated by a number of processes that obscure source variation, including pre-entrapment fractional crystallization, post-entrapment diffusive re-equilibration, crustal assimilation, and degree, type and depth of melting [7–16].

Studies delineating Pb-isotope diversity in melt inclusions have demonstrated that heterogeneous melt source compositions are an important factor in generating compositional variability [17–21]. A landmark Pb-isotope study of melt inclusions hosted in basalts from Mangaia Island in the Cook Islands revealed significantly more isotopic heterogeneity than is found in whole rocks from the island [17]. The results indicate the presence of an unradiogenic Pb-isotope endmember in the melt inclusions not discernable in whole-rock basalts. Problematically, this unradiogenic Pb endmember has been poorly characterized, owing partly to the large uncertainties associated with in situ Pb-isotope measurements: Pb-isotope data from melt inclusions generally are limited to $^{208}Pb/^{206}Pb$ versus $^{207}Pb/^{206}Pb$ isotope projections (due to the inability to collect precise ^{204}Pb data on silicate melt inclusions), which place DMM (depleted MORB mantle, low $^{3}He/^{4}He$, low $^{87}Sr/^{86}Sr$), FOZO (*Fo*cus *Zo*ne, high $^{3}He/^{4}He$, low $^{87}Sr/^{86}Sr$), PHEM (*P*rimitive *He*lium *M*antle, high $^{3}He/^{4}He$, middle-range $^{87}Sr/^{86}Sr$) and EM2 (enriched mantle 2, low $^{3}He/^{4}He$, high $^{87}Sr/^{86}Sr$) in such close graphical proximity that they cannot be unequivocally resolved. The true pedigree of the unradiogenic Pb endmember in Mangaia is still unknown, and could be similar to any of these four endmembers.

An advantage to the Sr-isotope system is that the EM2 endmember has dramatically higher $^{87}Sr/^{86}Sr$ ratios (~0.7089) [4] than the DMM (0.7026) [22], PHEM (0.7045) [23] and FOZO (0.7030) [24] mantle endmembers, and can be readily differentiated from the three less radiogenic endmembers. PHEM hosts significantly more radiogenic Sr than DMM and FOZO and is easily resolved from these two components. Unfortunately, DMM and FOZO exhibit similar $^{87}Sr/^{86}Sr$ ratios and it will be difficult to differentiate between these two components as potential sources of the isotopic diversity in melt inclusions.

We present Sr-isotope data from olivine-hosted melt inclusions recovered from Samoan basalts, some of which lie near the EM2 mantle endmember, with the goal of better understanding the puzzling unradiogenic component sampled by melt inclusions. To this end, we also contribute Sr-isotope data measured on melt inclusions from a recently discovered high $^{3}He/^{4}He$ basalt from Samoa [25]. Our strategy is to analyze Sr isotopes in melt inclusions from EM2 and high $^{3}He/^{4}He$ endmember basalts from Samoa, to constrain the role of the various components–EM2, PHEM, DMM and FOZO–that may be contributing to the Sr-isotope diversity in the Samoan plume.

2. Methods

A detailed description of the protocol used for in situ measurement of Sr isotopes in basaltic glasses (and melt inclusions) by LA-MC-ICPMS is provided in the Supplementary data. In order to measure Sr-isotope ratios in situ, we use a 213 nm NewWave laser ablation system coupled to a Themo-Finnigan Neptune MC-ICPMS, located in the Plasma Facility at Woods Hole Oceanographic Institution (WHOI). During analytical runs, the laser is run in aperture mode with 100% power, a pulse rate of 20 Hz and a spot size of 120 μm. The raster pattern varies depending on the size and shape of the melt inclusion, and the line speed is 4 μm/s. Surface contamination is removed by pre-ablation using the same raster and spot size, but with a pulse rate of 5 Hz, 45% power and a raster speed of 30 μm/s.

During each analytical session, we measure intensities on masses 82 through 88. Raw data are exported to an offline data correction program (TweaKr) for correcting the Rb and Kr isobaric interferences. Runs with low intensities (i.e., < 1 V on mass 88, due to small size or low Sr content) were discarded as they are prone to large systematic errors [26]. Masses 85 and 88 are pure Rb and Sr, respectively, with no significant known interferences, and require correction only for mass fractionation. We correct for Kr interferences on masses 84 and 86 so that the mass fractionation-corrected $^{84}Sr/^{86}Sr$ value is canonical (0.0565725). The protocol for correcting mass 87 for the Rb interference is the following: A Samoan basalt glass with known $^{87}Sr/^{86}Sr$, from analysis by conventional Thermal Ionization Mass Spectrometry

Table 1
Corrected and normalized $^{87}Sr/^{86}Sr$ melt inclusion and whole-rock data, including Rb/Sr ratios and raw exported Neptune data (in volts)

Sample name and grain #	Disc #	Mass 82 meas'd-V	Mass 83 meas'd-V	Mass 84 meas'd-V	Mass 85 meas'd-V	Mass 86 meas'd-V	Mass 87 meas'd-V	Mass 88 meas'd-V	$^{85}Rb/^{87}Rb$ required	$^{87}Sr/^{86}Sr$ corr'd[a]	$^{87}Sr/^{86}Sr$ corr'd[b]	Int. prec.	Rb/Sr	Int. prec.	# Cycles	Type	Oliv Fo
AVON3-78-1 (whole rock):											0.70890		0.1255				
78-1Z	Year1	0.0013	0.0011	0.0193693	0.158083	0.263023	0.250903	2.25759	2.58966	0.70791	0.70784	87	0.0746	1.82	14[c]	C	84.6
78-1#7[d]	Disc1	0.0020	0.0022	0.0193323	0.164332	0.188415	0.199670	1.60867	2.58811	0.70927	0.70926	123	0.1081	2.47	9	H	84.6
78-1#9[d]	Disc1	0.0019	0.0021	0.0178511	0.111482	0.163039	0.159876	1.38845	2.58811	0.70733	0.70732	103	0.0850	1.90	6	H	84.4
78-1#6[d]	Disc2	0.0031	0.0034	0.0297219	0.341900	0.308400	0.354647	2.62064	2.58593	0.70846	0.70843	99	0.1397	2.63	32	H	83.6
78-1#9[d]	Disc2	0.0031	0.0034	0.0316443	0.384820	0.340724	0.395010	2.89882	2.58593	0.70873	0.70870	94	0.1421	3.08	30	H	82.8
78-1#10[d]	Disc2	0.0030	0.0031	0.0241696	0.094343	0.202069	0.179689	1.70410	2.58663	0.70845	0.70842	104	0.0593	3.21	16	H	83.6
78-1#4[d]	Disc3	0.0049	0.0057	0.0638080	0.704962	0.756968	0.817352	6.43584	2.58694	0.70869	0.70866	44	0.1179	0.60	40	G	85.2
78-1inside	Disc3	0.0048	0.0049	0.0311385	0.155536	0.152840	0.165959	1.25071	2.58564	0.70689	0.70686	139	0.1337	2.20	16	C	84.3
78-1B	Disc3	0.0044	0.0043	0.0327454	0.189114	0.222802	0.230356	1.86119	2.58675	0.70791	0.70788	127	0.1089	5.76	10	C	84.2
78-1C	Disc3	0.0041	0.0043	0.0408646	0.414636	0.401444	0.448986	3.40453	2.58675	0.70866	0.70863	38	0.1304	1.96	24	C	83.9
78-1D	Disc3	0.0048	0.0048	0.0313504	0.130366	0.156852	0.158811	1.28485	2.58675	0.70699	0.70696	119	0.1091	3.79	14	C	85.3
AVON3-71-2 (whole rock):											0.70594		0.0754				
71-2C[d]	Year1	0.0015	0.0012	0.0241555	0.131881	0.348997	0.301171	2.99950	2.58977	0.70488	0.70481	50	0.0469	4.99	10[c]	G	88.8
71-2C[e]	Disc3	0.0049	0.0051	0.0423813	0.151006	0.357484	0.309961	3.00928	2.58772	0.70487	0.70484	60	0.0539	2.09	19	G	88.8
71-2Da	Year1	0.0014	0.0012	0.0190549	0.143364	0.258958	0.241512	2.22256	2.58977	0.70555	0.70549	53	0.0687	3.92	12[c]	C	90.1
71-2i_mi1[d]	Disc1	0.0041	0.0042	0.0293387	0.151118	0.188888	0.190950	1.57393	2.58696	0.70605	0.70602	42	0.1028	0.89	19	G	90.7
71-2#6_sao11	Disc1	0.0040	0.0044	0.0392836	0.237282	0.399731	0.376067	3.39132	2.58675	0.70532	0.70529	63	0.0750	2.45	32	C	90.3
71-2#6_sao12	Disc1	0.0038	0.0039	0.0311684	0.151330	0.259691	0.241924	2.18859	2.58675	0.70511	0.70508	90	0.0741	3.15	15	C	90.5
71-2pentagon	Disc1	0.0035	0.0036	0.0274768	0.164455	0.221630	0.220515	1.86556	2.58653	0.70603	0.70600	69	0.0944	1.40	35	C	91.1
71-2#5[d]	Disc3	0.0049	0.0055	0.0608667	0.440578	0.704362	0.672560	5.98503	2.58694	0.70537	0.70534	34	0.0792	1.23	40	G	91.0
71-2#5[e]	Disc3	0.0049	0.0057	0.0600272	0.456791	0.688053	0.667289	5.84446	2.58694	0.70537	0.70534	34	0.0841	1.21	40	G	91.0
71-2#6[d]	Disc3	0.0050	0.0053	0.0461581	0.261970	0.420138	0.399032	3.54513	2.58674	0.70602	0.70600	53	0.0794	1.35	40	G	85.7
71-2#6[e]	Disc3	0.0050	0.0054	0.0511361	0.320998	0.514222	0.489758	4.35389	2.58674	0.70600	0.70598	32	0.0793	1.19	40	G	85.7
71-2Z	Disc3	0.0041	0.0042	0.0286629	0.120538	0.176062	0.169532	1.46336	2.58809	0.70576	0.70573	97	0.0882	2.60	21	C	86.1
71-2N	Disc3	0.0041	0.0043	0.0326106	0.171904	0.249420	0.242412	2.09517	2.58778	0.70554	0.70551	48	0.0879	2.74	26	C	90.5
71-2imi_run2	Disc3	0.0046	0.0048	0.0392641	0.162916	0.326152	0.292704	2.74335	2.58778	0.70520	0.70518	112	0.0638	2.80	12	C	91.0
71-2V	Disc3	0.0034	0.0037	0.0358138	0.196791	0.370738	0.339729	3.15166	2.58754	0.70461	0.70459	122	0.0668	4.32	13	C	87.4
OFU-04-06 (whole rock):											0.70458		0.0458				
OFU-04-06-13[d]	Ofu	0.0012	0.0004	0.0123598	0.087599	0.202878	0.179279	1.74009	2.58774	0.70458	0.70457	226	0.0541	6.04	6	H	79.8
OFU-04-06-15[d]	Ofu	0.0008	0.0006	0.0166800	0.116272	0.260130	0.231639	2.23575	2.58791	0.70443	0.70443	128	0.0556	1.62	13	H	77.3

OFU-04-06-25[d]	Ofu	0.0009	0.0008	0.0272537	0.215485	0.450579	0.407078	3.87445	2.58797	0.70455	0.70454	60	0.0595	3.24	20	H	77.2
OFU-04-06-26[d]	Ofu	0.0007	0.0006	0.0135577	0.076760	0.200599	0.173323	1.72195	2.58771	0.70443	0.70443	86	0.0476	2.73	16	H	76.5
OFU-04-06-28[d]	Ofu	0.0007	0.0006	0.0138764	0.082936	0.207139	0.180426	1.77796	2.58777	0.70435	0.70434	164	0.0499	1.97	11	H	78.4
OFU-04-06-03[d]	Ofu	0.0004	0.0005	0.0090473	0.057761	0.131245	0.115793	1.11700	2.58747	0.70443	0.70443	92	0.0560	2.67	15	H	83.8
OFU-04-06-02[d]	Ofu	0.0007	0.0006	0.0126725	0.082453	0.187441	0.166696	1.61548	2.58588	0.70469	0.70469	184	0.0542	0.96	7	H	76.5
AVON3-71-11 (whole rock):											0.70550		0.0700				
71-11a[d]	Disc1	0.0035	0.0035	0.0250240	0.083017	0.152405	0.138888	1.27387	2.58654	0.70653	0.70653	83	0.0691	1.22	16	G	83.0
71-11a[e]	Disc1	0.0019	0.0021	0.0204900	0.125897	0.216562	0.204083	1.85257	2.58857	0.70692	0.70692	109	0.0720	0.92	15	G	83.0
71-11#1[d]	Disc3	0.0048	0.0048	0.0316250	0.103649	0.160366	0.150752	1.31592	2.58772	0.70683	0.70680	144	0.0846	5.70	8	G	81.4
AVON3-68-3 (whole rock):											0.70539		0.0688				
68-3#6mi1[d]	Disc1	0.0020	0.0021	0.0186133	0.117638	0.165627	0.163878	1.40909	2.58798	0.70625	0.70624	75	0.0884	3.01	20	G	87.9
68-3#6mi2	Disc1	0.0038	0.0040	0.0305189	0.209211	0.258789	0.264567	2.18215	2.58653	0.70577	0.70575	87	0.1027	1.92	12	C	87.9
68-3#6mi2[e]	Disc1	0.0037	0.0041	0.0371899	0.294848	0.389761	0.392493	3.31142	2.58653	0.70577	0.70574	93	0.0954	1.73	9	C	87.9
68-3Ami	Disc3	0.0041	0.0042	0.0302365	0.092078	0.197293	0.173102	1.64414	2.58754	0.70482	0.70480	144	0.0600	6.45	10	C	90.1
AVON3-63-2 (whole rock):											0.70540		0.0679				
63-2mi	Disc3	0.0049	0.0051	0.0641890	0.514757	0.759082	0.741869	6.46111	2.58815	0.70599	0.70596	58	0.0856	2.68	31	C	–
63-2mi[e]	Disc3	0.0047	0.0056	0.0601701	0.544474	0.708353	0.718034	6.03171	2.58815	0.70616	0.70613	69	0.0969	1.22	36	C	–
63-2ami	Disc3	0.0044	0.0045	0.0283814	0.086324	0.138106	0.128251	1.13104	2.58815	0.70522	0.70520	181	0.0818	4.84	11	C	87.1
63-2bmi1	Disc3	0.0044	0.0045	0.0334163	0.133112	0.234231	0.215648	1.95929	2.58815	0.70528	0.70525	55	0.0728	3.15	23	C	86.6
AVON3-74-1 (whole rock):											0.70469		0.0484				
74-1mi	Year1	0.0015	0.0012	0.0174643	0.076749	0.224099	0.189719	1.91969	2.58895	0.70483	0.70477	157	0.0426	1.38	9[c]	C	85.1
S11 (whole rock):											0.70620		0.0597				
S11mi	Disc3	0.0048	0.0048	0.0330920	0.078499	0.189324	0.161268	1.56507	2.58564	0.70520	0.70518	125	0.0539	6.13	11	C	76.5
AVON3-78-3 (whole rock):											0.70889		0.1108				
78-3 mi	Year1	0.0014	0.0012	0.0184433	0.207247	0.241204	0.254752	2.06790	2.58966	0.70814	0.70807	61	0.1068	3.51	18[c]	C	84.1

All samples, except for OFU-04-06 and S11, are dredge samples from the AVON3 dredging cruise. Melt inclusion type refers to whether it was homogenized (H), glassy (G) or crystalline (C). Host olivine forsterite contents are given in the last column. Internal precision (Int. prec.) is standard error (2σ) and is in ppm ($^{87}Sr/^{86}Sr$) or % (Rb/Sr). Melt inclusion $^{87}Sr/^{86}Sr$ ratios are corrected for the isobaric interference from Rb by use of the bracketing method (see text for details). All melt inclusion analyses were performed on 01/27/04, 01/10/05, 01/11/05, 08/09/05 and 08/10/06 and corrected for the isobaric Rb interference using the Samoan glass standard analyses from those 5 days (see Supplementary data). Melt inclusion Sr-isotope and Rb/Sr data from a particular sample are listed immediately below the equivalent whole-rock data.

[a] Sr-isotopes are corrected for Kr and Rb interferences and fractionation-corrected.

[b] After correction for Rb and Sr interferences and fractionation, melt inclusions are corrected for 987 standard solution runs for each analytical session.

[c] Cycle length for melt inclusions from disc "Year1" are 16 s integrations during analysis. Cycles for all other measurements are 8 s integration.

[d] Has major and/or trace element data in Table 2.

[e] Replicate analysis of a melt inclusion is listed immediately below first analysis. Six melt inclusions were large enough to permit replicate analyses. Melt inclusion sample Year1_71-2 was replicated over a 1-year period, and was renamed Disc3_71-2C for the replicate analysis. All other replicate analyses were made during the same analytical session.

(TIMS), is measured by laser ablation, Kr-corrected, and the $^{85}Rb/^{87}Rb$ ratio is adjusted until the known TIMS $^{87}Sr/^{86}Sr$ value of the glass is achieved. We adopted the strategy of using the required $^{85}Rb/^{87}Rb$ of the Samoan basalt glass standards to bracket the $^{85}Rb/^{87}Rb$ of the basalt glass unknowns. In order to estimate the overall accuracy associated with this technique, we apply contiguous bracketing of the glass standard runs, and we are able to reproduce the known TIMS values to within an average of ±320 ppm (2σ standard deviation). However, due to uncertainty associated with the $^{85}Rb/^{87}Rb$ ratio (2.5875±0.00275, 2σ), the final, corrected $^{87}Sr/^{86}Sr$ ratio exhibits an error magnification that is directly proportional to the Rb/Sr ratio of the sample. Samples with low Rb/Sr will exhibit less error from the Rb correction (145 ppm, Rb/Sr=0.04) than samples with high Rb/Sr (505 ppm, Rb/Sr=0.14) (see Supplementary data). However, over the range of Rb/Sr in the Samoan basalt glass standards (0.045-0.126), we find no relationship between the internal (in-run) precision of $^{87}Sr/^{86}Sr$ ratios (which average 45 ppm, 2σ standard deviation) and Rb/Sr during analyses of basalt glasses by laser ablation. Similarly, there does not appear to be a relationship between Kr/Sr and the internal precision or reproducibility (external precision) of the $^{87}Sr/^{86}Sr$ ratios in Samoan glass standards over the range of ratios that we have observed during melt inclusion analysis ($^{82}Kr/^{88}Sr$ from 0.00013 to 0.004). Finally, the reproducibility of $^{87}Sr/^{86}Sr$ measurement does not appear to be related to Sr intensity over the range of Sr intensities observed in lasering Samoan glasses, a range that encompasses the melt inclusion analyses.

Six melt inclusions were large enough for replicate analysis (one melt inclusion, 71-2C, was replicated over a one-year period), and five of their $^{87}Sr/^{86}Sr$ ratios were reproducible within the quoted precision. However, the replicate analysis of melt inclusion 71-11a was different by 550 ppm (see Table 1), while error resulting from the Rb correction is only 260 ppm (2σ) on Samoan glass standards with similar Rb/Sr ratios. The internal precision of the replicate analysis of this melt inclusion was ~100 ppm (2σ). Data from this melt inclusion indicates that larger-than-usual $^{85}Rb/^{87}Rb$ variations over time can occasionally generate uncertainties (above the 2σ level) in $^{87}Sr/^{86}Sr$ that are somewhat larger than error predicted by the data from Samoan glass standards.

An upper limit for the $^{87}Sr/^{86}Sr$ measurement precision on Samoan melt inclusions with low Rb/Sr can be inferred from the near-uniform ratios obtained on melt inclusions from the high $^{3}He/^{4}He$ Ofu basalt. The Rb/Sr values were among the lowest during analysis of Ofu melt inclusions, and the tight clustering of the Ofu melt inclusions may be partially explained by decreased error of $^{87}Sr/^{86}Sr$ measurement for these samples compared to other, higher Rb/Sr Samoan glasses and melt inclusions from Vailulu'u and Malumalu. If we assume that the Ofu melt inclusions are isotopically homogeneous, then the external precision on these 7 melt inclusions is ±335 ppm (2σ). Some of the apparent variability may be a result of error from the Rb correction, which is ±190 ppm (2σ) at Rb/Sr ratios of 0.053, and may not reflect true variability. Additionally, internal precision varied from 60 to 226 ppm (2σ standard error) on the seven Ofu melt inclusions.

Masses 85 and 88 represent pure Rb and Sr, respectively, so that fairly precise measurement of Rb/Sr ratios can be generated. After correcting for mass fractionation (≈1.5%/amu), Rb/Sr ratios on Samoan basalt glasses measured by laser ablation are reproduceable to 17% (2σ, compared to ratios obtained by XRF/ICP techniques on the same samples), and precise (1.7%, 2σ) during multiple runs on the same glass (see Supplementary data).

Major element compositions of glassy and homogenized melt inclusions were obtained with a JEOL-733 automated electron microprobe at the Massachusetts Institute of Technology using an electron beam with current of 10 nA and accelerating potential of 15 kV focused to a spot of 1–2 μm in diameter for olivine analyses, and defocused to 10 μm for glass analyses. Trace element contents were determined with a Cameca IMS 3f ion microprobe following the techniques described in [27,28]. A small beam (5 μm diameter spot), combined with a high-energy filtering technique (80–100 eV window), was used to determine trace element concentrations. Precision for Sr, La, Zr, Y is estimated to be ±15%, and ±20–30% for Ba, Nb and Rb. Homogenization of olivine-hosted melt inclusions was performed in a furnace at 1187–1220 C (depending on olivine composition) at 1 atm pressure for 5 min in a graphite capsule.

To correct for the effects of crystallization of olivine in the glassy and homogenized melt inclusions, we add equilibrium olivine to the melt inclusions in 0.1% increments until equilibrium with mantle olivine (Fo_{90}) is achieved, assuming olivine-melt partitioning of Fe and Mg from [29]. Instead of correcting the melt inclusions to be in equilibrium with the host olivine, this correction scheme is chosen so that we can compare them to similarly corrected Samoan whole-rock lavas (after discarding data from the most evolved–MgO<6.5 wt.%–whole-rock samples).

3. Results

3.1. Sr-isotope variability in melt inclusions

Sr-isotopes were measured in melt inclusions from nine geochemically well-characterized basalt samples [4,25] from five islands and seamounts located along the Samoan hotspot track. Olivines (Fo_{76-91}) with large ellipsoidal melt inclusions (50–250 μm diameter) were separated from the basalt samples for melt inclusion exposure and isotopic analysis. Most of the melt inclusions were crystalline and usually contained dendritic clinopyroxene in a glassy matrix, with spinel and rare sulfide globules; some (≈5%) of the melt inclusions were glassy. The high $^3He/^4He$ basalt sample OFU-04-06 was unique in that amphibole and apatite were common melt inclusion phases, and carbonate was also observed.

Olivines (Fo_{82-85}) hosting melt inclusions were separated from Malumalu seamount dredge sample 78-1, a picrite with the highest $^{87}Sr/^{86}Sr$ ratio (0.7089) of any OIB [4]. Melt inclusion-rich olivines were also recovered from dredge sample 71-2 (Fo_{84-91}) from Vailulu'u, a seamount that displays intermediate enrichment relative to the other Samoan islands and seamounts (bulk rock $^{87}Sr/^{86}Sr$ isotope ratios from 0.7052 to 0.7067, $n=20$). From Ofu Island, olivines (Fo_{76-84}) were recovered from ankaramite dike sample OFU-04-06, which exhibits the highest $^3He/^4He$ measured in a Samoan basalt [25]. Lavas from Ofu are the most isotopically homogeneous of the volcanoes in the Samoan chain ($^{87}Sr/^{86}Sr$ from 0.70444 to 0.70480, $n=12$). Finally, a smaller number of olivines were separated for melt inclusion analysis from Vailulu'u dredge samples 71-11 (Fo_{81-83}), 63-2 (Fo_{86-87}) and 68-3 (Fo_{87-90}), Malumalu dredge sample 78-3 (Fo_{84}), Ta'u Island dredge sample 74-1 (Fo_{85}), and Savai'i subaerial post-erosional sample S11 (Fo_{76}).

The Sr-isotope data from melt inclusions in just three Samoan whole-rock samples (OFU-04-06, 78-1 and 71-2) define a broad array that encompasses the entire spectrum of Sr-isotope variability (0.70434–0.70926) recorded in Samoan basalts (Fig. 1 and Table 1). Eleven melt inclusions from 78-1 display $^{87}Sr/^{86}Sr$ values of 0.70686–0.70926, and encompass over 30% of the isotope variability observed in the OIB mantle. Vailulu'u melt inclusions from dredge samples 71-2 ($^{87}Sr/^{86}Sr=0.70459–0.70602$, $n=12$ melt inclusions) and 68-3 ($^{87}Sr/^{86}Sr=0.70480–0.70624$, $n=3$) exhibit a smaller range of Sr-isotope values than 78-1. However, the magnitude of the Sr-isotope heterogeneity in the melt inclusions from these two samples is approximately equal to the variability observed in Vailulu'u seamount lavas, although the melt inclusions sample a more depleted component than observed in whole rocks from this seamount. Among the Vailulu'u samples, only sample 71-11 ($^{87}Sr/^{86}Sr=0.70653–0.70692$, $n=2$)

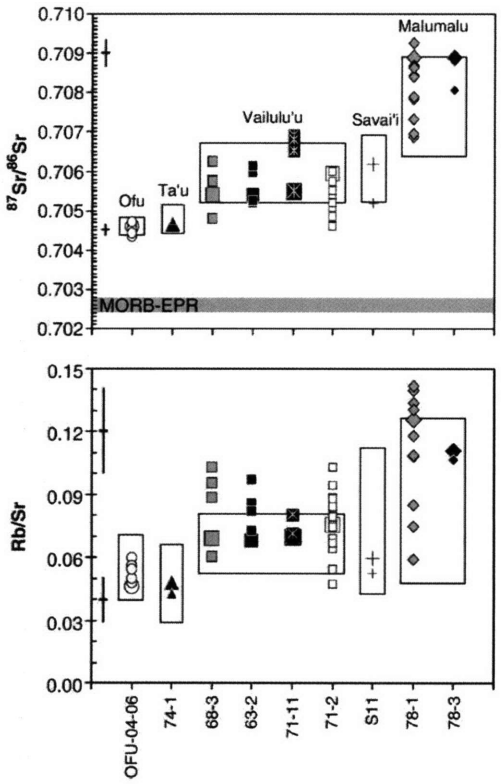

Fig. 1. $^{87}Sr/^{86}Sr$ (upper panel) and Rb/Sr (lower panel) in melt inclusions from nine basalt samples compared to the total variation in each island/seamount (shown by boxes). References for whole-rock data can be found in [4]. The nine whole rocks from which the melt inclusions were separated are represented by larger symbols. No melt inclusions are more isotopically depleted than the most depleted lava measured in the island chain ($^{87}Sr/^{86}Sr>0.7044$). The range for EPR N-MORB [22] (averaged by segment) plots significantly below the Samoan whole rocks and melt inclusions. Replicate analyses on the same melt inclusion are averaged. The Rb/Sr for Savai'i whole-rock sample SAV1-25 is not included because of alteration. Internal precision (2σ, standard error) for $^{87}Sr/^{86}Sr$ is approximately the size of the data symbols. $^{87}Sr/^{86}Sr$ error bars represent error propagated from the Rb correction, as determined on Samoan glass standards, and dominates the error associated with $^{87}Sr/^{86}Sr$ measurement by LA-ICP-MS; maximum and minimum (500 and 150 ppm) errors are shown for reference. Error bars for Rb/Sr are ±17% (2σ, standard deviation), and are based on the reproduceability of Rb/Sr measurement on Samoan glass standards; internal precision for Rb/Sr averages an order of magnitude better. Samples are listed in order of increasing whole-rock $^{87}Sr/^{86}Sr$, from left to right.

hosts inclusions that sample compositions similar to the most enriched isotopic compositions observed in Vailulu'u volcano. Like sample 71-11, isotopic analyses of melt inclusions from sample 63-2 ($^{87}Sr/^{86}Sr$=0.70520–0.70613, n=3) lie completely within the isotopic range found in the whole rocks from Vailulu'u seamount. OFU-04-06 melt inclusions exhibit the least isotopic variability ($^{87}Sr/^{86}Sr$=0.70434–0.70469, n=7) among the samples with isotopic analyses on more than two different inclusions, and this variability is similar to the variability sampled by whole-rock lavas from the island. There is only a single melt inclusion analysis from each of basalt samples 78-3 (0.70807), 74-1 (0.70477) and S11 (0.70518); the Sr-isotope ratios lie within the range observed in the respective host volcanoes.

Although melt inclusions show more depleted isotopic compositions than the island or seamount from which they were recovered, they are not observed to sample compositions more depleted than whole rocks from the Samoan hotspot ($^{87}Sr/^{86}Sr \geq 0.7044$). Therefore, the least radiogenic Sr-isotope ratios in Samoan basalts and melt inclusions are significantly more enriched than the depleted upper mantle sampled by MORB along the EPR (East Pacific Rise; 0.70228–0.70287, N-MORB segment averages from [22]); the old oceanic crust upon which the Samoan island chain is constructed is probably isotopically similar to these modern EPR basalts.

Rb/Sr ratios measured by LA-ICP MS on the same set of melt inclusions tell a story similar to that of the isotopes. Melt inclusions in sample 78-1 exhibit the largest variation in Rb/Sr ratios (0.0593–0.1421), and the variability is similar to that observed in the whole rocks measured from Malumalu seamount. The Rb/Sr ratios in OFU-04-06 melt inclusions show some heterogeneity (Rb/Sr from 0.0476 to 0.0595, n=7), but this variability is smaller than the variability sampled by whole-rock lavas from the island. Vailulu'u melt inclusions from dredge samples 71-2 (Rb/Sr from 0.0469 to 0.1028, n=12 melt inclusions) and 68-3 (Rb/Sr from 0.060 to 0.1027, n=3) exhibit a range of Rb/Sr values that falls between 78-1 and OFU-04-06. Unlike the isotopes, however, the magnitude of the Rb/Sr heterogeneity in the melt inclusions from samples 71-2 and 68-3 is greater than the variability observed in Vailulu'u seamount lavas, and, within error of measurement, do not sample a component with lower Rb/Sr than observed in whole rocks from this seamount.

The present dataset suggests that the isotopic variability exhibited by the melt inclusions in a basalt sample may be a function of the whole-rock isotopic composition. In Fig. 2, the Sr-isotope variability of melt inclusions in three basalt samples–those with the largest number of melt inclusion analyses–is plotted against the bulk $^{87}Sr/^{86}Sr$ composition of the respective whole rocks. The $^{87}Sr/^{86}Sr$ variability, determined by the difference between the highest and the lowest $^{87}Sr/^{86}Sr$

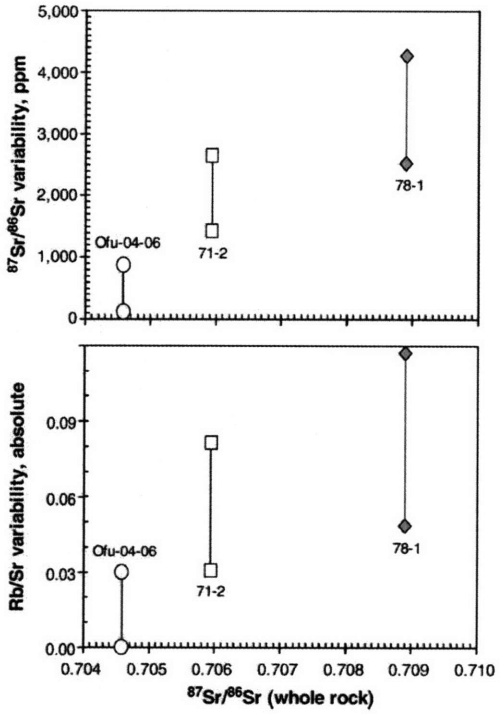

Fig. 2. Upper panel: Melt inclusion isotopic variability (in ppm) as a function of whole-rock $^{87}Sr/^{86}Sr$ ratio for the three Samoan lavas with the greatest number of melt inclusion analyses. Melt inclusion isotopic variability increases with increasing $^{87}Sr/^{86}Sr$ (and decreasing $^{3}He/^{4}He$, not shown) in the three Samoan basalts. Variability is determined by the difference between the most isotopically extreme melt inclusions in a basalt sample. The maximum and minimum values for this variability are a result of the uncertainty introduced by the Rb correction, which is directly related to the Rb/Sr of the melt inclusion. For example, the maximum variability in basalt sample 78-1 is determined by the difference between the highest (0.7092 plus 391 ppm uncertainty) and lowest plausible $^{87}Sr/^{86}Sr$ (0.7072 minus 393 ppm uncertainty). The minimum variability is determined by the difference between the lowest plausible $^{87}Sr/^{86}Sr$ in the most enriched melt inclusion (i.e., 0.7089, or 0.7092 minus 389 ppm uncertainty) and the highest plausible $^{87}Sr/^{86}Sr$ in the most depleted melt inclusion (0.7074, or 0.7072 plus 393 ppm uncertainty). Lower panel: Melt inclusion Rb/Sr variability (absolute) as a function of whole-rock $^{87}Sr/^{86}Sr$ ratio. Maximum and minimum variability is determined the same way, but assumes an uncertainty for Rb/Sr of 17%. The magnitude of variability due to internal precision is approximated by the size of the data symbols in both panels.

ratios from melt inclusions in a given basalt sample, exhibits a maximum and a minimum due to the uncertainty introduced by the Rb correction. Although the number of data points is limited, the data are consistent with melt inclusion isotopic diversity increasing with increasing $^{87}Sr/^{86}Sr$ (increasing EM2 component) and decreasing $^{3}He/^{4}He$ (not shown). The range of variability for Malumalu sample 78-1 is larger than, but overlaps with, the range of values from Vailulu'u sample 71-2. The melt inclusions from the high $^{3}He/^{4}He$ Ofu basalt exhibit the smallest range of probable $^{87}Sr/^{86}Sr$ ratios, and they do not overlap with the range from samples 71-2 and 78-1. A similar observation can be made for the variability of Rb/Sr ratios in the melt inclusions, where Rb/Sr tends toward greater melt inclusion variability in samples 78-1 and 71-2; the Ofu sample has the smallest range of variability, and overlaps slightly with the lowest probable variability in sample 71-2. It is notable that OFU-04-06 exhibits the highest $^{3}He/^{4}He$ ratio (and low $^{87}Sr/^{86}Sr$) found in Samoa, an observation that may be linked to the small degree of isotopic and trace element variability in its melt inclusions.

3.2. Major and trace element characteristics of melt inclusions

Rb/Sr and $^{87}Sr/^{86}Sr$ ratios from the melt inclusions define a broad array that encompasses the entire spectrum of Sr-isotope and Rb/Sr variability recorded in Samoan basalts (Fig. 3). Curiously, the melt inclusions from Malumalu do not form an array by themselves, but plot over a broad region. The Rb/Sr and Sr-isotope data array form a crude mantle isochron of 1.1 Ga.

Major and trace elements were measured on melt inclusions from Vailulu'u, Malumalu and Ofu basalts, and they reveal a large range of compositions (Table 2). Although the trace element compositions of Vailulu'u melt inclusions are similar to whole-rock analyses from this seamount, melt inclusions from EM2 endmember basalt 78-1 record a greater degree of trace element variability than all of the whole rocks measured from Malumalu. One

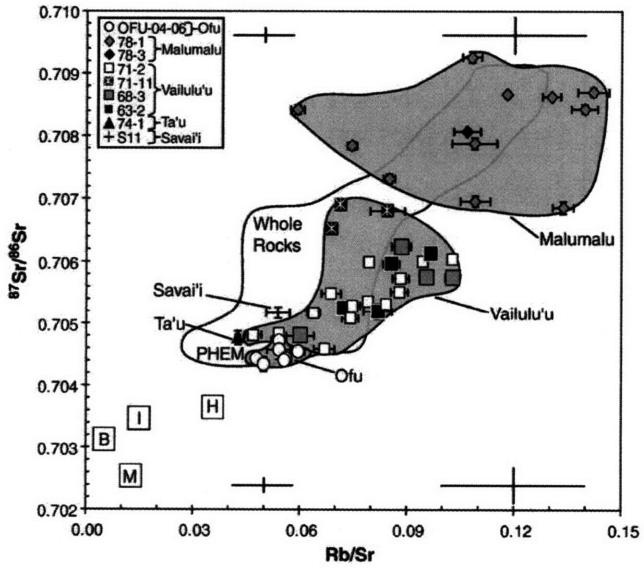

Fig. 3. $^{87}Sr/^{86}Sr$ versus Rb/Sr ratios for Samoan whole rocks and melt inclusions, determined by laser ablation. The shaded regions represent the extent of melt inclusion variability for the volcanoes (Vailulu'u, Malumalu and Ofu). The open region encompasses the least evolved (MgO ≥ 6.5 wt.%) whole-rock measurements from these three volcanoes and Ta'u, thus encompassing islands and seamounts only on the eastern half of the Samoan hotspot track (where ~98% of the analyzed melt inclusions were recovered). Whole-rock data from Ofu is unpublished, and for the other volcanoes is from [4]. MORB range is limited to EPR N-MORB (M) segment averages [22]. High $^{3}He/^{4}He$ basalts from Hawaii (H) [37], Iceland (I) [38] and Baffin Island (B) [39] provide an approximation for FOZO (higher $^{3}He/^{4}He$ ratios exist for Hawaiian basalts [40], but $^{87}Sr/^{86}Sr$ data are not available for these samples; Rb/Sr data for high $^{3}He/^{4}He$ samples from Baffin Island are found in [41]). Error bars on symbols are internal precision of measurement (2σ, mean deviation). Error bars on periphery of figure denote external precision of measurements, as determined by Samoan glass standards with compositions similar to the melt inclusions: Rb/Sr error is 17% (2σ, standard deviation) and $^{87}Sr/^{86}Sr$ error is based on error associated with the Rb correction (2σ, standard deviation). Replicate analyses of the same melt inclusion are shown. The melt inclusion data form a crude mantle isochron age of ~1.1 Ga.

Table 2
Melt inclusion major and trace element data (uncorrected for olivine fractionation), and host olivine composition

Sample #	Disc #	Grain #	SiO_2	TiO_2	Al_2O_3	FeO	MnO	MgO	CaO	Na_2O	K_2O	P_2O_5	Total	Mg #	OlFo	Rb	Sr	Y	Zr	Nb	Ba	La	$^{87}Sr/^{86}Sr^a$	Type
78-1	Disc1	#7	45.64	3.77	12.97	14.11	0.14	6.85	9.53	3.46	2.16	0.46	99.19	49.0	84.6	181	1176	83.6	979	–	–	–	0.70926	H
78-1	Disc1	#9	46.57	2.99	13.06	10.75	0.16	8.02	13.09	2.94	1.57	0.44	99.74	59.6	84.4	49	443	33.0	245	–	–	45.6	0.70732	H
78-1	Disc1	#10–11	44.98	3.22	12.84	11.18	0.14	9.26	11.29	2.62	1.76	0.39	98.10	62.1	84.0	75	507	28.1	269	–	–	–	–	H
78-1	Disc1	#12	46.37	3.76	13.09	11.51	0.17	8.03	11.38	2.93	1.91	0.40	99.65	58.0	84.4	59	545	33.2	339	73.1	390	–	–	H
78-1	Disc2	#5	45.16	3.42	12.62	11.09	0.17	9.15	12.42	2.46	1.42	0.42	98.68	62.0	84.3	130	1127	75.5	568	132.9	796	96.1	–	H
78-1	Disc2	#6	47.22	3.45	13.60	11.80	0.23	7.10	10.17	3.13	2.10	0.42	99.38	54.4	83.6	115	926	54.1	543	122.4	666	93.8	0.70843	H
78-1	Disc2	#7	47.20	2.92	13.65	9.94	0.14	7.83	11.36	2.73	2.00	0.40	98.49	60.9	83.9	–	–	–	–	–	–	–	–	H
78-1	Disc2	#8	45.57	3.20	12.26	11.20	0.17	9.26	11.33	2.71	1.33	0.47	97.88	62.1	83.6	71	679	40.6	360	76.0	409	57.7	–	H
78-1	Disc2	#9	46.81	3.46	14.03	11.81	0.16	7.34	10.54	2.93	1.91	0.43	99.59	55.2	82.8	76	655	38.7	400	84.8	482	72.3	0.70870	H
78-1	Disc2	#10	46.32	3.46	13.16	11.01	0.15	7.65	11.60	4.80	1.27	0.46	100.01	57.9	83.6	33	631	37.3	346	73.4	450	65.1	0.70842	H
78-1	Disc2	#11Le	46.32	3.24	12.74	11.04	0.14	8.18	12.72	3.18	1.33	0.39	99.67	59.5	83.6	55	598	36.7	281	56.1	401	45.5	–	H
78-1	Disc2	#11RtS	–	–	–	–	–	–	–	–	–	–	–	–	83.2	194	1694	100.5	871	193.5	1258	173.6	–	H
78-1	Disc2	#11RtL	44.61	3.77	12.99	11.76	0.19	6.23	13.20	2.70	1.57	0.44	97.85	51.2	83.2	299	2480	158.7	1310	293.5	1887	246.6	–	H
78-1	Disc2	#3	46.09	3.23	12.50	10.68	0.15	8.85	11.47	2.59	1.59	0.43	97.91	62.1	84.1	135	1038	62.5	579	126.8	719	100.6	–	H
78-1	Disc2	#4	46.45	2.99	12.17	10.32	0.15	9.22	12.92	2.37	1.37	0.40	98.80	63.9	83.9	104	901	55.1	465	110.9	686	78.9	–	H
78-1	Disc3	#4	46.07	3.81	13.22	10.47	0.12	6.00	12.52	2.93	1.80	0.42	97.81	53.1	85.2	69	555	26.4	297	64.8	370	55.4	0.70866	G
71-2	Disc1	g#3–4	48.50	2.66	12.55	9.41	0.14	7.38	14.63	2.33	0.84	0.35	99.13	60.8	87.4	26	384	23.0	185	30.4	124	22.4	–	G
71-2	Disc1	i	48.13	2.57	12.54	9.21	0.14	8.07	13.85	2.48	0.78	0.27	98.40	63.4	90.7	–	–	–	–	–	–	–	0.70602	G
71-2	Disc3	#3	46.12	3.48	13.06	10.94	0.15	5.81	14.09	2.55	1.29	0.32	98.23	51.3	84.3	50	517	29.5	237	52.7	347	40.9	–	G
71-2	Disc3	#5	46.71	3.10	12.72	9.66	0.15	7.90	13.10	2.45	1.24	0.32	97.72	61.8	91.0	45	504	27.1	243	58.8	314	35.3	0.70534	G
71-2	Disc3	#6	46.46	3.23	12.31	10.52	0.17	7.54	13.64	2.64	1.14	0.36	98.50	58.7	85.7	50	579	33.3	281	60.1	342	49.9	0.70599	G
71-2	Disc3	C	48.87	3.33	13.16	8.77	0.15	7.63	12.81	2.68	0.83	0.39	98.94	63.3	88.8	27	437	22.2	232	42.6	177	33.9	0.70482	G
71-11	Disc3	#1	49.01	3.13	12.53	11.05	0.18	6.15	12.01	2.85	0.94	0.40	98.51	52.4	81.4	34	419	27.1	232	41.4	205	35.6	0.70680	G
71-11	Disc1	a	49.28	2.82	12.70	10.94	0.14	6.89	11.63	2.60	1.01	0.37	98.73	55.5	83.0	36	409	30.3	223	40.9	214	33.0	0.70672	G
68-3	Disc1	#6mi1	48.77	2.88	14.30	8.75	0.13	4.68	14.74	2.64	1.35	0.37	98.98	51.4	87.9	54	533	27.0	260	62.5	378	46.3	0.70624	G
OFU-04-06	Ofu	13	44.25	3.31	12.60	10.10	0.11	7.99	13.38	3.40	0.94	0.50	96.75	61.4	79.8	52	856	41.6	464	76.8	343	106.2	0.70457	H
OFU-04-06	Ofu	14	46.33	3.07	14.03	8.64	0.07	8.03	11.89	3.52	1.08	0.53	97.24	54.9	80.4	61	613	33.3	352	55.6	311	77.8	–	H
OFU-04-06	Ofu	15	46.47	2.81	13.67	10.58	0.14	7.20	10.64	3.96	1.09	0.33	96.96	60.5	77.3	60	700	30.0	374	54.8	303	82.1	0.70443	H
OFU-04-06	Ofu	16	46.74	3.13	14.12	7.00	0.09	8.26	13.11	3.76	1.19	0.45	97.97	49.5	81.9	68	760	38.6	393	72.5	363	91.1	–	H
OFU-04-06	Ofu	18	50.44	1.16	14.17	7.56	0.07	7.33	11.22	4.69	1.38	0.39	98.67	51.4	79.3	63	926	33.8	460	84.1	399	113.9	–	H
OFU-04-06	Ofu	19	47.15	2.14	11.15	17.06	0.21	13.83	2.72	1.56	1.71	0.46	98.00	75.2	76.6	–	–	–	–	–	–	–	–	H
OFU-04-06	Ofu	20	47.36	2.90	14.50	9.00	0.13	7.59	10.84	4.02	1.06	0.39	97.84	55.1	78.6	81	909	39.0	438	70.3	402	32.5	–	H
OFU-04-06	Ofu	24rep	46.35	3.58	13.47	8.58	0.09	8.11	13.70	3.23	0.72	0.29	98.13	55.8	83.0	–	–	–	–	–	–	–	–	H
OFU-04-06	Ofu	25	45.74	3.16	13.55	11.98	0.12	7.71	11.15	3.54	0.89	0.42	98.33	63.6	77.2	59	659	38.1	383	48.7	243	–	0.70454	H
OFU-04-06	Ofu	26	46.14	2.51	12.70	10.60	0.10	8.04	13.61	3.01	0.74	0.34	97.93	62.3	76.5	45	573	37.7	338	42.3	191	–	0.70443	H

OFU-04-06	Ofu	27	44.62	3.36	13.38	10.12	0.10	7.99	12.36	3.35	0.91	0.49	96.82	60.0	79.5	55	807	40.2	457	75.8	321	111.4	–	H
OFU-04-06	Ofu	28	47.60	2.70	13.87	9.87	0.08	7.49	10.92	4.18	0.94	0.33	98.13	58.5	78.4	58	744	34.6	382	71.1	322	94.3	0.70434	H
OFU-04-06	Ofu	30	47.23	3.03	13.82	7.23	0.09	7.78	12.39	3.74	1.15	0.24	96.79	50.9	82.3	63	634	32.8	324	54.0	283	76.6	–	H
OFU-04-06	Ofu	31	42.22	2.01	13.18	14.43	0.12	7.24	12.41	4.17	1.14	0.43	97.95	68.4	80.3	87	1006	46.6	515	79.4	445	136.2	–	H
OFU-04-06	Ofu	33	41.65	2.83	13.21	16.38	0.17	6.96	10.68	3.77	1.06	0.34	97.17	71.1	77.7	66	961	39.1	479	81.9	391	105.9	–	H
OFU-04-06	Ofu	2	46.18	3.00	13.70	9.93	0.13	7.53	11.26	3.70	0.99	0.32	96.80	58.9	76.5	50	800	35.5	409	81.5	326	80.9	0.70469	H
OFU-04-06	Ofu	3	45.75	3.12	13.20	7.91	0.10	8.20	13.67	3.01	0.83	0.37	96.24	54.3	83.8	41	714	36.8	398	72.2	301	72.4	0.70443	H
OFU-04-06	Ofu	4	45.71	3.05	13.40	10.95	0.06	7.62	10.88	3.93	0.93	0.33	96.89	61.8	77.2	56	772	33.6	420	73.2	326	70.2	–	H
OFU-04-06	Ofu	5	47.03	3.01	14.37	8.75	0.12	7.66	11.77	3.70	1.21	0.19	97.92	54.7	81.4	79	661	31.6	333	63.5	393	78.9	–	H
OFU-04-06	Ofu	8	45.83	3.21	13.50	10.96	0.13	7.74	11.19	4.06	0.98	0.36	98.04	61.6	77.7	63	861	40.0	462	81.2	363	102.5	–	H
OFU-04-06	Ofu	9	44.84	3.37	13.52	12.21	0.15	6.89	10.62	4.25	1.04	0.32	97.31	64.1	77.4	77	1006	42.7	528	98.4	444	104.7	–	H
OFU-04-06	Ofu	22	38.04	4.65	10.75	12.83	0.18	9.84	17.18	1.15	0.12	0.59	95.55	70.3	80.9	18	1161	72.4	821	121.9	255	38.9	–	H
OFU-04-06	Ofu	21	45.30	4.63	14.07	10.83	0.20	6.89	9.58	4.35	1.57	0.74	98.40	60.4	78.1	67	779	34.8	417	51.7	271	51.4	–	H
OFU-04-06	Ofu	23	45.58	5.87	12.35	8.58	0.12	8.17	13.00	3.71	1.32	0.84	99.47	57.9	80.6	85	1042	48.6	551	78.9	374	38.4	–	H
OFU-04-06	Ofu	7(fir)	–	–	–	–	–	–	–	–	–	–	–	–	–	110	894	21.2	289	112.8	588	97.6	–	H
OFU-04-06	Ofu	7(sec)	–	–	–	–	–	–	–	–	–	–	–	–	–	65	809	37.5	428	74.1	365	104.7	–	H

Rb/Sr ratios by LA-ICP-MS are considered to be more accurate than those obtained by ion probe. Any discrepancy between the Rb/Sr ratios measured by the two methods is probably due to the difficulty of measuring Rb by ion probe techniques. Samples 78-1, 71-2, 71-11 and 68-3 are from the Samoan AVON3 dredging cruise, and their sample names are preceded by the prefix "AVON3."
Major element data are in wt.%, and trace elements are in ppm. Forsterite contents of the host olivines (Ol Fo) are also given. Glassy (G) or Homogenized (H).
[a] See data in Table 1 for Sr-isotope data.

melt inclusion from sample 78-1 displays high Sr and Ba concentrations (2500 and 1900 ppm, respectively) that are 6 times more enriched than any whole-rock lavas examined from Malumalu. This ultra-enriched composition is significantly more enriched than observed in any Samoan basalts, and is derived from either an extremely enriched source or from very small degrees of melting.

Melt inclusions from OFU-04-06 also exhibit some unusual major and trace element compositions. One Ofu melt inclusion exhibits unusually low K_2O concentrations. Additionally, the OFU-04-06 melt inclusions exhibit a large range in SiO_2, including one sample with unusually low SiO_2 (38.0%) and high CaO (17.2%). These uncommon major element compositions may be due to the combination of unusual phases present in the OFU-04-06 melt inclusions prior to homogenization in the lab. Low glass totals in the OFU-04-06 inclusions are likely due to high volatile contents in the homogenized glasses, a hypothesis consistent with the volatile-rich phases in melt inclusions from this sample.

In addition to Rb/Sr ratios, several other major and trace element parameters correlate with $^{87}Sr/^{86}Sr$ in the melt inclusions. Melt inclusions from Ofu, Vailulu'u and Malumalu exhibit negative Ba anomalies that also are observed in Samoan shield-stage lavas [4] (Fig. 4). An approximation for this Ba anomaly is $(Ba/Nb)_N$ (normalized to PUM, primitive upper mantle [30]), a ratio which correlates with $^{87}Sr/^{86}Sr$ in whole rocks and melt inclusions (Fig. 5). The $(Ba/Nb)_N$ values are lowest (largest Ba-anomaly) in the basalts and melt inclusions with low $^{87}Sr/^{86}Sr$, and highest in the basalts and melt inclusions with elevated $^{87}Sr/^{86}Sr$ ratios. It is notable that basalts and melt inclusions associated with elevated $^{3}He/^{4}He$ ratios, and not the high $^{87}Sr/^{86}Sr$ EM2 end-member basalts, have the largest Ba anomalies. The mechanism that generates this anomaly is unknown [4], and the anomaly also exists in MORB and HIMU basalts, but not in basalts with EM1 characteristics.

The negative K_2O anomaly in the Samoan melt inclusions (Fig. 4) is commonly observed in OIBs. Curiously, however, PUM-normalized K exhibits little variability regardless of the degree of enrichment of the other trace elements (with the exception of a single Ofu melt inclusion). Despite the limited variability, olivine fractionation-corrected K_2O concentrations exhibit a relationship with $^{87}Sr/^{86}Sr$ in the melt inclusions (Fig. 5).

Nb/Zr also correlates with $^{87}Sr/^{86}Sr$ in Samoan basalts and melt inclusions (Fig. 5). The lowest Nb/Zr ratios are associated with unradiogenic $^{87}Sr/^{86}Sr$ values. Nb/Zr ratios correlate with Pb-isotopes [4] and inversely with $^{3}He/$

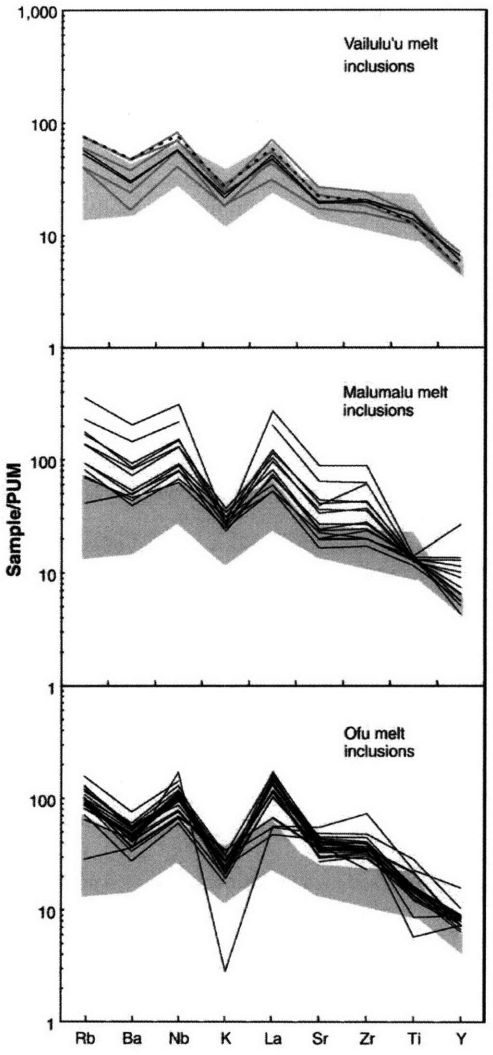

Fig. 4. PUM-normalized trace element patterns of Samoan basalts and melt inclusions; melt inclusion data is from ion probe analysis, except for K and Ti, which were measured by electron probe. Vailulu'u melt inclusions are from three samples: 71-2 (grey lines), 68-3 (dashed line), 71-11 (solid black lines). Malumalu and Ofu melt inclusions are from samples 78-1 and OFU-04-06, respectively. All melt inclusions (except for one melt inclusion from 78-1 and two from OFU-04-06 that have no major element compositions, see Table 2) are corrected for olivine fractionation to be in equilibrium with mantle olivine of Fo_{90} (see text for correction scheme). The grey field encloses the range of whole-rock patterns from the least evolved basalts (>6.5 wt.% MgO) from Vailulu'u, Ofu and Malumalu; whole-rock compositions have been corrected for olivine addition/fractionation. PUM values from [30].

^{4}He (not shown) in Samoan basalts. Nb/Zr may serve as a proxy for ^{3}He/^{4}He isotopes in Samoan melt inclusions; therefore, it may be important that the Nb/Zr ratios in several of the Ofu-04-06 melt inclusions exhibit values lower than the ratios observed in whole rocks.

3.3. Melting models of the EM2 source

It is important to place constraints on the trace element variability introduced by melting processes. A plot of Sr versus Ti/Zr shows that the majority of the melt inclusions form an array that extends outside of the whole-rock field to enriched Sr and low Ti/Zr values (Fig. 6). The low Ti/Zr ratios (15-88) observed in the melt inclusions extend to lower values than observed in whole-rock basalts from the eastern Samoa islands and seamounts (63-130). Such low values cannot be produced by crystal fractionation of melts before olivine entrapment, and assimilation of MORB (Ti/Zr=88) also fails to produce low Ti/Zr values [31]. A model of the Samoan EM2 source composition [4] provides a robust estimate for the mantle source sampled by the extreme EM2 basalt sample 78-1, and variable degrees of aggregated modal fractional melts of this source (Sr=20.0 ppm, Ti/Zr=101.9) in the garnet and spinel stability fields can describe much of the melt inclusion array in Fig. 6. Consistent with the model of the EM2 source as a metasomatized harzburgite [4], we adopt a harzburgite source lithology (1% spinel, 3.6% clinopyroxene [cpx], 20.6% orthopyroxene [opx] and 74.8% olivine), with mineral modes from [32] and mineral/melt partition coefficients from [33]. We assume the mineral modes of a similar bulk composition for melting in the garnet stability field (3.8% garnet, 2.7% cpx, 17.7% opx and 75.8% olivine) using the spinel to garnet conversion from [34]. The two melting models follow similar trajectories, but melting in the spinel stability field is required to generate the exceptionally high Sr and low Ti/Zr observed in the ultra-enriched Malumalu melt inclusions. Interestingly, if the EM2 source [4] has a more cpx-rich lithology than the harzburgite in our melting model, it will not produce melts with the Sr concentrations observed in the most enriched melt inclusion at reasonable degrees (>1%) of melting (Fig. 7).

Other geochemical indicators, including Y/Zr ratios, more clearly resolve the relative roles of melting in the garnet and spinel stability fields. Due to the relative compatibility of Y in residual garnet, low Y/Zr ratios are consistent with melting in the presence of garnet. A role for melting in the garnet stability field is suggested in a plot of Y/Zr against Nb/Zr in Fig. 6. This is particularly true for the Ofu melt inclusions, which trend to the lowest Y/Zr ratios

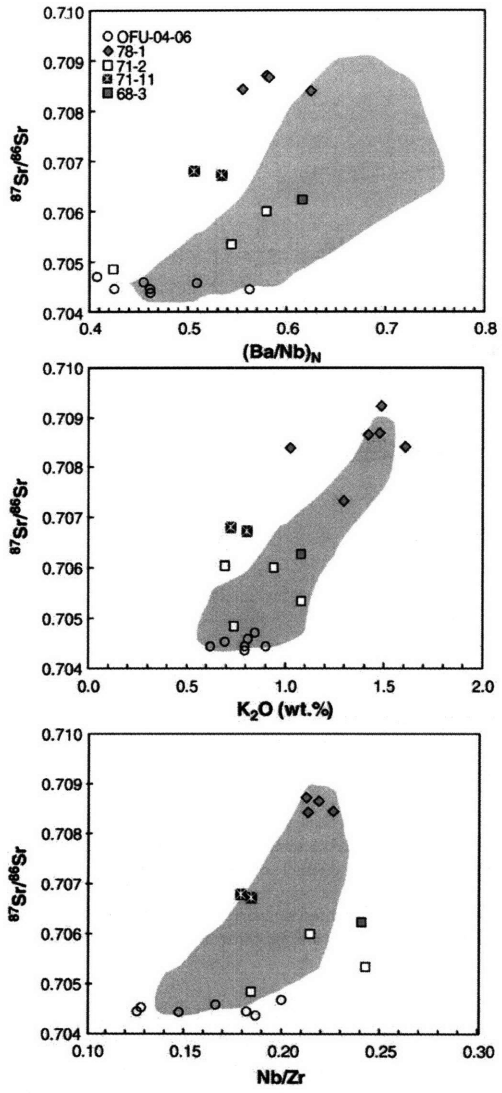

Fig. 5. Nb/Zr, K_2O and Ba/Nb_N versus $^{87}Sr/^{86}Sr$. K_2O measured by electron probe, and Nb, Zr and Ba by ion probe. $(Ba/Nb)_N$ (normalized to PUM) is used as a proxy for the pervasive negative Ba anomaly in Samoan shield-stage basalts. The EM2 basalts and melt inclusions are associated with elevated Nb/Zr, K_2O and $(Ba/Nb)_N$ (smaller negative Ba anomalies), and the low $^{87}Sr/^{86}Sr$ basalts exhibit lower Nb/Zr, K_2O and $(Ba/Nb)_N$ (larger negative Ba anomalies). All melt inclusions are corrected for olivine fractionation. The grey fields enclose the range of whole-rock patterns from the least evolved basalts (>6.5 wt.% MgO) from Vailulu'u, Ofu and Malumalu (whole-rock compositions have been corrected for olivine addition/fractionation). Symbols are the same as Fig. 3. $^{87}Sr/^{86}Sr$ internal precision (2σ, standard error) is approximately the size of the symbol.

observed in the melt inclusions suite and straddle the garnet melting trend at 5% melt. This is similar to the Ti/Zr versus Sr plot, where the garnet melting curve trends through the Ofu melt inclusion field at ~4% melt. Malumalu and Vailulu'u melt inclusions (and Samoan whole rocks) are offset to higher Y/Zr ratios, perhaps suggesting a larger role for melting in the spinel stability field, an observation that is consistent with the same subset of melt inclusions in the Ti/Zr versus Sr melt model.

No single melting model of the EM2 source perfectly describes the melt inclusion fields for all three volcanoes, but we find that a combination of melting and mixing satisfactorily reproduces the melt inclusion geochemical variability. The relative roles of melting and mixing of different components can be partially deconvolved in a plot of $^{87}Sr/^{86}Sr$ versus 1/Sr (Fig. 8), where two-component mixing trajectories are linear and variable degrees of melting result in horizontal trajectories. The Ofu melt inclusions lie on a horizontal trend, which can be described by various degrees of melting of a single source that exhibits a $^{87}Sr/^{86}Sr$ ratio of ~0.7045, and the Malumalu and Vailulu'u melt inclusions form a diagonal array that suggests a role for two-component mixing.

4. Discussion

4.1. A homogeneous source for PHEM basalts

Compelling evidence that the Samoan melt inclusions sample a heterogeneous source comes from Sr-isotope analysis of the melt inclusions from Vailulu'u and Malumalu basalts. However, the uniformly unradiogenic character of the Ofu melt inclusions precludes a significant contribution from an enriched, radiogenic (EM2) component. This suggests that Samoan melts with high $^3He/^4He$ sample a homogeneous source and do not mix with melts of an enriched component. By comparison, the melt inclusions from Malumalu and Vailulu'u span a large range of Sr concentrations and isotopic compositions, indicating that both variable degrees of melting and mixing have occurred. An aggregated fractional melt trajectory for the garnet stability field is plotted (Fig. 8) for the EM2 source [4], and the Malumalu and Vailulu'u melt inclusions form a broad array that trends diagonally away from the horizontal Ofu melting trajectory toward low degree (~1%) melts of the EM2 source; the Vailulu'u and Malumalu melt inclusions can be produced by aggregated melts of an Ofu source that then mix with aggregated fractional garnet melts of the EM2 source.

Unlike the EM2 source, the trace element source composition of the high $^3He/^4He$, lower $^{87}Sr/^{86}Sr$ Ofu source component is less clear. Called PHEM [23], this

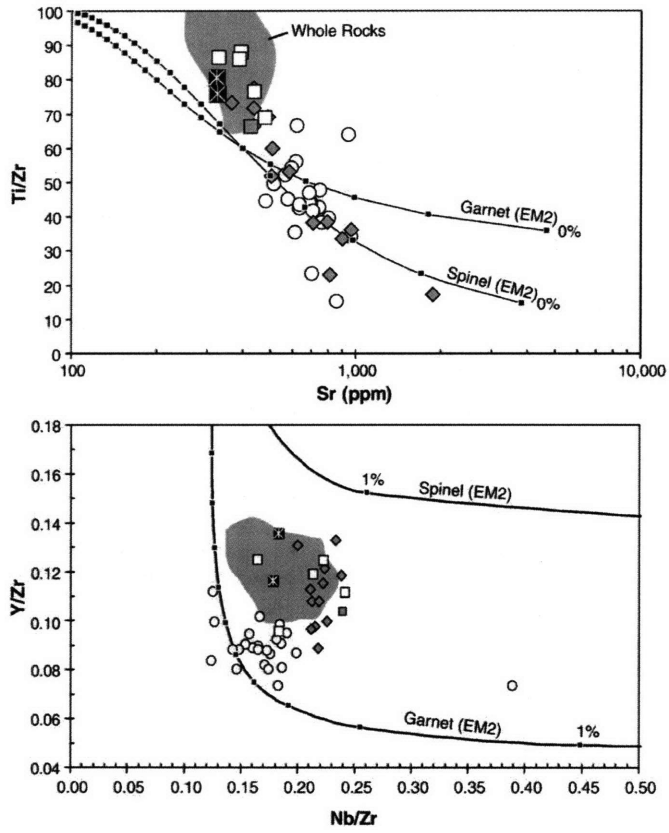

Fig. 6. Upper panel: Ti/Zr versus Sr concentration in melt inclusions and whole rocks with melting models. All melt inclusions and whole rocks are corrected for olivine fractionation to be in equilibrium with mantle olivine. Grey field is for whole-rock samples from Vailulu'u, Malumalu and Ofu. Lines with closed boxes represent aggregated fractional melting trends of the EM2 source [4] in the garnet and spinel stability fields, using partition coefficients from [33]. Harzburgite mineral modes are from [32]. All melting is non-modal. Tick marks are every 1% melting, beginning at 0% and increasing to the left. Lower panel: Y/Zr versus Nb/Zr in melt inclusions and whole rock, including melting models in the garnet and spinel stability fields. Tick marks are every 1% and the degree of melting increases to the left. Melting parameters and grey field are the same as upper panel.

component melts to form basalts and melt inclusions from Ofu. However, it is possible to bracket the source composition of this component and estimate the degree of melting captured in the Ofu melt inclusions. Although the Ofu basalts are more isotopically depleted than the EM2 basalts, an isotopically and trace element depleted DMM lherzolite source (7 ppm Sr) [35] fails to produce the high Sr concentrations observed in the Ofu melt inclusions (Fig. 7). This would suggest that the Ofu source is either more refractory or more trace element enriched, or both, than the lherzolitic [35] DMM source. The first option can be explored by invoking a more refractory, harzburgitic DMM source. However, only unreasonably low ($F<1\%$) degrees of melting can produce the most enriched Sr concentration observed an Ofu melt inclusion. The second scenario can be tested by invoking the trace element enriched EM2 source, and assigning it a lherzolitic lithology that is similar to DMM. At reasonable degrees of melting ($F=1.5\%$), such a source can generate melts with sufficiently high Sr contents to match the range observed in Ofu. Finally, a harzburgitic EM2 source, which is both more refractory and trace element enriched than DMM, can generate the most enriched melt inclusions from Malumalu and Ofu between 1% and 2% melting. The harzburgitic EM2 source can serve as a probable upper limit for the trace element enrichment of the PHEM source because we consider it unlikely for the less isotopically enriched PHEM component to exhibit greater trace element enrichment than EM2. However,

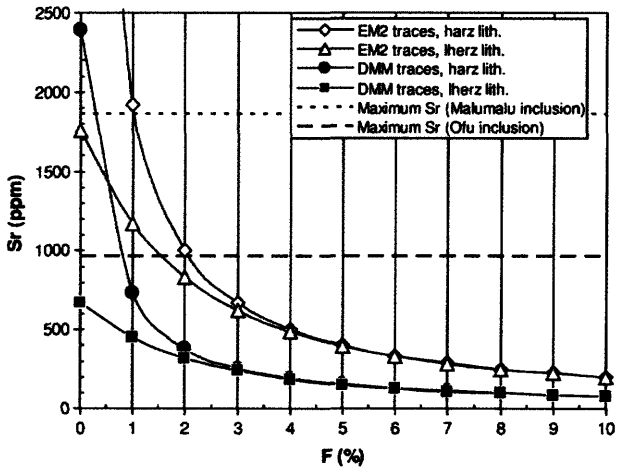

Fig. 7. Sr in melt versus degree of melting (F) for various combinations of two lithologies and two trace element source abundances. Two dashed lines represent olivine fractionation-corrected Sr concentrations in the most enriched melt inclusions from Malumalu sample 78-1 (upper line) and Vailulu'u sample 71-2 (lower line). DMM trace element source and lherzolite lithology from [35], converted to equivalent garnet facies lithology using relationship from [34]. EM2 source from [4]. Harzburgite lithology from [32]. Note that only the EM2 source with a harzburgite lithology can produce the highest Sr concentration observed in the melt inclusion from sample 78-1 at $F \geq 1\%$. All melting is non-modal in the garnet stability field. Neither modal melting nor melting in the spinel stability field significantly changes our conclusions at $F \geq 1\%$.

a PHEM source with a lithology (and/or Sr concentrations) intermediate between DMM and EM2 cannot be ruled out. If PHEM has the same Sr content and lithology as the EM2 source, the Vailulu'u and Malumalu melt inclusion arrays can be explained as mixtures of 6.5±1.5% melts of PHEM and ~1% melts of EM2. However, the degree of melting of the PHEM source that contributes to the Malumalu–Vailulu'u mixing array should be taken as a maximum.

Unlike the Ofu melt inclusions, which sample a pure PHEM source, no melt inclusions sample a pure EM2 melt (as calclulated by [4], using ultra-enriched Sr-isotope compositions from Samoan xenoliths [36]). Mixing lines in Fig. 8 between a 1% EM2 melt and 6.5±1.5% PHEM melts indicate that the subset of Vailulu'u and Malumalu melt inclusions with both $^{87}Sr/^{86}Sr$ and Sr concentration data are dominated by a PHEM component, and exhibit less than a ~30% contribution from the EM2 component. However, one Malumalu melt inclusion exhibits a much larger contribution from an EM2 component, as indicated by its high (~1865 ppm) Sr content and low (~17) Ti/Zr ratio (Fig. 6). The PHEM–EM2 melt mixing lines in Fig. 8 suggest that this melt inclusion contains more than a 70% contribution from the EM2 melt component. The mixing model suggests that a 70% contribution from an EM2 melt would produce an extrapolated $^{87}Sr/^{86}Sr$ ratio of ~0.712, which is a significantly higher ratio than has been observed in a Samoan basalt, but close to the $^{87}Sr/^{86}Sr$ of cpx in metasomatized xenoliths from Savai'i in western Samoa. Unfortunately, this ultra-enriched melt inclusion was too small for isotopic analysis.

4.2. Isotopic variability in Samoan melt inclusions: MORB or FOZO?

Correlations between trace elements and Sr isotopes suggest that trace element variability in Samoan basalts and melt inclusions may reflect heterogeneity in the Samoan mantle. Rb/Sr, K_2O, $(Ba/Nb)_N$ and Nb/Zr ratios correlate with Sr isotopes in Samoan lavas and melt inclusions, suggesting that these trace elements are heterogeneous in the Samoan mantle source. However, a combination of melting processes and variable source lithology may drive the observed correlations, limiting the role for source heterogeneity. For example, the relatively constant K_2O concentrations and negative (PUM-normalized) anomalies in Samoan lavas may be a result of residual phlogopite, which may cause K_2O to behave more compatibly in the Samoan source during melting. However, K_2O correlates with $^{87}Sr/^{86}Sr$ in the whole rocks and melt inclusions (Fig. 5), suggesting a role for K_2O heterogeneity in the Samoan source, and that K_2O concentrations in Samoan basalts and melt inclusions may be controlled only partially by melting processes.

Assuming that Rb/Sr variability in Samoan melts reflects source variability, the array formed by the $^{87}Sr/$

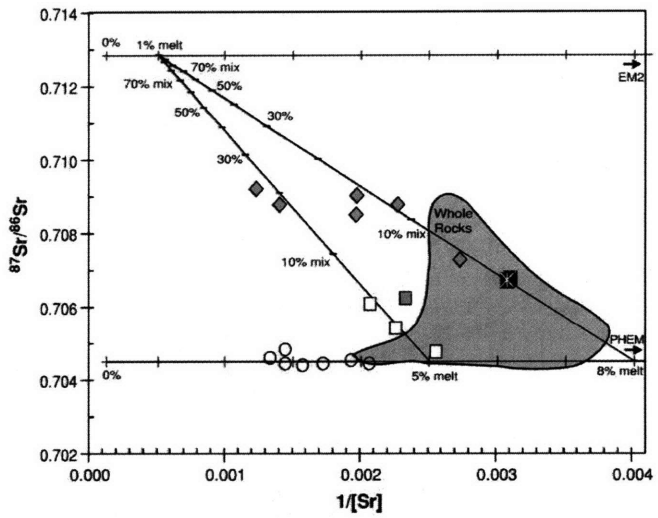

Fig. 8. $^{87}Sr/^{86}Sr$ versus 1/[Sr] for Samoan melt inclusions and basalts. Malumalu and Vailulu'u melt inclusions form a quasi-linear array extending away from the whole-rock basalts from Malumalu, Ofu and Vailulu'u (grey field, same as Fig. 6). Ofu melt inclusions fall off this array, plotting at lower $^{87}Sr/^{86}Sr$ at a given Sr concentration. Aggregated non-modal fractional melting trends of the EM2 and PHEM sources in the garnet stability field are shown as horizontal lines (tick marks are every 1% melting, beginning at 0% and increasing to the right). Two mixing lines, both extending diagonally from a 1% EM2 melt to 5% and 8% PHEM melts, are shown (each tick represents 10% mixture, starting at 0% EM2 and increasing to the upper left). Ofu melt inclusions lie on the melting trend for PHEM, and require no mixing with an EM2 component. Malumalu and Vailulu'u melt inclusions can be described by mixing of melts from the EM2 and PHEM sources. Sr concentrations in melt inclusions and whole rocks are corrected for olivine fractionation. PHEM and EM2 source compositions plot outside of the figure as indicated, at 1/Sr values of ~0.05 (Sr concentrations of 20.0 ppm). The published source for EM2 [4] is used in this figure. As a limit, PHEM is given the trace element source abundances and lithology of EM2 in the melt model. Symbols same as in Fig. 3.

^{86}Sr and Rb/Sr data can be modeled as binary mixing between a PHEM and an EM2 component, a model originally proposed by Farley et al. [23]. Such a model is consistent with the trace element melting/mixing model proposed above, which suggests that the Ofu melt inclusions sample only a high $^{3}He/^{4}He$ PHEM mantle reservoir and the Vailulu'u and Malumalu melt inclusions result from mixing melts from both the PHEM and EM2 mantle reservoirs.

Previous work on the Pb-isotopic variability in melt inclusions [17] suggested that the unradiogenic endmember in EM2 basalts from Tahaa may be depleted (MORB or FOZO?), and thus lie at even lower $^{87}Sr/^{86}Sr$ values than observed in the high $^{3}He/^{4}He$ PHEM lavas from Ofu (Fig. 3). In fact, an extrapolation of the Samoa melt inclusion and whole-rock basalt array in Fig. 3 does indeed trend toward one of two depleted components that are significantly less radiogenic than PHEM: MORB [22] or a common high $^{3}He/^{4}He$ mantle component, called FOZO [24] (Fig. 3). The FOZO component is represented by basalts with the highest $^{3}He/^{4}He$ from Hawaii [37], Iceland [38] and Baffin Island [39]. Both MORB and FOZO lie on a similar extension of the Samoa melt inclusion $^{87}Sr/^{86}Sr$–Rb/Sr array, so it is difficult to distinguish which, if either, of these two components is sampled by the Samoan melt inclusions. If the depleted component is MORB, it may be entrained in melt inclusions by shallow anatexis due to preferential cooling and olivine crystallization near magma chamber and conduit walls [7,8,21]. However, the presence of FOZO (or any other high $^{3}He/^{4}He$ component) in the Samoan melt inclusions would require that the isotopic variability in melt inclusions reflect true source heterogeneity, assuming that a high $^{3}He/^{4}He$ component does not exist in the oceanic crust or lithosphere.

4.3. The case against MORB

It may be possible to look at other lines of geochemical evidence to discern whether MORB or FOZO play a role in augmenting the isotopic diversity in Samoan melt inclusions. Models suggesting that melt inclusion isotopic variability is caused only by contamination from unradiogenic oceanic crust and lithosphere at shallow levels do not explain how several Samoan melt inclusions have higher $^{87}Sr/^{86}Sr$ ratios than their host

bulk rock compositions (see Fig. 1). For example, Samoan whole-rock basalt sample 71-11 hosts several melt inclusions that have $^{87}Sr/^{86}Sr$ ratios (up to 0.70692) that are significantly more enriched than its host rock (0.70550). The presence of $^{87}Sr/^{86}Sr$ ratios in melt inclusions that are higher than the bulk rock require that at least some of the isotopic variability present in melt inclusions is derived from the mantle source, because the enriched component in melt inclusion 71-11a is too enriched to be found in the oceanic crust and lithosphere. Therefore, if assimilation of oceanic crust and lithosphere contributes heterogeneity to the Samoan melt inclusions, it cannot be the only means by which isotopic heterogeneity is produced in Samoan melt inclusions, and some contribution from the melt source must be involved as well.

On a different tack, the case for the less radiogenic melt inclusions sampling the depleted oceanic crust and lithosphere by assimilation is limited severely by the observation that, within analytical uncertainty, not a single melt inclusion has an $^{87}Sr/^{86}Sr$ ratio that is lower than the least radiogenic ($^{87}Sr/^{86}Sr=0.7044$) whole-rock basalt measured in the Samoan islands (Fig. 1). The Samoan melt inclusions trace out a range of Sr-isotope variability that is confined to the region of Sr-isotope space defined by the Samoan whole-rock data (Fig. 3). On an island-by-island basis, the interpretation is more complicated, as melt inclusions from two Vailulu'u whole-rocks sample a component more depleted than found in whole rocks measured from the seamount. However, the least radiogenic component found in Vailulu'u melt inclusions is also found in lavas from nearby Samoan islands (e.g., Ta'u and Ofu), exhibits elevated $^{3}He/^{4}He$ ratios, and is thus known to exist in the Samoan plume. Many of the downstream Samoan seamounts also are dominated by $^{87}Sr/^{86}Sr$ between 0.7044 and 0.7049 [3]. It seems unnecessary, therefore, to invoke contamination from the oceanic crust and lithosphere to explain the presence of the less radiogenic component when it already exists inside the plume! Although the argument can be made that an insufficient number of melt inclusions have been analyzed to detect a component more depleted than what is found in whole rocks, the number of melt inclusions analyzed for Sr isotopes ($n=41$) is already significant, and is equal to ~30% of the number of published $^{87}Sr/^{86}Sr$ whole-rock analyses from the Samoan hotspot.

The high $^{3}He/^{4}He$, unradiogenic Sr component in Samoan basalts (PHEM) is unique in that it exhibits $^{87}Sr/^{86}Sr$ ratios more enriched than in the high $^{3}He/^{4}He$ Hawaii, Iceland or Baffin Island basalts, suggesting that the high $^{3}He/^{4}He$ reservoir in the mantle is at least mildly heterogeneous in $^{87}Sr/^{86}Sr$ ratios. The same line of reasoning that precludes the presence of entrained melts from oceanic lithosphere in the Samoan melt inclusions also minimizes the possibility that a traditional, depleted FOZO-like component ($^{87}Sr/^{86}Sr=0.7030$ [24]) serves as the unradiogenic Sr component: If melt inclusion diversity were a result of entrainment of a component (MORB or FOZO) more depleted than found in Samoan basalts, then the melt inclusions would extend to $^{87}Sr/^{86}Sr$ ratios lower than found in whole rocks (0.7044). However, the high $^{3}He/^{4}He$ Samoan sample OFU-04-06 defines the lowest $^{87}Sr/^{86}Sr$ portion of the Samoan whole-rock mixing array (see Fig. 3) and the melt inclusions are identical to the whole rock, suggesting that the least radiogenic Sr composition sampled by the Ofu basalts is the same component found in the melt inclusions. Therefore, we maintain that the unradiogenic Sr component in Samoan melt inclusions is more enriched than MORB or FOZO, and is likely the same PHEM component sampled by the high $^{3}He/^{4}He$ Samoan basalts, suggesting that a two-component EM2–PHEM mixing model may be the most appropriate for melt inclusions originating in the enriched Samoan mantle. Scatter around such a mixing model (Fig. 8) may be due to minor contributions from other components [4] that may exist in the Samoan mantle.

4.4. Implications for source heterogeneity (or lack thereof)

The results for Sr-isotope measurements in Samoan melt inclusions support an argument for an origin of the isotopic variability in the melt source, not contamination by oceanic crust and lithosphere. We assume that the isotopic variability (or lack thereof) in Samoan melt inclusions is not a product of variable degrees of homogenization in magma conduits and chambers before olivine entrapment, but rather that the isotopic variability in melt inclusions reflects the heterogeneity of the melt source: When the melt source is heterogeneous, melt inclusions capture the range of heterogeneity while the isotopic composition of the bulk rock lava represents an average of the heterogeneity sampled in the melt. By extension, we infer that the high $^{3}He/^{4}He$ whole-rock sample OFU-04-06 tends to sample a more homogeneous source, as the melt inclusions are nearly isotopically homogeneous and identical to the bulk rock. Perhaps, then, only melting of a pure PHEM source allows the high $^{3}He/^{4}He$ composition to persist in the

Ofu whole-rock lavas. Vailulu'u and Malumalu melt inclusions are more isotopically heterogeneous, and thus are inferred to sample a heterogeneous source that captures much of the mixing spectrum between the EM2 and PHEM components. The contribution of an EM2 component may explain the diminished $^{3}He/^{4}He$ composition in the lavas from these two volcanoes. Although $^{87}Sr/^{86}Sr$ analyses of the melt inclusions from high $^{3}He/^{4}He$ basalts from other localities are not yet available, perhaps the high $^{3}He/^{4}He$ mantle that these basalts sample is homogeneous and devoid of enriched domains. This hypothesis is consistent with the melting–mixing model above (see Fig. 8), which suggests that the isotopically homogeneous melt inclusions from the high $^{3}He/^{4}He$ basalt from Ofu exhibit no evidence of mixing with an EM2 component.

It is notable that while near-pure PHEM melts are observed in Samoan melt inclusions, pure EM2 melts ($^{87}Sr/^{86}Sr=0.7128$ [4,36]) were not unequivocally detected in this study (i.e., by measurement of Sr isotopes). Several melt inclusions with ultra-enriched trace element patterns were observed, but most of the melt inclusions are composed of <30% EM2 component. Perhaps this indicates that, compared to the PHEM component, the EM2 component in the Samoan plume is rare. Alternatively, the EM2 component may not be rare in the Samoan plume, but is more refractory and produces less melt than the PHEM component. In this way, perhaps, EM2 melts are less frequently sampled by melt inclusions. Future work on melt inclusions will help resolve the relative contributions of the enriched and high $^{3}He/^{4}He$ sources to OIB lavas.

5. Summary

The following conclusions can be drawn from this study:

1.) The Sr-isotopic diversity in melt inclusions from Samoan basalts does not extend significantly above or below the range defined by whole rocks from the Samoan hotspot.
2.) A few melt inclusions exhibit $^{87}Sr/^{86}Sr$ ratios significantly higher than their host whole rock. This is taken as evidence that assimilation of MORB lithosphere cannot be the only mechanism that contributes isotopic diversity to the melt inclusions.
3.) The $^{87}Sr/^{86}Sr$ ratio of the high $^{3}He/^{4}He$ basalt is essentially indistinguishable from the Sr-isotope ratios (0.7044) measured in its melt inclusions, and the $^{87}Sr/^{86}Sr$ ratios in melt inclusions from other Samoan basalts do not exhibit ratios lower than 0.7044. This observation is consistent with the hypothesis that a high $^{3}He/^{4}He$ component, not MORB, is the unradiogenic Sr endmember in Samoan melt inclusions.
4.) Melt inclusions from a high $^{3}He/^{4}He$ Samoan basalt (with less radiogenic $^{87}Sr/^{86}Sr$) are isotopically more homogeneous than the melt inclusions from basalts with higher $^{87}Sr/^{86}Sr$ (more contribution from an EM2 component). This may indicate that the Samoan high $^{3}He/^{4}He$ basalts sample a source that is more isotopically homogeneous than the source that produces basalts with an EM2 component.

Acknowledgements

We thank Lary Ball for his generous analytical wizardry with the NEPTUNE. J. Blusztajn and R. Workman helped document the Sr-isotope basalt glass standards. We also thank N. Shimizu, A. Saal, M. Kurz, J. Wang, A. Koleszar and C. Waters for discussions. Simon Thorrold loaned us his sclerosponge standards, and helped with many technical discussions arising from his unparallel laser ablation Sr isotope work on carbonates. Frank Ramos provided a preprint of his paper, and numerous insightful discussions. Reviews from Vincent Salters and an anonymous reviewer greatly improved the manuscript. An NSF Graduate Research Fellowship is gratefully acknowledged (to MGJ). This research was supported by NSF grant EAR-0125917 (to SRH).

Appendix A. Supplementary data

Supplementary data associated with this article can be found, in the online version, at doi:10.1016/j.epsl.2006.02.040.

References

[1] A. Zindler, S.R. Hart, Chemical geodynamics, Annu. Rev. Earth Planet. Sci. 14 (1986) 493–571.
[2] A.W. Hofmann, Mantle geochemistry: the message from oceanic volcanism, Nature 385 (1997) 219–229.
[3] S.R. Hart, M. Coetzee, R.K. Workman, J. Blusztajn, K.T.M. Johnson, J.M. Sinton, B. Steinberger, J.W. Hawkins, Genesis of the Western Samoa seamount province: age, geochemical fingerprint and tectonics, Earth Planet. Sci. Lett. 227 (2004) 37–56.
[4] R.K. Workman, S.R. Hart, M. Jackson, M. Regelous, K.A. Farley, J. Blusztajn, M. Kurz, H. Staudigel, Recycled metasomatized lithosphere as the origin of the Enriched Mantle II (EM2) endmember: evidence from the Samoan volcanic chain, Geochem. Geophys. Geosyst. 5 (2004), doi:10.1029/2003GC000623.

[5] W.J. Morgan, Convection plumes in the lower mantle, Nature 230 (1971) 42–43.
[6] R.K. Workman, E. Hauri, S.R. Hart, J. Wang, J. Blusztajn, Volatile and trace elements in basaltic glasses from Samoa: implications for water distribution in the mantle, Earth Planet. Sci. Lett. 24 (2006) 932–951.
[7] L.V. Danyushevsky, M.R. Perfit, S.M. Eggins, T.J. Falloon, Crustal origin for coupled 'ultra-depleted' and 'plagioclase' signatures in MORB olivine-hosted melt inclusions: evidence from the Siquieros Transform Fault, East Pacific Rise, Contrib. Mineral. Petrol 144 (2003) 619–637.
[8] L.V. Danyushevsky, R.A.J. Leslie, A.J. Crawford, P. Durance, Melt inclusions in primitive olivine phenocrysts: the role of localized reaction processes in the origin of anomalous compositions, J. Pet. 45 (2004) 2531–2553.
[9] A.V. Sobolev, N. Shimizu, Ultra-depleted primary melt included in an olivine from the Mid-Atlantic Ridge, Nature 363 (1993) 151–154.
[10] A.A. Gurenko, M. Chaussidon, Enriched and depleted primitive melts included in olivine from Icelandic tholeiites: origin by continuous melting of a single mantle column, Geochim. Cosmochim. Acta 59 (1995) 2905–2917.
[11] J.C. Lassiter, E.H. Hauri, I.K. Nikogosian, H.G. Barsczus, Chlorine–potassium variations in melt inclusions from Raivavae and Rapa, Austral Islands: constraints on chlorine recycling in the mantle and evidence for brine-induced melting of oceanic crust, Earth Planet. Sci. Lett. 202 (2002) 525–540.
[12] E. Cottrell, M. Spiegelman, C.H. Langmuir, Consequences of diffusive reequilibration for the interpretation of melt inclusions, Geochem. Geophys. Geosyst. 3 (2002), doi:10.1029/2001GC000205.
[13] G.A. Gaetani, E.B. Watson, Modeling the major-element evolution of olivine-hosted melt inclusions, Chem. Geol. 183 (2002) 25–41.
[14] G.A. Gaetani, E.B. Watson, Open system behavior of olivine-hosted melt inclusions, Earth Planet. Sci. Lett. 183 (2000) 27–41.
[15] P. Schiano, R. Clocchiatti, Worldwide occurrence of silica-rich melts in sub-continental and sub-oceanic mantle minerals, Nature 368 (1994) 621–624.
[16] V. Kamenetsky, Methodology for the study of melt inclusions in Cr-spinel, and implications for parental melts of MORB from FAMOUS area, Earth Planet. Sci. Lett. 142 (1996) 477–484.
[17] A.E. Saal, S.R. Hart, N. Shimizu, E.H. Hauri, G.D. Layne, Pb isotopic variability in melt inclusions from oceanic island basalts, Polynesia, Science 282 (1998) 1481–1484.
[18] K. Kobayashi, R. Tanaka, T. Moriguti, K. Shimizu, E. Nakamura, Lithium, boron, and lead isotope systematics of glass inclusions in olivines from Hawaiian lavas: evidence for recycled components in the Hawaiian plume, Chem. Geol. 212 (2004) 143–161.
[19] H. Yurimoto, T. Kogiso, K. Abea, H.G. Barsczus, A. Utsunomiya, S. Maruyama, Lead isotopic compositions in olivine-hosted melt inclusions from HIMU basalts and possible link to sulfide components, Phys. Earth Planet. Inter. 146 (2004) 231–242.
[20] K.P. Jochum, B. Stoll, A.W. Hofmann, Pb isotopes and trace elements in melt inclusions from Hawaiian basalts using LA-ICPMS and SRXRF, Geochim. Cosmochim. Acta 68 (Sup.1) (2004) A564.
[21] A.E. Saal, S.R. Hart, N. Shimizu, E.H. Hauri, G.D. Layne, J.M. Eiler, Pb isotopic variability in melt inclusions from the EMI–EMII–HIMU mantle end-members and the role of the oceanic lithosphere, Earth Planet. Sci. Lett. 240 (2005) 605–620.
[22] Y. Su, C.H. Langmuir, Global MORB chemistry compilation at the segment scale, Ph.D. Thesis, Department of Earth and Environmental Sciences, Columbia University (2003). Available at: http://petdb.ldeo.columbia.edu/documentation/morbcompilation/.
[23] K.A. Farley, J.H. Natland, H. Craig, Binary mixing of enriched and undegassed (primitive?) components (He, Sr, Nd, Pb) in Samoan lavas, Earth Planet. Sci. Lett. 111 (1992) 183–199.
[24] S.R. Hart, E.H. Hauri, L.A. Oschmann, J.A. Whitehead, Mantle plumes and entrainment—isotopic evidence, Science 256 (1992) 517–520.
[25] M.G. Jackson, M.D. Kurz, S.R. Hart, R. Workman, Implications of new high $^{3}He/^{4}He$ values from the Samoan hotspot, Abstr. EOS Tran. AGU, 86, Fall Meet. Suppl., 2005, pp. V41D–V1485.
[26] F.C. Ramos, J.A. Wolff, D.L. Tollstrup, Measuring $^{87}Sr/^{86}Sr$ variations in minerals and groundmass from basalts using LA-MC-ICPMS, Chem. Geol. 211 (2004) 135–158.
[27] N. Shimizu, C.J. Allegre, Geochemistry of transition elements in garnet lherzolite nodules in kimberlites, Contrib. Mineral. Petrol. 67 (1978) 41–50.
[28] N. Shimizu, A.P. Le Roex, The chemical zoning of augite phenocrysts in alkaline basalts from Gough Island, South Atlantic, J. Volcanol. Geotherm. Res. 29 (1978) 149–199.
[29] P.L. Roeder, R.F. Emslie, Olivine-liquid equilibrium, Contrib. Mineral. Petrol. 29 (1970) 275–289.
[30] W.F. McDonough, S.S. Sun, The composition of the Earth, Chem. Geol. 120 (1995) 223–253.
[31] N. Shimizu, The geochemistry of olivine-hosted melt inclusions in a FAMOUS basalt ALV519-4-1, Phys. Earth Planet. Inter. 107 (1998) 183–201.
[32] H.J.B. Dick, R.L. Fisher, W.B. Bryan, Mineralogic variability of the uppermost mantle along the mid-ocean ridges, Earth Planet. Sci. Lett. 69 (1984) 88–106.
[33] P.B. Kelemen, G.M. Yogodzinski, D.W. Scholl, Along-strike variation in lavas of the Aleutian island arc: implications for the genesis of high Mg# andesite and the continental crust, in: J. Eiler (Ed.), Inside the Subduction Factory, AGU Monograph, vol. 138, AGU, 2004, pp. 223–276.
[34] E. Takazawa, F. Frey, N. Shimizu, M. Obata, Evolution of the Horoman peridotite (Hokkaido, Japan): implications from pyroxenite compositions, Chem. Geol. 134 (1996) 3–26.
[35] R.K. Workman, S.R. Hart, Major and trace element composition of the depleted MORB mantle (DMM), Earth Planet. Sci. Lett. 231 (2005) 53–72.
[36] E.H. Hauri, N. Shimizu, J. Dieu, S.R. Hart, Evidence for hotspot-related carbonatite metasomatism in the oceanic upper mantle, Nature 365 (1993) 221–227.
[37] M.D. Kurz, W.J. Jenkins, S.R. Hart, D. Clague, Helium isotopic variations in volcanic rocks from Loihi seamount and the Islands of Hawaii, Earth Planet. Sci. Lett. 66 (1983) 388–406.
[38] D.R. Hilton, K. Grönvold, C.G. Macpherson, P.R. Castillo, Extreme $^{3}He/^{4}He$ ratios in northwest Iceland: constraining the common component in mantle plumes, Earth Planet. Sci. Lett. 173 (1999) 53–60.
[39] F.M. Stuart, S. Lass-Evans, J.G. Fitton, R.M. Ellam, High $^{3}He/^{4}He$ ratios in picritic basalts from Baffin Island and the role of a mixed reservoir in mantle plumes, Nature 424 (2003) 57–59.
[40] P.J. Valbracht, T. Staudacher, A. Malahoff, C.J. Allegre, Noble gas systematics of deep rift zone glasses from Loihi Seamount, Hawaii, Earth Planet. Sci. Lett. 150 (1997) 399–411.
[41] S. Lass-Evans, The anatomy of the ancestral Iceland plume: a chemical and isotopic study of the Tertiary basalts and picrites from Baffin Island, Ph.D. Thesis, School of GeoSciences, University of Edinburgh (2005).

Appendix A. Supplementary data (as it appears, published, on the Elsevier website)

Background Datasets Text,Figs&Tables
Click here to download Background Datasets: SuppDataFigsTables.pdf

Supplementary Data (Jackson and Hart, 2006)

Sr isotopes by laser ablation PIMMS: Application to Samoan basaltic melt inclusions

1. Introduction

We have thoroughly, but not exhaustively, investigated the parameters necessary for precise and accurate Sr isotope analysis of basalt glasses by *in situ* laser ablation PIMMS. The lower limit of external precision attained under optimal conditions for the SRM987 Sr solution standard is ± 5 ppm (>25 volt data, 1σ), and is fairly comparable to good TIMS data. For lower intensity data (~ 1-5 volts), more comparable to our typical laser ablation work, the external solution precision is in the 20-80 ppm range. We have instituted a new method for Kr correction that is based on ^{84}Kr, and a method for Rb correction that utilizes basalt glass standards with significant Rb/Sr ratios and known ^{87}Sr/^{86}Sr ratios. Even in basalts requiring very large Rb corrections, we are able to obtain ^{87}Sr/^{86}Sr data with ~320 ppm external precision and 45 ppm internal (in-run) precision (2σ standard deviation) on a suite of Samoan glasses with known ^{87}Sr/^{86}Sr ratios.

We developed an analytical protocol for the measurement of Sr isotope ratios by Laser Ablation PIMMS for analysis of melt inclusions in olivine phenocrysts in OIBs (ocean island basalts) from the EM2 (Samoa), EM1 (Pitcairn, Christmas) and HIMU (Mangaia) mantle end-members. We acknowledge a significant existing body of work on Sr isotope measurement by laser ablation PIMMS, but will not attempt to review this literature or compare it with the protocols we have installed on the NEPTUNE at the Woods Hole Oceanographic Institution [1-6].

2. Techniques

2.1. Instrumental Description

The data discussed here were obtained with a ThermoFinnigan NEPTUNE multicollector ICP-MS, coupled to a NEW Wave UP213 laser, housed in the Plasma Facility at the Woods Hole Oceanographic Institution. This NEPTUNE was installed in June 2003, replacing an earlier one that had been installed in February 2002, but damaged by the October 2002 fire in the Ion Probe Facility.

The typical operating parameters of the NEPTUNE and laser are given in Table 1 (note that our techniques have evolved over time, and some earlier data may have utilized somewhat different protocols). Currently, we aspirate clean dilute (5%) nitric acid during the lasering, to allow solution standards to be interspersed with laser runs when needed. The arrangement of Faraday cups, and the relevant isotopic masses that are collected, is given in Table 2. Amplifiers are not rotated, as this rotates the Faraday (off-mass) baselines as well. The mean raw Faraday intensities are transferred after all analyses to an offline data reduction program (TweaKr), for the various corrections.

We have opted to run the laser at 100% power and in apertured mode. While we could likely emplace higher energy density in focused mode, this tends to throw off larger chips and particles, particularly from basalt glass samples. We have not made any

investigations of the effects of particle size on mass bias, interferences, and the like. Each analysis takes about 6.5 minutes of lasering, including offpeak baseline integration for 64 seconds and 20 cycles of 16 second integrations (and, more recently, 40 cycles of 8 second integrations). With a 120 μm spot and 200 μm long raster lines (see Table 1), spaced at only 20 μm, the final ablation pit is pyramidal, approximately 300 x 300 μm, and 250 μm deep. Typically, there will be little or no drift of ^{88}Sr intensity with time during ablation of homogeneous basalt glass standards, and the 1σ standard deviation of intensity will fall in the range 5-15%.

2.2. Standards and Canonical Isotope Abundances

For Rb and Sr isotope standards, we have used NIST standards SRM984 and SRM987. The certified values for these standards are listed in Table 3, along with the quoted uncertainties. Note that $^{85}Rb/^{87}Rb$ in SRM 984 is only certified to ± 423 ppm, $^{87}Sr/^{86}Sr$ and $^{88}Sr/^{86}Sr$ to only 380 ppm, and $^{84}Sr/^{86}Sr$ to 0.25%. It is likely that the uncertainties in $^{87}Sr/^{86}Sr$ and $^{88}Sr/^{86}Sr$ are not independent, but possibly related by some fractionation-dependence. Note also that the certified $^{86}Sr/^{88}Sr$ value is 0.1193515, not the consent value of 0.119400 adopted by the community. We have corrected all of the SRM 987 certificate ratios, by exponential law, to be consistent with the consent value of 0.1194. Ironically, this results in a "corrected" $^{87}Sr/^{86}Sr$ ratio of 0.7101938, which is lower than (but marginally within errors of) the value commonly adopted by the community of 0.710240 (which is itself different from the "uncorrected" certificate value of 0.710339). It will obviously be important for published papers to be very clear as to their usage of SRM 987 standard values. For Kr, we adopt the isotope abundances compiled by Ozima and Podosek (2001).

2.3. Backgrounds and Baselines

The NEPTUNE software allows a choice of baseline protocols. PIMMS users frequently use "on-peak" baselines, after sample wash-out [1, 3-6]; the NEPTUNE also allows a "defocused" beam baseline. Our experience is that baselines can be measurably (> 50 μV) elevated across a broad mass region during actual sample analysis and thus different from those measured in a defocused "beam-off" state, or while running gas or acid blanks. We have chosen therefore to adopt the common TIMS procedure of running "off-peak" baselines while sample analysis is underway; while this consumes part of the sample, we see no other way to ensure reliability of baselines. (However, baselines on Samoan basalt standards and basaltic melt inclusions do not change significantly over the course of an analytical session, and we have adopted the practice of applying baselines from larger melt inclusions—run during the same analytical session—to exceptionally small melt inclusions to save precious material). We have chosen to measure baselines at a position 0.70 amu below each mass; this avoids potential baseline interferences from doubly-charged half-mass REE peaks, allows the Faradays that are intentionally set at 83.5 and 85.5 in order to monitor these REE^{+2} to offset 0.2 amu below mass 83 and 85 during baseline measurement, and places the ^{88}Sr cup near the minimum in the valley between ^{87}Sr and ^{88}Sr during baseline measurement. With this protocol, the only baseline that will have a significant tail contribution is ^{87}Sr. With the measured abundance sensitivity at Sr mass of ~ 1ppm at 1 amu, the $^{87}Sr/^{86}Sr$ ratio will be elevated by < 12

ppm; this error is small compared to our external precision goal, and will also be normalized, to first order, through the use of the SRM987 standard.

2.4. Kr Correction

As is well known, there are interferences at ^{84}Sr and ^{86}Sr masses from Kr. Conventionally, the Kr is considered to be a contaminant in the Ar plasma gas, and is corrected by measurement of ^{82}Kr or ^{83}Kr. Over the past two years of measurement ~~here~~, our ^{83}Kr intensity has varied from ~ 0.05 mV to ~ 20 mV, and we believe that not all of it comes in with the argon, nor is all of mass 83 actually Kr. Typically, after changing samples in the laser cell, there is a component of air Kr which slowly decreases as the chamber is purged. Ultimately, the Kr intensity with He flowing from the cell into the machine will decrease substantially below that in aspirated solutions (because the He has less Kr than the argon). It appears to us that there is a component of atmospheric Kr dissolved in aspirated solutions and this contributes to the Kr background. This could be possibly moderated by hermetically isolating the solutions from the atmosphere. Air entrainment by the plasma at the torch is also probable, but has proven difficult to constrain.

We have typically measured both ^{82}Kr and ^{83}Kr during all Sr analyses. Deviations of up to a factor of two from the canonical $^{83}Kr/^{82}Kr$ ratio of ~ 1 are very common in laser runs, with values most often above one, but also frequently below one (Fig. 1). Even solution runs on the 987 standard will frequently show 10-20% deviations from a ratio of 1, typically with the ratios being too low (interferences on mass 82). Clearly there exist isobaric interferences that seriously hamper efforts to use either of these masses to correct for Kr. We have adopted an alternative scheme which basically uses the most abundant Kr isotope at mass 84 (~57%) to make the Kr correction on mass 86. This mass has a Sr "interference" on it, but for ^{88}Sr intensities in the 1-2 volt range, the Kr makes up 35-75% of the mass 84 peak (i.e. the Kr and Sr are approximately equal in intensity). By "subtracting" Kr until the $^{84}Sr/^{88}Sr$ ratio equals the canonical value of 0.00675476 (while iterating the mass-bias correction), this allows a robust correction to be made on mass 86 (there is a large error demagnification in this process, due to the fact that $^{86}Kr/^{84}Kr$ is ~ 0.30, while the $^{86}Sr/^{84}Sr$ ratio is ~ 17.7). Obviously, this technique relies on the absence of any other significant isobaric interferences at mass 84; in any event, these are likely to be less fatal than those at mass 83, because of the $^{84}Kr/^{83}Kr$ ratio of ~ 5. One indication that this calculation method is helpful is the observation that the external precision of samples and standards run at low-intensity (1-2 volts on mass 88) is typically improved by 30-50%, compared to the same data corrected with ^{83}Kr. Further discussion of isobaric interference issues may be found in section II*F*, below.

We are able to correct for Kr interferences so that elevated Kr/Sr ratios do not noticeably diminish the precision or accuracy of glass analysis while using our protocol, provided that the ^{88}Sr intensity is > 1 V and $^{82}Kr/^{88}Sr$ is < 0.004 (Table 4). At exceptionally high Kr/Sr ratios, there may be a tendency for measurement precision to degrade. Therefore, analyses of unknowns that exhibit high Kr/Sr ratios ($^{82}Kr/^{88}Sr$ > 0.004) are discarded.

Uncertainty in the isotopic ratios of Kr used in our correction scheme does not significantly contribute to diminishing the accuracy of $^{87}Sr/^{86}Sr$ analyses by laser ablation. At elevated Kr/Sr ($^{82}Kr/^{88}Sr$ = 0.004) —where such uncertainties will play the

largest role in affecting the final Kr-corrected $^{87}Sr/^{86}Sr$ ratio—a 1% uncertainty in any or all of the Kr-isotope ratios will change the final corrected $^{87}Sr/^{86}Sr$ ratio by <15 ppm. Additionally, allowing the Kr-isotope ratios to fractionate by up to 2% (before or during entry into the plasma) changes the $^{87}Sr/^{86}Sr$ by <15 ppm.

2.5. Rb Correction

The analysis of basaltic melt inclusions typically involves samples in which 20-50% of intensity on mass 87 is due to Rb, and large Rb corrections are required. Our goal was to devise a protocol where the Rb-corrected $^{87}Sr/^{86}Sr$ ratios are accurate to within a few hundred ppm. We adopted the strategy of using natural basalt glasses (Table 5) with precisely known $^{87}Sr/^{86}Sr$ ratios (obtained by TIMS) to bracket the basalt glass unknowns; for each "standard" glass, the $^{85}Rb/^{87}Rb$ ratio required to give the TIMS $^{87}Sr/^{86}Sr$ is calculated, and these bracketing $^{85}Rb/^{87}Rb$ ratios are then used for the Rb corrections in the unknown glasses. This method depends only on the Rb mass bias being relatively invariant on short time scales (20 minutes), and not being a function of the particular major element composition of the various glasses analyzed.

To assess these issues, we performed laser ablation analyses of a suite of 14 Samoan basalt glasses of known $^{87}Sr/^{86}Sr$, with significant variability in major and trace element composition. The results of nine one-day analysis campaigns are shown in Fig. 2; interspersed with these laser ablation analyses during the first two days were a series of runs on mixed 984-987 Rb-Sr solutions. While the total variability of the "Required $^{85}Rb/^{87}Rb$" (basically the variability of the Rb mass bias factor) is substantial (2317 ppm, excluding the 987-984 Rb-Sr solution runs), the variation with time is relatively smooth, such that the bracketing technique will be fairly effective (note that the error on ^{87}Sr due to the Rb effect is de-magnified by a factor of ~2.59 due to the $^{85}Rb/^{87}Rb$ ratio).

Several things may be noted. First, the "empirically" determined Rb ratio in lasered basalts has an average value of 2.58745, which is some 2100 ppm lower than the canonical value certified for the SRM984 Rb standard (the stated uncertainty in SRM984 is ± 770 ppm). Whether this reflects the existence of natural isotope variations in Rb, or simply an underestimate of the SRM certified value is unclear. If the former, then it will perhaps be important to use basalt glass standards that are petrogenetically related the unknowns. Secondly, there is a clear tendency for the Rb-Sr solution runs to lie at the high side of the data series, averaging 2.5900 (1200 ppm lower than the canonical value for the SRM984 Rb standard). This would suggest a slight difference in Rb mass bias for solution runs versus laser ablation runs (and this would not be surprising, given the much larger plasma loading from the laser runs).

To assess the overall accuracy of this correction scheme, we have "corrected" each run in two ways: first, using the contiguous bracketing runs, and secondly, correcting each run with the global average "required" $^{85}Rb/^{87}Rb$ ratio of 2.58745. The resulting "corrected" $^{87}Sr/^{86}Sr$ ratios are then compared with the known values (note that the internal precision of the solution runs averaged about ± 10 ppm (1σ, standard error); that of the laser runs averaged ±17 ppm, with 88 intensities ranging from 1-12 volts). For the "bracketing technique", the mean deviation (measured against TIMS) for the nine analytical sessions is 127 ppm (320 ppm, 2σ standard deviation, assuming a Gaussian distribution); for the "global average" technique, the mean deviation is 155 ppm (Fig. 3). We adopt the first scheme to correct unknowns and when discussing the accuracy of

standard glass (and melt inclusion) runs; this technique has the advantage of capturing the downward drift of the $^{85}Rb/^{87}Rb$ required values over time (see Fig. 2). While obviously not as precise as TIMS analyses, this level of reproducibility is excellent for an *in situ* technique, and will allow us to embark on a realistic program of melt-inclusion analysis.

Due to the uncertainty of the $^{85}Rb/^{87}Rb$ required value, there will be an error magnification on the corrected $^{87}Sr/^{86}Sr$ ratios of basaltic unknowns as Rb/Sr increases. In order to model this effect, we selected several glass standard runs with different Rb/Sr ratios and similar, low Kr/Sr ratios, and varied the $^{85}Rb/^{87}Rb$ ratio by 2 standard deviations about the mean global value of 2.58745 (±0.00278, 2σ standard deviation). The propagated error increases linearly to 630 ppm when Rb/Sr is 0.14, and the accuracy appears to scale with the Rb/Sr such that the uncertainty in $^{85}Rb/^{87}Rb$ magnifies the error on the final $^{87}Sr/^{86}Sr$ (Fig. 4). However, the "bracketing method" for the Rb correction reduces the uncertainty in the $^{85}Rb/^{87}Rb$ required value by ~20%, so that the propagated error from the reduced uncertainty translates to an improvement in the accuracy of the $^{87}Sr/^{86}Sr$ r (i.e., to 505 ppm when Rb/Sr is 0.14). The internal precision for $^{87}Sr/^{86}Sr$ measurements on lasered glasses is generally an order of magnitude better than the accuracy (this is also true for the Rb/Sr measurements), and does not appear to worsen with increasing Rb/Sr ratios. However, the internal precision of the $^{87}Sr/^{86}Sr$, but not the accuracy, does vary with Sr intensities (Fig. 5), and, to a lesser extent, the number and length (8 or 16 second integrations) of cycles of analysis. The precision on the melt inclusion analyses also varies as a function of Sr intensity and the number and length of cycles. However, because the accuracy of the $^{87}Sr/^{86}Sr$ of Samoan glasses is not related to Sr intensity over the range of 1-12 Volts on mass 88 (Table 4), somewhat lower Sr intensities during the melt inclusion runs (1-6.5 Volts) should not affect the overall accuracy of $^{87}Sr/^{86}Sr$.

2.6. Other Interferences

We have directly measured possible isobaric mass interferences resulting from Ca dimers and argides, FeO_2, doubly-charged Er and Yb and KrH. The Ca dimers and argides invoke errors of less than <10 ppm, for Ca/Sr ratios typical of alkali basalts; there is no straightforward way to monitor or correct for these. Similarly, in a typical basalt laser run (with 500 ppm Sr), the total propagated error in $^{87}Sr/^{86}Sr$ from FeO_2 will then be less than 40 ppm (and could be nil). Additionally, the REE^{++} invoke errors of <30 ppm for typical Sr/REE ratios in alkali basalts; these can in principal be corrected for by monitoring the 83.5 and 85.5 half-mass peaks due to $^{167}Er^{++}$ and $^{171}Yb^{++}$. Finally, there seems to be some evidence for the formation of KrH in the plasma, with Kr/KrH exhibiting ratios from 35-70. Kr hydrides create isobaric interferences on masses 83, 84, 85 and 87, and they may play an important role when Kr/Sr ratios are elevated. In practice, however, it appears that there are frequently other unexplained interferences at these masses, as well as at the Kr and Rb masses, so that correction for these isobaric interferences is not always successful. These problems not only limit the attainable precision of laser ablation analyses, but can limit the precision of straightforward Sr solution analyses as well, even of the SRM987 standard. A continuing investigation of these issues (and a fuller discussion of interferences from Ca dimers, argides, FeO_2, KrH and doubly charged Er and Yb) is underway (Hart *et al.*, in prep).

2.7. Measurement of Rb/Sr by LA-ICP-MS

Masses 85 and 88 represent pure Rb and Sr, respectively, so that fairly precise measurement of Rb/Sr ratios can be generated. After correcting for mass fractionation during each run, Rb/Sr ratios on Samoan basalt glasses measured by laser ablation are accurate to 7% (1 mean deviation, compared to ratios obtained by XRF/ICP techniques on the same glasses), and precise (0.67%, 1 mean deviation) during multiple runs on a suite of Samoan glasses (Fig. 6). We note that this technique does not appear to work when running a "dry" plasma; Rb and Sr are strongly fractionated from each other, so that the measured Rb/Sr ratios are up to 80% higher than in the standard glass (see last 4 analyses in Table 4).

2.8. Replicability

We have not yet made a comprehensive study of reproducibility of sample analyses. We have done an analysis of a group of 50 runs on the SRM987 standard, spread over a 17 month time period, using solutions varying in concentration from 10 ppb to 600 ppb. All errors discussed here will be given at the 1σ level. Considering first the 200 and 600 ppb solutions, the average internal precision for these was 7 ppm (for ^{88}Sr intensities varying from 8-28 volts). The average external precision, calculated from the variations within a single day's analysis session, was 12 ppm (and the number of standards run during each of these sessions varied from 2-6). While the overall ratio of external to internal precision was ~1.8, there was not a significant correlation between external and internal precision on a session-to-session basis (i.e. the internal precision on individual runs is not a good guide to the expected external precision). For the daily means of 11 sessions over the 17 month time period, the average $^{87}Sr/^{86}Sr$ was 0.710255, with a 1σ standard deviation of a single analysis of 15 ppm. We should note that this time period involved a number of different baseline protocols and cup configurations, so the statistics may not be representative of our current procedures. There is one obvious conclusion, however, and that is that the precision on a daily basis is similar to the long-term precision; in other words, the variability in standard runs has almost as much "daily" scatter as it does "yearly" scatter.

Within this data set, there is a fair correlation between Sr intensity and the precision of the data; external precision for a given session is ± 5 ppm for >25 volt data, ±7-20 ppm for 9-15 volt data and ±50-80 ppm for 0.3-1 volt data. Overall, the 1σ external precision in ppm, as a function of ^{88}Sr intensity in volts, may be empirically expressed as: $\sim [80/(volts)^{0.8}]$.

3. Summary

The Finnigan NEPTUNE multi-collector ICP-MS has proven to be an excellent instrument for developing robust Sr isotope analysis protocols. Among its advantages are the stability of the Faraday-amplifier system, the ability to run with intensities up to 50 volts, and the stability of the mass bias for Sr and Rb. While the external precision of solution analyses are not yet comparable to the best TIMS techniques, the *in situ* laser ablation technique appears to be a reliable and very promising tool for the study of small scale-length isotopic heterogeneities, even in samples with a significant Rb component.

References Cited

[1] M. Bizzarro, A. Simonetti, R. K. Stevenson, and S. Kurszlaukis, In situ $^{87}Sr/^{86}Sr$ investigation of igneous apatites and carbonates using laser-ablation MC-ICP-MS, Geochim. Cosmochim. Acta, 67 (2003) 289-302.

[2] J.N. Christensen, A. N. Halliday, D. C. Lee, and C. M. Hall, In situ isotopic analysis by laser ablation, Earth Planet. Sci. Lett., 136 (1995) 79-85.

[3] J.P Davidson, F. J. Tepley, Z. Palacz and S. Meffan-Main, Magma recharge, contamination and residence times revealed by in situ laser ablation isotopic analysis of feldspar in volcanic rocks, Earth Planet. Sci. Lett., 184 (2001) 427-442.

[4] S.S. Schmidberger, Simonetti, A., and D. Francis, Small-scale Sr isotope investigation of clinopyroxenes from peridotite xenoliths by laser ablation MC-ICP-MS–Implications for mantle metasomatism, Chemical Geology, 199 (2003) 317-329.

[5] T. Waight, J. Baker and D. Peate, Sr isotope ratio measurements by double-focusing MC-ICPMS: techniques, observations and pitfalls, International Journal of Mass Spectrometry, 221 (2002) 229-244.

[6] F.C. Ramos, J. A. Wolff and D. L. Tollstrup, Measuring $^{87}Sr/^{86}Sr$ variations in minerals and groundmass from basalts using LA-MC-ICPMS, Chemical Geology, 211 (2004) 135-158.

[7] R.K. Workman, S. R. Hart, M. Jackson, M. Regelous, K. A. Farley, J. Blusztajn, M. Kurz, H. Staudigel, Recycled metasomatized lithosphere as the origin of the Enriched Mantle II (EM2) end-member: Evidence from the Samoan volcanic chain, Geochem. Geophys. Geosys. 5 (2004), doi:10.1029/2003GC000623.

Figure Captions

Fig. 1. Variation of intensity ratio of mass 82 to mass 83 over time. Series of Samoan basalt glasses analyzed by laser ablation (colored symbols) and mixed Sr-Rb standard solutions (SRM987-SRM984, black diamonds). The certificate value for $^{82}Kr/^{83}Kr$ is 1.004. We observe no relationship between mass 82/mass 83 and the precision or accuracy of $^{87}Sr/^{86}Sr$ measurement by LA-MC-ICPMS.

Fig. 2. $^{85}Rb/^{87}Rb$ ratio required to give correct $^{87}Sr/^{86}Sr$ of a series of Samoan basalt glasses (analyzed by TIMS, open diamonds) and mixed Sr-Rb standard solutions (SRM987-SRM984, filled diamonds). The certificate value for $^{85}Rb/^{87}Rb$ in SRM984 is 2.593 ± 0.002; all of the "calculated" Rb ratios are lower than the certificate value, and outside quoted error limits. Runs using a dry plasma not shown.

Fig. 3. Reproducibility of $^{87}Sr/^{86}Sr$ for 12 Samoan basalt glass standards (with known 87Sr/86Sr by TIMS) by LA-MC-ICPMS. Two data trends represent reproducibility (external precision) using the "global average" and the "bracketing" correction schemes for the isobaric interference of Rb on mass 87. The bracketing method gives better overall external precision, and is adopted as the correction scheme in the manuscript. Mixed NBS987 and NBS984 solution runs not included in the figure. The downward drift of $^{85}Rb/^{87}Rb$ (see Fig. 2) is noted in the downward drift of error using the "global average" Rb correction scheme. Error bars on symbols are internal (in-run) precision (2 mean deviations). Dashed lines mark external precision of ±320 ppm (2σ, standard deviation). Larger scatter in later runs is due to higher Rb/Sr ratios of the glass standards analyzed. Better external precision in early runs is due to smaller variation in $^{85}Rb/^{87}Rb$ over time. The glass standard runs at the beginning and the end of each analytical session are not correctible using the bracketing technique and are not plotted. However, all glass standards are correctible using the "global average" Rb correction scheme, so more data points are plotted for this latter correction scheme.

Fig. 4. Rb/Sr vs. propagated error on $^{87}Sr/^{86}Sr$ measurement due to uncertainty of the $^{85}Rb/^{87}Rb$ required value. The average $^{85}Rb/^{87}Rb$ required values (used for correcting the ^{87}Rb isobaric interference on ^{87}Sr) during all laser runs on Samoan glass standards is 2.58745 (±0.00278, 2σ), and this uncertainty generates larger errors on the final $^{87}Sr/^{86}Sr$ at higher Rb/Sr ratios. The upper model line shows the error (2σ, standard deviation) on final $^{87}Sr/^{86}Sr$ ratio when using the "global average" technique for the Rb correction (see text for description). Symbols on line represent error propagation on (from the uncertainty on the $^{85}Rb/^{87}Rb$) using actual basalt analyses by laser ablation. Alternatively, error using the "bracketing" method for the Rb correction is 20% lower, and is described by the lower line. The Rb correction contributes the vast majority of the error on the final $^{87}Sr/^{86}Sr$ in our protocol for measuring basal glasses by LA-MC-ICPMS. Therefore, we consider the lower model curve to be a good approximation of the reproducibility of our method.

Fig. 5. Relationship between intensity on mass 88 and internal precision during laser ablation analysis of Samoan glass standards. Various Neptune and laser operating conditions and variations in basalt and plasma chemistry, inclusing Rb/Sr and Kr/Sr, show little or no relationship with measurement precision. The curve models the relationship between intensity and internal precision (1 mean deviation), and is described by the following relationship: Precision = 45*($\sqrt{}$Intensity)/Intensity.

Fig. 6. Samoan glass Rb/Sr measured by LA-MC-ICPMS Neptune plotted against Rb/Sr measured by standard techniques (XRF or ICP) on powders of the same glasses. Error bars (2σ standard deviation from the mean of measured values) are shown on samples with at least 9 laser analyses. All other glasses had one or two analyses. One-to-one line is solid, and weighted least squares regression (including equation) is dashed.

Table 1. Typical NEPTUNE and Laser Operating Parameters

RF Power	1200 W
Argon cooling gas, flow rate	15L/min
Ar auxiliary gas, flow rate	0.8 L/min
He sample gas, flow rate	0.5 L/min
Interface cones	X-cones
Mass analyzer pressure	$5x10^{-9}$ mbar
Resolution mode	Low (400)
Abundance sensitivity	~ 1 ppm at -1 amu, mass 88 (RPQ off)
Detection system	Faraday cups (9)
Signal analysis set-up	8 sec or 16 sec integration/cycle, 40 or 20 cycles
Background-baseline protocol	1 min integration pre-analysis, -0.7 amu all Faradays
Nebuliser and uptake rate	Elemental Scientific, Inc., PFA 20-50 microliters per minute
Spray chamber	Elemental Scientific, Inc., Stable Introduction System (SIS)
Sensitivity, solution Sr	75 V ^{88}Sr per ppm Sr in 5% HNO_3
Sensitivity, laser Sr	~ 1 volt ^{88}Sr per 100 ppm Sr in basalt at 1 mj
Laser type	New Wave UP213, quad Nd YAG 213 nm
Carrier gas	Helium
Beam optics	Apertured mode
Spot size	120 um (60 um or less in high-Sr carbonates)
Raster pattern	200 x 200 um, 20 um line spacing, 4 um/sec
Pulse rate	20 Hz
Power setting	100% (lower for high-Sr carbonates)
Power delivered	~ 1.0-1.3 mj
Pre-ablation	same raster and spot size, 5 Hz, 45% power, 30 um/sec

Table 2. Faraday Cup Configuration Laser Ablation Sr Isotope Analysis

Cup	Mass
H4	88
H3	87
H2	86
H1	85
C	84
L1	83
L2	82.5
L3	82
L4	81.5

Centered for Sr amu; C ~ 83.913

Table 3. Adopted Isotopic Abundances.

Krypton	Isotopic Abunance
78	0.003469
80	0.02257
82	0.11523
83	0.11477
84	0.56998
86	0.17398

From Ozima and Podosek, 2001

Strontium SRM987	Isotopic Abundance**	Isotopic Abundance*
84	0.005578	0.005574
86	0.098600	0.098566
87	0.070029	0.070015
88	0.825793	0.825845

	Isotopic Ratios**	Isotopic Ratios*		
84/86	0.056573	0.056549	±2529	ppm
87/86	0.710194	0.710339	±367	ppm
88/86	8.375209	8.37861	±388	ppm
84/88	0.006755	0.006749	±2529	ppm
86/88	0.119400	0.119352	±388	ppm

*NIST Certificate Values for SRM987 with quoted uncertainties.

**Renormalized to 0.1194 using exponential law; this value has been used by community consensus for decades. The corresponding $^{87}Sr/^{86}Sr$ value adopted by most of the community is 0.71024.

Rubidium SRM984			
85	0.72168		
87	0.27832		
85/87*	2.593	±771	ppm

*NIST Certificate Values for SRM984, with quoted uncertainties.

Table 4. Corrected and normalized $^{87}Sr/^{86}Sr$ glass standard data, including Rb/Sr ratios and raw exported Neptune data (in Volts) on masses 82 to 88

Date	Glass Name[a]	Mass 82 Meas'd	Mass 83 Meas'd	Mass 84 Meas'd	Mass 85 Meas'd	Mass 86 Meas'd	Mass 87 Meas'd	Mass 88 Meas'd	$^{85}Rb/^{87}Rb$ Required[j]	Mass Bias[k]	$^{87}Sr/^{86}Sr$ Laser[c]	$^{87}Sr/^{86}Sr$ Laser[d]	$^{87}Sr/^{86}Sr$ Laser[m]	I. Prec.[e]	E. Prec.[f]	E. Prec.[l]	$^{87}Sr/^{86}Sr$ TIMS[g]	Rb/Sr Laser[d]	Rb/Sr I. Prec.[e]	Rb/Sr E. Prec.[f]	Rb/Sr XRF[g]	mass 82/88[h]	# of Cycles[i]
01/26/04	75-10	0.0019	0.0015	0.070160	0.383076	1.161550	0.981164	9.99332	2.58799	1.45	0.70451	0.70450	--	10	41	--	0.704533	0.041	1.18	8.4	0.045	0.00019	20
01/26/04	75-10	0.0019	0.0015	0.068130	0.410805	1.130253	0.970173	9.72817	2.58762	1.47	0.70452	0.70452	0.70454	11	19	12	0.704533	0.045	0.42	0.9	0.045	0.00020	20
01/26/04	75-10	0.0019	0.0015	0.066972	0.316560	0.928578	0.799522	7.99056	2.58761	1.48	0.70452	0.70452	0.70456	10	16	39	0.704533	0.042	0.97	5.4	0.045	0.00023	20
01/26/04	75-10	0.0018	0.0014	0.038589	0.210660	0.591571	0.505435	5.08531	2.58887	1.49	0.70447	0.70448	0.70450	11	97	41	0.704533	0.044	1.00	1.1	0.045	0.00035	20
01/26/04	75-10	0.0019	0.0015	0.059566	0.310559	0.979671	0.821938	8.42300	2.58865	1.48	0.70448	0.70447	0.70456	9	85	34	0.704533	0.038	3.32	12.0	0.045	0.00022	20
01/26/04	76-13	0.0017	0.0014	0.055907	0.544459	0.915110	0.871425	7.87805	2.58963	1.50	0.70620	0.70619	0.70633	13	285	89	0.706395	0.074	0.30	4.5	0.077	0.00022	20
01/26/04	76-8	0.0017	0.0014	0.054455	0.526363	0.889211	0.845639	7.65417	2.58922	1.49	0.70621	0.70621	0.70639	11	231	22	0.706374	0.073	0.16	9.8	0.081	0.00023	20
01/26/04	63-13	0.0017	0.0013	0.045648	0.441395	0.731734	0.698360	6.29660	2.58914	1.50	0.70536	0.70536	0.70547	11	226	71	0.705520	0.075	0.90	4.7	0.071	0.00028	20
01/26/04	68-3	0.0018	0.0013	0.045375	0.373755	0.727534	0.668448	6.26096	2.58796	1.50	0.70535	0.70534	0.70542	15	62	51	0.705388	0.064	0.60	7.3	0.069	0.00029	20
01/26/04	72-2	0.0019	0.0013	0.048745	0.436044	0.789158	0.737371	6.79224	2.58771	1.50	0.70537	0.70537	0.70538	19	37	16	0.705395	0.069	0.37	15.1	0.060	0.00028	20
01/26/04	73-12	0.0019	0.0013	0.045637	0.450865	0.733196	0.704204	6.30990	2.58719	1.50	0.70668	0.70667	0.70670	14	28	63	0.706653	0.076	0.58	0.1	0.076	0.00030	18
01/26/04	71-2	0.0019	0.0013	0.046247	0.412129	0.726657	0.683560	6.25381	2.58762	1.50	0.70593	0.70592	0.70597	14	27	37	0.705843	0.070	0.22	6.8	0.075	0.00030	20
01/26/04	73-1	0.0018	0.0013	0.050270	0.533292	0.818134	0.797957	7.04356	2.58866	1.51	0.70660	0.70660	0.70666	10	175	86	0.706720	0.081	0.49	0.3	0.081	0.00026	20
01/26/04	70-1	0.0016	0.0010	0.036367	0.270199	0.577103	0.519443	4.86111	2.58846	1.43	0.70530	0.70530	0.70540	14	107	41	0.705371	0.058	0.70	2.1	0.060	0.00033	20
01/26/04	71-11	0.0016	0.0010	0.036493	0.316405	0.590123	0.547012	5.07213	2.58908	1.43	0.70526	0.70526	0.70537	12	184	27	0.705394	0.067	0.27	4.7	0.070	0.00031	20
01/26/04	71-22	0.0017	0.0013	0.041431	0.362145	0.673708	0.625087	5.79313	2.58923	1.44	0.70533	0.70532	--	14	211	--	0.705473	0.067	0.55	6.1	0.071	0.00029	20
01/27/04	73-1	0.0015	0.0010	0.042357	0.501491	0.715500	0.713457	6.18177	2.58963	1.65	0.70655	0.70648	--	14	336	--	0.706720	0.086	0.54	7.0	0.081	0.00024	20
01/27/04	76-13	0.0012	0.0009	0.041502	0.427055	0.703095	0.674792	6.07676	2.58938	1.67	0.70628	0.70621	0.70641	14	259	25	0.706395	0.075	0.45	3.4	0.077	0.00020	17
01/27/04	63-13	0.0011	0.0009	0.035692	0.355703	0.599686	0.571649	5.18396	2.58951	1.69	0.70539	0.70533	0.70553	17	270	8	0.705620	0.073	1.43	1.8	0.071	0.00021	20
01/27/04	78-1	0.0011	0.0008	0.041195	0.639397	0.702572	0.761301	6.07662	2.58977	1.70	0.70862	0.70856	0.70875	16	462	185	0.708886	0.112	1.26	11.1	0.126	0.00018	20
01/27/04	75-10	0.0011	0.0008	0.042356	0.280778	0.725189	0.631281	6.27295	2.58813	1.70	0.70455	0.70449	0.70463	12	61	137	0.704533	0.047	0.41	6.1	0.045	0.00017	20
01/27/04	76-13	0.0016	0.0013	0.055752	0.552520	0.923794	0.881225	7.95726	2.58977	1.51	0.70624	0.70618	0.70632	12	304	111	0.706395	0.074	0.27	4.1	0.077	0.00020	10
01/27/04	76-13	0.0016	0.0013	0.055497	0.554683	0.920418	0.879848	7.93062	2.58968	1.53	0.70625	0.70619	0.70641	10	295	17	0.706395	0.075	0.26	3.5	0.077	0.00020	20
01/27/04	76-13	0.0016	0.0013	0.058108	0.578687	0.970494	0.925562	8.36648	2.58986	1.55	0.70624	0.70617	0.70638	11	315	24	0.706395	0.074	0.41	0.8	0.077	0.00019	20
01/27/04	76-13	0.0015	0.0013	0.049800	0.506317	0.817493	0.786891	7.04391	2.58966	1.54	0.70625	0.70618	--	12	301	--	0.706395	0.077	0.42	4.6	0.077	0.00022	20
02/13/04	71-11	0.0020	0.0020	0.052127	0.412318	0.785318	0.723659	6.73813	2.58794	1.41	0.70542	0.70535	--	13	62	--	0.705394	0.065	0.21	6.5	0.070	0.00030	20
02/13/04	78-8	0.0020	0.0019	0.049567	0.579772	0.740226	0.759702	6.35140	2.58835	1.42	0.70757	0.70750	--	13	159	--	0.707614	0.098	0.40	0.5	0.097	0.00032	20
03/26/04	70-1	0.0019	0.0016	0.046911	0.327674	0.704302	0.633370	6.06027	2.58680	1.56	0.70545	0.70541	--	17	60	--	0.705371	0.058	0.27	3.2	0.060	0.00032	20
12/09/04	75-10	0.0027	0.0026	0.062513	0.321199	0.902189	0.770682	7.75525	2.58856	1.56	0.70485	0.70458	--	9	64	--	0.704533	0.044	0.34	1.4	0.045	0.00035	49
12/09/04	75-10	0.0025	0.0025	0.062778	0.327432	0.917974	0.785039	7.90098	2.58872	1.61	0.70484	0.70457	0.70459	10	52	82	0.704533	0.044	0.17	1.5	0.045	0.00032	48
12/09/04	76-13	0.0025	0.0024	0.063843	0.557662	0.950939	0.902924	8.19690	2.58901	1.67	0.70632	0.70625	0.70629	10	203	144	0.706395	0.072	0.13	6.5	0.077	0.00030	49

12/09/04	76-13	0.0024	0.0024	0.062189	0.541662	0.926303	0.879131	7.98773	2.58901	1.69	0.70632	0.70625	0.70624	9	203	215	0.706395	0.072	0.13	6.9	0.077	0.00030	48
12/09/04	75-10	0.0021	0.0022	0.041088	0.190853	0.563339	0.478042	4.85665	2.58560	1.77	0.70469	0.70463	0.70466	16	133	175	0.704533	0.042	1.64	7.0	0.045	0.00043	50
12/09/04	75-10	0.0020	0.0019	0.044719	0.210583	0.648179	0.547229	5.59980	2.58695	1.82	0.70462	0.70456	--	12	32	--	0.704533	0.040	2.09	11.2	0.045	0.00035	50
01/10/05	76-13	0.0029	0.0032	0.062592	0.558316	0.908212	0.873053	7.83316	2.58638	1.73	0.70650	0.70649	--	12	136	--	0.706395	0.076	0.17	2.2	0.077	0.00037	37
01/10/05	76-13	0.0028	0.0031	0.062148	0.561306	0.908499	0.874702	7.83946	2.58683	1.74	0.70645	0.70645	0.70634	11	76	76	0.706395	0.076	0.19	1.8	0.077	0.00036	38
01/10/05	71-2	0.0033	0.0035	0.045848	0.326355	0.560609	0.529545	4.81303	2.58615	1.70	0.70606	0.70605	0.70601	15	158	95	0.705943	0.072	0.24	4.7	0.075	0.00069	38
01/10/05	71-2	0.0035	0.0038	0.053988	0.403808	0.691899	0.654374	5.94536	2.58697	1.69	0.70599	0.70598	0.70585	12	54	132	0.705943	0.072	0.30	4.5	0.075	0.00059	40
01/10/05	76-13	0.0036	0.0044	0.065799	0.643348	0.910299	0.907215	7.83305	2.58571	1.66	0.70658	0.70658	0.70655	13	258	223	0.706395	0.087	0.36	12.9	0.077	0.00046	40
01/10/05	71-2	0.0033	0.0034	0.031707	0.179591	0.292804	0.278502	2.49353	2.58737	1.73	0.70595	0.70595	0.70589	19	5	81	0.705943	0.076	0.51	1.2	0.075	0.00133	38
01/10/05	71-2	0.0019	0.0019	0.019831	0.129680	0.205503	0.197576	1.75832	2.58781	1.78	0.70591	0.70590	0.70600	26	56	75	0.705943	0.078	0.34	3.4	0.075	0.00106	40
01/10/05	71-2	0.0019	0.0020	0.018789	0.111868	0.176592	0.169506	1.50584	2.58933	1.77	0.70576	0.70575	0.70575	43	268	278	0.705943	0.079	0.68	4.2	0.075	0.00129	27
01/10/05	76-13	0.0021	0.0027	0.040442	0.401984	0.569223	0.567925	4.90895	2.58686	1.76	0.70646	0.70645	0.70685	19	83	360	0.706395	0.087	0.38	12.2	0.077	0.00043	40
01/10/05	76-13	0.0021	0.0026	0.027671	0.212827	0.335122	0.323659	2.87663	2.58910	1.71	0.70624	0.70623	0.70619	47	233	290	0.706395	0.078	0.98	1.5	0.077	0.00073	30
01/10/05	76-13	0.0019	0.0025	0.034968	0.346399	0.485332	0.485705	4.18601	2.58712	1.78	0.70643	0.70643	0.70663	19	44	338	0.706395	0.088	0.30	13.3	0.077	0.00046	40
01/10/05	71-2	0.0018	0.0018	0.016824	0.097919	0.154975	0.148658	1.32174	2.58951	1.82	0.70574	0.70574	--	43	291	--	0.705943	0.078	0.84	3.8	0.075	0.00133	31
01/11/05	71-2	0.0046	0.0051	0.069247	0.570788	0.881891	0.852357	7.52080	2.58694	1.29	0.70599	0.70596	--	18	26	--	0.705943	0.082	0.66	8.1	0.075	0.00061	40
01/11/05	71-2	0.0045	0.0051	0.058418	0.470999	0.717218	0.695719	6.11468	2.58698	1.33	0.70601	0.70599	0.70592	17	60	36	0.705943	0.083	0.58	9.6	0.075	0.00073	40
01/11/05	71-2	0.0040	0.0048	0.061762	0.582067	0.830511	0.822118	7.10423	2.58651	1.38	0.70607	0.70604	0.70597	16	135	39	0.705943	0.088	0.63	16.3	0.075	0.00056	40
01/11/05	76-13	0.0031	0.0035	0.042900	0.404831	0.547640	0.550584	4.68347	2.58655	1.44	0.70652	0.70649	0.70636	19	135	53	0.706395	0.092	0.65	19.6	0.077	0.00066	40
01/11/05	76-13	0.0034	0.0041	0.054000	0.586498	0.753766	0.770557	6.45857	2.58594	1.43	0.70659	0.70657	0.70643	16	245	48	0.706395	0.097	0.66	25.8	0.077	0.00052	40
01/11/05	76-13	0.0035	0.0044	0.053429	0.584683	0.737877	0.758293	6.31971	2.58591	1.42	0.70660	0.70658	0.70648	16	255	126	0.706395	0.099	0.47	28.2	0.077	0.00055	40
01/11/05	71-2	0.0046	0.0049	0.064039	0.471377	0.775869	0.736914	6.60756	2.58735	1.29	0.70597	0.70595	0.70584	17	7	149	0.705943	0.077	0.54	1.6	0.075	0.00070	40
01/11/05	76-13	0.0049	0.0053	0.064899	0.528307	0.775994	0.759615	6.60372	2.58653	1.27	0.70651	0.70649	0.70650	16	128	148	0.706395	0.086	0.60	11.3	0.077	0.00074	40
01/11/05	71-2	0.0048	0.0050	0.063217	0.452777	0.746571	0.708570	6.35639	2.58772	1.31	0.70594	0.70591	0.70589	20	43	79	0.705943	0.076	0.49	1.4	0.075	0.00075	40
01/11/05	71-2	0.0050	0.0052	0.059835	0.419486	0.671236	0.641146	5.70452	2.58771	1.29	0.70594	0.70591	0.70585	17	42	131	0.705943	0.079	0.47	4.7	0.075	0.00087	40
01/11/05	76-13	0.0052	0.0066	0.099696	1.041701	1.410914	1.417626	12.0573	2.58577	1.27	0.70661	0.70658	0.70649	10	260	135	0.706395	0.093	0.23	20.2	0.077	0.00043	40
01/11/05	76-13	0.0050	0.0065	0.096919	1.069271	1.373301	1.402463	11.7439	2.58552	1.31	0.70664	0.70662	0.70656	11	315	227	0.706395	0.098	0.46	26.6	0.077	0.00043	40
01/11/05	71-2	0.0048	0.0050	0.053745	0.351423	0.586159	0.539079	4.80269	2.58798	1.29	0.70592	0.70589	0.70584	12	78	142	0.705943	0.079	0.39	4.2	0.075	0.00101	40
01/11/05	71-2	0.0042	0.0044	0.045297	0.297450	0.470912	0.450860	4.00124	2.58832	1.40	0.70588	0.70585	0.70590	26	126	55	0.705943	0.080	0.71	5.5	0.075	0.00106	26
01/11/05	71-2	0.0042	0.0045	0.058865	0.471070	0.730507	0.706057	6.24085	2.58785	1.42	0.70593	0.70590	0.70596	15	63	22	0.705943	0.081	0.58	7.0	0.075	0.00067	40
01/11/05	71-2	0.0039	0.0044	0.054667	0.450610	0.678735	0.661178	5.79870	2.58770	1.42	0.70594	0.70591	0.70594	14	43	11	0.705943	0.083	0.24	10.2	0.075	0.00067	40
01/11/05	71-2	0.0048	0.0055	0.079954	0.671602	1.063082	1.022383	9.08473	2.58739	1.35	0.70597	0.70594	0.70601	15	1	94	0.705943	0.079	0.35	5.1	0.075	0.00053	40
01/11/05	71-2	0.0047	0.0050	0.052864	0.347356	0.566080	0.537973	4.80994	2.58846	1.35	0.70587	0.70584	--	26	141	--	0.705943	0.077	0.89	2.6	0.075	0.00098	40
08/09/05	71-2	0.0014	0.0011	0.022728	0.258610	0.388432	0.379989	3.33312	2.58724	1.28	0.70596	0.70596	--	19	23	--	0.705943	0.083	1.38	10.5	0.075	0.00041	37

09/09/05 71-2	0.0010	0.0012	0.039667	0.410998	0.676025	0.646988	5.81840	2.58823	1.44	0.70587	0.70587	0.70593	21	108	20	0.705843	0.076	0.77	0.1	0.075	0.00017	40
09/09/05 75-10	0.0010	0.0009	0.041922	0.267759	0.717313	0.618485	6.17226	2.58758	1.43	0.70453	0.70452	0.70460	13	15	96	0.704533	0.046	1.00	3.8	0.045	0.00016	40
09/09/05 71-2	0.0009	0.0009	0.034364	0.350906	0.581416	0.555389	5.00466	2.58932	1.46	0.70577	0.70577	0.70574	16	249	288	0.705843	0.075	0.42	0.7	0.075	0.00019	40
09/09/05 75-10	0.0010	0.0012	0.044398	0.305593	0.761972	0.685350	6.55471	2.58863	1.41	0.70458	0.70458	0.70468	14	67	209	0.704533	0.050	0.81	11.6	0.045	0.00015	40
09/09/05 76-13	0.0009	0.0011	0.040285	0.445631	0.686601	0.668344	5.90585	2.58878	1.41	0.70626	0.70626	0.70619	18	192	291	0.706395	0.081	0.51	4.5	0.077	0.00016	40
09/09/05 76-13	0.0011	0.0021	0.058298	0.720332	1.014084	1.011925	8.72086	2.58876	1.38	0.70647	0.70646	0.70663	16	97	331	0.706395	0.088	0.79	14.5	0.077	0.00013	40
09/09/05 71-2	0.0005	0.0005	0.017692	0.167519	0.288194	0.271203	2.45862	2.58909	1.03	0.70580	0.70580	0.70570	22	210	347	0.705843	0.074	0.79	2.2	0.075	0.00020	40
09/09/05 75-10	0.0006	0.0008	0.029739	0.191258	0.502920	0.433086	4.29411	2.58584	1.03	0.70463	0.70462	--	19	127	--	0.704533	0.048	1.71	7.8	0.045	0.00015	40
09/10/05 71-2	0.0008	0.0008	0.030262	0.298953	0.507454	0.483010	4.38372	2.58702	1.65	0.70598	0.70598	--	16	48	--	0.705843	0.072	0.63	4.0	0.075	0.00018	40
09/10/05 75-10	0.0008	0.0010	0.038555	0.249734	0.660744	0.572473	5.70962	2.58474	1.65	0.70469	0.70469	0.70462	17	217	123	0.704533	0.046	0.83	3.9	0.045	0.00015	40
09/10/05 76-13	0.0010	0.0017	0.046609	0.547945	0.808282	0.798610	6.98314	2.58548	1.63	0.70659	0.70659	0.70646	17	280	92	0.706395	0.083	0.77	8.0	0.077	0.00014	40
09/10/05 71-2	0.0008	0.0009	0.031222	0.316861	0.530073	0.506826	4.58580	2.58748	1.72	0.70594	0.70594	0.70574	22	10	290	0.705843	0.073	0.28	2.9	0.075	0.00018	40
09/10/05 75-10	0.0008	0.0009	0.038968	0.201179	0.669617	0.559369	5.78558	2.58498	1.64	0.70464	0.70464	0.70466	12	157	177	0.704533	0.037	4.72	17.4	0.045	0.00013	40
09/10/05 71-2	0.0007	0.0006	0.018731	0.177420	0.298953	0.284978	2.58205	2.58792	1.70	0.70590	0.70590	0.70570	26	67	348	0.705843	0.073	0.85	3.4	0.075	0.00029	38
09/10/05 76-13	0.0010	0.0021	0.053202	0.659724	0.930221	0.931071	8.04115	2.58547	1.65	0.70660	0.70660	--	20	295	--	0.706395	0.087	0.80	12.8	0.077	0.00013	40
09/11/05 71-2	0.0008	0.0008	0.028474	0.280326	0.481040	0.457445	4.16744	2.58755	1.80	0.70593	0.70593	--	19	19	--	0.705843	0.071	0.54	5.7	0.075	0.00019	40
09/11/05 71-2	0.0008	0.0009	0.025628	0.249742	0.428075	0.407073	3.70673	2.58701	1.78	0.70598	0.70598	0.70597	21	49	43	0.705843	0.071	0.58	5.5	0.075	0.00021	40
09/11/05 71-2	0.0008	0.0008	0.027774	0.267364	0.463111	0.439103	4.00773	2.58715	1.75	0.70596	0.70596	0.70592	20	31	33	0.705843	0.071	1.25	6.4	0.075	0.00021	33
09/11/05 71-2	0.0006	0.0008	0.025284	0.255547	0.433576	0.413754	3.75980	2.58877	1.83	0.70600	0.70600	0.70597	23	80	36	0.705843	0.072	0.48	4.8	0.075	0.00016	40
09/11/05 71-2	0.0007	0.0008	0.026528	0.274040	0.455628	0.436904	3.94988	2.58897	1.83	0.70598	0.70598	0.70597	26	56	42	0.705843	0.073	1.15	2.9	0.075	0.00017	28
09/11/05 71-2	0.0007	0.0006	0.022004	0.216339	0.367855	0.350677	3.18822	2.58782	1.83	0.70590	0.70591	0.70588	19	53	93	0.705843	0.072	0.40	5.0	0.075	0.00021	40
09/11/05 71-2	0.0007	0.0008	0.024642	0.251123	0.417276	0.400127	3.61669	2.58720	1.82	0.70596	0.70596	0.70597	19	25	40	0.705843	0.073	0.51	2.8	0.075	0.00019	40
09/11/05 71-2	0.0007	0.0008	0.025226	0.256815	0.427220	0.410275	3.70300	2.58721	1.82	0.70596	0.70596	0.70598	21	25	54	0.705843	0.074	0.34	2.2	0.075	0.00019	40
09/11/05 71-2	0.0007	0.0007	0.023358	0.232289	0.395225	0.376807	3.42680	2.58804	1.84	0.70589	0.70589	--	17	81	--	0.705843	0.072	0.31	5.1	0.075	0.00019	40
01/16/06 78-1	0.0062	0.0061	0.070911	0.689532	0.782508	0.818940	6.52057	2.58430	1.69	0.70947	0.70932	--	13	610	--	0.708886	0.112	0.65	10.6	0.126	0.00096	45
01/16/06 78-1	0.0059	0.0058	0.060415	0.365045	0.405995	0.432392	3.43846	2.58490	1.72	0.70939	0.70924	0.70891	22	494	36	0.708886	0.113	1.03	10.3	0.126	0.00172	45
01/16/06 78-1[i]	0.0058	0.0057	0.089039	1.008890	1.140008	1.219198	9.79527	2.58586	1.68	0.70925	0.70909	0.70881	16	294	106	0.708886	0.109	0.72	12.9	0.126	0.00060	45
01/16/06 78-1[i]	0.0056	0.0055	0.062132	0.584565	0.661023	0.704447	5.65186	2.58572	1.70	0.70927	0.70911	0.70878	28	323	148	0.708886	0.110	0.90	12.6	0.126	0.00098	39
01/16/06 78-1[i]	0.0053	0.0053	0.042605	0.276774	0.311453	0.329490	2.62646	2.58406	1.71	0.70951	0.70935	0.70913	21	654	340	0.708886	0.112	0.32	11.0	0.126	0.00201	45
01/16/06 78-1[i]	0.0050	0.0050	0.033419	0.140970	0.164176	0.169158	1.35428	2.58587	1.72	0.70925	0.70910	0.70873	33	296	214	0.708886	0.110	0.58	12.1	0.126	0.00371	45
01/16/06 78-1[i]	0.0050	0.0050	0.036845	0.206490	0.230955	0.243559	1.93289	2.58548	1.70	0.70931	0.70916	0.70910	35	382	306	0.708886	0.113	0.85	9.7	0.126	0.00259	27
01/16/06 78-1[i]	0.0085	0.0085	0.049816	0.121730	0.146878	0.145002	1.15711	2.58816	1.77	0.70894	0.70878	0.70854	52	148	489	0.708886	0.111	0.56	11.3	0.126	0.00732	45
01/16/06 71-2[i]	0.0155	0.0157	0.091273	0.139273	0.263105	0.227057	2.06873	2.58584	1.76	0.70624	0.70608	0.70605	28	197	147	0.705843	0.071	0.37	5.4	0.075	0.00752	45
01/16/06 71-2[i]	0.0183	0.0185	0.123513	0.333251	0.611060	0.551464	5.04318	2.58586	1.72	0.70623	0.70608	--	13	190	--	0.705843	0.070	0.37	7.2	0.075	0.00364	45

01/16/06	78-1[j]	0.0105	0.0098	0.071513	0.683739	0.460786	0.592918	3.84615	2.58924	1.48	0.70862	0.70846	--	37	602	--	0.708886	0.190	0.19	51.3	0.126	0.00273	41
01/16/06	78-1[j]	0.0111	0.0104	0.090872	1.314651	0.775036	1.069266	6.54519	2.58742	1.44	0.70904	0.70888	--	24	8	--	0.708886	0.215	0.82	71.1	0.126	0.00169	45
01/16/06	71-2[j]	0.0119	0.0112	0.086823	0.653507	0.631526	0.700407	5.29883	2.58759	1.45	0.70607	0.70591	--	27	43	--	0.705943	0.132	0.55	74.8	0.075	0.00225	45
01/16/06	71-2[j]	0.0126	0.0119	0.093511	0.738091	0.694135	0.778190	5.82947	2.58734	1.45	0.70611	0.70595	--	20	14	--	0.705943	0.135	0.38	79.4	0.075	0.00217	45

Analyses are listed in chronological order. Cycles are 16 second integrations of measurement during analysis until 3/26/04. Cycles are 8 second integrations thereafter.

[a] All samples are dredge samples from the AVON3 dredging cruise (Workman *et al*., 2004) [7]

[b] $^{85}Rb/^{87}Rb$ required values are obtained after correcting for Kr and Rb interferences, fractionation correction, and normalization to NBS 987 solution run during each analytical session. The average $^{85}Rb/^{87}Rb$ required value is 2.58745, which is used to obtain the Rb correction using the "global average" technique

[c] Sr-isotopes are corrected for Kr and Rb interferences and fractionation corrected

[d] After correction for Rb and Sr interferences and fractionation, glass standard runs are corrected for 987 standard solution runs for each analytical session

[e] Internal (in-run) precision (I. Prec.) is quoted as 1σ standard error, and is calculated offline using the TweaKr program. In the above dataset, the average internal precision is 17 ppm for $^{87}Sr/^{86}Sr$, and 0.67% for Rb/Sr.

[f] External precision (E. Prec.) is calculated assuming that the TIMS $^{87}Sr/^{86}Sr$ (ppm) and XRF Rb/Sr (%) values obtained on bulk powders are correct. The average external precision of $^{87}Sr/^{86}Sr$ measurements on the above glass standards is 155 ppm mean deviation (1σ), which translates to 388 ppm standard deviation (2σ) if a Gaussian distribution is assumed. The average external precision on Rb/Sr measurements on glass standards is 6.7% (mean deviation, 1σ), which translates to a standard deviation of 16.7% (2σ). Uses global average $^{85}Rb/^{87}Rb$ value (2.58745) for isobaric Rb interference.

[g] $^{87}Sr/^{86}Sr$ and Rb/Sr values obtained by conventional methods (XRF or ICP) are reported in Workman *et al*., 2004 [7].

[h] Raw voltages on mass 82 divided by mass 88. This is a proxy for Kr/Sr during analysis

[i] Samples are run at less than 100% laser power (between 45-90% power)

[j] Unlike all other Samoan glass standard and melt inclusion analyses, these four analyses were performed with a "dry" plasma (i.e., no aspiration of the 5% nitric solution during laser analysis). These dry runs are not used in calculations or in the figures, and were performed for comparative purposes only. We find that the Rb is strongly fractionated from Sr, and that the $^{85}Rb/^{87}Rb$ required and mass bias tend to me lower than similar runs made with a wet plasma during the same analytical session.

[k] The amount of mass bias correction required to obtain the canonical value for $^{86}Sr/^{88}Sr$. Units are %/amu.

[l] External precision is calculated assuming that the TIMS $^{87}Sr/^{86}Sr$ is correct. External precision is calculated using the "bracketing" technique for the correction of the isobaric interference from Rb on mass 87. The external precision is somewhat improved (127 ppm, 1 mean deviation) compared to the global average technique for the Rb correction (155 ppm) when comparing the same set of glass analyses. Bracketing is a useful technique for individual, 1-day analytical sessions only, as $^{85}Rb/^{87}Rb$ values can change significantly between analytical sessions. Therefore, the first and last runs of the Samoan glass standards of each analytical session cannot be corrected with the bracketing technique. Runs with a dry plasma are not examined.

[m] Same as previous column, but $^{87}Sr/^{86}Sr$ values calculated by correcting for the Rb interferece using the "bracketing method", our preferred correction scheme and the one adopted in the manuscript for correcting unknowns.

Table 5. Compositions of Samoan glasses ("standards") used in determining $^{85}Rb/^{87}Rb$ required values in this study.

Glass Nam	76-8	78-1	78-8	76-13	75-10	63-13	70-1	71-11	71-22	72-2	73-1	73-12	71-2	68-3
Volcano	Malumalu	Malumalu	Malumalu	Malumalu	Ta'u	Vailulu'u	Vailulu'u	Vailulu'u	Vailulu'u	Vailulu'u	Vailulu'u	Vailulu'u	Vailulu'u	Vailulu'u
$^{86}Sr/^{87}Sr$	0.706374	0.708988	0.707614	0.706395	0.704533	0.705520	0.705371	0.705394	0.705473	0.705395	0.706720	0.706853	0.705943	0.705388
SiO_2	47.04	45.54	47.33	46.35	47.10	47.16	47.57	47.57	45.21	45.53	47.14	47.10	43.85	47.84
Al_2O3	13.69	8.94	14.19	13.55	16.29	14.76	13.63	13.71	8.13	14.10	13.97	12.07	6.37	11.86
TiO_2	3.88	1.96	3.29	3.86	4.02	3.01	2.91	2.75	1.68	3.31	2.80	2.46	1.44	2.55
FeO*	11.93	11.89	11.45	12.78	12.56	11.59	11.44	10.64	10.77	12.13	11.26	10.25	10.80	10.51
MnO	0.18	0.17	0.17	0.20	0.20	0.18	0.18	0.18	0.17	0.19	0.18	0.18	0.17	0.17
CaO	11.86	8.23	11.47	11.80	9.11	12.37	13.05	12.72	9.99	11.88	12.93	12.80	8.07	12.75
MgO	6.27	19.68	6.93	6.42	5.16	6.57	7.58	8.60	21.79	8.56	7.52	11.70	27.44	10.68
K_2O	1.92	1.41	2.05	1.94	1.46	1.28	0.98	1.15	0.67	1.40	1.37	1.15	0.59	0.99
Na_2O	2.75	1.92	2.74	2.61	3.47	2.72	2.35	2.35	1.39	2.54	2.50	2.02	1.11	2.36
P_2O5	0.49	0.27	0.40	0.49	0.63	0.37	0.34	0.33	0.20	0.37	0.34	0.28	0.17	0.29
Pre-total	99.27	100.27	99.74	99.12	99.58	99.01	98.81	98.74	98.71	98.39	99.10	99.13	98.50	99.49
Ni	65	616	97	71	5	59	57	135	778	110	79	220	1080	285
Cr	137	1289	106	130	15	110	98	316	1687	227	202	768	2141	822
V	356	194	342	384	282	339	338	324	212	367	325	295	177	300
Ga	22	14	21	26	26	20	21	19	14	23	14	17	9	20
Cu	72	49	79	95	21	58	82	91	156	79	70	59	138	82
Zn	121	102	104	125	140	95	92	92	78	102	86	77	77	89
Cs	0.51	0.39	0.60	0.5	0.39	0.28	0.31	0.34	0.21	0.39	0.38	0.31	0.19	0.30
Rb	44.3	41.8	51.4	42.8	27.6	33.6	25.0	30.4	19.0	29.3	38.1	30.4	16.9	26.6
Ba	355	255	372	341	264	279	203	247	149	287	347	282	128	218
Th	6.4	6.0	6.3	5.3	4.9	5.2	4.2	4.4	2.6	5.0	6.1	4.9	2.3	4.0
U	1.30	1.05	1.36	1.29	1.10	1.07	0.93	0.95	0.56	1.11	1.15	0.87	0.49	0.87
Nb	56.7	39.0	59.0	57.5	51.3	45.1	37.1	40.5	24.7	47.5	46.7	38.2	20.7	36.4
Ta	3.9	2.6	3.8	3.8	3.6	3.1	2.5	2.9	1.6	3.2	3.1	2.5	1.4	2.5
La	48.4	39.4	52.0	48.6	43.1	37.4	31.0	32.9	20.2	38.3	44.2	36.1	17.1	29.3
Ce	95.9	73.0	98.8	96.3	90.5	74.4	65.0	65.6	40.4	76.3	83.6	68.8	34.4	58.7
Pb	4.2	4.2	4.6	5.2	3.3	2.8	2.2	2.3	1.6	2.5	4.8	6.2	1.3	2.5
Pr	11.2	7.9	11.5	11.8	11.1	8.7	7.6	7.9	4.7	9.1	9.4	7.8	4.0	6.9
Nd	46.3	31.0	44.2	47.2	48.0	35.4	31.5	31.6	19.0	37.2	36.0	30.2	16.5	28.5
Sr	544	333	529	554	617	470	420	434	287	492	473	398	224	387
Zr	276	183	256	281	327	218	198	186	117	221	212	177	98	168
Hf	7.2	4.7	6.4	7.1	8.3	5.8	5.4	5.2	3.1	5.9	5.8	4.9	2.6	4.4
Sm	10.5	6.5	9.1	10.2	11.6	7.8	7.5	7.3	4.4	8.4	7.8	6.7	3.7	6.5
Eu	3.2	1.9	2.5	2.9	3.8	2.5	2.3	2.3	1.4	2.6	2.4	2.1	1.1	2.0
Gd	9.5	5.8	8.0	9.1	10.7	7.1	6.8	6.4	3.9	7.3	6.8	6.0	3.2	5.8
Tb	1.4	0.8	1.1	1.3	1.6	1.1	1.0	1.0	0.6	1.1	1.1	0.9	0.5	0.9
Dy	7.4	4.4	5.8	6.6	8.8	5.9	5.7	5.4	3.3	6.0	5.6	5.0	2.7	4.8
Ho	1.3	0.8	1.0	1.2	1.6	1.1	1.0	1.0	0.6	1.1	1.0	0.9	0.5	0.9
Y	32.2	19.6	30.5	33.1	40.2	27.5	26.4	25.9	15.6	29.3	27.3	23.5	12.6	22.5
Er	3.0	1.8	2.5	2.8	3.8	2.7	2.5	2.4	1.4	2.7	2.5	2.2	1.2	2.1
Tm	0.38	0.23	0.34	0.37	0.50	0.35	0.33	0.32	0.19	0.35	0.33	0.28	0.16	0.28
Yb	2.05	1.24	1.97	2.13	2.80	2.02	1.87	1.83	1.11	2.02	1.90	1.64	0.87	1.63
Lu	0.29	0.19	0.29	0.31	0.40	0.30	0.27	0.27	0.16	0.29	0.28	0.23	0.13	0.24
Sc	31.0	25.2	28.5	25.0	20.5	33.4	41.9	39.2	36.0	38.0	39.1	42.7	29.8	40.9

Most glass data can be found in [7]. Major element data normalized to 100%. All glass standards names have the prefix "AVON3"

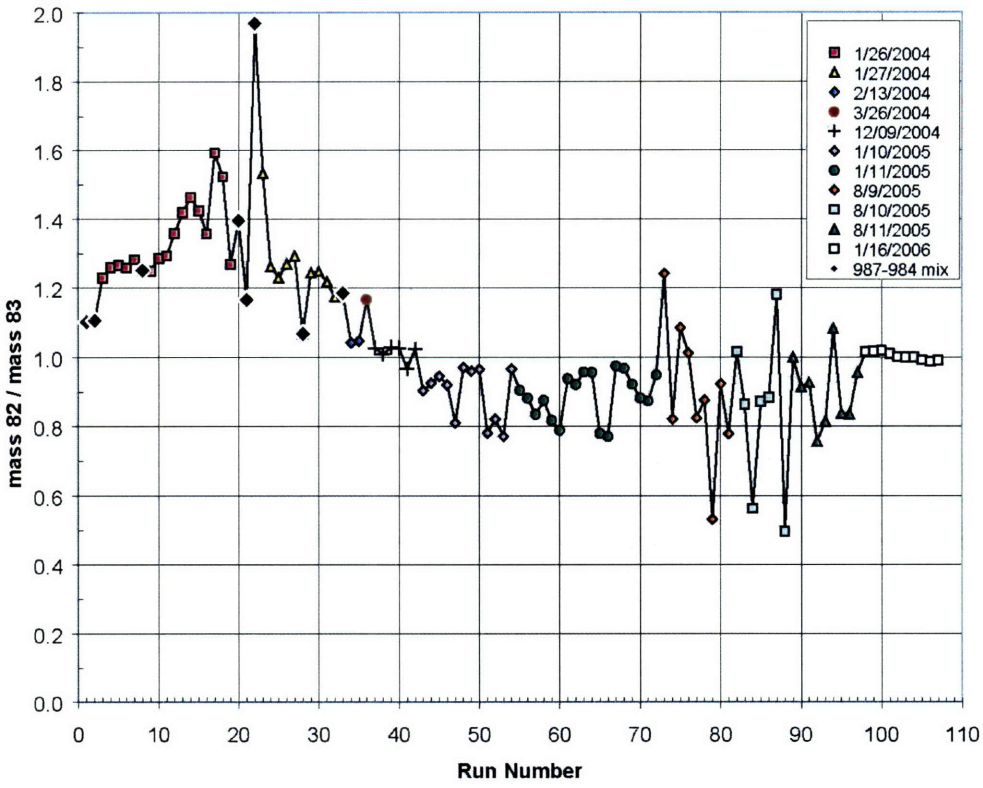
mass 82 / mass 83
Run Number
0.0
0.2
0.4
0.6
0.8
1.0
1.2
1.4
1.6
1.8
2.0
0
10
20
30
40
50
60
70
80
90
100
110
1/26/2004
1/27/2004
2/13/2004
3/26/2004
12/09/2004
1/10/2005
1/11/2005
8/9/2005
8/10/2005
8/11/2005
1/16/2006
987-984 mix

Fig. 1

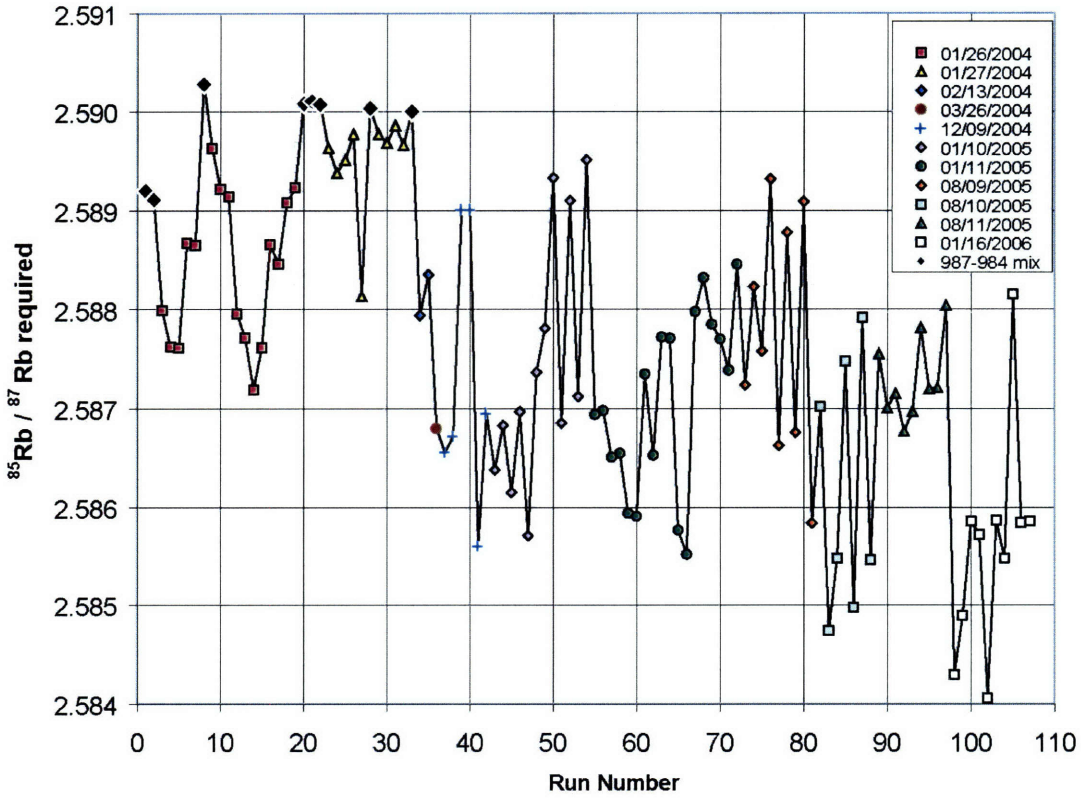
2.591
2.590
2.589
2.588
2.587
2.586
2.585
2.584
0
10
20
30
40
50
60
70
80
90
100
110
Run Number
85Rb / 87Rb required
01/26/2004
01/27/2004
02/13/2004
03/26/2004
12/09/2004
01/10/2005
01/11/2005
08/09/2005
08/10/2005
08/11/2005
01/16/2006
987-984 mix

Fig. 2

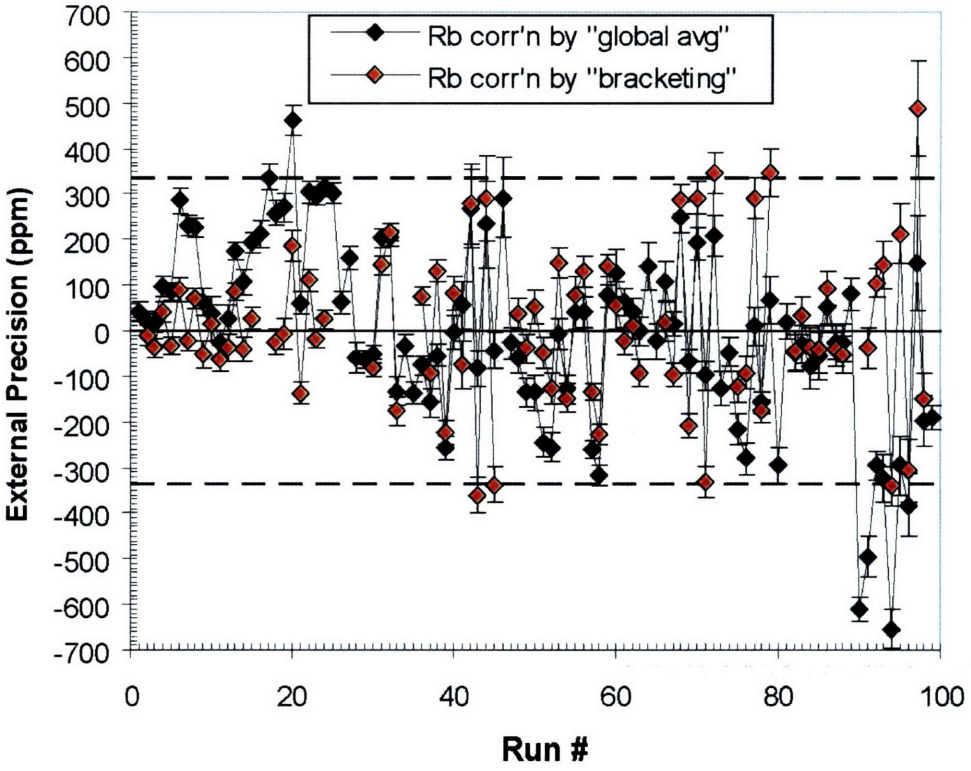
Rb corr'n by "global avg"
Rb corr'n by "bracketing"
External Precision (ppm)
700
600
500
400
300
200
100
0
-100
-200
-300
-400
-500
-600
-700
0
20
40
60
80
100
Run #

Fig. 3

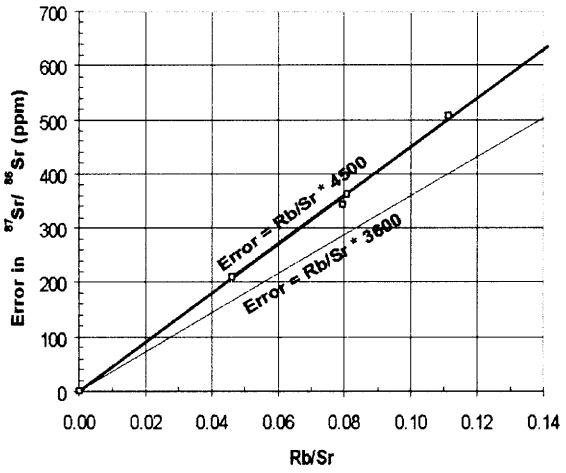

Supp Data Fig. 4

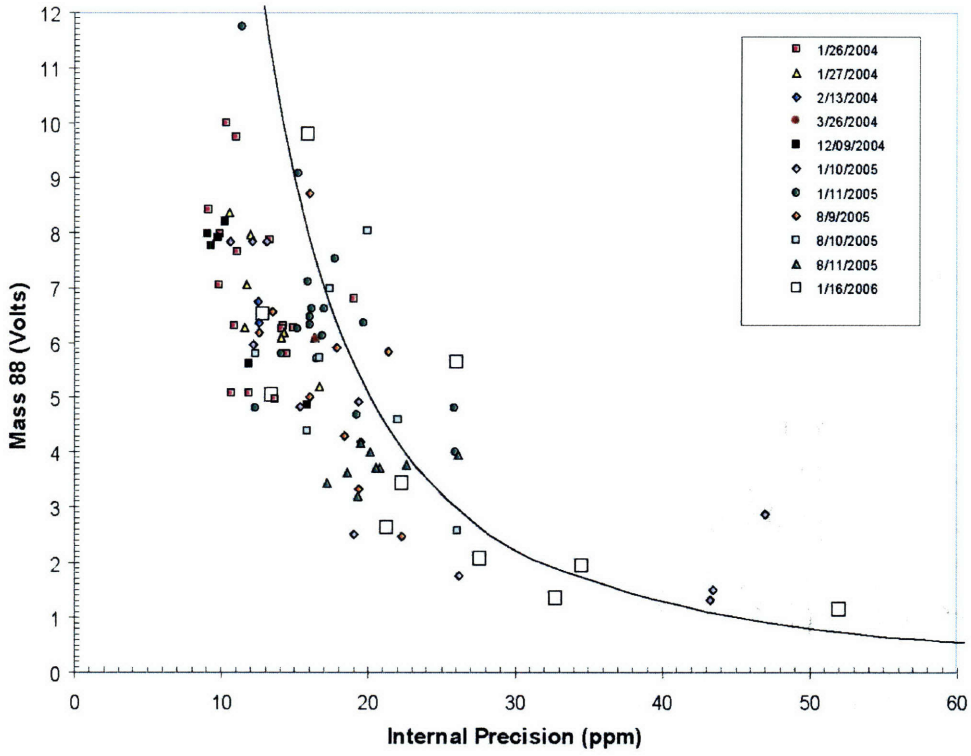
Mass 88 (Volts)
Internal Precision (ppm)
0
1
2
3
4
5
6
7
8
9
10
11
12
0
10
20
30
40
50
60
1/26/2004
1/27/2004
2/13/2004
3/26/2004
12/09/2004
1/10/2005
1/11/2005
8/9/2005
8/10/2005
8/11/2005
1/16/2006

Fig. 5

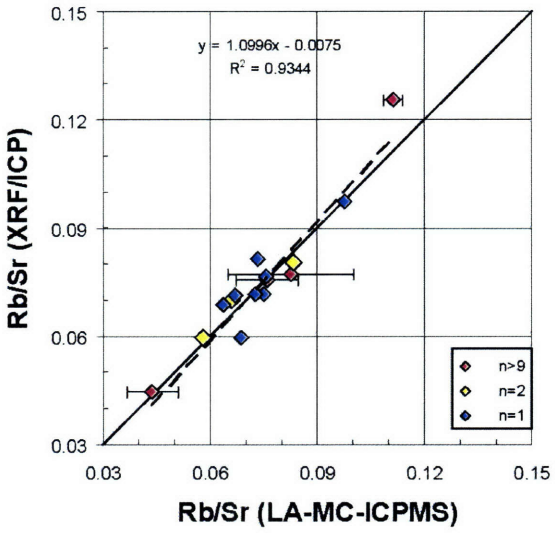
y = 1.0996x - 0.0075
R² = 0.9344
0.15
0.12
0.09
0.06
0.03
Rb/Sr (XRF/ICP)
0.03
0.06
0.09
0.12
0.15
Rb/Sr (LA-MC-ICPMS)
n>9
n=2
n=1

Fig. 6

Chapter 2

The return of subducted continental crust in Samoan lavas*

Abstract

Substantial quantities of terrigenous sediments are known to enter the mantle at subduction zones, but little is known about their fate in the mantle[1]. Subducted sediment may be entrained in buoyantly upwelling plumes and returned to the Earth's surface at hotspots[2–5], but the proportion of recycled sediment in the mantle is small, and clear examples of recycled sediment in hotspot lavas are rare[6,7]. Here we report remarkably enriched $^{87}Sr/^{86}Sr$ and $^{143}Nd/^{144}Nd$ isotope signatures in Samoan lavas from three dredge locations on the underwater flanks of Savai'i island, Western Samoa. The submarine Savai'i lavas represent the most extreme $^{87}Sr/^{86}Sr$ isotope compositions reported for ocean island basalts to date. The data are consistent with the presence of a recycled sediment component (with a composition similar to the upper continental crust) in the Samoan mantle. Trace-element data show affinities similar to those of the upper continental crust—including exceptionally low Ce/Pb and Nb/U ratios[8]—that complement the enriched $^{87}Sr/^{86}Sr$ and $^{143}Nd/^{144}Nd$ isotope signatures. The geochemical evidence from these Samoan lavas significantly redefines the composition of the EM2 (enriched mantle 2; ref. 9) mantle endmember, and points to the presence of an ancient recycled upper continental crust component in the Samoan mantle plume.

*Published as: M. G. Jackson, S. R. Hart, A. A. P. Koppers, H. Staudigel, J. Konter, J. Blusztajn, M. Kurz and J. A. Russell, The return of subducted continental crust in Samoan lavas, *Nature, v. 448*, pp. 684-687, 2007, doi: 10.1038/nature06048.

nature Vol 448|9 August 2007|doi:10.1038/nature06048

LETTERS

The return of subducted continental crust in Samoan lavas

Matthew G. Jackson[1], Stanley R. Hart[2], Anthony A. P. Koppers[3,4], Hubert Staudigel[3], Jasper Konter[3], Jerzy Blusztajn[2], Mark Kurz[2] & Jamie A. Russell[3]

Substantial quantities of terrigenous sediments are known to enter the mantle at subduction zones, but little is known about their fate in the mantle[1]. Subducted sediment may be entrained in buoyantly upwelling plumes and returned to the Earth's surface at hotspots[2–5], but the proportion of recycled sediment in the mantle is small, and clear examples of recycled sediment in hotspot lavas are rare[6,7]. Here we report remarkably enriched $^{87}Sr/^{86}Sr$ and $^{143}Nd/^{144}Nd$ isotope signatures in Samoan lavas from three dredge locations on the underwater flanks of Savai'i island, Western Samoa. The submarine Savai'i lavas represent the most extreme $^{87}Sr/^{86}Sr$ isotope compositions reported for ocean island basalts to date. The data are consistent with the presence of a recycled sediment component (with a composition similar to the upper continental crust) in the Samoan mantle. Trace-element data show affinities similar to those of the upper continental crust—including exceptionally low Ce/Pb and Nb/U ratios[8]—that complement the enriched $^{87}Sr/^{86}Sr$ and $^{143}Nd/^{144}Nd$ isotope signatures. The geochemical evidence from these Samoan lavas significantly redefines the composition of the EM2 (enriched mantle 2; ref. 9) mantle endmember, and points to the presence of an ancient recycled upper continental crust component in the Samoan mantle plume.

The Earth's mantle, as sampled by ocean island basalts erupted at hotspots, is chemically and isotopically heterogeneous. However, the origin of the geochemical heterogeneity of the mantle is not well understood. One model for the geochemical evolution of the mantle assumes that much of the chemical diversity is a result of subduction, a tectonic process that introduces enriched oceanic crust and compositionally heterogeneous sediment into a largely primitive (or slightly depleted) mantle[5,10,11]. Following subduction, these surface materials mix with a peridotitic mantle, thus imprinting their enriched chemical and isotopic signatures on its various domains. A number of isotopically distinct geochemical reservoirs, as sampled by ocean island basalts, have resulted from this process. The isotopic endmembers are often referred to as HIMU (high $\mu = {}^{238}U/^{204}Pb$), EM1 (enriched mantle 1) and EM2 (enriched mantle 2) and DMM (depleted mid-ocean-ridge basalt mantle)[9]. Although the most radiogenic Pb isotope ratios observed in the HIMU component have been proposed to result from a contribution of recycled oceanic crust[8,12], most models for the creation of the EM1 and EM2 mantle reservoirs invoke a small portion of lithologically distinct sediments that have been recycled into the mantle[9,13].

The volcanically active Samoan islands and seamounts define a hotspot track with a classical EM2 pedigree[7,14,15]. The first high-precision $^{87}Sr/^{86}Sr$ and $^{143}Nd/^{144}Nd$ measurements from Samoan lavas were interpreted as evidence of sediment recycling[5]. Recently, however, the proposed recycled sediment origin of the enriched Samoan basalts has been questioned (see Supplementary Discussion), and an alternative model favouring source enrichment by metasomatic processes was proposed[7]. The extreme isotopic and chemical enrichment in the new Samoan EM2 lavas exhibit distinctly continental fingerprints, and argue for a role for a component similar to ancient recycled upper continental crust (UCC) in the Samoan plume (see Supplementary Discussion for the ALIA 2005 cruise dredge locations and geochemical data).

The most isotopically enriched Samoan whole-rock $^{87}Sr/^{86}Sr$ signature (0.720469, Mg# = 57.2) is recorded in a trachyandesite, dredge sample D115-21, which was taken from the southwestern flank of Savai'i. Clinopyroxene mineral separates from the same sample yielded an even higher $^{87}Sr/^{86}Sr$ ratio (0.721630). A trachybasalt (D115-18) hosts the second-most-enriched $^{87}Sr/^{86}Sr$ (0.718592, Mg# = 58.7), and clinopyroxene mineral separates from the sample also gave more enriched ratios (0.720232–0.720830). Six other lavas recovered in the same dredge also exhibit enriched $^{87}Sr/^{86}Sr$ ratios (0.708175–0.716394, Mg# = 52.0–65.1). Dredge D118, located on the far western end of the Savai'i lineament, contained an alkali basalt with enriched $^{87}Sr/^{86}Sr$ (0.710337, measured on fresh clinopyroxene). Dredge D128, taken on the northeastern flanks of Savai'i, yielded a transitional basalt with a high $^{87}Sr/^{86}Sr$ ratio (0.712500, Mg# = 70.5) and several other basalts with less enriched $^{87}Sr/^{86}Sr$ (0.706397–0.708170, Mg# = 61.2–63.9). Dredge D114, taken on the southwestern flanks of Savai'i, provided younger shield basalts of transitional chemistry and normal $^{87}Sr/^{86}Sr$ (0.705422–0.705435, Mg# = 67.2 and 76.3).

The $^{87}Sr/^{86}Sr$ isotopes in the basalts from all three ultra-enriched sampling localitites are complemented by enriched (low) $^{143}Nd/^{144}Nd$ and the lowest $^{3}He/^{4}He$ ratios (4.31–4.93 Ra, or ratio to atmosphere) observed in Samoan basalts. Together, the new data extend the Samoan isotope array to a region outside the global ocean island basalt field (Fig. 1). Highly enriched EM2 signatures have previously been observed only in metasomatized xenoliths from Savai'i ($^{87}Sr/^{86}Sr$ up to 0.712838; ref. 16), and the Samoan EM2 basalts provide the first evidence that the enriched component hosted in these xenoliths also occurs as erupted basalts. The enriched $^{87}Sr/^{86}Sr$ and $^{143}Nd/^{144}Nd$ isotope ratios, coupled with the low $^{3}He/^{4}He$, are consistent with a recycled UCC component in the mantle source of the Samoan EM2 basalts.

The UCC reservoir exhibits several diagnostic trace-element characteristics that can be useful for detecting its presence in Samoan EM2 lavas. Compared to ocean island basalt and mid-ocean-ridge basalt lavas, UCC displays exceptional depletion in Nb (and Ta), Ti and Eu, and enrichment in Pb (Fig. 2). Samoan basalts have

[1]Massachusetts Institute of Technology, Woods Hole Oceanographic Institution Joint Program, [2]Woods Hole Oceanographic Institution, Woods Hole, Massachusetts 02543-1525, USA. [3]Scripps Institution of Oceanography, University of California, San Diego, La Jolla, California 92093-0225, USA. [4]College of Oceanic and Atmospheric Sciences, Oregon State University, Corvallis, Oregon 97331-5503, USA.

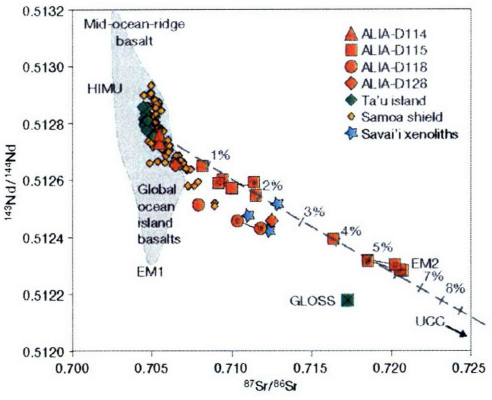

Figure 1 | $^{87}Sr/^{86}Sr$ and $^{143}Nd/^{144}Nd$ isotope ratios of new enriched Samoan lavas. The values are compared with other Samoan shield basalts[7], global ocean island basalt compositions and GLOSS (global subducting sediment)[1]. Analyses in which whole-rock (w) powders and clinopyroxene (c) analyses are performed on the same sample are connected by a tie-line. A model mixing line between depleted Ta'u peridotite and UCC is marked at 1% intervals, with increasing contribution from the latter component. The hypothetical UCC mixing endmember lies outside the figure. Approximately 5% UCC is required to produce the spidergram of sample D115-18 (see Supplementary Discussion), and ~6% is required to generate the $^{87}Sr/^{86}Sr$ and $^{143}Nd/^{144}Nd$ in D115-21.

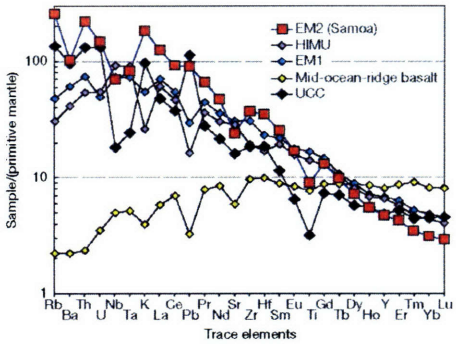

Figure 2 | Primitive-mantle-normalized[27] trace-element patterns for the Samoan EM2 endmember. The EM2 spidergram is the most isotopically enriched Samoan lava, sample D115-21 ($^{87}Sr/^{86}Sr = 0.720469$, Mg# = 57). The other mantle endmembers (corrected to Mg# numbers of 60–62) and UCC[17] are plotted for comparison. Similar to UCC, the Samoan EM2 lava exhibits large negative Ti and Nb (and Ta) anomalies and an excess of Pb (and K).

trace-element characteristics that are increasingly similar to UCC with more enriched $^{87}Sr/^{86}Sr$ and $^{143}Nd/^{144}Nd$ values (Fig. 3). Although the most isotopically depleted basalts from Samoa show slight positive anomalies in Nb and Ti, the magnitude of these anomalies decreases monotonically towards the most enriched Samoan EM2 basalts. Similarly, a correlation exists between greater Pb enrichment and increasing isotopic enrichment in Samoan basalts. Importantly, the Eu anomaly is increasingly negative in the most isotopically enriched Samoan EM2 lavas (excluding basalts with MgO < 6.5 wt%), and the Rb/Sr and U/Pb are too low in the lower (or middle) continental crust[17] to be consistent with the new Samoan Sr and Pb isotope data; these observations rule out the involvement of lower (or middle) continental crust. Furthermore, rare xenoliths with enriched $^{87}Sr/^{86}Sr$ and $^{143}Nd/^{144}Nd$ from the subcontinental lithospheric mantle[9] suggest that this mantle domain can be isotopically enriched. However, the subcontinental lithospheric mantle does not appear to exhibit the trace-element anomalies observed in the most isotopically enriched Samoan lavas[18]. Instead, isotope ratios

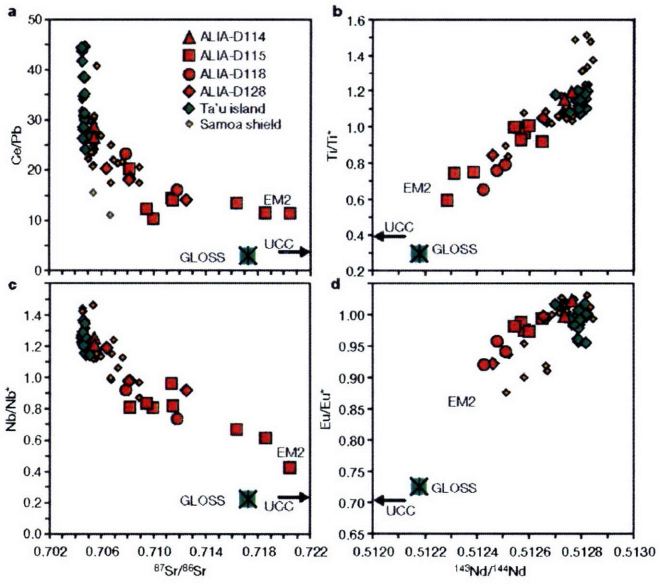

Figure 3 | $^{87}Sr/^{86}Sr$ and $^{143}Nd/^{144}Nd$ ratios suggest the presence of a UCC component in Samoan EM2 lavas. The $^{87}Sr/^{86}Sr$ and $^{143}Nd/^{144}Nd$ ratios are plotted against diagnostic UCC trace-element indicators in Samoan basalts: the more isotopically enriched Samoan basalts exhibit trace-element characteristics that are increasingly similar to UCC. UCC[17] plots outside the panels, and its trace-element and isotopic composition is indicated by the level (and direction) of the arrows. **a**–**c**, All submarine Savai'i samples are plotted, as are other Samoan shield lavas with MgO > 6.5 wt%. **d**, Submarine Savai'i samples with MgO < 6.5% are excluded (avoiding possible effects of plagioclase fractionation). All trace-element data shown are by ICP-MS (inductively coupled plasma mass spectrometry). Element anomalies are calculated as follows (where subscript N means normalized to primitive mantle[27]): $Ti/Ti^* = Ti_N/(Nd_N^{0.0555} \times Sm_N^{0.333} \times Gd_N^{0.722})$; $Nb/Nb^* = Nb_N/\sqrt{(Th_N \times La_N)}$; $Eu/Eu^* = Eu_N/\sqrt{(Sm_N \times Gd_N)}$.

and trace-element anomalies (Nb, Ti, Eu and Pb) in Samoan basalts generate arrays that trend towards a composition similar to UCC.

We can exclude a shallow origin for the anomalous enrichment observed in the Samoan EM2 lavas. Owing to the close proximity of the Tonga trench, located only 120 km south of Savai'i, rapid cycling of sediment from the subduction zone into the Samoan plume was proposed as a mechanism for generating the extreme isotopic enrichment in Samoan lavas[14]. However, at the time that the submarine Savai'i lavas were erupted 5 Myr ago[31], plate reconstructions indicate that the northern terminus of the Tonga trench was located 1,300 km to the west of Savai'i (ref. 19), and sediment input from the Tonga trench can be ruled out as a source of enrichment in these lavas.

Evidence from Pb isotopes suggests that it is unlikely that shallow-level contamination by modern marine sediments is responsible for the isotopic enrichment in the Samoan EM2 basalts. In $\Delta^{207}Pb/^{204}Pb - \Delta^{208}Pb/^{204}Pb$ isotope space, Samoan basalts and global marine sediments[1] exhibit non-overlapping fields with diverging trends (Fig. 4). Moreover, three composite cores taken from the Samoan region, and a single ferromanganese crust from the flanks of Savai'i, plot in the global marine sediment field and exhibit no geochemical relationship with the extremely enriched Samoan lavas. It is also unlikely that the Samoan plume has been contaminated by stranded continental crust, such as was found beneath the Kerguelen plateau[20] and the southern Mid-Atlantic Ridge[21], or by ancient limestone blocks like those discovered in the Romanche fracture zone[22]. The tectonic history of the Samoan region places it neither at the locus of continental rifting, which was responsible for the marooned Kerguelen and southern Atlantic continental blocks, nor in proximity to any Pacific fracture zones[23].

Large quantities of sediment derived from UCC have entered the mantle at subduction zones over geologic time[1], and such a reservoir is ideally suited as an enriched source for the Samoan plume. The array formed by the Samoan EM2 basalts in $^{143}Nd/^{144}Nd–^{87}Sr/^{86}Sr$ isotope space is anchored on the depleted end by basalts from Ta'u, one of the youngest, easternmost Samoan islands. The $^{143}Nd/^{144}Nd–^{87}Sr/^{86}Sr$ array suggests mixing between this dominant, slightly depleted Ta'u component and a rare, enriched component that exhibits isotope and trace-element characteristics similar to UCC. The proportion of the enriched component in the Samoan EM2 lavas can be estimated by calculating trace-element concentrations in the depleted Ta'u mantle and mixing this composition with UCC (see Supplementary Discussion). A contribution of 5% UCC to the depleted Ta'u mantle generates a composition that, after mixing and melting, produces a trace-element pattern similar to that observed in Samoan EM2 sample D115-18 (with $^{87}Sr/^{86}Sr$ of 0.718592). Fixing the proportions of the depleted and UCC components in the Samoan EM2 source in this way then defines the $^{87}Sr/^{86}Sr$ and $^{143}Nd/^{144}Nd$ isotopic composition of this material as 0.7421 and 0.5117, respectively. The most isotopically enriched Samoan lavas have higher $^{87}Sr/^{86}Sr$ than the average continental crust inferred from suspended river sediments ($^{87}Sr/^{86}Sr \approx 0.716$; ref. 24) and global marine sediments (~0.717; ref. 1), values that are biased towards younger continental crust. However, composites of directly sampled ancient continental shield rocks show isotopically enriched compositions[25] that bracket the calculated composition of the recycled UCC sediment in the Samoan mantle. The new ultra-enriched EM2 lavas suggest an unusually enriched recycled protolith in the Samoan mantle.

Despite the large volumes of sediment entering the mantle at subduction zones (estimated at 0.5–0.7 $km^3 yr^{-1}$; ref. 1), isotopic signatures associated with recycled UCC are rare in ocean island basalts[26]. This enriched component is also uncommon in the Samoan plume, where the highly enriched Samoan EM2 lava D115-18 is calculated to have only 5% recycled UCC (and 95% depleted Ta'u source), and 90% of the remaining Samoan basalts exhibit depleted $^{143}Nd/^{144}Nd$ ratios (>0.512638). In addition to being rare in other ocean island basalts, recycled UCC may exist in low abundance in the Samoan plume. The reason for this may be that most subducted sediment melts and is rapidly returned to the surface in subduction zone volcanoes, or is simply scraped off onto the forearc and is never subducted. Alternatively, if a significant portion of UCC has been subducted over the past 4 Gyr (0.5–0.7 $km^3 yr^{-1}$) and has survived subduction zone melting, the resulting accumulated reservoir in the mantle will constitute only ~0.15% of its mass. Such a small reservoir may be diluted by the ambient mantle after convective stirring, a mechanism that efficiently attenuates mantle heterogeneities. Therefore, recycled crustal signatures can be greatly diluted and difficult to detect. By contrast, the recycled UCC component in the Samoan plume is an anomalous survivor in a chaotic mantle.

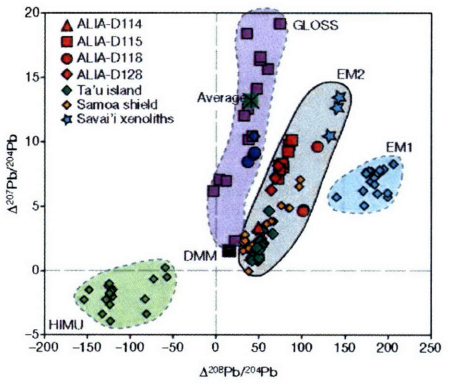

Figure 4 | ΔPb isotope compositions of Samoan lavas and marine sediment samples indicate that the Samoan EM2 lavas are not contaminated with modern marine sediment. Samoan basalts show no overlap with oceanic sediments contributing to GLOSS[1] (purple squares, where the GLOSS average composition is represented by a green crossed 'average' square), composite sections from three sediment cores taken in the Samoan region (blue circles), and a Samoan ferromanganese rind (blue diamond). Pb-isotope data for mantle endmembers DMM (using data from mid-ocean ridge basalt normal segments, as defined and catalogued by ref. 28), EM1 (Pitcairn), and HIMU (Mangaia and Tubuai) are from the literature (see Supplementary Information for reference citations). The use of ΔPb isotope notation[29] to identify sediment components in ocean island basalts is discussed elsewhere[30]. All Samoan data shown are determined using a high-precision Tl-spike protocol[7].

Received 26 January; accepted 22 June 2007.

1. Plank, T. & Langmuir, C. H. The chemical composition of subducting sediments and its consequences for the crust and mantle. *Chem. Geol.* **145**, 325–394 (1998).
2. Allegre, C. J. & Turcotte, D. L. Geodynamic mixing in the mesosphere boundary layer and the origin of oceanic islands. *Geophys. Res. Lett.* **12**, 207–210 (1985).
3. Cohen, R. S. & O'Nions, R. K. Identification of recycled continental material in the mantle from Sr, Nd and Pb isotope investigations. *Earth Planet. Sci. Lett.* **61**, 73–84 (1982).
4. Hawkesworth, C. J., Norry, M. J., Roddick, J. C. & Vollmer, R. $^{143}Nd/^{144}Nd$ and $^{87}Sr/^{86}Sr$ ratios from the Azores and their significance in LIL-element enriched mantle. *Nature* **280**, 28–31 (1979).
5. White, W. M. & Hofmann, A. W. Sr and Nd isotope geochemistry of oceanic basalts and mantle evolution. *Nature* **296**, 821–825 (1982).
6. White, W. M. & Duncan, R. A. in *Earth Processes: Reading the Isotopic Code* (eds Basu, A. & Hart, S. R.) 183–206 (Geophys. Monogr. 95, AGU, Washington DC, 1996).
7. Workman, R. K. *et al.* Recycled metasomatized lithosphere as the origin of the Enriched Mantle II (EM2) endmember: evidence from the Samoan volcanic chain. *Geochem. Geophys. Geosyst.* **5**, doi:10.1029/2003GC000623 (2004).
8. Hofmann, A. W., Jochum, K. P., Seufert, M. & White, W. M. Nb and Pb in oceanic basalts: new constraints on mantle evolution. *Earth Planet. Sci. Lett.* **79**, 33–45 (1986).
9. Zindler, A. & Hart, S. R. Chemical geodynamics. *Annu. Rev. Earth Planet. Sci.* **14**, 493–571 (1986).

10. Hofmann, A. W. & White, W. M. Mantle plumes from ancient oceanic crust. *Earth Planet. Sci. Lett.* **57**, 421–436 (1982).
11. Chase, C. G. Oceanic island Pb: two-stage histories and mantle evolution. *Earth Planet. Sci. Lett.* **52**, 277–284 (1981).
12. Zindler, A., Jagoutz, E. & Goldstein, S. Nd, Sr and Pb isotopic systematics in a three-component mantle: a new perspective. *Nature* **298**, 519–523 (1982).
13. Weaver, B. L. The origin of ocean island basalt end-member compositions: Trace element and isotopic constraints. *Earth Planet. Sci. Lett.* **104**, 381–397 (1991).
14. Farley, K. A., Natland, J. H. & Craig, H. Binary mixing of enriched and undegassed (primitive?) mantle components (He, Sr, Nd, Pb) in Samoan lavas. *Earth Planet. Sci. Lett.* **111**, 183–199 (1992).
15. Wright, E. & White, W. M. The origin of Samoa: new evidence from Sr, Nd and Pb isotopes. *Earth Planet. Sci. Lett.* **82**, 151–162 (1987).
16. Hauri, E. H., Shimizu, N., Dieu, J. & Hart, S. R. Evidence for hotspot-related carbonatite metasomatism in the oceanic upper mantle. *Nature* **365**, 221–227 (1993).
17. Rudnick, R. L. & Gao, S. in *The Crust* (ed. Rudnick, R. L.) 1–64, Vol. 3 of *Treatise in Geochemistry* (Elsevier, Amsterdam, 2003).
18. McDonough, W. F. Constraints on the composition of the continental lithospheric mantle. *Earth Planet. Sci. Lett.* **101**, 1–18 (1990).
19. Hart, S. R. *et al.* Genesis of the Western Samoa seamount province: age, geochemical fingerprint and tectonics. *Earth Planet. Sci. Lett.* **227**, 37–56 (2004).
20. Frey, F. A., Weis, D., Borisova, A. Y. & Xu, G. Involvement of continental crust in the formation of the Cretaceous Kerguelen plateau: new perspectives from ODP Let 120 sites. *J. Petrol.* **43**, 1207–1239 (2002).
21. Kamenetsky, V. S. *et al.* Remnants of Gondwanan continental lithosphere in oceanic upper mantle: evidence from the South Atlantic Ridge. *Geology* **29**, 243–246 (2001).
22. Bonatti, E. *et al.* Lower Cretaceous deposits trapped near the equatorial Mid-Atlantic Ridge. *Nature* **380**, 518–520 (1996).
23. Taylor, B. The single largest oceanic plateau: Ontong Java-Manihiki-Hikurangi. *Earth Planet. Sci. Lett.* **241**, 372–380 (2006).
24. Goldstein, S. J. & Jacobsen, S. B. Nd and Sr isotopic systematics of river water suspended material: implications for crustal evolution. *Earth Planet. Sci. Lett.* **87**, 249–265 (1988).
25. McCulloch, M. T. & Wasserburg, G. J. Sm-Nd and Rb-Sr chronology of continental crust formation. *Science* **200**, 1003–1011 (1978).
26. Hofmann, A. W. Mantle geochemistry: The message from oceanic volcanism. *Nature* **385**, 219–229 (1997).
27. McDonough, W. F. & Sun, S. S. The composition of the Earth. *Chem. Geol.* **120**, 223–253 (1995).
28. Su, Y. *Global MORB Chemistry Compilation at the Segment Scale*. Thesis, Columbia Univ. (2003).
29. Hart, S. R. A large-scale isotope anomaly in the Southern Hemisphere mantle. *Nature* **309**, 753–757 (1984).
30. Hart, S. R. Heterogeneous mantle domains: signatures, genesis and mixing chronologies. *Earth Planet. Sci. Lett.* **90**, 273–296 (1988).
31. Koppers, A. A. P., Russell, J. A., Jackson, M. G., Konter, J., Staudigel, H. & Hart, S. R. Samoa reinstated as a primary hotspot trail. *Geology* (submitted).

Supplementary Information is linked to the online version of the paper at www.nature.com/nature.

Acknowledgements We thank A. Hofmann and W. White for reviews. We thank N. Shimizu, R. Workman and R. Rudnick for discussions, and J. Natland for sharing unpublished data. This study was supported by National Science Foundation grants. We are grateful to the scientific party and ships crew of the R/V *Kilo Moana* for the success of the ALIA 2005 expedition (http://earthref.org/ERESE/projects/ALIA/).

Author Contributions M.G.J. performed most of the experimental work, developed the model and wrote the paper. S.R.H. and H.S. conceived the project, and were co-chiefs of the ALIA expedition. A.A.P.K. and J.K. were responsible for the cruise bathymetry, and A.A.P.K. greatly improved the figures. J.B. and M.K. provided analytical assistance and access to facilities. A.A.P.K., J.B., J.K. and J.A.R. helped with sample preparation. All authors participated in the discussion and interpretation of results, and commented on the manuscript.

Author Information Reprints and permissions information is available at www.nature.com/reprints. The authors declare no competing financial interests. Correspondence and requests for materials should be addressed to M.G.J. (mjackson@whoi.edu).

SUPPLEMENTARY INFORMATION

Contents of Supplementary Information (in a merged PDF titled jacksonsuppinfo.pdf; Size: 0.7 MB total):

The file contains a Supplementary Discussion that gives a model of the Samoan EM2 source, including calculations and assumptions. The file also contains a Supplementary Table 1 and a Supplementary Table 2 that together provide the model parameters used to calculate the depleted Ta'u and EM2 Samoan sources, respectively. The file also contains a Supplementary Table 3 that provides the new Samoan geochemical data. Four supplementary figures also are included in the file: Supplementary Figure 1 shows new helium isotope data from the remarkably enriched Samoan lavas; Supplementary Figure 2 is an expanded view of main text Figure 1, and shows the composition of the Samoan lavas in the context of individual samples from the upper continental crust; Supplementary Figure 3 compares the spidergram of a model melt of the EM2 source with the spidergram of an isotopically-enriched Samoan EM2 lava. Supplementary Figure 4 provides a model that explains the correlation between SiO_2 and $^{87}Sr/^{86}Sr$ in lavas from dredge ALIA D115.

1. Supplementary Discussion

Recycled UCC in the Samoan EM2 mantle. The standard model for the genesis of the EM2 reservoir suggests a role for recycled sediment, probably terrigenous in origin[1-7]. However, a number of problems with the standard model were outlined in ref. 8, and an alternative origin of the Samoan EM2 source (recycled, metasomatized lithosphere) was proposed. In light of the remarkably enriched Samoan lavas presented in this paper, we reconsider the arguments against a recycled terrigenous component in the EM2 plume. We demonstrate that recycled upper continental crust (UCC) can have an important role in the origin of the EM2 source. However, we maintain that it is (most likely) not "upper continental crust" (UCC) that is being recycled, but sediment with a composition resembling that of UCC. While the sediment recycling model presented here does not invalidate the metasomatic model for the lavas presented earlier[8], the new lavas presented in this study are consistent with a recycled sediment component.

The problems with recycled marine sediment in the Samoan EM2 mantle source (as outlined in ref. 8) are as follows. The variation in $^{187}Os/^{188}Os$ in Samoan lavas is not consistent with mixing between recycled marine sediment and depleted MORB mantle (DMM). Such a scenario would require 35% marine sediment in the EM2 source, a quantity not observed in the trace element patterns of Samoan basalts. Additionally, the smooth trace element spidergrams observed in Samoan EM2 lavas were suggested to be inconsistent with a sediment component in the Samoan EM2 source. This is because, unlike Samoan EM2 lavas presented earlier[8], marine sediments exhibit "jagged" spidergrams, marked by large negative anomalies for Nb (and Ta), Ti and Eu and large positive anomalies for Pb (and K). It was also noted that EM2 lavas exhibit negative Ba-

anomalies, a feature not characteristic of marine sediments[8]. Furthermore, because EM2 lavas exhibit high $^{3}He/^{4}He$ ratios (~8 Ra, ratio to atmosphere, or $\sim 1.4\times10^{-6}$), a trait not shared with the low $^{3}He/^{4}He$ ratios in sediments (0.05-1 Ra)[9] and continental crust (0.007 Ra)[10], it was suggested that the Samoan EM2 source does not host a sediment component[8]. Finally, Pb-isotope composition of modern marine sediment was observed to be unsuitable as an endmember for the enriched Samoan basalts[8]: Modern marine sediments exhibit $^{208}Pb/^{204}Pb$ ratios that are too low at a given $^{206}Pb/^{204}Pb$ to serve as mixing endmembers for the Samoan EM2 lavas.

Below, we suggest that, instead of a marine sediment composition such as GLOSS (Global Subducting Sediment[11]), sediment with a composition like UCC (a composition here approximated by UCC from ref. 12) is more suitable for generating a source sampled by the most isotopically-enriched Samoan lavas. A small portion (~5%) of (sediment with the composition of) UCC mixed with a depleted Samoan plume component generates a peridotite that, when melted, produces a spidergram similar to that observed in the most isotopically-enriched Samoan lavas. Like Samoan EM2 lavas, UCC exhibits a negative Ba anomaly, a feature not shared with GLOSS[11]. Furthermore, published Os-isotopes[8] in enriched Samoan EM2 lavas are not inconsistent with a UCC component in the plume. The Os-isotope signature in Samoan basalts is not likely a result of mixing between DMM ($^{187}Os/^{188}Os = 0.125$) and marine sediment; however, a mixture of UCC ($^{187}Os/^{188}Os = 1.05$, [Os] = 30 ppt[13]) and a depleted Samoan plume component generates a mixing trend that describes the Os-isotope data for Samoan shield basalts (excluding samples with <100 ppt Os, and assuming measurement precision of ±1.5% in data from ref. 8). This mixing scenario uses measured Ta'u $^{187}Os/^{188}Os$ ratios

of 0.129[8] and assumes that the Ta'u peridotite source also has Os concentrations that are depleted relative to primitive mantle (>3,900 ppt[14]). Moreover, new helium isotope data for Samoan EM2 lavas exhibit low ratios (<5 Ra) that plot on a trajectory that trends to UCC, and are consistent with the existence of a recycled UCC component in the Samoan plume (Supplementary Figure 1). Finally, our model for the formation of the EM2 mantle agrees with Pb-isotope constraints. UCC exhibits a large range of Pb-isotope values, and the Samoan EM2 lavas exhibit Pb-isotope values that plot in the field previously defined for UCC[15].

Model for the EM2 source. In order to model the generation of the mantle source sampled by the new Samoan EM2 lavas, we take advantage of the array formed by Samoan basalts in $^{87}Sr/^{86}Sr$–$^{143}Nd/^{144}Nd$ isotope space. The array suggests that the most enriched Samoan basalts were formed as products of mantle-mixing between a depleted component (here represented by the mantle source sampled by the isotopically-depleted and remarkably homogeneous lavas from Ta'u island) and a component similar to UCC (Supplementary Figure 2). In order to determine the proportion of UCC in the Samoan plume, we first calculate a trace element peridotite source for the depleted Ta'u endmember that is consistent with the radiogenic isotopes of Nd, Hf, Sr and Pb. We then determine the amount of UCC that must be added to the depleted Ta'u peridotite source so that the final mixture, an enriched peridotite, can be melted to generate a spidergram similar to the new Samoan EM2 lavas.

In the following modeling exercise, we generate a model for the EM2 source that describes the array formed by the most isotopically-enriched submarine Savai'i lavas from dredge D115, and we make no attempt to model the other components previously

identified[8] in lavas from the Samoan hotspot. We emphasize that the model is just one possible model that is consistent with the isotopes and trace elements in Samoan EM2 lavas. The model is presented only to demonstrate that recycling sediment into Samoan EM2 lavas is possible.

Composition of the depleted Ta'u peridotite source. Following ref. 8, we generate an average olivine fractionation corrected trace element budget for Ta'u lavas (Supplementary Figure 3 and Supplementary Table 1). In order to determine a trace element mantle source sampled by the average Ta'u lava composition, we first assume a peridotite source lithology, an aggregated fractional melting model, and we adopt mineral-melt partition coefficients from ref. 16 (Supplementary Table 1). We also assume a two-stage isotope model for the evolution of the depleted Ta'u source, and that this differentiation event of a primitive mantle composition occurred at 1.8 Ga. This age is commonly quoted as the average mantle differentiation age[17], and is an age that is consistent with the array formed by Ta'u lavas in $^{207}Pb/^{204}Pb$ vs. $^{206}Pb/^{204}Pb$ isotope space (see Fig. 7 in ref. 8). Given these assumptions, a Ta'u source is calculated so that parent-daughter ratios—Sm/Nd and Lu/Hf—will generate the present-day depleted $^{143}Nd/^{144}Nd$ (Ta'u average is 0.512789[8]) and $^{176}Hf/^{177}Hf$ (Ta'u average is 0.282987[18]) isotopes measured in Ta'u lavas given the two-stage isotope model. The Ta'u source is not very sensitive to its age of formation: ages of 1.0-2.5 Ga require only small variations in melting—4.5 to 5.5%—to generate the average Ta'u lava. However, assuming a formation age of 1.8 Ga, a 5.1% melt (with ~50.6% garnet melting) of the hypothetical Ta'u source will generate a model melt with a spidergram that is both identical to the average measured Ta'u lava and consistent with isotopic constraints. These highly

specific melting parameters are presented only to generate an average Ta'u source that is consistent with isotopic constraints, and by presenting them we are not suggesting such precise knowledge of the actual mantle "plumbing" beneath Ta'u island.

The $^{87}Sr/^{86}Sr$ of primitive mantle is unconstrained, so it is not possible to evaluate whether the $^{87}Sr/^{86}Sr$ measured in Ta'u lavas is enriched or depleted relative to primitive mantle. However, the average $^{87}Sr/^{86}Sr$ in Ta'u lavas (0.704650) and the Rb/Sr of the Ta'u source (0.0268) can be modeled as having evolved from primitive mantle at 1.8 Ga if the present-day primitive mantle $^{87}Sr/^{86}Sr$ is 0.70508, a value that is in the range typically assigned to primitive mantle. In order for the two-stage isotope model to produce the observed average Ta'u $^{206}Pb/^{204}Pb$ (19.271) and $^{206}Pb/^{204}Pb$ (15.597) (excluding T14 and considering only Tl-spiked data[8]), the proportion of sulfide[19] in the Ta'u source mineralogy is adjusted to obtain an appropriate parent-daughter U/Pb source ratio. The resulting calculated Th/Pb source ratio is within error of the Th/Pb ratio required to produce the average Ta'u $^{208}Pb/^{204}Pb$ composition (39.424) in 1.8 Ga. While non-unique (a different melt model could be chosen or the Ta'u source formation age may be different, etc.), the trace element source calculated from Ta'u lavas is consistent (within the uncertainties of the data) with constraints from radiogenic isotopes.

Generation of a source for the Samoan EM2 lavas. Determining the precise nature of the recycled component contributing to the enrichment in the Samoan plume is not straightforward. UCC rocks and individual marine sediment cores show a large degree of trace element heterogeneity that varies considerably with geography and provenance[11,12], and the composition of a recycled sediment may depend on the geography of the subduction zone. More problematic is the issue of temporal variability[20,21]: the trace

element budgets of sediments encountered in modern oceans may be poor analogues for the sediments subducted in the past. Finally, the poorly constrained processes operating in subduction zones, including fluid loss and/or melting of sediments, may modify the composition of the subducted sediment component[22-25].

With these caveats aside, we take a simple approach. We assume that the compositions of subducted material are conserved in the subduction zone. Perhaps fluids and melts are removed from the slab and inoculated into the mantle wedge; but the resulting slab residue and the fertilized mantle wedge may in some cases stay together as a package. This package is what enters the general circulation, to eventually be remixed to end up looking like "closed system" slab recycling. While the composition of the original material sent into the subduction zone is underconstrained, we explore whether or not a modern UCC composition, when mixed with the depleted Ta'u source, can generate a suitable source for the Samoan EM2 lava D115-18. We assume that after the depleted Ta'u source mixed completely with the enriched UCC component, the resulting peridotite (treated here as a single lithology) was melted in a modal, aggregated fractional melting system. The modal abundances of the mantle phases, the contribution of UCC to the depleted Ta'u source, and the degree of melting (and the proportion of garnet and spinel melting) of the resulting mixture (the EM2 source) are all adjusted to generate a trace element spidergram that is similar to the enriched Samoan EM2 basalts. The combination of these parameters that generates a "best-fit" spidergram to the Samoan EM2 lava composition is given in Supplementary Table 2. The agreement between the model spidergram and the spidergram for Samoan EM2 lava D115-18 is optimized (the

fit is within 14% for all the trace elements considered, or ~11% if U is excluded) when the contribution of the UCC component is ~5%.

Having fixed the proportions of UCC (5%) and the depleted Ta'u source (95%) in the EM2 source sampled by lava D115-18 (with $^{87}Sr/^{86}Sr$ and $^{143}Nd/^{144}Nd$ of 0.718592 and 0.512314, respectively), we use trace element budgets and isotopic constraints to calculate the $^{87}Sr/^{86}Sr$ and $^{143}Nd/^{144}Nd$ of the UCC component. Assuming a measured isotopic ($^{87}Sr/^{86}Sr = 0.704650$ and $^{143}Nd/^{144}Nd = 0.512789$) and calculated trace element composition (Supplementary Table 1) of the Ta'u source and a trace element composition of UCC[12], we calculate the Sr and Nd isotopic composition of the UCC component in the Samoan plume to be 0.7421 and 0.5117, respectively. The $^{87}Sr/^{86}Sr$ and $^{143}Nd/^{144}Nd$ values calculated for the UCC endmember in the Samoan plume are within the range of values measured in ancient UCC shield rocks[26] (Supplementary Figure 2).

While the addition of UCC to the depleted Ta'u source generates a spidergram that is a close match to Samoan EM2 lavas, the fit is not perfect. In particular, the element that exhibits the least perfect fit to the data is U. Samoan EM2 lavas have lower U concentrations than the model result, and the disagreement may be a result of U-loss during weathering (note the high Th/U in sample D115-18; Supplementary Table 3).

Addressing contamination by marine sediment. Implicit in the model of the EM2 source is the assumption that the sediment signature in the Samoan EM2 lavas is a primary mantle signal and not a result of shallow-level sediment contamination. A plot of $\Delta^{207}Pb/^{204}Pb–\Delta^{208}Pb/^{204}Pb$ (see Main Text Figure 4) indicates that sediment contamination is not an issue. Further evidence comes from $^{87}Sr/^{86}Sr$ measurements in sediments from the Samoan region, which exhibit $^{87}Sr/^{86}Sr$ ratios (0.70614 to 0.70824)

that are much lower than the most enriched Samoan EM2 lavas (0.72047 in whole-rock sample D115-21). It is very difficult to generate the high $^{87}Sr/^{86}Sr$ observed in the new Samoan EM2 lavas by sediment contamination. For example, the GLOSS average $^{87}Sr/^{86}Sr$ composition is only 0.7173 (327 ppm Sr)[11], a value that is much lower than the most isotopically-enriched lavas from Samoa. Even if the most isotopically-enriched marine sediment ($^{87}Sr/^{86}Sr$ = 0.73493, 251 ppm Sr) in the compilation from ref. 11 were added to the least isotopically-enriched submarine Savai'i lava ($^{87}Sr/^{86}Sr$ = 0.705435, 374 ppm Sr), over 60% sediment assimilation would be required to generate the most radiogenic $^{87}Sr/^{86}Sr$ observed in the Samoan lavas. Such large quantities of sediment are not visible in the trace element spidergrams of the most enriched Samoan lavas.

In general, Samoan lavas do not show a correlation between $^{87}Sr/^{86}Sr$ and SiO_2 (Supplementary Figure 4). However, $^{87}Sr/^{86}Sr$ ratios in whole-rock lavas from dredge D115 do correlate with SiO_2. Having ruled out sediment assimilation using Sr and Pb isotope data, the $^{87}Sr/^{86}Sr$ – SiO_2 array formed by ALIA D115 samples is interpreted to be a result of magma mixing between an evolved (high SiO_2), isotopically-enriched magma and a less evolved, less isotopically-enriched magma. Other major and trace element data are consistent with this scenario (see Supplementary Figure 4). Perhaps the isotopically-enriched magmatic endmember evolved by crystal fractionation in a magma chamber and, just before eruption, mixed with a later pulse of a less evolved, less isotopically-enriched magma. Magma mixing is not an uncommon phenomenon; heterogeneous $^{87}Sr/^{86}Sr$ ratios recorded in olivine-hosted melt inclusions from individual Samoan basalt samples suggest that mixing of magmas from isotopically-distinct sources is not uncommon in Samoa[27].

Data sources for HIMU and EM1 lavas. In Fig. 2 and Fig. 4 of the main text, trace element and Pb-isotope data for the HIMU endmember are from samples collected at Mangaia and Tubuai islands and are reported in refs. 41 and 42. Trace element and Pb-isotope data from the EM1 endmember are from samples collected at Pitcairn and include data from ref. 43 and unpublished data (S.R. Hart and E.H. Hauri). Only data from the freshest, most isotopically-extreme samples were used.

References Cited

1. White, W.M. & Hofmann, A.W. Sr and Nd isotope geochemistry of oceanic basalts and mantle evolution. *Nature* **296**, 821-825 (1982).

2. Zindler, A. & Hart, S.R. Chemical Geodynamics. *Ann. Rev. Earth Planet. Sci.* **14**, 493–571 (1986).

3. Allegre, C.J. & Turcotte, D.L. Geodynamic mixing in the mesosphere boundary layer and the origin of oceanic islands. *Geophys. Res. Lett.* **12**, 207-210 (1985).

4. Cohen, R.S. & O'Nions, R.K. Identification of recycled continental material in the mantle from Sr, Nd and Pb isotope investigations. *Earth Planet. Sci. Lett.* **61**, 73-84 (1982).

5. Hawkesworth, C.J., Norry, M.J., Roddick, J.C. & Vollmer, R. $^{143}Nd/^{144}Nd$ and $^{87}Sr/^{86}Sr$ ratios from the Azores and their significance in LIL-element enriched mantle. *Nature* **280**, 28-31 (1979).

6. Hofmann, A.W. Mantle geochemistry: The message from oceanic volcanism. *Nature* **385**, 219–229 (1997).

7. Weaver, B.L. The origin of ocean island basalt end-member compositions: Trace element and isotopic constraints. *Earth Planet. Sci. Lett.* **104**, 381–397 (1991).

8. Workman, R.K. *et al.* Recycled metasomatized lithosphere as the origin of the Enriched Mantle II (EM2) endmember: evidence from the Samoan volcanic chain. *Geochem. Geophys. Geosyst.* **5**, 10.1029/2003GC000623 (2004).

9. Podosek, F.A., Honda, M. & Ozima M. Sedimentary noble gases. *Geochim. Cosmochim. Acta* **44**, 1875–1884 (1980).

10. Ballentine, C.J. & Burnard, P.G. Production, release and transport of noble gases in the continental crust. *Rev. Min. Geochem.* **47**, 481–538 (2002).

11. Plank, T. & Langmuir, C.H. The chemical composition of subducting sediment and its consequences for the crust and mantle. *Chemical Geology* **145**, 325–394 (1998).

12. Rudnick, R. L. & Gao, S. in *The Crust* (ed. Rudnick, R. L.) 1-64, Vol. 3 of *Treatise in Geochemistry* (Elsevier, Amsterdam, 2003).

13. Peucker-Ehrenbrink, B. & Jahn, B.M. Rhenium osmium isotope systematics and platinum group element concentrations: Loess and the upper continental crust, *Geochem. Geophys. Geosyst.* **2**, 10.1029/2001GC000172 (2001).

14. Becker, H. *et al.* Highly siderophile element composition of the Earth's primitive upper mantle: constraints from new data on peridotite massifs and xenoliths. *Geochim. Cosmochim. Acta.* **70**, 4528-4550 (2006).

15. Zartman, R.E. & Doe, B.R. Plumbotectonics—The model. *Tectonophysics* **75**, 135-142 (1981).

16. Kelemen, P.B., Yogodzinski, G.M. & Scholl, D.W. in *Inside the Subduction Factory* (ed Eiler, J.) 223-276 (Geophys. Monogr. 138, AGU, Washington DC, 2004).

17. Hart, S. R. A large-scale isotope anomaly in the Southern Hemisphere mantle. *Nature* **309**, 753-57 (1984).

18. Salters, V. Coupled Trace Element and Isotope Variations in Oceanic Basalts: recycling re-examined. *EOS* **86**, Abstract V41D-1486 (2005).

19. Hart, S.R. & Gaetani, G.A. Mantle Pb paradoxes: the sulfide solution. *Contrib. Mineral. Petrol.* **152**, 295–308 (2006).

20. Ronov, A.B., Khain, V.E., Balukhovsky, A.N. & Seslavinsky, K.B. Quantitative analysis of Phanerozoic sedimentation. *Sedimentary Geology* **25**, 311-325 (1980).

21. Wilkinson, B.H. & Walker, J.C.G. Phanerozoic cycling of sedimentary carbonate. *Am. J. Sci.* **289**, 525-548 (1989).

22. Kelley, K.A., Plank, T., Farr, L., Ludden, J. & Staudigel, H. Subduction cycling of U, Th, and Pb. *Earth Planet. Sci. Lett.* **234**, 369-383 (2005).

23. Kessel, R., Schmidt, M.W., Ulmer, P. & Pettke, T. Trace element signature of subduction-zone fluids, melts and supercritical liquids at 120-180 km depth. *Nature* **437**, 724-727 (2005).

24. Johnson, M.C. & Plank, T. Dehydration and melting experiments constrain the fate of subducted sediments. *Geochem. Geophys. Geosyst.* **1**, 10.1029/1999GC000014 (1999).

25. Elliott, T., Plank, T., Zindler, A., White, W. & Bourdon, B. Element transport from slab to volcanic front at the Mariana Arc. *J. Geophys. Res.* **102**, 14991-15019 (1997).

26. McColluch, M.T. & Wasserburg, G.J. Sm-Nd and Rb-Sr chronology of continental crust formation. *Science* **200**, 1003-1011 (1978).

27. Jackson, M.G. & Hart, S.R. Strontium isotopes in melt inclusions from Samoan basalts: implications for heterogeneity in the Samoan plume. *Earth Planet. Sci. Lett.* **245**, 260–277 (2006).

28. McDonough, W.F. & Sun, S.S. The composition of the Earth. *Chem. Geol.* **120**, 223–253 (1995).

29. Hofmann, A.W. & White, W.M. Ba, Rb and Cs in the Earth's mantle. *Zeitschrift fur Naturforschung* **38**, 256–266 (1983).

30. Hart, S.R. & Blusztajn, J. Age and geochemistry of the mafic sills, ODP site 1276, Newfoundland margin. *Chem. Geol.* **235**, 222-237 (2006).

31. Hooper, P.R. & Johnson, D.M., Conrey, R.M. Major and trace element analyses of rocks and minerals by automated X-ray spectrometry, Washington State Univ. open-file report, Pullman (1993).

32. Govindaraju, K. Compilation of working values and sample description for 383 geostandards. *Geostandards Newsletter* **18**, 1-158 (1994).

33. Govindaraju, K. Working values with confidence limits for twenty-six CRPG, ANRT and IWG-GIT geostandards. *Geostandards Newsletter* **19**, 1-32 (1995).

34. Taras, B.D. & Hart, S.R. Geochemical evolution of the New England seamount chain: isotopic and trace-element constraints. *Chem. Geol.* **64**, 35-54 (1987).

35. Galer, S.J.G. *Chemical and isotopic studies of crust–mantle differentiation and the generation of mantle heterogeneity*, Thesis, Univ. of Cambridge (1986).

36. Abouchami, W., Galer, S.J.G., & Koschinsky, A. Pb and Nd isotopes in NE Atlantic Fe–Mn crusts: proxies for trace metal paleosources and paleocean circulation. *Geochim Cosmochim Acta* **63**, 1489–1505 (1999).

37. Todt, W., Cliff, R.A., Hanser, A. & Hofmann, A.W. in *Earth Processes: Reading the Isotopic Code Geophysical Monograph* (eds Basu, A. & Hart, S.R.) 429-437 (Geophys. Monogr. 95, AGU, Washington DC, 1996).

38. Hart, S.R., Workman, R.K., Coetzee, M., Blusztajn, J., Ball, L. & Johnson, K.T.M. The Pb isotope pedigree of Western Samoan Volcanics: new insights from high-precision analysis by NEPTUNE ICP/MS. *EOS* **83**, Abstract F20 (2002).

39. Kurz, M.D., Curtice, J.C., Lott, D.E. & Solow, A. Rapid helium isotopic variability in Mauna Kea shield lavas from the Hawaiian Scientific Drilling Project. *Geochem. Geophys. Geosyst.* **4**, 10.1029/2002GC000439 (2004).

40. Farley, K.A., Natland, J.H. & Craig, H. Binary mixing of enriched and undegassed (primitive?) mantle components (He, Sr, Nd, Pb) in Samoan lavas. *Earth Planet. Sci. Lett.* **111** 193-199 (1992).

41. Hauri, E.H. & Hart, S.R. Re-Os isotope systematics of HIMU and EMII oceanic island basalts from the south Pacific Ocean. *Earth Planet. Sci. Lett.* **114**, 353-371 (1993).

42. Woodhead, J.D. Extreme HIMU in an oceanic setting: the geochemistry of Mangaia Island (Polynesia), and temporal evolution of the Cook-Austral hotspot. *J. Volcanol. Geotherm. Res.* **72**, 1-19 (1996).

43. Eisele, J., Sharma, M., Galer, S.J.G., Blichert-Toft, J., Devey, C.W. & Hofmann, A.W. The role of sediment recycling in EM-1 inferred from Os, Pb, Hf, Nd, Sr isotope and trace element systematics of the Pitcairn hotspot. *Earth Planet. Sci. Lett.* **196**, 197-212 (2002).

2. Supplementary Figures

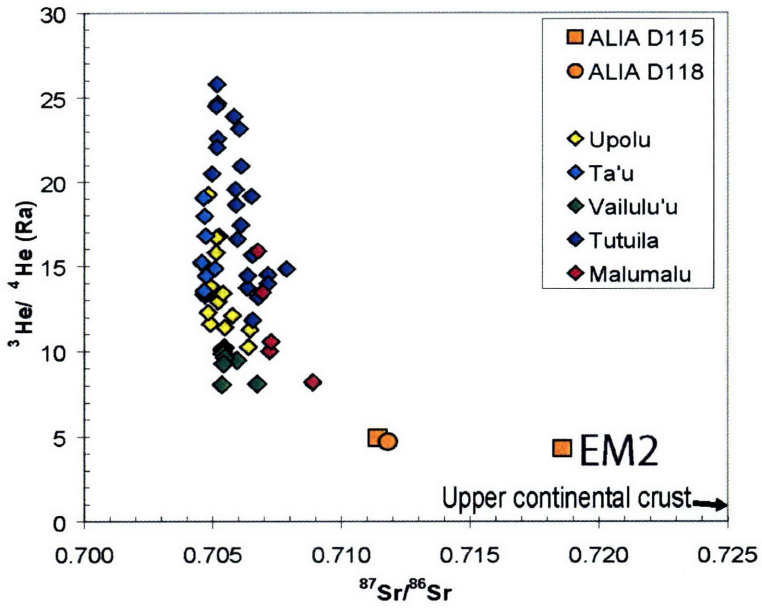

Supplementary Figure 1 $^{87}Sr/^{86}Sr$ vs. $^{3}He/^{4}He$ isotopes in Samoan basalts. New $^{3}He/^{4}He$ ratios in the enriched Samoan EM2 basalts are low (<5 Ra), and plot on a trajectory that extrapolates to a UCC component with low $^{3}He/^{4}He$ (0.007 Ra)[10] and high $^{87}Sr/^{86}Sr$ (0.7421). Data for the other Samoan islands and seamounts are from refs 8 and 40.

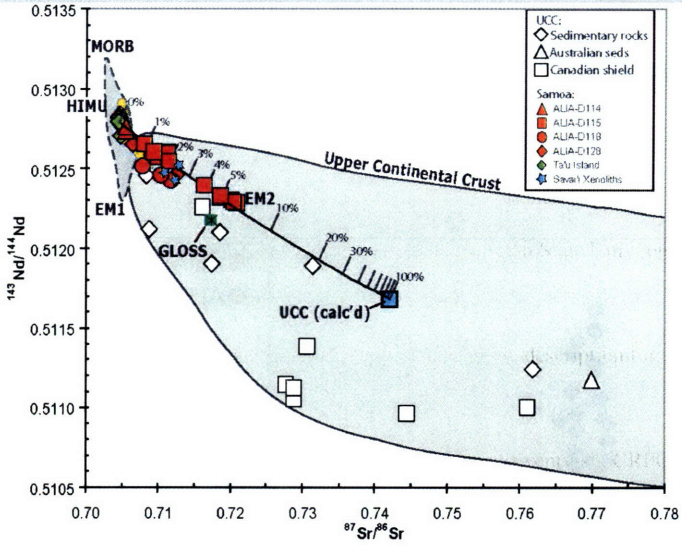

Supplementary Figure 2 $^{87}Sr/^{86}Sr$ vs. $^{143}Nd/^{144}Nd$ of Samoan shield basalts compared with samples from upper continental crust (UCC) from ref. 26. The grey field (with solid outline) encompasses Sr and Nd isotopic analyses on UCC samples[26], and extends outside of the figure to values of 1.1862 and 0.51023, respectively. The grey field (with dashed outline) encompasses the non-Samoan OIB field. The orange field describes Samoan shield basalts observed in previous studies; the new Samoan EM2 basalts (red) extend well into the field for UCC. Tic marks represent addition of the UCC component to the depleted peridotite Ta'u source. The isotopic composition of the UCC endmember in the Samoan plume is calculated to have $^{87}Sr/^{86}Sr$ and $^{143}Nd/^{144}Nd$ of 0.7421 and 0.5117, respectively (light blue box, see Supplementary Discussion), and lies in the range of values previously measured on UCC rocks[26]. 5% of this hypothetical UCC composition is required to generate the spidergram of Samoan sample D115-18 (and an estimated 6% UCC is required to generate the $^{87}Sr/^{86}Sr$ ratios in the most enriched cpx from sample D115-21).

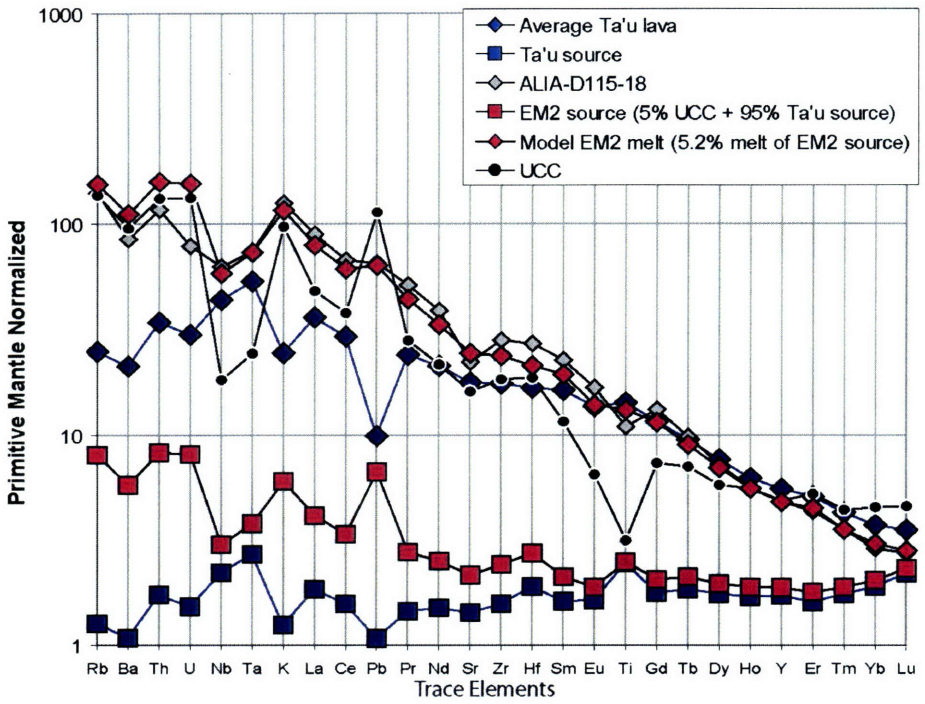

Supplementary Figure 3 Primitive mantle[28] normalized trace element patterns for Samoan basalts and peridotite sources. These compositions are used in a sediment recycling model for generating a Samoan EM2 mantle source. Ta'u lavas are assumed to be melts of a depleted plume component, and the average, olivine-fractionation corrected Ta'u lava composition is plotted. A Ta'u source for the average Ta'u lava is calculated to satisfy isotopic constraints. 5% of UCC[12] is added to 95% of the Ta'u source to make the EM2 source sampled by the Samoan lava D115-18, and the model melt of the EM2 peridotite source is plotted. The spidergram of the model melt is similar to sample D115-18 (the second most isotopically-enriched Samoan sample). The most isotopically-enriched lava, D115-21, is too evolved to reliably reconstruct its trace element composition. Plotted compositions can be found in Supplementary Tables 1 & 2.

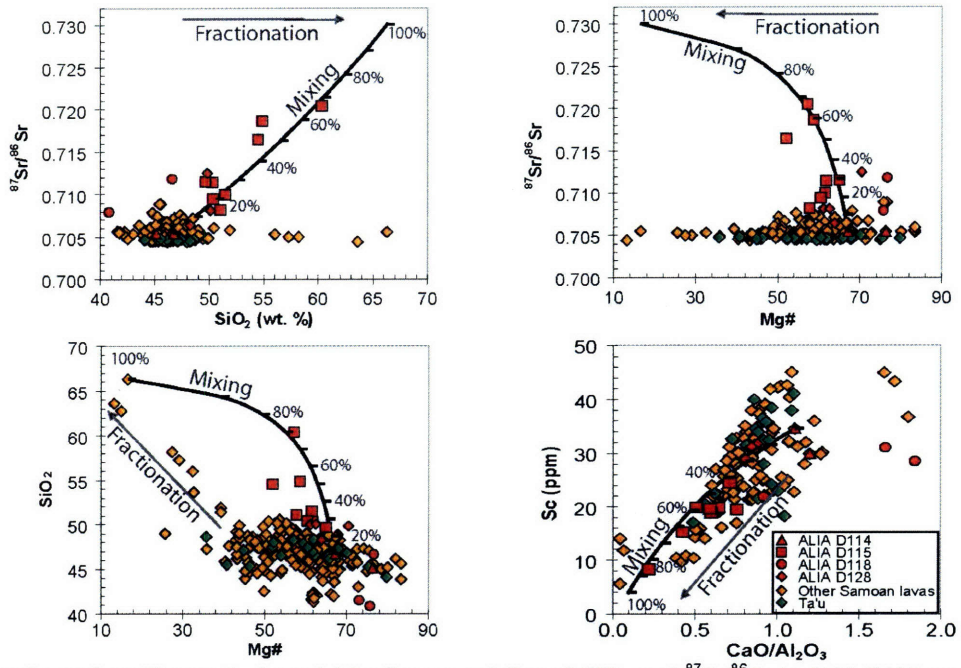

Supplementary Figure 4 A model for the co-variation of SiO_2 and $^{87}Sr/^{86}Sr$ in ALIA D115 samples. Samoan lavas do not exhibit a one-to-one relationship between SiO_2 (or Mg#) and $^{87}Sr/^{86}Sr$; evolved Samoan lavas exhibit both high (up to 0.7205) and low (0.7044) $^{87}Sr/^{86}Sr$ ratios. However, lavas from dredge ALIA D115 exhibit a correlation between $^{87}Sr/^{86}Sr$ and SiO_2. We explain this correlation in ALIA D115 lavas as a result of mixing between a highly evolved, isotopically-enriched magma and a less evolved, less isotopically-enriched magma. In this scenario, the mixing endmembers are a Savai'i submarine lava sample (ALIA D114-01; Supplementary Table 3) and a highly evolved lava from Tutuila (91TP-128; SiO_2 = 66.30 wt.%, MgO = 0.41 wt.%, FeO = 4.06 wt.%, CaO = 1.62 wt.%, Al_2O_3 = 17.03 wt.%, Sr = 395 ppm; Natland unpubl. data). The measured $^{87}Sr/^{86}Sr$ of the Tutuila lava is 0.705535[8]. However, for the sake of argument, this sample is given an $^{87}Sr/^{86}Sr$ ratio of 0.730 in the mixing model in order to determine whether mixing between an evolved magma and a less evolved magma can generate a mixing array consistent with the data from dredge ALIA D115. Sc was not measured on the Tutuila lava, but its concentration is assumed to be 4 ppm. The reduction of Sc and CaO/Al_2O_3 (including reduced Mg#'s and increased SiO_2) in the most isotopically-enriched lavas from ALIA D115 is consistent with cpx fractionation. Crystal fractionation of an isotopically-enriched magma followed by mixing with a less evolved, less isotopically-enriched magma describes the geochemical data from dredge ALIA D115.

3. Supplementary Tables

Supplementary Table 1. Calculation of the depleted component in the Samoan plume, using lavas from Ta'u island

	Primitive mantle[1]	Avg. Ta'u lava[2] (olivine corr'd to Fo_{90})	Variability in 18 Ta'u lavas (1σ, std. dev., %)	Bulk partition coefs[3] (garnet field)	Bulk partition coefs[3] (spinel field)	Depleted Ta'u source[4] (calculated from avg. Ta'u lava)
Rb	0.6	14.9	16.5	0.000144	0.000124	0.759
Ba	6.6	140	11.9	0.000144	0.000124	7.14
Th	0.0795	2.71	13.4	0.00219	0.00178	0.138 (0.117)[5]
U	0.0203	0.61	12.7	0.00074	0.00018	0.0309
Nb	0.658	28.53	11.5	0.00393	0.00302	1.45
Ta	0.037	1.97	11.7	0.00393	0.00302	0.10
K	240	5860	9.8	0.00150	0.00128	299
La	0.648	23.27	11.0	0.0114	0.00983	1.20
Ce	1.675	48.93	10.3	0.0191	0.0161	2.64
Pb	0.15	1.49	18.4	0.0834	0.0816	0.161
Pr	0.254	6.09	10.0	0.0314	0.0247	0.368
Nd	1.25	26.58	9.1	0.0463	0.0357	1.88
Sr	19.9	354.1	9.9	0.0665	0.0364	28.3
Zr	10.5	184	9.9	0.0867	0.0371	16.5
Hf	0.283	4.74	9.0	0.114	0.0607	0.538
Sm	0.406	6.64	7.8	0.0868	0.0574	0.657
Eu	0.154	2.10	7.9	0.121	0.0671	0.253
Ti	1205	17190	7.4	0.176	0.122	2960
Gd	0.544	6.32	7.8	0.179	0.0769	0.965
Tb	0.099	0.94	8.1	0.254	0.0876	0.18
Dy	0.674	5.17	8.2	0.316	0.0964	1.18
Ho	0.149	0.93	8.1	0.402	0.0972	0.25
Y	4.30	23.86	7.3	0.475	0.102	7.40
Er	0.438	2.24	7.3	0.481	0.105	0.70
Tm	0.068	0.29	7.2	0.673	0.110	0.12
Yb	0.441	1.65	7.1	0.865	0.115	0.84
Lu	0.0675	0.24	7.5	1.09	0.124	0.148

[1] Primitive mantle is from ref 28.

[2] Ta'u basalts (with MgO > 6.5 wt.%) used in the average lava composition include: T10, T16, T19, T22, T23, T25, T30, T32, T33, T44, T45, T46, T47, T48, T51, T54, T55, and 74-1. T14 is suspected of Pb contamination and is not included. The 18 Ta'u basalts were individually corrected for olivine fractionation to be in equilibrium with a mantle olivine composition of Fo_{90} (assuming Fe^{2+}/Fe_{total} is 0.90), trace element corrected, and then averaged.

[3] Bulk partition coefficients are calculated by assuming the following modal abundances: spinel stability field: 3.72% spinel, 17.8% clinopyroxene, 26% orthopyroxene, 52.39% olivine, 0.162% sulfide; garnet stability field: 10.7% garnet, 20.8% clinopyroxene, 13.4% orthopyroxene, 55.1% olivine, 0.161% sulfide. Mineral-melt partition coefficients are from ref. 16, with the following additions and modifications: Ba and Ta are assumed to have the same bulk partition coefficients as Rb and Nb, respectively; Tm and Sr are assumed to have a bulk partition coefficient that is the average of the elements that bracket them on the spidergram; the sulfide-melt partition coefficient for Pb is assumed to be 42. The mineral modes in the garnet and spinel stability fields are calculated to agree with a primitive mantle major element composition. Although the Ta'u source is slightly depleted, and therefore has suffered a small amount of melt extraction during its history, the low degree of melt extraction will not significanlty change the calculated mineral modes.

[4] The Ta'u source assumes that the average, olivine-fractionation corrected Ta'u lava resulted from a 5.1% modal aggregated fractional melt with a 50.6% melt contribution from the garnet stability field (and the remainder from the spinel stability field). This precise set of melting parameters allows the parent-daughter ratios (Lu/Hf and Sm/Nd) in the Ta'u source to be consistent with the $^{176}Hf/^{177}Hf$ and $^{143}Nd/^{144}Nd$ ratios measured in the Ta'u lavas (given a two-stage evolution model, with differentiation from primitive mantle at 1.8 Ga).

[5] The Th concentration in parenthesis, which yields a Th/Pb ratio of 0.727, provides a value required for the Ta'u source to be consistent with constraints from $^{208}Pb/^{204}Pb$ isotopes measured in Ta'u lavas. The other Th value for the Ta'u source is calculated by adjusting the modal sulfide abundance to give U/Pb ratios that are consistent with $^{206}Pb/^{204}Pb$ and $^{207}Pb/^{204}Pb$. This Th svalue (0.138) generates a Th/Pb ratio (0.855) that is within error (18%) of the measured Th/Pb variability (±23%) in Ta'u lavas, and is therefore (within uncertainty of the data available on Ta'u lavas) consistent with measured $^{208}Pb/^{204}Pb$ ratios.

3. Supplementary Tables

Supplementary Table 1. Calculation of the depleted component in the Samoan plume, using lavas from Ta'u island

	Primitive mantle[1]	Avg. Ta'u lava[2] (olivine corr'd to Fo_{90})	Variability in 18 Ta'u lavas (1σ, std. dev., %)	Bulk partition coefs[3] (garnet field)	Bulk partition coefs[3] (spinel field)	Depleted Ta'u source[4] (calculated from avg. Ta'u lava)
Rb	0.6	14.9	16.5	0.000144	0.000124	0.759
Ba	6.6	140	11.9	0.000144	0.000124	7.14
Th	0.0795	2.71	13.4	0.00219	0.00178	0.138 (0.117)[5]
U	0.0203	0.61	12.7	0.00074	0.00018	0.0309
Nb	0.658	28.53	11.5	0.00393	0.00302	1.45
Ta	0.037	1.97	11.7	0.00393	0.00302	0.10
K	240	5860	9.8	0.00150	0.00128	299
La	0.648	23.27	11.0	0.0114	0.00983	1.20
Ce	1.675	48.93	10.3	0.0191	0.0161	2.64
Pb	0.15	1.49	18.4	0.0834	0.0816	0.161
Pr	0.254	6.09	10.0	0.0314	0.0247	0.368
Nd	1.25	26.58	9.1	0.0463	0.0357	1.88
Sr	19.9	354.1	9.9	0.0665	0.0364	28.3
Zr	10.5	184	9.9	0.0867	0.0371	16.5
Hf	0.283	4.74	9.0	0.114	0.0607	0.538
Sm	0.406	6.64	7.8	0.0868	0.0574	0.657
Eu	0.154	2.10	7.9	0.121	0.0671	0.253
Ti	1205	17190	7.4	0.176	0.122	2960
Gd	0.544	6.32	7.8	0.179	0.0769	0.965
Tb	0.099	0.94	8.1	0.254	0.0876	0.18
Dy	0.674	5.17	8.2	0.316	0.0964	1.18
Ho	0.149	0.93	8.1	0.402	0.0972	0.25
Y	4.30	23.86	7.3	0.475	0.102	7.40
Er	0.438	2.24	7.3	0.481	0.105	0.70
Tm	0.068	0.29	7.2	0.673	0.110	0.12
Yb	0.441	1.65	7.1	0.865	0.115	0.84
Lu	0.0675	0.24	7.5	1.09	0.124	0.148

[1] Primitive mantle is from ref 28.

[2] Ta'u basalts (with MgO > 6.5 wt.%) used in the average lava composition include: T10, T16, T19, T22, T23, T25, T30, T32, T33, T44, T45, T46, T47, T48, T51, T54, T55, and 74-1. T14 is suspected of Pb contamination and is not included. The 18 Ta'u basalts were individually corrected for olivine fractionation to be in equilibrium with a mantle olivine composition of Fo_{90} (assuming Fe^{2+}/Fe_{total} is 0.90), trace element corrected, and then averaged.

[3] Bulk partition coefficients are calculated by assuming the following modal abundances: spinel stability field: 3.72% spinel, 17.8% clinopyroxene, 26% orthopyroxene, 52.39% olivine, 0.162% sulfide; garnet stability field: 10.7% garnet, 20.8% clinopyroxene, 13.4% orthopyroxene, 55.1% olivine, 0.161% sulfide. Mineral-melt partition coefficients are from ref. 16, with the following additions and modifications: Ba and Ta are assumed to have the same bulk partition coefficients as Rb and Nb, respectively; Tm and Sr are assumed to have a bulk partition coefficient that is the average of the elements that bracket them on the spidergram; the sulfide-melt partition coefficient for Pb is assumed to be 42. The mineral modes in the garnet and spinel stability fields are calculated to agree with a primitive mantle major element composition. Although the Ta'u source is slightly depleted, and therefore has suffered a small amount of melt extraction during its history, the low degree of melt extraction will not significanlty change the calculated mineral modes.

[4] The Ta'u source assumes that the average, olivine-fractionation corrected Ta'u lava resulted from a 5.1% modal aggregated fractional melt with a 50.6% melt contribution from the garnet stability field (and the remainder from the spinel stability field). This precise set of melting parameters allows the parent-daughter ratios (Lu/Hf and Sm/Nd) in the Ta'u source to be consistent with the $^{176}Hf/^{177}Hf$ and $^{143}Nd/^{144}Nd$ ratios measured in the Ta'u lavas (given a two-stage evolution model, with differentiation from primitive mantle at 1.8 Ga).

[5] The Th concentration in parenthesis, which yields a Th/Pb ratio of 0.727, provides a value required for the Ta'u source to be consistent with constraints from $^{208}Pb/^{204}Pb$ isotopes measured in Ta'u lavas. The other Th value for the Ta'u source is calculated by adjusting the modal sulfide abundance to give U/Pb ratios that are consistent with $^{206}Pb/^{204}Pb$ and $^{207}Pb/^{204}Pb$. This Th svalue (0.138) generates a Th/Pb ratio (0.855) that is within error (18%) of the measured Th/Pb variability (±23%) in Ta'u lavas, and is therefore (within uncertainty of the data available on Ta'u lavas) consistent with measured $^{208}Pb/^{204}Pb$ ratios.

Supplementary Table 3. Isotope, major and trace element analyses for Samoan (submarine Savai'i) lavas and mineral separates, including sediment cores and a ferromanganese crust from the Samoan region.

Sample ID	D114-01	D114-03	D115-03	D115-07	D115-18	D115-18 rep[1]	D115-20	D115-21	D115-22	D115-26	D115-28	D118-13	D118-22	D118-23	D128-01	D128-17	D128-19	D128-21	RC 13-43[2]	VM-19-253[2]	RC-12-207[2]	D118-22crust[3]	W-2	BHVO-1
Latitude (°S)	13.875	13.875	14.090	14.090	14.090	14.090	14.090	14.090	14.090	14.090	14.090	13.325	13.325	13.325	13.213	13.213	13.213	13.213	12.25	12.233	14.617	13.325		
Longitude (°W)	172.724	172.724	172.898	172.898	172.898	172.898	172.898	172.898	172.898	172.898	172.898	173.430	173.430	173.430	172.093	172.093	172.093	172.093	171.683	169	168.5	173.430		
Water Depth (m)	2490	2490	3220	3220	3220	3220	3220	3220	3220	3220	3220	2660	2660	2660	2560	2560	2560	2560	4872	5286	5037	2660		
Lithology	Basalt	Picrite	Hawaiite	Basalt	Trachybasalt		Hawaiite	Trachy-andesite	Basalt	Trachy-basalt	Hawaiite	Alkali basalt	Alkali basalt	Alkali basalt	Basalt	Basalt	Basalt	Basalt	sediment	sediment	sediment	Fe-Mn crust		
SiO_2	46.38	44.82	49.18	46.30	52.28		48.65	57.20	47.38	51.88	50.00	39.82	39.71	42.23	48.94	47.73	46.36	48.95	35.62					
Al_2O_3	10.00	7.42	12.59	11.53	14.20		13.16	14.63	12.64	14.26	13.44	7.66	7.42	7.81	12.68	12.07	12.61	12.11	9.85					
TiO_2	4.00	3.00	3.50	3.13	2.45		3.55	1.72	3.43	2.71	3.30	3.46	3.20	2.21	2.80	3.09	2.85	2.28	2.23					
FeO*[4]	11.78	12.33	9.74	9.19	7.09		9.13	5.35	9.85	7.46	7.88	12.06	10.82	10.08	9.73	11.31	9.81	9.67	8.28					
MnO	0.18	0.18	0.13	0.13	0.07		0.13	0.05	0.12	0.09	0.12	0.19	0.15	0.11	0.17	0.17	0.16	0.17	0.23					
CaO	11.08	8.89	8.17	8.75	6.08		7.89	3.21	7.47	7.27	9.62	12.70	13.68	7.26	10.58	10.60	10.54	9.81	12.81					
MgO	12.16	20.07	7.97	8.63	5.09		6.34	3.61	7.47	4.08	6.37	16.63	17.13	16.74	9.22	10.10	7.88	11.65	6.86					
K_2O	1.13	0.83	3.09	2.68	4.01		2.57	5.05	2.31	3.52	2.73	1.01	1.32	0.99	1.58	1.33	1.56	1.23	1.26					
Na_2O	2.09	1.55	2.85	2.41	3.64		3.32	3.68	3.11	3.50	3.15	1.58	1.78	2.61	2.41	2.15	2.40	2.12	3.78					
P_2O_5	0.48	0.36	0.51	0.45	0.36		0.61	0.31	0.52	0.42	0.52	0.81	0.61	0.48	0.37	0.35	0.36	0.25	0.31					
Pre-total	99.28	99.65	97.73	93.21	95.28		95.35	94.82	94.10	95.20	97.10	95.91	94.81	90.81	97.68	98.92	96.64	98.24	81.22					
Mg#[5]	67.15	76.32	61.84	65.06	59.73		57.89	57.24	60.52	52.02	61.63	73.20	75.81	76.68	62.60	63.89	61.17	70.46	62.11					
LOI	0.29	nil	1.90	6.25	4.40		4.27	4.88	5.56	4.42	2.51	3.63	4.72	8.97	2.00	0.75	3.05	1.43	18.48					
Ni	377	920	222	365	116		191	53	145	108	180	478	472	528	142	207	106	265	166					
Cr	1001	1418	370	464	244		292	79	298	494	464	872	830	855	438	557	393	713	325					
V	328	258	237	226	154		274	99	256	221	270	280	283	169	284	312	281	261	203					
Ga	20	13	24	21	27		25	27	22	27	24	12	14	14	20	21	19	19	15					
Cu	64	76	41	52	23		56	17	52	53	52	70	47	45	56	59	62	41	85					
Zn	125	127	120	119	111		122	78	142	150	103	80	98	92	108	116	114	115	106					
Cs	0.30	0.22	0.70	0.68	0.59		0.81	1.07	0.29	0.58	0.66	0.33	0.61	4.19	0.59	0.4	0.56	0.41	0.79	1.05	0.92	0.15	0.89	0.10
Rb	22.5	14.2	93.1	80.0	97.4		74.0	155.8	57.4	99.8	81.4	33.2	44.5	28.5	44.2	32.4	42.3	28.4	26.1	32.8	27.1	9.1	20.4	9.7
Ba	244	177	569	1736	646		486	683	466	586	510	216	477	701	345	257	326	240	369	350	276	1761	171	130
Th	4.44	3.28	7.13	7.84	10.74		10.13	17.46	8.26	10.31	8.99	15.45	14.04	12.93	6.53	5.21	6.28	4.29	4.00	4.64	3.61	9.95	2.15	1.27
U	0.96	0.83	1.83	2.89	1.84		2.04	2.99	1.67	2.10	1.77	1.48	1.97	1.56	1.38	1.10	1.31	0.72	0.98	1.07	0.74	8.08	0.51	0.43
Nb	47.81	33.64	54.12	49.84	47.48		59.73	46.14	52.26	47.73	54.31	107.52	98.75	74.53	49.97	50.79	48.45	31.26	34.75	40.93	24.84	157.4	6.64	17.2
Ta	3.34	2.31	3.68	3.39	3.17		3.95	3.08	3.50	3.23	3.61	7.18	6.64	4.55	3.43	3.47	3.33	2.17	2.56	2.98	1.69	9.39	0.46	1.17
La	39.13	28.05	53.17	55.63	66.92		64.01	81.33	56.82	59.58	61.04	113.07	98.37	95.85	47.92	41.65	46.44	32.25	29.16	34.38	24.85	110.7	10.9	15.6
Ce	78.61	60.69	104.2	110.9	130.1		129.3	154.5	114.2	118.6	119.4	209.2	194.9	172.8	96.96	81.65	94.30	66.79	56.84	66.72	50.69	680.2	23.3	38.0
Pb	2.78	2.28	7.27	7.95	11.29		6.42	13.56	9.31	8.84	11.61	9.03	8.42	10.90	5.37	4.02	5.13	4.77	8.29	9.55	7.87	694.4	7.71	2.03
Pr	9.59	7.75	11.97	12.99	15.02		15.17	16.97	13.43	14.39	13.76	24.97	22.12	19.42	11.60	9.32	11.32	8.55	6.87	8.26	6.25	16.24	3.06	5.44
Nd	40.69	32.01	48.31	48.91	55.89		58.29	58.94	51.35	55.43	52.43	92.59	82.00	67.46	44.89	37.85	44.23	34.67	29.08	34.92	26.72	69.46	13.0	24.6
Sr	499	374	617	714	511		662	479	589	526	645	515	627	317	496	466	481	363	709	690	382	1062	192	385
Zr	253	186	305	289	341		358	390	302	320	313	284	260	243	248	227	242	179	168	208	157	642	92	167
Hf	6.60	4.60	8.02	7.35	8.86		8.81	9.87	7.60	8.26	7.88	7.34	6.94	6.37	6.38	5.88	6.36	5.02	4.22	5.11	4.20	16.41	2.56	4.44
Sm	9.56	7.06	10.69	10.02	10.66		11.75	10.24	10.42	11.24	10.46	15.38	13.87	11.96	8.98	8.27	8.93	7.50	6.68	8.26	6.72	14.10	3.31	6.11
Eu	2.97	2.22	3.14	2.91	3.00		3.52	2.62	3.07	3.20	3.14	4.16	3.85	3.12	2.74	2.55	2.69	2.17	2.11	2.54	2.09	4.14	1.08	2.06
Gd	8.61	6.20	9.02	8.16	8.34		9.92	7.19	8.89	9.20	9.01	11.40	10.15	8.94	7.81	7.35	7.76	6.86	6.55	7.92	6.33	17.03	3.58	6.19
Tb	1.23	0.90	1.25	1.16	1.13		1.41	0.97	1.24	1.28	1.24	1.45	1.27	1.16	1.14	1.10	1.14	1.02	0.98	1.16	0.98	2.89	0.61	0.93
Dy	6.52	4.89	6.44	5.93	5.67		7.38	4.86	6.58	6.66	6.65	7.28	6.27	5.83	6.27	6.17	6.28	5.49	5.43	6.35	5.58	20.42	3.86	5.33
Ho	1.14	0.86	1.06	1.01	0.97		1.26	0.82	1.12	1.15	1.15	1.24	1.05	0.98	1.14	1.11	1.13	1.03	0.98	1.16	1.03	4.74	0.82	1.00
Y	29.14	20.58	27.26	24.47	24.05		31.03	20.29	27.44	28.79	28.16	36.16	26.42	25.93	27.93	28.52	27.68	25.78	26.63	31.32	25.92	113.70	21.6	26.4
Er	2.66	2.00	2.36	2.31	2.20		2.92	1.87	2.58	2.65	2.69	2.89	2.29	2.20	2.73	2.70	2.75	2.47	2.47	2.82	2.53	13.62	2.22	2.55
Tm	0.33	0.25	0.30	0.28	0.28		0.36	0.24	0.33	0.33	0.33	0.36	0.28	0.28	0.37	0.37	0.36	0.34	0.32	0.36	0.34	2.08	0.32	0.33
Yb	1.96	1.41	1.59	1.54	1.47		1.99	1.38	1.82	1.87	1.89	1.95	1.55	1.47	2.14	2.09	2.11	1.98	1.87	2.10	1.98	13.18	2.01	1.90
Lu	0.27	0.20	0.22	0.23	0.21		0.27	0.20	0.25	0.27	0.27	0.30	0.22	0.22	0.32	0.31	0.32	0.29	0.28	0.32	0.30	2.07	0.31	0.27
Sc	34.6	28.9	19.8	19.3	15.2		18.8	8.3	19.6	18.8	24.4	31.0	28.5	21.9	31.2	31.7	31.0	28.9	21.7	24.0	26.3	11.7	35.6	31.9
$^{87}Sr/^{86}Sr$ (W.R.)	0.705422	0.705435	0.711409	0.711481	0.718592	0.718583	0.708175	0.720469	0.709450	0.716394	0.709985		0.707902	0.711808	0.708117	0.706387	0.708170	0.712500	0.708247	0.707807	0.706140			
$^{87}Sr/^{86}Sr$ (cpx)			0.709171		0.720630 (gr), 0.720232 (bl)			0.721630						0.710337										
$^{143}Nd/^{144}Nd$ (W.R.)	0.512736	0.512763	0.512583	0.512544	0.512314	0.512328	0.512851	0.512287	0.512601	0.512398	0.512670	0.512512	0.512511	0.512426		0.512653		0.512459						
$^{143}Nd/^{144}Nd$ (cpx)			0.512588		0.512285 (gr), 0.512300 (bl)									0.512453										
$^{206}Pb/^{204}Pb$ (W.R.)	18.317	19.322	19.011	19.042	18.957		19.063	18.954	19.070	19.009	19.034	19.557	19.557	19.967	19.150	19.150	19.151	18.963	18.844	18.849	18.932	18.764		
$^{207}Pb/^{204}Pb$ (W.R.)	15.618	15.619	15.633	15.638	15.643		15.628	15.646	15.637	15.644	15.634	15.658	15.657	15.643	15.639	15.630	15.640	15.628	15.624	15.624	15.628	15.629		
$^{208}Pb/^{204}Pb$ (W.R.)	39.473	39.475	39.347	39.418	39.399		39.396	39.424	39.419	39.452	39.419	40.290	40.285	39.738	39.465	39.418	39.465	39.273	38.650	38.649	38.888	38.757		
$^3He/^4He$ (Ra)			4.93		4.31									4.71										

Basalt samples and the ferromanganese crust were dredged from the submarine flanks of Savai'i island during the 2005 ALIA cruise of the R/V Kilo Moana. The prefix "ALIA" has been deleted from the sample ID of the lavas and the ferromanganese rind in the table.

In spite of being sampled in a submarine setting, the state of preservation for most samples is quite good. The Th/U of the new Samoan samples generally fall in the same range (4.5±1.5) observed in other submarine and subaerial basalts reported in ref. 8. The exceptions include sample D115-07 (Th/U = 2.7; the LOI in this sample is the highest from dredge D115) and all three samples from dredge D118 (where Th/U range from 7.1 to 10.4, suggesting U loss). Excluding these 4 samples, a rough correlation exists between Th/U and U conentrations. However, the high Th/U (~5.8) in the two most isotopically-enriched lavas may be a result of U-loss. The two samples with the highest LOI values (D115-07 and D118-23) have Ba/Rb ratios greater than 20. Excluding sample D115-07 and all samples from dredge D118, Ba/Rb values fall in a range of 4.4 to 12 (the canonical ratio in fresh OIBs is ~12 from ref. 28) and show an excellent negative correlation with Rb concentrations and a positive correlation with Nd-isotopes. Due to these correlations, we consider the low Ba/Rb rabos in the most enriched samples to be a signature of the highly enriched EM2 source. Excluding samples from dredge D118, Rb/Cs rabos fall in the range of 66-203, with an average value of 98 that is close to the canonical range of 85-95 from ref. 28. Excluding the sample with the highest Rb/Cs ratio (D115-22) and all the samples from dredge D118, the Rb/Cs ratios in the new Samoan lavas exhibit good correlations with Rb concentrations and Sr-isotopes. These three proxies of alteration (Th/U, Ba/Rb and Rb/Cs) suggest that elements equally or less mobile than U, Rb and Cs can provide useful petrogenetic information for most samples, excluding the three highly altered samples from dredge D118, sample D115-07 and possibly the U concentrations in D115-21 and D115-18. However, due to intensive acid leaching before analyses (see below), we consider all the isotope rabos to reflect source compositions. Major and trace element analyses were performed on unleached whole-rock (W.R.) powders at the Washington State University GeoAnalytical lab. Major elements and Ni, Cr, V, Ga, Cu and Zn were measured by XRF, and all other traces by ICP-MS. Errors associated with measurement of element concentrations in basalts can be found in refs 30 and 31: errors for major elements are 0.11-0.33% (1σ) of the amount present (SiO_2, Al_2O_3, TiO_2, P_2O_5) and 0.38-0.71% (other major elements); for trace elements analysed by ICP-MS, the reproducibility is 0.77-3.2% (1σ) for all elements except for U (9.5%) and Th (9.3%), and is based on 50 analyses of in internal standard (BCR-P). For day to day calibration of the ICP-MS, the GeoAnalytical Lab uses three

in house standards (BCR-P, BMP-01 and MON-01) that are dissolved and processed with each batch of unknowns. The calibration values for these three standards were determined in 2001 using 17 international reference materials, including, BCR-1 (Basalt), W-2 (Diabase), G-2 (Granite), DNC-1 (Diabase), AGV-1 (Andesite), BIR-1 (Basalt), BHVO-1 (Basalt), AC-E (Granite), QLC-1 (Qtz Latite), GSP-1 (Granodiorite), DNC-1 (Dolerite), FK-N (K-feldspar), JG-1 (Granodiorite), JB-1a (Basalt), etc. The accepted values for these standards are taken from refs 32 and 33 and the GEOREM database. Single analyses of the international standards W-2 and BHVO-1, run as an "unknowns", are reported in the table above.

Basalt Sr, Nd and Pb isotope analyses were performed on the same powder following 3 hours of leaching in 6.2 N HCl at 100 °C. Sr and Nd isotopes were also measured on leached cpx separates (following ref. 34) from selected samples (two separate cpx populations distinguished by colour--black [bl] and green [gr]--were extracted from sample D115-18), and the data are reported along with the whole rock data above. Signal intensities during Sr and Nd isotope measurements of cpx separates and whole rock basalt powders were similar, as were the associated errors. Sr and Nd chemistry was done with conventional ion chromatography using DOWEX 50 cation resin and HDEHP-treated teflon for Nd separation (following ref. 34); the HBr-HNO3 procedure of refs. 35 and 36 were used for Pb chemistry, with a single column pass. Sr, Nd, and Pb isotope analyses were done on the NEPTUNE multi-collector ICP-MS at WHOI. The protocol and associated errors and standard normalizations can be found in ref. 30. Internal precision is 5-10 ppm (2σ) for Sr and Nd isotope measurements, and after adjusting to 0.710240 (SRM987 Sr standard) and 0.511847 (La Jolla Nd standard), the corresponding external precision for Sr and Nd is estimated at 15-25 ppm (2σ). The internal precision for Pb isotope measurements on XXX/204 ratios is 15-30 ppm. SRM997 Tl was used as an internal standard, and external reproducibility following full chemistry ranges from 17 ppm (2σ) for $^{207}Pb/^{206}Pb$ to 117 ppm (2σ) for $^{208}Pb/^{204}Pb$. Pb isotope ratios are adjusted to the SRM 981 values of ref. 37. Further documentation of the precision for Pb-isotope measurment at WHOI (on a standard solution and a basalt) can be found in ref. 38.

Helium isotopes were measured at WHOI (see ref. 39) on cpx (in samples D118-23 and D115-18) and olivine (in sample D115-03) mineral separates. Gas contents were 2.5×10^{-8}, 1.9×10^{-8} and 1.7×10^{-8} cc/g, respectively, with 1σ internal precision of ±0.10, ±0.1 and ±0.064 Ra (Ra, or ratio to atmosphere, is 1.384×10^{-6}). All helium data were obtained by crushing of cpx and olivine in vacuum. It is assumed here that radiogenic contributions are negligible. However, without total fusion helium data, we cannot exclude the possibility of implanted radiogenic ^4He from the basalt matrix.

[1]Replicate measurement was made on a leached powder prepared from a different batch of rock chips from the same rock sample.

[2]Cores available at Lamont-Doherty Earth Observatory core repository, and all cores were taken in the region of the Samoan islands and seamounts. Care was taken to sample all lithologies and, when making a composite of each core, the lithologies sampled were combined in approximately the same proportions as found in the respective cores. Composites were not subject to leaching prior to isotopic and major and trace element analyses.

[3]The ferromanganese rind was taken from the rim of basalt sample D118-22. The Mn-rind was powdered before analysis and not subjected to leaching.

[4]All Fe reported as FeO.

[5]Mg# = molar ratio of MgO/(MgO + 0.9xFeO)

Chapter 3

New Samoan lavas from Ofu Island reveal a hemispherically heterogeneous high $^{3}He/^{4}He$ mantle *

Abstract

New measurements of high $^{3}He/^{4}He$ ratios in Samoan lavas from Ofu Island (19.5–33.8 times atmospheric) extend the known range for $^{3}He/^{4}He$ in the southern hemisphere mantle. The Ofu data suggest that the high $^{3}He/^{4}He$ mantle component thought to be common to all oceanic hotspots, called FOZO (Focus Zone), is not homogeneous. Sr, Nd and Pb isotopes in Ofu lavas indicate that the Samoan high 3He/4He component is isotopically distinct from the high $^{3}He/^{4}He$ lavas from Hawaii, Iceland and Galapagos. Along with Samoa, the highest $^{3}He/^{4}He$ sample from each southern hemisphere high $^{3}He/^{4}He$ hotspot exhibits lower $^{143}Nd/^{144}Nd$ ratios than their counterparts in the northern hemisphere (excluding lavas erupted in continental, back-arc, and submarine ridge environments). The observation of a large-scale isotopic enrichment (generally higher $^{87}Sr/^{86}Sr$ and lower $^{143}Nd/^{144}Nd$) in the FOZO-A (austral) high 3He/4He mantle compared to the FOZO-B (boreal) high $^{3}He/^{4}He$ mantle is similar to the DUPAL anomaly, a globe-encircling feature of isotopic enrichment observed primarily in southern hemisphere ocean island basalts. The recent discovery that terrestrial samples have $^{142}Nd/^{144}Nd$ ratios higher than chrondrites has potentially important implications for the origin of the FOZO reservoirs, and suggest that the high $^{3}He/^{4}He$ mantle has been re-enriched.

*In Press as: M. G. Jackson, M. D. Kurz, S. R. Hart, R. K. Workman, The Samoan lavas from Ofu Island reveal a hemispherically heterogeneous high $^{3}He/^{4}He$ mantle, *Earth Planet. Sci. Lett.*, 2007, accepted manuscript, doi: 10.1016/j.epsl.2007.09.023.

+ MODEL

ARTICLE IN PRESS

EPSL-08914; No of Pages 15

Available online at www.sciencedirect.com

ScienceDirect

EPSL

ELSEVIER

Earth and Planetary Science Letters xx (2007) xxx – xxx

www.elsevier.com/locate/epsl

New Samoan lavas from Ofu Island reveal a hemispherically heterogeneous high $^{3}He/^{4}He$ mantle

Matthew G. Jackson [a,*], Mark D. Kurz [b], Stanley R. Hart [b], Rhea K. Workman [c]

[a] *Massachusetts Institute of Technology — Woods Hole Oceanographic Institution Joint Program, USA*

[b] *Woods Hole Oceanographic Institution, Woods Hole, MA 02543, USA*

[c] *School of Ocean and Earth Science and Technology, University of Hawaii, Honolulu, HI 96822, USA*

Received 16 May 2007; received in revised form 14 September 2007; accepted 17 September 2007

Editor: R.W. Carlson

Abstract

New measurements of high $^{3}He/^{4}He$ ratios in Samoan lavas from Ofu Island (19.5 33.8 times atmospheric) extend the known range for $^{3}He/^{4}He$ in the southern hemisphere mantle. The Ofu data suggest that the high $^{3}He/^{4}He$ mantle component thought to be common to all oceanic hotspots, called FOZO (*Focus Zone*), is not homogeneous. Sr, Nd and Pb isotopes in Ofu lavas indicate that the Samoan high $^{3}He/^{4}He$ component is isotopically distinct from the high $^{3}He/^{4}He$ lavas from Hawaii, Iceland and Galapagos. Along with Samoa, the highest $^{3}He/^{4}He$ sample from each southern hemisphere high $^{3}He/^{4}He$ hotspot #exhibits lower $^{143}Nd/^{144}Nd$ ratios than their counterparts in the northern hemisphere (excluding lavas erupted in continental, back-arc, and submarine ridge environments). The observation of a large-scale isotopic enrichment (generally higher $^{87}Sr/^{86}Sr$ and lower $^{143}Nd/^{144}Nd$) in the FOZO-A (austral) high $^{3}He/^{4}He$ mantle compared to the FOZO-B (boreal) high $^{3}He/^{4}He$ mantle is similar to the DUPAL anomaly, a globe-encircling feature of isotopic enrichment observed primarily in southern hemisphere ocean island basalts. The recent discovery that terrestrial samples have $^{142}Nd/^{144}Nd$ ratios higher than chrondrites has potentially important implications for the origin of the FOZO reservoirs, and suggest that the high $^{3}He/^{4}He$ mantle has been re-enriched.

Keywords: Samoa; FOZO; PHEM; C; 3He/4He; mantle; basalt; geochemistry; DUPAL; hotspot

1. Introduction

Oceanic lavas with high $^{3}He/^{4}He$ signatures are rare, and derive from ancient reservoirs in the earth's mantle. Volcanically active hotspots with high $^{3}He/^{4}He$ lavas, such as Samoa and Hawaii, sample melts of buoyantly upwelling regions of the deep mantle where the high $^{3}He/^{4}He$ reservoir is thought to reside (Kurz et al., 1982; Hart et al., 1992; Class and Goldstein, 2005). Consequently, ocean island basalts (OIBs) erupted at hotspots provide a unique tool for probing the composition and history of the deep mantle. Radiogenic isotopes in OIBs are commonly used as tracers for the various mantle components revealed at hotspots, and show a diverse range of compositions, or endmembers, including DMM (depleted mid-ocean ridge basalt [MORB] mantle), HIMU (high 'μ', or $^{238}U/^{204}Pb$ mantle), EM1 and EM2 (enriched mantle 1 and 2) (Zindler and Hart, 1986).

* Corresponding author. Woods Hole Oceanographic Institution, MS #24, Woods Hole, MA 02543-1525, USA.

E-mail address: mjackson@whoi.edu (M.G. Jackson).

0012-821X/$ - see front matter © 2007 Published by Elsevier B.V.

doi:10.1016/j.epsl.2007.09.023

Please cite this article as: Jackson, M.G., et al., New Samoan lavas from Ofu Island reveal a hemispherically heterogeneous high $^{3}He/^{4}He$ mantle, Earth Planet. Sci. Lett. (2007), doi:10.1016/j.epsl.2007.09.023

Emerging from this taxonomic diversity, a unifying theory in mantle geochemistry maintains that a single mantle component exists that is common to all hotspots (Hart et al., 1992): Mixing arrays from individual ocean islands originate near the mantle endmembers in various radiogenic isotope spaces and converge on a region characterized by depleted isotope ratios that is distinct from normal MORB (Hart et al., 1992). Lavas plotting in this region of convergence often exhibit elevated $^{3}He/^{4}He$ ratios, and are suggested to sample a component in the mantle common to all hotspots. Variably called FOZO (Hart et al., 1992), PHEM (*P*rimitive *He*lium *M*antle; Farley et al., 1992), or C (*C*ommon; Hanan and Graham, 1996), the high $^{3}He/^{4}He$ common component is thought to be a relatively less degassed region of the (lower?) mantle (Kurz et al., 1982; Class and Goldstein, 2005).

New geochemical data from the Samoan hotspot are not entirely consistent with this view of the mantle. The new $^{3}He/^{4}He$ ratios (up to 33.8±0.2 Ra, ratio to atmosphere) from the Samoan Island of Ofu are the highest yet recorded in the southern hemisphere, and are significantly higher than $^{3}He/^{4}He$ ratios previously measured (25.8 Ra) in Samoan basalts and xenoliths (Farley et al., 1992; Poreda and Farley, 1992; Workman et al., 2004). The new helium isotope data from Samoa extend the range of observed $^{3}He/^{4}He$ up to values comparable to those found in Hawaii (32.3 Ra; Kurz et al., 1982), Iceland (37.7 Ra; Hilton et al., 1999) and the Galapagos (30.3 Ra; Kurz and Geist, 1999; Saal et al., 2007), referred to here as HIG. The Ofu lavas are isotopically more enriched (higher $^{87}Sr/^{86}Sr$ and lower $^{143}Nd/^{144}Nd$) than the high $^{3}He/^{4}He$ samples from HIG and exhibit elevated incompatible trace element concentrations. Due to this isotopic and trace element enrichment relative to HIG lavas, the new data from Samoan high $^{3}He/^{4}He$ lavas are inconsistent with recent models that describe the evolution of the high $^{3}He/^{4}He$ mantle, and the Ofu data suggest that the high $^{3}He/^{4}He$ mantle domain is isotopically heterogeneous.

2. Methods and results

2.1. Sample location and state of preservation

Ofu Island is located in the eastern province of the Samoan archipelago, an age-progressive hotspot track (Hart et al., 2004; Koppers et al., submitted for publication) located just north of the northern terminus of the Tonga subduction zone. The samples were collected at various locations on the perimeter of Ofu and Olosega islands (Ofu hereafter; sample location map is available in the supplementary data in the Appendix). Tholeiitic lavas in Samoa are rare (Natland, 1980; Workman et al., 2004), and with the exception of a cumulate (OFU-04-14) and a gabbro (OFU-04-17), the Ofu lavas presented in this study are alkali basalts (Table 1). The Ofu samples are generally quite fresh. With the exception of sample OFU-04-12, which has a Th/U ratio of 4.8 (and may indicate U-loss during subaerial weathering), the range of Th/U ratios in the Ofu sample suite is 4.0–4.4. The Ba/Rb ratios for Ofu samples (9.1 ± 1.1 at 1σ) are similar to the values for young Samoan basalts reported previously (Workman et al., 2004), and somewhat lower than the canonical value of ~12 for fresh OIB lavas (Hofmann and White, 1983). Excluding the cumulate sample OFU-04-14, which has a Rb/Cs ratio of 280, the range of Rb/Cs values from the Ofu samples (from 73 to 137) is close to the canonical range of 85–95 (Hofmann and White, 1983). These weathering proxies indicate that elements equally or less mobile than U, Rb and Cs yield useful petrogenetic information.

2.2. He, Sr, Nd and Pb isotopes in Ofu lavas

New $^{3}He/^{4}He$ values (19.5 to 33.8 Ra) were measured at Woods Hole Oceanographic Institution on olivine and clinopyroxene (cpx) phenocrysts separated from 12 hand samples (Table 1). Measurements were made by crushing and fusion *in vacuo*, following the protocol reported in (Kurz et al., 2004). The sample with the highest $^{3}He/^{4}He$ value, OFU-04-06, was taken from an ankaramite dike exposed at 2 m depth in a recent road cut. Olivines from this sample are relatively gas rich (67.5×10^{-9} cm^3 STP g^{-1}, the sum of crushing and fusion) and yielded similar $^{3}He/^{4}He$ ratios on two separate crushes of the same olivine separate (OFU-04-06cr1 followed by OFU-04-06cr2). Following the crushing experiments, a fusion extraction of the resulting olivine powder (OFU-04-06fus) yielded lower $^{3}He/^{4}He$, indicating the presence of ingrown radiogenic helium, probably implanted from the Th and U-rich matrix. Two different olivine populations (lighter and darker olivines) separated from sample OFU-04-06 yielded similar $^{3}He/^{4}He$ ratios (33.4 and 33.6 Ra). These fusion and crushing experiments, coupled with sampling depths, preclude the influence of cosmogenic helium for this important sample. The lava with the second highest $^{3}He/^{4}He$ value measured by crushing–sample OFU-04-15–also yielded lower $^{3}He/^{4}He$ ratios upon fusion (OFU-04-15fus) of the crushed olivine powder. Additionally, crushing experiments of sample OFU-04-03 (OFU-04-03cr1 followed by OFU-04-03cr2) yielded

Please cite this article as: Jackson, M.G., et al., New Samoan lavas from Ofu Island reveal a hemispherically heterogeneous high $^{3}He/^{4}He$ mantle, Earth Planet. Sci. Lett. (2007), doi:10.1016/j.epsl.2007.09.023

Table 1
Isotopic and (selected) trace element analyses of Ofu and Moorea lavas

Sample	Phase analyzed for helium	Rock type	Geological formation	^{4}He (10^{-9}cm^3 STP g^{-1})	^{3}He/^{4}He (R/R_a)	1σ	^{87}Sr/^{86}Sr	^{143}Nd/^{144}Nd	^{206}Pb/^{204}Pb	^{207}Pb/^{204}Pb	^{208}Pb/^{204}Pb	Th	Sr	Th/U	Ba/Rb	Rb/Cs	Ba/Nb	Pb/Pb*
OFU-04-02	Olivine	Ankaramite	Dike	38.6	24.6	0.1	NA	NA	NA	NA	NA	NA	NA	NA	NA	NA	NA	NA
OFU-04-03cr1	Olivine	Ankaramite	Dike	119	24.0	0.1	0.704756	0.512811	19.257	15.591	39.418	3.26	390	4.29	7.19	117.1	5.3	0.44
OFU-04-03cr2	Olivine	Ankaramite	Dike	11.5	23.9	0.2	"	"	"	"	"	"	"	"	"	"	"	"
OFU-04-05	Olivine	Ankaramite	Dike	70.8	24.4	0.1	0.704793	0.512814	19.254	15.589	39.412	4.24	546	4.26	7.81	136.7	5.6	0.43
OFU-04-06cr1	Olivine	Ankaramite	Dike	44.0	33.7	0.2	0.704584	0.512827	19.189	15.571	39.202	3.96	599	3.99	9.71	77.7	4.9	0.42
OFU-04-06cr2	Olivine	Ankaramite	Dike	5.0	33.8	0.2	"	"	"	"	"	"	"	"	"	"	"	"
OFU-04-06 fus	Olivine	Ankaramite	Dike	18.5	27.0	0.1	"	"	"	"	"	"	"	"	"	"	"	"
OFU-04-06 (light olivines)	Olivine	Ankaramite	Dike	27.3	33.4	0.2	"	"	"	"	"	"	"	"	"	"	"	"
OFU-04-06 (dark olives)	Olivine	Ankaramite	Dike	40.0	33.6	0.1	"	"	"	"	"	"	"	"	"	"	"	"
OFU-04-06[a]	cpx	Ankaramite	Dike	0.2	26.1	3.4	"	"	"	"	"	"	"	"	"	"	"	"
OFU-04-07	none	Trachybasalt	Dike	NA	NA	NA	0.704623	0.512814	19.177	15.582	39.268	5.24	767	4.04	9.59	122.0	5.0	0.39
OFU-04-08	Olivine	Ankaramite	Dike	4.5	21.3	0.3	0.704703	0.512802	19.207	15.586	39.291	4.06	573	4.11	8.78	77.5	4.7	0.42
OFU-04-09	Olivine	Ankaramite	Flow	3.2	25.6	0.5	0.704538	0.512835	19.165	15.577	39.208	3.25	503	4.03	10.20	131.6	5.4	0.46
OFU-04-10	Olivine	Alkali Basalt	Flow	8.0	22.0	0.2	"	"	"	"	"	"	"	"	"	"	"	"
OFU-04-10	cpx	Alkali Basalt	Flow	1.0	19.7	0.6	0.704648	0.512815	19.187	15.585	39.261	3.65	495	4.39	10.79	73.0	5.8	0.43
OFU-04-11	None	Trachybasalt	Flow	NA	NA	NA	0.704635	0.512804	19.184	15.594	39.299	6.60	929	4.30	9.09	108.0	5.3	0.45
OFU-04-12	Olivine	Alkali Basalt	Flow	3.5	21.2	0.3	0.704795	0.512800	19.202	15.594	39.403	3.29	331	4.78	10.36	118.3	6.2	0.42
OFU-04-13	None	Hawaiite	Flow	NA	NA	NA	0.704625	0.512816	19.176	15.581	39.264	5.02	723	4.07	9.09	99.2	4.8	0.40
OFU-04-14	Olivine	Cumulate	Boulder	4.5	25.0	0.2	0.704517	0.512819	19.126	15.584	39.164	2.95	292	4.39	9.88	280.2	4.9	0.37
OFU-04-15	Olivine	Ankaramite	Boulder	14.3	29.6	0.2	0.704559	0.512822	19.141	15.580	39.169	3.89	601	4.02	9.28	88.0	4.8	0.43
OFU-04-15 fus	Olivine	Ankaramite	Boulder	3.2	21.2	0.2	"	"	"	"	"	"	"	"	"	"	"	"
OFU-04-16	cpx	Alkali Basalt	Boulder	0.2	19	1	0.704438	0.512834	19.216	15.587	39.276	3.54	639	3.96	8.60	129.6	5.3	0.46
OFU-04-17	Olivine	Gabbro	Boulder	1.0	26.4	0.4	0.704498	0.512844	19.160	15.576	39.173	2.18	310	4.14	7.30	118.2	5.1	0.41
MO01-01 (Moorea)[b]	Olivine	Ankaramite	NA	1.3	17.0	1.6	0.704621	0.512774	19.216	15.603	38.933	2.11	381	3.75	11.14	270.4	8.5	0.50

Samples were collected at Ofu Island, American Samoa in August of 2004. All ^{3}He/^{4}He ratios are reported relative to atmospheric (R/Ra) using an atmospheric value of 1.384×10^{-6}. The Sr, Nd, and Pb chemistry, mass spectrometry and associated measurement precision are reported in Hart and Blusztajn (2006). Sr, Nd and Pb-isotope analyses were performed on leached whole-rock powders. Trace elements analyses were performed on unleached whole-rock powders by ICP at the Washington State University GeoAnalytical Lab.

Errors associated with trace element analyses can be found in Jackson et al. (2007). Only two samples (OFU-04-06 fus and OFU-04-15 fus) were fused for helium isotope measurement. All other helium measurements were made by crushing. When an olivine sample was crushed and measured more than once, the crush experiment is labeled as "cr1 or cr2".

[a] Required a blank correction of 46% due to low gas concentrations. The ^{3}He/^{4}He ratio on this clinopyroxene measurement is similar to the olivine crush values at the 2σ level.

[b] The sample is from Moorea in the Societies island chain, a hotspot that exhibits EM2 affinities. Helium isotope data were previously published on Societies sample MO01-01 in Hanyu and Kaneoka (1997). Sr, Nd and Pb isotopes by same method as Ofu rocks.

Please cite this article as: Jackson, M.G., et al., New Samoan lavas from Ofu Island reveal a hemispherically heterogeneous high ^{3}He/^{4}He mantle, Earth Planet. Sci. Lett. (2007), doi:10.1016/j.epsl.2007.09.023

reproducible results. The reproducibility of the measurements for Ofu samples, the relatively high helium concentrations, the absence of higher $^3He/^4He$ ratios on melting, and shielding of many of the samples all indicate that cosmogenic ^3He is not a factor in generating the remarkably high $^3He/^4He$ ratios.

The Sr, Nd, and Pb chemistry, mass spectrometry, associated measurement precision and standard normalizations are reported in Hart and Blusztajn (2006) and references therein. Basalt Sr, Nd and Pb-isotope analyses were performed on the same powder following 1 h of leaching in 6.2 N HCl at 100 °C. Sr and Nd chemistry was done with conventional ion chromatography using DOWEX 50 cation resin and HDEHP-treated teflon for Nd separation (Taras and Hart, 1987). An $HBr–HNO_3$ procedure (Galer, in press; Abouchami et al., 1999) was used for Pb chemistry, with a single column pass. Sr, Nd, and Pb-isotope analyses were done on the NEPTUNE multi-collector ICP-MS at WHOI. Internal precision is 5–10 ppm (2σ) for Sr and Nd-isotope measurements. Adjusting to 0.710240 (SRM987 Sr standard) and 0.511847 (La Jolla Nd standard) gives an estimated external precision for Sr and Nd of 15–25 ppm (2σ). The internal precision for Pb-isotope ratios is better than 15–30 ppm, and using SRM997 Tl as an internal standard, the external reproducibility following full chemistry ranges from ~20 ppm (2σ) for $^{207}Pb/^{206}Pb$ to ~120 ppm (2σ) for $^{208}Pb/^{204}Pb$ (Hart and Blusztajn, 2006). Pb-isotope ratios are adjusted to the SRM 981 values of Todt et al. (1996).

Ofu lavas exhibit slight variations in the radiogenic isotope ratios of $^{87}Sr/^{86}Sr$ (0.704438–0.704795), $^{143}Nd/^{144}Nd$ (0.512800 to 0.512844) and $^{206}Pb/^{204}Pb$ (19.126 to 19.257) (Fig. 1 and Table 1). Together with Ofu, data from Samoan lavas in general define a wedge-like shape in $^3He/^4He$–$^{87}Sr/^{86}Sr$ isotope space: lavas with the highest (more enriched) $^{87}Sr/^{86}Sr$ ratios exhibit low $^3He/^4He$ ratios and samples with the least radiogenic $^{87}Sr/^{86}Sr$ ratios, found primarily at Ofu, are associated with the highest $^3He/^4He$ ratios (Fig. 1). Similarly, Samoan lavas with the most enriched (lowest) $^{143}Nd/^{144}Nd$ have low $^3He/^4He$ ratios. However, Nd and Pb isotopes measured in Ofu lavas do not define end-member values for Samoa, but instead fall toward the upper end found in the hotspot.

In order to further constrain the nature of elevated $^3He/^4He$ lavas associated with EM2 hotspots, we present Sr, Nd and Pb isotopes for a high $^3He/^4He$ sample from

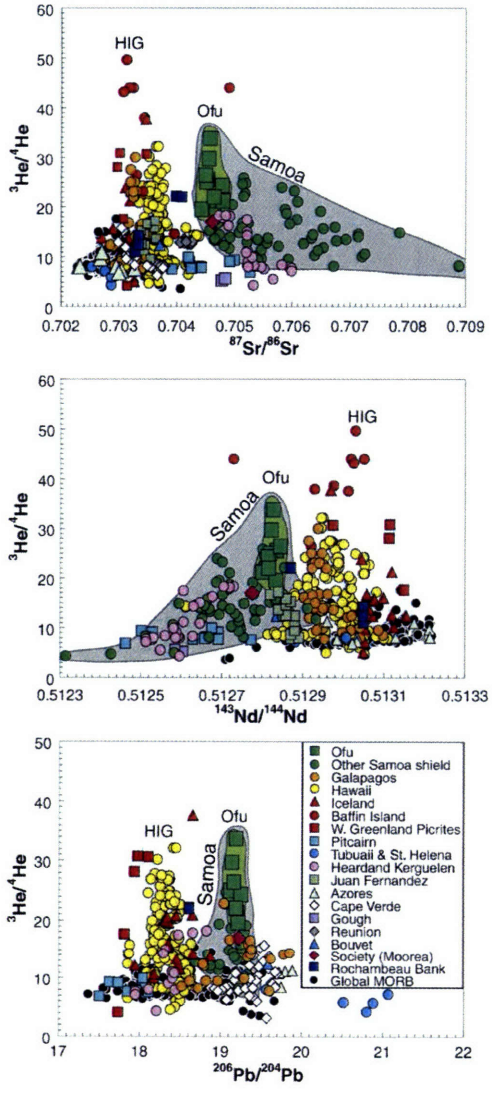

Fig. 1. The new Ofu data indicate that the Samoan high $^3He/^4He$ lavas have more enriched $^{87}Sr/^{86}Sr$ and $^{143}Nd/^{144}Nd$ than the highest $^3He/^4He$ lavas from Hawaii, Iceland and Galapagos (abbreviated HIG). The field of Samoan shield basalts is shaded grey, and the field of Samoan lavas from Ofu Island is shaded green (see Table 1). HIG lavas trend to a more isotopically depleted high $^3He/^4He$ component than lavas from Ofu. A single sample from Baffin Island is an exception to the Sr and Nd-isotope separation between the Ofu and HIG lavas, but was indicated by Stuart et al. (2003) to be crustally contaminated. Data sources are summarized in Graham (2002) or noted in Table 2. In the isotope projections shown in this figure, the separation between the highest $^3He/^4He$ samples from the northern and southern hemisphere high $^3He/^4He$ hotspots is not perfect. For example, the Pb-isotopes of the highest $^3He/^4He$ lavas from Samoa and the Galapagos overlap. However, the isotopic and hemispheric separation of FOZO-A and FOZO-B samples (Table 2) is observed in the isotope projections shown in Fig. 2. (For interpretation of the references to color in this figure legend, the reader is referred to the web version of this article.)

Please cite this article as: Jackson, M.G., et al., New Samoan lavas from Ofu Island reveal a hemispherically heterogeneous high $^3He/^4He$ mantle, Earth Planet. Sci. Lett. (2007), doi:10.1016/j.epsl.2007.09.023

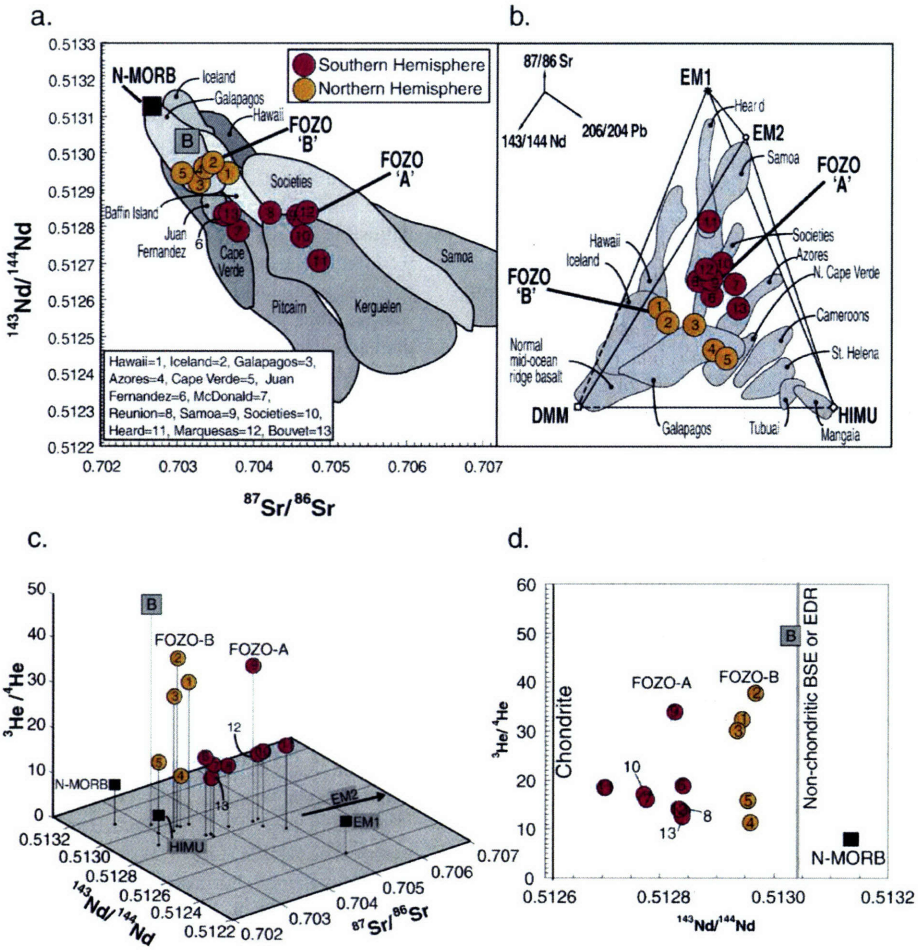

Fig. 2. The highest $^3He/^4He$ lavas from northern hemisphere (FOZO-B) hotspots separate from the highest $^3He/^4He$ samples from southern hemisphere (FOZO-A) hotspots in a.) $^{87}Sr/^{86}Sr$–$^{143}Nd/^{144}Nd$ space, b.) the mantle tetrahedron, c.) a "helium balloon" pinplot showing $^{87}Sr/^{86}Sr$–$^{143}Nd/^{144}Nd$–$^3He/^4He$, and d.) $^{143}Nd/^{144}Nd$–$^3He/^4He$ isotope spaces. The criteria for selecting high $^3He/^4He$ lavas with Sr–Nd–Pb isotopes most representative of the OIB mantle are described in Table 2 and Sections 3 and 4.1 of the text. The EDR and the non-chondritic BSE are described in Fig. 6. Although the Baffin Island lava (square marked with a "B") is erupted in a continental setting, and is thus excluded from the compilation of high $^3He/^4He$ lavas (see Table 2), it hosts the highest magmatic $^3He/^4He$ on record and is included in the figure for reference. The highest $^3He/^4He$ lavas from each hotspot (and the high $^3He/^4He$ Baffin Island lava) are significantly more enriched than the N-MORB composition from Su (in press), consistent with earlier observations (Hart et al., 1992). Compared to other southern hemisphere high $^3He/^4He$ lavas, Samoan high $^3He/^4He$ lavas do not exhibit anomalous Sr, Nd and Pb isotopes.

Moorea island in the Societies hotspot. The high $^3He/^4He$ sample from Moorea, MO01-01, has a $^3He/^4He$ ratio of 17.0 Ra (Hanyu and Kaneoka, 1997), and has Sr, Nd and Pb-isotope ratios similar to Ofu basalts (Table 1).

3. Ofu in a global context

The $^{87}Sr/^{86}Sr$ and $^{143}Nd/^{144}Nd$ compositions of Ofu lavas show that the high $^3He/^4He$ reservoir sampled by the Samoan hotspot is more enriched than the high $^3He/^4He$ reservoir sampled by HIG lavas. Data in Fig. 1 show a clear "valley" between the highest $^3He/^4He$ Samoan and HIG lavas; samples with $^3He/^4He$ greater than ~22 Ra have not been found in this gap. The Ofu samples have $^{87}Sr/^{86}Sr$ ratios greater than 0.7044, while the high $^3He/^4He$ HIG lavas have $^{87}Sr/^{86}Sr$ less than 0.7038; a single Baffin Island sample, which is considered by Stuart et al. (2003) to be affected by contamination from

Please cite this article as: Jackson, M.G., et al., New Samoan lavas from Ofu Island reveal a hemispherically heterogeneous high $^3He/^4He$ mantle, Earth Planet. Sci. Lett. (2007), doi:10.1016/j.epsl.2007.09.023

t2.1 Table 2

t2.2 Summary of the radiogenic isotope data for the highest $^{3}He/^{4}He$ samples used to define FOZO-A and FOZO-B

t2.3 Hotspot	Island/ seamount/ region	ID of sample with highest $^{3}He/^{4}He$ used	$^{3}He/^{4}He$ ($\pm 1\sigma$)	$^{87}Sr/^{86}Sr$	$^{143}Nd/^{144}Nd$	$^{206}Pb/^{204}Pb$	$^{207}Pb/^{204}Pb$	$^{208}Pb/^{204}Pb$	Epsilon ^{143}Nd
t2.4 *FOZO-A*									
t2.5 Samoa [a]	Ofu	Ofu-04-06	33.8±0.2	0.704584	0.512827	19.189	15.571	39.202	4.2
t2.6 Societies [a]	Moorea	MO-01-01	17.0±1.6	0.704621	0.512774	19.216	15.603	38.933	3.2
t2.7 Macdonald [a]	Macdonald	SO-47 64DS2	15.8±0.3	0.703755	0.512777	19.46	15.61	39.27	3.2
t2.8 Juan Fernandez [b, c]	Mas a Tierra	PIN-8	17.2±0.3	0.70363	0.512840	*19.13*	*15.61*	*38.98*	4.5
t2.9 Reunion [b]	Reunion	VP1931	13.6±0.3	0.704130	*0.51284*	*18.88*	*15.59*	*38.96*	4.5
t2.10 Kerguelen [d]	Heard	HB24A	18.3±0.5	0.704862	0.512705	18.776	15.588	39.170	1.8
t2.11 Bouvet [b]	Bouvet	WJ8B	12.4±1	0.70371	*0.51284*	19.588	15.653	39.243	4.5
t2.12 Marquesas [a]	Hiva Oa	HO-AT-1	14.4±1.4	0.70471	0.512834	19.017	15.570	38.823	4.4
t2.13									
t2.14 *FOZO-B*									
t2.15 Hawaii [a, c]	Loihi	KK18-8	32.3±0.6	0.703680	0.512945	18.448	15.477	38.189	6.5
t2.16 Iceland [a]	Westfjords	SEL-97	37.7±2.0	0.703465	0.512969	18.653	15.473	38.453	7.0
t2.17 Galapagoes [a]	Fernandina	NSK 97-214	30.3±0.2	0.703290	0.512937	19.080	15.537	38.711	6.4
t2.18 Cape Verde [b]	San Nicolau	SN-10	15.7±0.1	0.703050	*0.51296*	19.538	15.586	38.964	6.7
t2.19 Azores [a, c]	Terciera	T2	11.3±0.8	0.703520	0.512960	19.883	15.630	39.310	6.8

t2.20 If Sr, Nd and Pb isotopes are unavailable for a sample with high $^{3}He/^{4}He$, they are estimated based on the criteria below and the estimated values are italicized in the table.

High $^{3}He/^{4}He$ lavas erupted at deep submarine ridge environments are excluded, and include the following locations as summarized in Graham (2002): Southeast Indian ridge near Amsterdam and St. Paul (14.1 Ra), east and west rifts of the Easter microplate (11.7 Ra), Gulf of Tadjoura near Afar (14.7 Ra), southern Mid-Atlantic ridge near Shona and Discovery (12.3 and 15.2 Ra, respectively), Southwest Indian Ridge near Bouvet Island (14.9 Ra) and the Manus Basin back-arc spreading center (15.1 Ra). However, sub-aerially erupted high $^{3}He/^{4}He$ lavas sampled at ridge-centered hotspots, including Bouvet Island (Kurz et al., 1998) and Iceland (Hilton et al., 1999), are included in the dataset. Additionally, high $^{3}He/^{4}He$ lavas erupted in continental settings are not considered, and include: Baffin Island (Stuart et al., 2003) and West Greenland picrites (Graham et al., 1998), Yellowstone (Graham et al., 2006) and Afar (Scarsi and Craig, 1996). Finally, high $^{3}He/^{4}He$ lavas erupted in back-arc environments, such as

t2.21 Rochambeau Bank (Poreda and Craig, 1992) and Manus Basin (Macpherson et al., 1998), are excluded from our treatment of the high $^{3}He/^{4}He$ mantle.

[a] Many of the high $^{3}He/^{4}He$ lavas in this table have a full complement of lithophile radiogenic isotope analyses measured on the same samples, and are from the following locations: The Galapagos (Kurz and Geist, 1999; Saal et al., 2007), Hawaii (Kurz et al., 1983; Staudigel et al., 1984), Samoa (Table 1), Iceland (Hilton et al., 1999), Societies (Hanyu and Kaneoka, 1997; Table 1), Marquesas (Castillo et al., 2007), Macdonald

t2.22 (Hémond et al., 1994; Moreira and Allègre, 2004) and Azores (Turner et al., 1997; Moreira et al., 1999).

[b] A full complement of Sr, Nd and Pb-isotope data do not exist for all the high $^{3}He/^{4}He$ samples listed in the table above. Values for the "missing" lithophile radiogenic isotopes (data in italics) are generated based on the following criteria. The high $^{3}He/^{4}He$ Cape Verde lava has Sr and Pb isotopes but lacks Nd isotopes (Doucelance et al., 2003). Sr and Nd-isotope data correlate well in the Cape Verde islands, and the Nd-isotope ratio for the Cape Verde sample is made by regression through existing data. The high $^{3}He/^{4}He$ Bouvet Island sample (Kurz et al., 1998) also has Sr and Pb-isotope data, but lacks a Nd-isotope measurement. The missing Nd isotopic value is estimated by averaging existing Bouvet island data from O'Nions et al. (1977). A high $^{3}He/^{4}He$ sample from Reunion with Sr isotope data (Graham et al., 1990) lacks Nd and Pb-isotope data; Reunion lavas are isotopically uniform, and the GEOROC database (http://georoc.mpch-mainz.gwdg.de/georoc/) was used to estimate the Nd and Pb isotopic compositions for the Reunion sample. Sr and Nd-isotope data are reported for a sample with the second highest $^{3}He/^{4}He$ measured from Juan Fernandez (Farley et al., 1993), but Pb-isotope data are missing; the high $^{3}He/^{4}He$ Juan Fernandez sample exhibits one of the least radiogenic Nd-isotope ratios (0.51284) in the Juan Fernandez suite, so Pb-isotope compositions ($^{206}Pb/^{204}Pb$ from 19.045 to 19.214) from three other Juan Fernandez samples (Gerlach et al., 1986) with

t2.23 the least radiogenic Nd isotopes (0.51282–0.51284) were averaged to generate a Pb-isotope composition for the high $^{3}He/^{4}He$ lava.

[c] When the $^{3}He/^{4}He$ ratios quoted above are lower than the maximum from a hotspot, it is because Sr, Nd and/or Pb-isotope ratios could not be estimated reliably for the sample, or because higher reported $^{3}He/^{4}He$ ratios were not measured as precisely (or were suspected of having a cosmogenic ^{3}He influence). For example, a $^{3}He/^{4}He$ value of 14.8 Ra was reported for an Azores lava (Madureira et al., 2005), but lithophile radiogenic isotopes were not reported and a cosmogenic ^{3}He influence cannot be ruled out for this sample. Similarly, a value of up to 35.3 Ra has been reported from Loihi

t2.24 (Valbracht et al., 1997), but analytical uncertainties on this measurement were large and lithophile isotopes were not reported.

[d] The Sr, Nd and Pb isotopes of the Heard sample (Barling and Goldstein, 1990; Hilton et al., 1995) were not measured on the same sample as the

t2.25 $^{3}He/^{4}He$, but they were measured on a sample (69244) from the same flow.

236 continental crust, is an exception to the separation of Ofu
237 and HIG lavas. Ofu's trend to a more enriched region
238 of Nd-isotope space than that sampled by the HIG lavas
239 is also clear ($^{143}Nd/^{144}Nd < 0.51285$ in Ofu versus $^{143}Nd/$
240 $^{144}Nd > 0.51290$ in HIG lavas). Previous work suggested
241 that the Samoan data trends toward a similar high $^{3}He/^{4}He$
242 component as the HIG lavas (Farley et al., 1992; Hart
243 et al., 1992). The new isotope data argue against this
244 hypothesis because Ofu has $^{3}He/^{4}He$ as high as HIG but
245 with more enriched $^{87}Sr/^{86}Sr$ and $^{143}Nd/^{144}Nd$.

Please cite this article as: Jackson, M.G., et al., New Samoan lavas from Ofu Island reveal a hemispherically heterogeneous high $^{3}He/^{4}He$ mantle, Earth Planet. Sci. Lett. (2007), doi:10.1016/j.epsl.2007.09.023

In order to place constraints on the Sr, Nd and Pb-isotope heterogeneity of the high $^3He/^4He$ mantle reservoir (Fig. 2), we have compiled a dataset of Sr, Nd and Pb isotopes for lavas that are representative of the high $^3He/^4He$ OIB mantle. We include only the hotspots that have $^3He/^4He > 11$ Ra, thereby excluding hotspots such as Tristan, Gough, and St. Helena, etc., that do not sample a component from the high $^3He/^4He$ mantle. We also limit our discussion to just the *single highest $^3He/^4He$ sample from each high $^3He/^4He$ hotspot*, in an attempt to define the Sr–Nd–Pb-isotope composition of the highest $^3He/^4He$ reservoir sampled by a hotspot. Finally, high $^3He/^4He$ lavas erupted at continental, back-arc and deep submarine ridge environments are excluded (see Table 2 for a list of specific samples from these three environments).

Using the above criteria, Table 2 lists the high $^3He/^4He$ samples that best represent the Sr, Nd and Pb compositions of the high $^3He/^4He$ OIB mantle reservoir. Combined with the new Ofu data, the high $^3He/^4He$ OIB dataset in Table 2 suggests the existence of two isotopically distinct high $^3He/^4He$ reservoirs in the mantle. These two high $^3He/^4He$ reservoirs separate in the northern (boreal) and southern (austral) hemispheres (Fig. 2). The highest $^3He/^4He$ samples from each of the southern hemisphere hotspots, Macdonald seamount, Bouvet, Kerguelen, Juan Fernandez, Societies, Reunion and Marquesas appear to sample the more isotopically enriched (or less isotopically depleted, see Section 4.5), high $^3He/^4He$ mantle component found in Ofu lavas. By contrast, HIG lavas and two other northern hemisphere hotspots–Cape Verde and Azores–sample a more isotopically depleted, high $^3He/^4He$ component than observed in southern hemisphere high $^3He/^4He$ lavas. The highest $^3He/^4He$ samples from the boreal and austral high $^3He/^4He$ hotspots separate toward the depleted and enriched ends, respectively, of the global $^{87}Sr/^{86}Sr$–$^{143}Nd/^{144}Nd$ OIB array (Fig. 2). Fig. 2 shows that there are two separate $^3He/^4He$ peaks in Sr–Nd–He isotope space: One peak is formed by the highest $^3He/^4He$ northern hemisphere samples and another peak, anchored by the high $^3He/^4He$ Ofu lava, is formed by the highest $^3He/^4He$ southern hemisphere samples. Samples with the highest $^3He/^4He$ from each of the boreal and austral FOZO hotspots also are distinguished isotopically inside the mantle tetrahedron formed by the isotopes of Sr, Nd and Pb. The boreal (FOZO-B) domain plots closer to the DMM-HIMU join while the austral (FOZO-A) domain plots closer to the EM1-EM2 join (Fig. 2). FOZO-A and FOZO-B also clearly separate in a mantle tetrahedron constructed from the isotopes of Pb (a figure of the Pb-isotope tetrahedron is available as supplementary data in the Appendix).

4. Discussion

4.1. FOZO-A and FOZO-B: some important caveats

Unfortunately, there are limited numbers of hotspots with moderately high $^3He/^4He$ (from 11.3–18.3 Ra, 9 hotspots) and very high $^3He/^4He$ (>30 Ra, 4 hotspots); lithophile isotope data on lavas from many of these high $^3He/^4He$ hotspots are also limited (see Table 2). Therefore, we cannot exclude the possibility that the apparent hemispheric separation is related to sparse data, and that existing He, Sr, Nd and Pb-isotope data do not yet adequately characterize the terrestrial mantle. Furthermore, the isotopic and hemispheric separation of the two FOZOs is not observed in all isotope projections: In $^3He/^4He$ vs. $^{206}Pb/^{204}Pb$ and $^3He/^4He$ vs. $^{87}Sr/^{86}Sr$ isotope spaces (not shown), the FOZO-A and FOZO-B fields overlap. However, in $^3He/^4He$ vs. $^{143}Nd/^{144}Nd$-isotope space the two FOZOs are completely resolved (Fig. 2).

An additional characteristic of the "two FOZOs" model is that the isotopic and hemispheric distinction is not always observed in the highest $^3He/^4He$ lavas erupted in continental, back-arc and deep submarine mid-ocean ridge settings. One possible explanation is that mantle plume interaction with the shallow geochemical reservoirs in these three environments can decouple the deep mantle $^3He/^4He$ signatures from the associated Sr, Nd and Pb isotopes. If so, then the high $^3He/^4He$ ratios measured in lavas from these three settings cannot be traced to the same source components as the Sr, Nd and Pb isotopes. High $^3He/^4He$ lavas erupted in continental settings may have suffered crustal assimilation such that the Sr, Nd and Pb isotopes are not representative of the high $^3He/^4He$ mantle. For example, a high $^3He/^4He$ Baffin Island sample (43.9 Ra; Stuart et al., 2003) with the least depleted $^{143}Nd/^{144}Nd$ in the suite–0.512730–is inferred to be crustally contaminated, and is not interpreted to be a northern hemisphere expression of FOZO-A. High $^3He/^4He$ lavas erupted in back-arc environments may not have lithophile isotope ratios that reflect the high $^3He/^4He$ mantle source, owing to possible involvement of slab-derived fluids that may affect the Sr, Nd and Pb isotopes (even though such fluids may have a negligible effect on the $^3He/^4He$ ratios; Macpherson et al., 1998). The high $^3He/^4He$ signatures observed in deeply erupted submarine ridge lavas may host Sr, Nd and Pb isotopes that reflect entrainment of the shallow depleted mantle. However, we presume that the high plume flux necessary for the generation of a sub-aerially-exposed, ridge-centered hotspot volcano enhances the plume contribution in the erupted lavas, thus overwhelming the depleted

Please cite this article as: Jackson, M.G., et al., New Samoan lavas from Ofu Island reveal a hemispherically heterogeneous high $^3He/^4He$ mantle, Earth Planet. Sci. Lett. (2007), doi:10.1016/j.epsl.2007.09.023

upper mantle component. Therefore, sub-aerially erupted Bouvet Island and Iceland high $^3He/^4He$ lavas are included in the database (both lavas host Sr, Nd and Pb isotopes that more enriched than nearby ridges, and are taken to reflect a plume component).

How can high $^3He/^4He$, deep mantle signatures be preserved and become decoupled from the deep mantle Sr, Nd and Pb signatures in continental, back-arc and deep submarine ridge environments? As a stimulus for further investigation, we suggest that the He/(Sr,Nd,Pb) ratios may be higher in the high $^3He/^4He$ mantle (or mantle melt) than in the shallow contaminating reservoirs found in these three geological settings. In this way, high $^3He/^4He$ signatures often may be little affected by contamination from shallow reservoirs while Sr, Nd and Pb isotopes in such lavas can be strongly decoupled from the original high $^3He/^4He$ mantle source.

4.2. FOZO-A vs. FOZO-B: is the difference sediment?

The isotopic enrichment observed in FOZO-A lavas, particularly from Ofu, relative to the FOZO-B reservoir is not easily reconciled with existing models for the evolution of the high $^3He/^4He$ mantle. One hypothesis for the generation of the relative lithophile isotope and trace element enrichment in high $^3He/^4He$ lavas from Samoa maintains that the high $^3He/^4He$ mantle beneath this hotspot was recently contaminated by rapidly cycled sediment from the nearby Tonga trench (Class and Goldstein, 2005). However, evidence from Pb-isotopes rules out modern marine sediment contamination of the Samoan high $^3He/^4He$ mantle. The sediment-OIB discriminating properties (Hart, 1988) of $\Delta^{207}Pb/^{204}Pb$–$\Delta^{208}Pb/^{204}Pb$-isotope space (Hart, 1984) show that Samoan basalts and modern global marine sediments (Plank and Langmuir, 1998) exhibit non-overlapping fields with diverging trends (Fig. 3) (Jackson et al., 2007). Pb-isotope data thus preclude the presence of modern marine sediment (including sediments outboard of the Tonga trench) in the FOZO-A mantle sampled by Ofu lavas.

Sr, Nd and Pb-isotope compositions for the high $^3He/^4He$ Moorea lava (Hanyu and Kaneoka, 1997) provide further evidence that the more enriched radiogenic isotope compositions of Samoan high $^3He/^4He$ lavas (compared to HIG lavas) are not necessarily a result of rapidly cycled, subducted sediment (Table 1). Moorea island is not located near a subduction zone, yet the high $^3He/^4He$ Moorea sample has $^{87}Sr/^{86}Sr$, $^{143}Nd/^{144}Nd$ and $^{206}Pb/^{204}Pb$-isotope ratios similar to Ofu basalts.

The observation of elevated trace element concentrations in Samoan high $^3He/^4He$ lavas (relative to HIG high $^3He/^4He$ lavas) has been used as evidence for recent

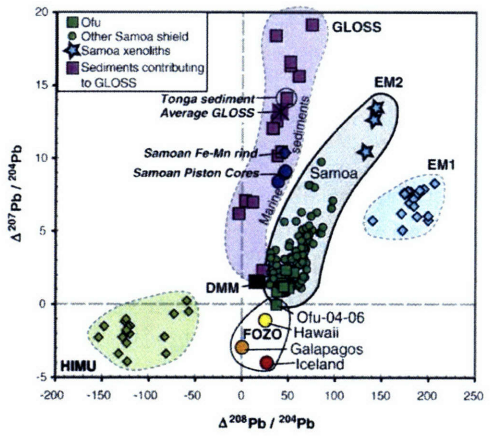

Fig. 3. In $\Delta^{207}Pb/^{204}Pb$–$\Delta^{208}Pb/^{204}Pb$-isotope space (Hart 1984, 1988), Samoan basalts (including Ofu basalts) and global marine sediments exhibit non-overlapping fields with diverging trends. The Samoan data are plotted with oceanic sediments (the Tonga sediment is circled) contributing to global subducting sediment (GLOSS) from Plank and Langmuir (1998). Samoan lavas from Ofu Island plot close to the highest $^3He/^4He$ lavas from Hawaii, Iceland and Galapagos. Samoan xenoliths from Savai'i island are plotted as stars (Hauri et al., 1993). Other plotted Pb-isotope data include endmember MORB (average of normal ridge segments; Su, in press), EM1 (Pitcairn; Eisele et al., 2002; Hart and Hauri, unpubl. data) and HIMU (Mangaia and Tubuai; Hauri and Hart, 1993; Woodhead, 1996). The figure is adapted from Jackson et al. (2007), and data for sediments from the Samoan region (piston cores) and the ferromanganese rind are from the same source. Pb-isotope data preclude the presence of modern marine sediment (including sediment recently subducted into the Tonga trench) in the FOZO-A mantle sampled by Ofu lavas.

sediment contamination of the Samoan high $^3He/^4He$ mantle (Class and Goldstein, 2005). However, our favored explanation for the elevated trace element concentrations in the Ofu (and Moorea) high $^3He/^4He$ lavas is that they are products of low degrees of melting, a mechanism that can greatly increase the trace element concentrations in lavas relative to their mantle source. Ofu and Moorea high $^3He/^4He$ lavas are alkaline, a petrologic feature that is uncommon among high $^3He/^4He$ HIG lavas and one that is likely to be a result of low degrees of mantle melting. Therefore, the alkaline nature of Samoan high $^3He/^4He$ lavas may help resolve the apparent paradox of high U and Th concentrations in Samoan lavas that also host high $^3He/^4He$ ratios (Fig. 4).

Although the Samoan plume exhibits a (low $^3He/^4He$) component with recycled sediment, the high $^3He/^4He$ Samoan lavas from Ofu exhibit no evidence for an ancient recycled sediment component. The most enriched lavas from Samoa display evidence for an ancient recycled sediment component (White and Hofmann, 1982; Wright

Please cite this article as: Jackson, M.G., et al., New Samoan lavas from Ofu Island reveal a hemispherically heterogeneous high $^3He/^4He$ mantle, Earth Planet. Sci. Lett. (2007), doi:10.1016/j.epsl.2007.09.023

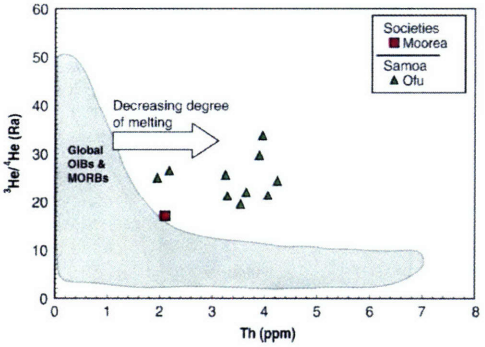

Fig. 4. ^{3}He/^{4}He–Th for Ofu lavas compared to other OIBs and MORBs. Ofu basalts and the high ^{3}He/^{4}He basalt from Moorea (MO-01-01) exhibit higher Th concentrations than high ^{3}He/^{4}He basalts from other hotspots (see Table 1). The field for global OIBs (excluding Samoa) and MORBs is from Class and Goldstein (2005). All Ofu and Moorea Th data shown are by ICP, and the Ofu Th data are not corrected for olivine or cpx fractionation. The high Th concentrations in the Ofu and Moorea high ^{3}He/^{4}He basalts are interpreted as resulting from lower degrees of melting, a hypothesis that is consistent with the alkaline nature of the lavas from these two islands.

and White, 1987; Farley et al., 1992), including high ^{87}Sr/^{86}Sr ratios (up to 0.7216) and low ^{3}He/^{4}He ratios (<5 Ra; Jackson et al., 2007). By contrast, ^{87}Sr/^{86}Sr and ^{143}Nd/^{144}Nd isotopes measured in Ofu lavas are among the most depleted in Samoa (Table 1). Furthermore, the positive Pb anomalies and high Ba/Nb ratios that are diagnostic of sediment are observed in the most isotopically enriched Samoan lavas, but are absent in the isotopically depleted Ofu lavas (Fig. 5). The Ba/Nb and Pb/Pb* measured in the HIG (FOZO-B) high ^{3}He/^{4}He lavas are indistinguishable from the Ofu lavas, providing further evidence that the Ofu lavas do not host an ancient recycled sediment component (Fig. 5).

4.3. Ofu lavas from recycled harzburgite?

Some recent models advocate a role for ancient, depleted, high ^{3}He/(U+Th) harzburgitic mantle lithosphere in the formation of the high ^{3}He/^{4}He mantle domain (Anderson, 1998; Parman et al., 2005; Heber et al., 2007). This assumes that cpx-poor melt residues may have the property of increased ^{3}He/(U+Th) relative to the initial, unmelted source (Parman et al., 2005), and thus may preserve high ^{3}He/^{4}He ratios over time. Trace element budgets in abyssal peridotites provide a critical test of the hypothesis that recycled harzburgite is involved in the source of high ^{3}He/^{4}He OIB lavas. While a harzburgite lithology is consistent with the cpx-poor nature of the upper oceanic lithosphere, the abyssal peridotites that comprise the upper oceanic lithosphere are too depleted in incompatible trace elements (Workman and Hart, 2005) to act as a source for the high ^{3}He/^{4}He Ofu basalts. For example, the maximum Sr concentration that can be generated by extremely low degrees of aggregated fractional melting of modern harzburgitic abyssal peridotites (samples with <5% cpx, with an average reconstructed bulk rock Sr concentration of ~0.02 ppm; see figure available as supplementary data in the Appendix) is ~5 ppm, which is far below the Sr concentrations (~600 ppm) of primary Ofu lavas. Trace element budgets in modern abyssal peridotites suggest that Ofu basalts are

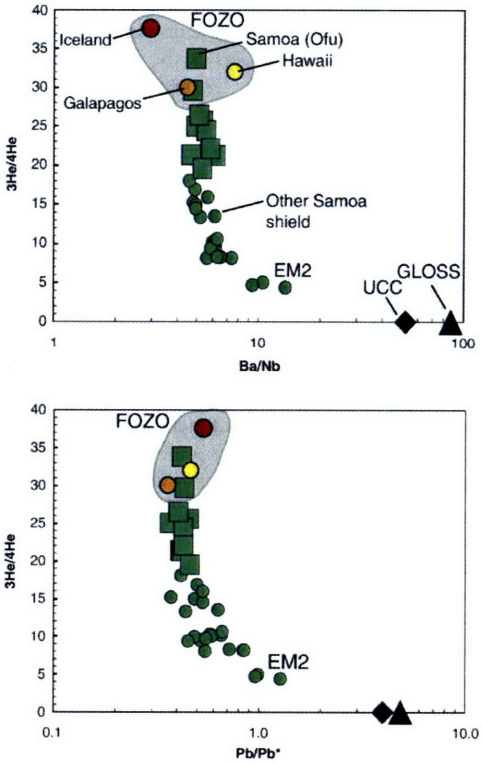

Fig. 5. ^{3}He/^{4}He variation with Ba/Nb and Pb/Pb* in Samoan lavas and high ^{3}He/^{4}He samples from Hawaii (Kurz et al., 1982), Iceland (Hilton et al., 1999) and the Galapagos (Kurz and Geist, 1999; Saal et al., 2007). Ba/Nb ratios in high ^{3}He/^{4}He lavas from all four hotspots are low, and do not indicate input from marine sediment (GLOSS; Plank and Langmuir, 1998) or upper continental crust (UCC; Rudnick and Gao, 2003). Pb/Pb* values in high ^{3}He/^{4}He lavas are also unlike GLOSS and UCC. On the other hand, the enriched (EM2) Samoan lavas have low ^{3}He/^{4}He, high Ba/Nb and high Pb/Pb*, values that suggest a recycled sediment signature (Jackson et al., 2007). All trace element data were measured by ICP, but trace element data from the Iceland and Hawaii samples are unpublished. $Pb/Pb^* = Pb_N / \sqrt{(Ce_N \times Nd_N)}$, where N signifies normalization to primitive mantle (McDonough and Sun, 1995).

Please cite this article as: Jackson, M.G., et al., New Samoan lavas from Ofu Island reveal a hemispherically heterogeneous high ^{3}He/^{4}He mantle, Earth Planet. Sci. Lett. (2007), doi:10.1016/j.epsl.2007.09.023

not the melts of ancient, recycled (depleted) oceanic upper mantle lithosphere.

The base of the oceanic mantle lithosphere, which is thought to have a lherzolitic composition similar to DMM (Workman and Hart, 2005), can produce the Sr concentrations observed in Ofu lavas if it is melted at low degrees. Lherzolitic melt residues also may have the property of increased $^{3}He/(U+Th)$ relative to the initial, unmelted source (Parman et al., 2005). However, results from recent helium partitioning experiments yield conflicting results (Heber et al., 2007; see Section 4.5 below), and suggest that lherzolitic melt residues will have greatly diminished $^{3}He/(U+Th)$. The observation of radiogenic $^{187}Os/^{188}Os$ in high $^{3}He/^{4}He$ lavas from Iceland is inconsistent with a purely peridotitic origin of the high $^{3}He/^{4}He$ mantle (Brandon et al., in press), and suggest that helium partitioning studies based on melting pure peridotite compositions may not be applicable to melting of the high $^{3}He/^{4}He$ reservoirs in the earth's mantle.

4.4. Ofu lavas from chondritic primitive (undegassed) mantle or regassed mantle?

An alternative hypothesis suggests that high $^{3}He/^{4}He$ Samoan lavas are derived from chondritic primitive mantle (referred to as PHEM; Farley et al., 1992). However, such a model fails to explain the non-chondritic $^{143}Nd/^{144}Nd$ and $^{206}Pb/^{204}Pb$ ratios obtained in Ofu lavas: the $^{143}Nd/^{144}Nd$ and $^{206}Pb/^{204}Pb$ ratios of Ofu lavas, which are 0.51283 and 19.19, respectively, are much higher than the corresponding chondritic primitive mantle values, which are 0.512611 (Boyet and Carlson, 2005) and 17.675, respectively.

Another, more recent model attempts to reconcile the non-chondritic lithophile isotopes in high $^{3}He/^{4}He$ lavas assumes that a depleted upper mantle source was "regassed" by mixing with a small proportion of helium-rich, high $^{3}He/^{4}He$ chondritic mantle (Stuart et al., 2003; Ellam and Stuart, 2004). This model suggested that regassed, depleted mantle is in the source of the high $^{3}He/^{4}He$ ratios found in basalts associated with the proto-Iceland plume (PIP). However, Ofu lavas fall well outside of the array formed by PIP lavas in $^{3}He/^{4}He$–$^{143}Nd/^{144}Nd$-isotope space (Ellam and Stuart, 2004), highlighting the need for a model that includes a heterogeneous high $^{3}He/^{4}He$ mantle.

4.5. Implications of $^{142}Nd/^{144}Nd$ for "re-enrichment" of the high $^{3}He/^{4}He$ mantle

The discovery of $^{142}Nd/^{144}Nd$ ratios in accessible terrestrial rocks that are higher than chondrite (Boyet and Carlson, 2005) has important consequences for the origin and evolution of the two FOZOs. The terrestrial $^{142}Nd/^{144}Nd$ anomaly indicates that all measured terrestrial rocks were derived from a reservoir that had superchronditic Sm/Nd during the lifetime of ^{146}Sm, as imperfect mixing of nucleosynthetic material in the solar nebula (Ranen and Jacobsen, 2006) does not explain the terrestrial excess in ^{142}Nd (Hidaka et al., 2003; Andreasen and Sharma, 2006; Carlson et al., 2007; Wombacher and Becker, 2007). For example, if Sm/Nd ratios were heterogeneously distributed in the solar nebula at the time of accretion, bulk silicate earth (BSE) may have acquired higher Sm/Nd and thus higher time-integrated $^{142}Nd/^{144}Nd$ ratios than chondrites (Boyet and Carlson, 2006). If the assumptions for a non-chondritic BSE are valid (Boyet and Carlson, 2006), then both FOZO-A and FOZO-B are isotopically enriched relative to BSE (Fig. 6, top panel). Alternatively, if BSE has chondritic Sm/Nd, the terrestrial $^{142}Nd/^{144}Nd$ anomaly in accessible terrestrial mantle rocks could have been generated by an early, global terrestrial differentiation event within 30 Myr of accretion (Boyet and Carlson, 2005). In this case, the resulting early depleted reservoir (EDR) has superchondritic Sm/Nd and evolves superchondritic $^{142}Nd/^{144}Nd$ (a complementary hidden early enriched reservoir, or EER, evolved sub-chondritic $^{142}Nd/^{144}Nd$; Boyet and Carlson, 2005). The FOZO reservoirs exhibit $^{143}Nd/^{144}Nd$ ratios that are lower (more enriched) than the minimum $^{143}Nd/^{144}Nd$ of the EDR (Fig. 6, bottom panel). If the FOZO reservoirs (like all accessible terrestrial mantle rocks) were ultimately derived from the EDR at some point in earth's history, then the high $^{3}He/^{4}He$ FOZO mantle has been re-enriched since the early differentiation event. In summary, if the terrestrial $^{142}Nd/^{144}Nd$ anomaly relative to chondrites is due to the decay of ^{146}Sm, the observed $^{143}Nd/^{144}Nd$ ratios in FOZO-A and FOZO-B lavas require that they were re-enriched relative to either a non-chondritic BSE or the EDR.

There are a number of mechanisms by which the high $^{3}He/^{4}He$ mantle could have been re-enriched. However, the enriched material added to the high $^{3}He/^{4}He$ reservoirs must also have the property of preserving a high $^{3}He/^{4}He$ signature over time. Thus, re-enrichment by addition of recycled sediments seems unlikely, as lavas exhibiting clear evidence of sediment recycling, such as the high $^{87}Sr/^{86}Sr$ Samoan lavas from Samoa, exhibit low $^{3}He/^{4}He$ (Jackson et al., 2007). On the other hand, re-enrichment by addition of recycled (oceanic crust) eclogite plums to a high $^{3}He/^{4}He$ mantle source may not necessarily diminish the high $^{3}He/^{4}He$ signature (Brandon et al., in press). As an alternative to re-enrichment by eclogite addition, depleted oceanic mantle lithosphere

Please cite this article as: Jackson, M.G., et al., New Samoan lavas from Ofu Island reveal a hemispherically heterogeneous high $^{3}He/^{4}He$ mantle, Earth Planet. Sci. Lett. (2007), doi:10.1016/j.epsl.2007.09.023

that has been re-enriched (metasomatized) with melt may serve as a source for high $^3He/^4He$ basalts (White, 2005). However, if the re-enriching melt is a result of imperfect melt extraction near a mid-ocean ridge (Workman et al., 2004), the $^3He/(U+Th)$ of the melt will have to be similar to or higher than DMM to preserve high $^3He/^4He$ in the recycled upper oceanic mantle lithosphere over time (i.e., following subduction and isolation in the lower mantle). This condition requires that the compatibility of helium is similar to or lower than U and Th during peridotite melting.

However, such partitioning behavior is inconsistent with the helium partitioning results of Parman et al. (2005). Recent helium partitioning results of Heber et al. (2007) do suggest that He is less compatible than U and Th during peridotite melting (assuming a DMM lherzolite lithology from Workman and Hart (2005) and U and Th partition coefficients from Kelemen et al. (2004)). If the partitioning results of Heber et al. (2007) are correct, then oceanic mantle lithosphere hosting trapped melt may preserve high $^3He/^4He$ over time. Thus, long-term isolation of melt-impregnated oceanic mantle lithosphere may provide a viable mechanism for preserving a high $^3He/^4He$ signature, and may have potential for describing the radiogenic isotope compositions and trace element budgets observed in global high $^3He/^4He$ lavas.

4.6. Origin of the hemispheric separation of FOZO-A and FOZO-B: hints from the DUPAL anomaly

The observation of a southern hemisphere high $^3He/^4He$ domain that is isotopically more enriched than its northern hemisphere counterpart is reminiscent of the DUPAL anomaly (Hart, 1984)–a globe-encircling feature of isotopic enrichment observed primarily in the southern hemisphere mantle–and indicates a long-term separation of the earth's northern and southern hemisphere high $^3He/^4He$ mantle. While there are a number of processes by which the re-enriched high $^3He/^4He$ mantle can be generated, the mechanisms responsible for the hemispheric separation, and long-term preservation, of two isotopically distinct FOZO reservoirs are elusive.

Like the high $^3He/^4He$ reservoir (Kurz et al., 1982; Hart et al., 1992) the DUPAL anomaly was suggested to be an ancient feature residing in the lower mantle (Hart, 1988; Castillo, 1988). The DUPAL anomaly is the only

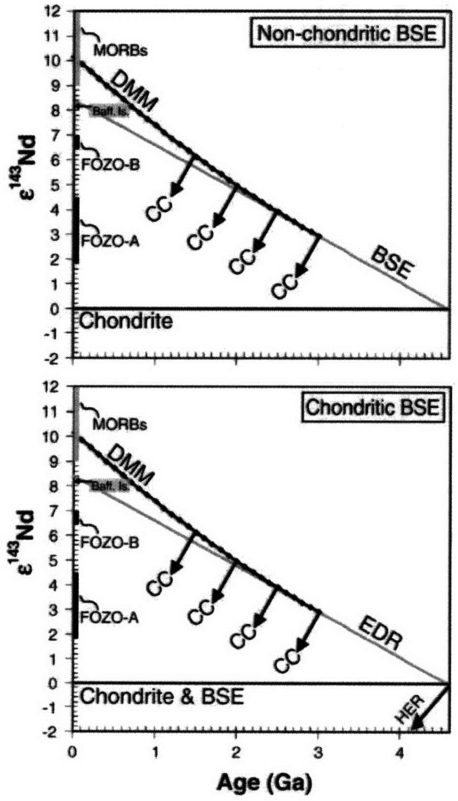

Fig. 6. Implications of terrestrial $^{142}Nd/^{144}Nd$ anomalies for the $^{143}Nd/^{144}Nd$ evolution of BSE and the origin of the two FOZOs. If the observed superchondritic terrestrial mantle $^{142}Nd/^{144}Nd$ ratios (Boyet and Carlson, 2005) were generated by ^{146}Sm decay, either 1.) (top panel) the earth accreted from non-chondritic material and BSE has superchondritic Sm/Nd, or 2.) (bottom panel) BSE is chondritic but underwent an early depletion event and all available terrestrial mantle rocks derive from an early depleted reservoir (EDR) with superchondritic Sm/Nd. All calculations are after Boyet and Carlson (2005, 2006), and assume a chondrite average $^{147}Sm/^{144}Nd$ of 0.1948, $^{143}Nd/^{144}Nd$ of 0.512611, a solar system initial $^{146}Sm/^{144}Sm$ of 0.008, and an identical age of 4.567 Ga for the accretion time of the earth (top panel) and for the early differentiation event (bottom panel). Given these assumptions, the non-chondritic BSE and the EDR require $^{147}Sm/^{144}Nd$ ratios of ~0.209 to generate the $^{142}Nd/^{144}Nd$ anomalies that are 20 ppm higher than chondrite (later formation times for the accretion of the earth, or for the early differentiation event, require even higher Sm/Nd ratios). Thus, the lowest present-day $^{143}Nd/^{144}Nd$ value for a non-chondritic BSE and the EDR is 0.51304 ($\varepsilon^{143}Nd=+8.4$). Both FOZOs exhibit $^{143}Nd/^{144}Nd$ values lower than the non-chondritic BSE (top panel) and the EDR (bottom panel), and *both FOZOs thus exhibit evidence for re-enrichment.* Starting at 3 Ga, the DMM reservoir evolved by continuous extraction of continental crust (Workman and Hart, 2005) from the non-chondritic BSE (top panel) or from the EDR (bottom panel); DMM calculations are identical to Boyet and Carlson (2006). The trajectories of CC and EER are estimated. CC is not extracted as a single event, but is continuously extracted after 3 Ga. The MORB field is from Boyet and Carlson (2005) and FOZO-A and FOZO-B are from Table 2; the Baffin Island (Baff. Is.) high $^3He/^4He$ lava (Stuart et al., 2003) is plotted for reference. $\varepsilon_{Nd}(t)=[^{143}Nd/^{144}Nd_{Sample}(t)/^{143}Nd/^{144}Nd_{Chondrite}(t)-1]\times10^4$.

Please cite this article as: Jackson, M.G., et al., New Samoan lavas from Ofu Island reveal a hemispherically heterogeneous high $^3He/^4He$ mantle, Earth Planet. Sci. Lett. (2007), doi:10.1016/j.epsl.2007.09.023

other mantle domain suggested to occupy similar, hemispheric proportions. The DUPAL anomaly shows that the southern hemisphere exhibits generally more isotopically enriched mantle domains than the northern hemisphere, and we find a similar southern hemisphere enrichment in the high $^3He/^4He$ FOZO-A reservoir; the depletion in the northern hemisphere DUPAL reference reservoir is mirrored in the FOZO-B reservoir. The geographic and geochemical similarities between the FOZO and DUPAL reservoirs suggest that their origin may have been linked.

One hypothesis for the formation of the DUPAL domain is that oceanic mantle and crustal lithosphere were injected into the mantle, thereby enriching this region of the mantle. This model has the advantage of being compatible with two of the possible re-enrichment mechanisms suggested for the FOZO reservoirs in Section 4.5: 1.) oceanic crustal eclogite plums were added to the depleted high $^3He/^4He$ mantle via subduction, or 2.) re-enriched (metasomatized by melt near a mid-ocean ridge) oceanic mantle lithosphere was subducted and isolated in the (deep?) mantle and became the high $^3He/^4He$ mantle domain. These injection models may produce a random pattern of isotopic enrichment throughout the mantle, with no coherent hemispheric pattern (Hart, 1984). However, if injection were focused around the perimeter of a supercontinent during a period of anomalous subduction, a hemispheric pattern in the FOZO and DUPAL reservoirs might emerge. This model would suggest that the hemispheric and isotopic separation may be a surviving artifact of the paleo-arrangement of the subduction zones and continents during the formation of the FOZO reservoirs. While the timing of the formation of the FOZO reservoirs is unknown, we note that the Northern Hemisphere Reference Line (NHRL) separates the two FOZOs in $^{207}Pb/^{204}Pb$–$^{206}Pb/^{204}Pb$-isotope space (see figure included in the supplementary data in the Appendix), possibly suggesting a similar formation time (~1.8 Ga) for the DUPAL and FOZO reservoirs (Pb-isotope ratios in high $^3He/^4He$ lavas are displaced from the Geochron and preclude coeval formation of the FOZO and the hypothetical EDR reservoirs).

4.7. FOZO-A and FOZO-B: implications for mantle dynamics

A clear implication of the isotopic and geographic separation of the two high $^3He/^4He$ reservoirs is that they had to be isolated from each other for long timescales. The long-term separation of the two FOZO domains requires preservation despite convective stirring, a mechanism that efficiently attenuates mantle heterogeneities (van Keken et al., 2002). However, the hemispheric heterogeneity in the high $^3He/^4He$ reservoir is apparently not a feature preserved in the convecting upper mantle sampled by mid-ocean ridges (see Sections 34.1). Thus, the shallow mantle may not be an ideal location for the preservation of the FOZO-A and FOZO-B mantle domains. However, the less rapid convective motions of the lower mantle may make it a more suitable home for the FOZOs (Hart et al., 1992; Macpherson et al., 1998; van Keken et al., 2002; Class and Goldstein, 2005).

One mechanism for the preservation of hemispheric-scale heterogeneity may be the isolation of the high $^3He/^4He$ domains in a dense boundary layer at the core–mantle boundary (CMB). Seismic tomography suggests that some hotspots, like Samoa and Hawaii, may well originate as upwellings from this region of the mantle (Montelli et al., 2006), and many hotspots with high $^3He/^4He$ have been associated with velocity anomalies in the deep mantle (Courtillot et al., 2003). The post-perovskite phase proposed to exist at this depth may exhibit a sufficiently large density contrast to isolate it from the overlying convecting mantle (Guignot et al., 2007), and a new seismic technique may allow detection of this phase at the base of the mantle (van der Hilst et al., 2007). Exploiting this new seismic tool, it may be possible to better resolve the spatial relationships between velocity anomalies at the CMB and high $^3He/^4He$ ocean islands at the earth's surface. Thus, a confluence of geochemical and geophysical observations may ultimately reveal the mechanism responsible for the long-term preservation of the hemispheric heterogeneity in the deep mantle, a feature that hinges on new observations of high $^3He/^4He$ in Samoan lavas from Ofu.

5. Conclusions

From this study we draw the following conclusions:

(1) New high $^3He/^4He$ ratios (19.5–33.8 times atmospheric) from Ofu island are the highest from Samoa (and the southern hemisphere), and place Samoa in the same category of high $^3He/^4He$ hotspots as Hawaii, Iceland and the Galapagos.

(2) The new Ofu data reveal that at least two distinct high $^3He/^4He$ reservoirs–one more isotopically enriched than the other–exist in the earth's mantle.

(3) The two high $^3He/^4He$ reservoirs separate in the earth's northern (FOZO-B, boreal) and southern (FOZO-A, austral) hemispheres.

(4) The trace element budgets and isotopic compositions of the new high $^3He/^4He$ samples from Samoa

Please cite this article as: Jackson, M.G., et al., New Samoan lavas from Ofu Island reveal a hemispherically heterogeneous high $^3He/^4He$ mantle, Earth Planet. Sci. Lett. (2007), doi:10.1016/j.epsl.2007.09.023

are inconsistent with derivation from recycled harzburgite. Additionally, the Samoan high $^{3}He/^{4}He$ mantle does not appear to be contaminated with rapidly cycled sediment from the Tonga subduction zone. Furthermore, the Nd and Pb isotopes of the highest $^{3}He/^{4}He$ Samoan basalts demonstrate that they were not derived from a chondritic primitive mantle.

(5) If the terrestrial $^{142}Nd/^{144}Nd$ anomaly relative to chondrites is due to the decay of ^{146}Sm, the observed $^{143}Nd/^{144}Nd$ ratios in FOZO-A and FOZO-B lavas require that they were re-enriched relative to either a non-chondritic BSE or the EDR.

(6) The high $^{3}He/^{4}He$ mantle is an ancient reservoir, and the discovery of isotopically distinct northern and southern hemisphere high $^{3}He/^{4}He$ mantle domains suggests that these regions of the mantle escaped the convective mixing and stirring that has efficiently attenuated heterogeneities in the upper mantle. This observation provides an important constraint for future dynamic and isotopic models describing the evolution of the earth's mantle.

Acknowledgements

We are indebted to D. Hilton and P. Castillo for supplying a high $^{3}He/^{4}He$ sample from Iceland for trace element analysis, and to T. Hanyu for supplying a high $^{3}He/^{4}He$ sample from Moorea. We thank W. White and C. Macpherson for helpful reviews, and R. Carlson for helpful comments and editorial handling. Discussion with F. Stuart, C. Class, A. Hofmann, N. Shimizu, A. Shaw and J. Blusztajn helped shape the thinking that went into this manuscript. We thank L. Ball for his assistance on the Neptune in the WHOI Plasma Facility, and J. Curtice for his invaluable help in the noble gas facility. Helium isotope measurements were supported by OCE 05-25864. Fa'afetai to the Malae family at Ofu's Vaoto Lodge for their hospitality during the 2004 and 2005 field seasons.

Appendix A. Supplementary data

Supplementary data associated with this article can be found, in the online version, at doi:10.1016/j.epsl.2007.09.023.

References

Abouchami, W., Galer, S.J.G., Koschinsky, A., 1999. Pb and Nd isotopes in NE Atlantic Fe–Mn crusts: proxies for trace metal paleosources and paleocean circulation. Geochim. Cosmochim. Acta 63, 1489–1505.

Anderson, D.L., 1998. A model to explain the various paradoxes associated with mantle noble gas geochemistry. Proc. Natl. Acad. Sci. U. S. A. 95, 9087–9092.

Andreasen, R., Sharma, M., 2006. Solar nebula heterogeneity in p-process samarium and neodymium isotopes. Science 314, 806–809.

Barling, J., Goldstein, S.L., 1990. Extreme isotopic variations in Heard Island lavas and the nature of mantle reservoirs. Nature 348, 59–62.

Boyet, M., Carlson, R.W., 2005. ^{142}Nd evidence for early (>4.53 Ga) global differentiation of the silicate earth. Science 309, 576–581.

Boyet, M., Carlson, R.W., 2006. A new geochemical model for the Earth's mantle inferred from ^{146}Sm–^{144}Nd systematics. Earth Planet. Sci. Lett. 250, 254–268.

Brandon, A.D., Graham, D.W., Waight, T., Gautason, B., in press. ^{186}Os and ^{187}Os enrichments in high-$^{3}He/^{4}He$ sources in the Earth's deep mantle: evidence from Icelandic picrites. Geochim. Cosmochim. Acta. Q1

Carlson, R.W., Boyet, M., Horan, M., 2007. Chondrite barium, neodymium, and samarium isotopic heterogeneity and early earth differentiation. Science 316, 1175–1178.

Castillo, P., 1988. The Dupal anomaly as a trace of the upwelling lower mantle. Nature 336, 667–670.

Castillo, P.R., Scarsi, P., Craig, H., 2007. He, Sr, Nd and Pb isotopic constraints on the origin of the Marquesas and other linear volcanic chains. Chem. Geol. 240, 205–221.

Class, C., Goldstein, S.L., 2005. Evolution of helium isotopes in the Earth's mantle. Nature 436, 1107–1112.

Courtillot, V., Davaille, A., Besse, J., Stock, J., 2003. Three distinct types of hotspots in the Earth's mantle. Earth Planet. Sci. Lett. 205, 295–308.

Doucelance, R., Escrig, S., Moreira, M., Gariépy, C., Kurz, M.D., 2003. Pb–Sr–He isotope and trace element geochemistry of the Cape Verde Archipelago. Geochim. Cosmochim. Acta 67, 3717–3733.

Eisele, J., Sharma, M., Galer, S.J.G., Blichert-Toft, J., Devey, C.W., Hofmann, A.W., 2002. The role of sediment recycling in EM-1 inferred from Os, Pb, Hf, Nd, Sr isotope and trace element systematics of the Pitcairn hotspot. Earth Planet. Sci. Lett. 196, 197–212.

Ellam, R.M., Stuart, F.M., 2004. Coherent He–Sr–Nd isotope trends in high $^{3}He/^{4}He$ basalts: implications for a common reservoir, mantle heterogeneity and convection. Earth Planet. Sci. Lett. 228, 511–523.

Farley, K.A., Natland, J.H., Craig, H., 1992. Binary mixing of enriched and undegassed (primitive?) mantle components (He, Sr, Nd, Pb) in Samoan lavas. Earth Planet. Sci. Lett. 111, 183–199.

Farley, K.A., Basu, A.R., Craig, H., 1993. He, Sr and Nd isotopic variations in lavas from Juan Fernandez Archipelago, SE Pacific. Contrib. Mineral. Petrol. 115, 75–87.

Galer, S.J.G., in press. Chemical and isotopic studies of crust–mantle differentiation and the generation of mantle heterogeneity. PhD, University of Cambridge. Q2

Gerlach, D.C., Hart, S.R., Morales, V.W.J., Palacios, C., 1986. Mantle heterogeneity beneath the Nazca plate: San Felix and Juan Fernandez islands. Nature 322, 165–169.

Graham, D.W., 2002. Noble gas isotope geochemistry of mid-ocean ridge and ocean island basalts; characterization of mantle source reservoirs. In: Porcelli, D., Ballentine, C.J., Wieler, R. (Eds.), Noble Gases in Geochemistry and Cosmochemistry. Reviews in Mineralogy and Geochemistry, vol. 47, pp. 247–318.

Graham, D.W., Lupton, J., Albarède, F., Condomines, M., 1990. Extreme temporal homogeneity of helium isotopes at Piton de la Fournaise, Reunion Island. Nature 347, 545–548.

Graham, D.W., Larsen, L.M., Hanan, B.B., Storey, M., Pedersen, A.K., Lupton, J.E., 1998. Helium isotope composition of the early Iceland

Please cite this article as: Jackson, M.G., et al., New Samoan lavas from Ofu Island reveal a hemispherically heterogeneous high $^{3}He/^{4}He$ mantle, Earth Planet. Sci. Lett. (2007), doi:10.1016/j.epsl.2007.09.023

mantle plume inferred from the Tertiary picrites of West Greenland. Earth Planet. Sci. Lett. 160, 241–255.

Graham, D.W., Reid, M.R., Jordan, B.T., Grunder, A.L., Leeman, W.P., Lupton, J.E., 2006. A helium isotope perspective on mantle sources for basaltic volcanism in the northwestern US. Eos Trans., vol. 87. American Geophysical Union. Abstract V43D-02.

Guignot, N., Andrault, D., Morard, G., Bolfan-Casanova, N., Mezouar, M., 2007. Thermoelastic properties of post-perovskite phase $MgSiO_3$ determined experimentally at core–mantle boundary P–T conditions. Earth Planet. Sci. Lett. 256, 162–168.

Hanan, B.B., Graham, D.W., 1996. Lead and helium isotope evidence from oceanic basalts for a common deep source of mantle plumes. Science 272, 991–995.

Hanyu, T., Kaneoka, I., 1997. The uniform and low $^3He/^4He$ ratios of HIMU basalts as evidence for their origin as recycled materials. Nature 390, 273–276.

Hart, S.R., 1984. A large-scale isotope anomaly in the Southern Hemisphere mantle. Nature 309, 753–757.

Hart, S., 1988. Heterogeneous mantle domains: signatures, genesis and mixing chronologies. Earth Planet. Sci. Lett. 90, 273–296.

Hart, S.R., Blusztajn, J., 2006. Age and geochemistry of the mafic sills, ODP site 1276, Newfoundland margin. Chem. Geol. 235, 222–237.

Hart, S.R., Hauri, E.H., Oschmann, L.A., Whitehead, J.A., 1992. Mantle plumes and entrainment: isotopic evidence. Science 256, 517–520.

Hart, S.R., Coetzee, M., Workman, R.K., Blusztajn, J., Johnson, K.T.M., Sinton, J.M., Steinberger, B., Hawkins, J.W., 2004. Genesis of the Western Samoa seamount province: age, geochemical fingerprint and tectonics. Earth Planet. Sci. Lett. 227, 37–56.

Hauri, E.H., Hart, S.R., 1993. Re–Os isotope systematics of HIMU and EMII oceanic island basalts from the south Pacific Ocean. Earth Planet. Sci. Lett. 114, 353–371.

Hauri, E.H., Shimizu, N., Dieu, J.J., Hart, S.R., 1993. Evidence for hotspot-related carbonatite metasomatism in the oceanic upper mantle. Nature 365, 221–227.

Heber, V.S., Brooker, R.A., Kelley, S.P., Wood, B.J., 2007. Crystal-melt partitioning of noble gases (helium, neon, argon, krypton, and xenon) for olivine and clinopyroxene. Geochim. Cosmochim. Acta 71, 1041–1061.

Hémond, C., Devey, C.W., Chauvel, C., 1994. Source compositions and melting processes in Society and Austral plumes (South Pacific Ocean): element and isotope (Sr, Nd, Pb, Th) geochemistry. Chem. Geol. 115, 7–45.

Hidaka, H., Ohta, Y., Yoneda, S., 2003. Nucleosynthetic components of the early solar system inferred from Ba isotopic compositions in carbonaceous chondrites. Earth Planet. Sci. Lett. 214, 455–466.

Hilton, D.R., Barling, J., Wheller, G.E., 1995. Effect of shallow-level contamination on the helium isotope systematics of ocean–island lavas. Nature 373, 330–333.

Hilton, D.R., Grönvold, K., Macpherson, C.G., Castillo, P.R., 1999. Extreme $^3He/^4He$ ratios in northwest Iceland: constraining the common component in mantle plumes. Earth Planet. Sci. Lett. 173, 53–60.

Hofmann, A.W., White, W.M., 1983. Ba, Rb and Cs in the Earth's mantle. Z. Naturforsch 38 (a), 256–266.

Jackson, M.J., Hart, S.R., Koppers, A.A.P., Staudigel, H., Konter, J., Blusztajn, J., Kurz, M.D., Russell, J.A., 2007. Evidence for the return of subducted continental crust in Samoan lavas. Nature 448, 684–697.

Kelemen, P.B., Yogodzinski, G.M., Scholl, D.W., 2004. Alongstrike variation in lavas of the Aleutian island arc: implications for the genesis of high Mg# andesite and the continental crust. In: Eiler, J. (Ed.), Inside the Subduction Factory. AGU Geophysical Monograph.

Koppers, A.A.P., Russell, J.A., Jackson, M.G., Konter, J., Staudigel, H., Hart, S.R., submitted for publication. Samoa reinstated as a primary hotspot trail, Geology.

Kurz, M.D., Geist, D.J., 1999. Dynamics of the Galapagos hotspot from helium isotope geochemistry. Geochim. Cosmochim. Acta 63, 4139–4156.

Kurz, M.D., Jenkins, W.J., Hart, S.R., 1982. Helium isotopic systematics of oceanic islands and mantle heterogeneity. Nature 297, 43–47.

Kurz, M.D., Jenkins, W.J., Hart, S.R., Clague, D., 1983. Helium isotopic variations in volcanic rocks from Loihi Seamount and the Island of Hawaii. Earth Planet. Sci. Lett. 66, 388–406.

Kurz, M.D., Le Roex, A.P., Dick, H.J.B., 1998. Isotope geochemistry of the oceanic mantle near Bouvet triple junction. Geochim. Cosmochim. Acta 62, 841–852.

Kurz, M.D., Curtice, J.C., Lott III, D.E., Solow, A., 2004. Rapid helium isotopic variability in Mauna Kea shield lavas from the Hawaiian Scientific Drilling Project. Geochem., Geophys., Geosyst. 4, Q04G14. doi:10.1029/2002GC000439.

Macpherson, C.G., Hilton, D.R., Sinton, J.M., Poreda, R.J., Craig, H., 1998. High $^3He/^4He$ ratios in Manus backarc basin: implications for mantle mixing and the origin of plume in the western Pacific Ocean. Geology 26, 1007–1010.

Madureira, P., Moreira, M., Mata, J., Allègre, C.J., 2005. Primitive neon isotopes in Terceira Island (Azores archipelago). Earth Planet. Sci. Lett. 233, 429–440.

McDonough, W.F., Sun, S.S., 1995. The composition of the earth. Chem. Geol. 120, 223–253.

Montelli, R., Nolet, G., Dahlen, F.A., Masters, G., 2006. A catalogue of deep mantle plumes: new results from finite-frequency tomography. Geochem., Geophys., Geosystem 7, Q11007. doi:10.1029/2006GC001248.

Moreira, M., Allègre, C.J., 2004. Helium isotopes on the Macdonald seamount (Austral chain): constraints on the origin of the superswell. C. R. Géosci. 336, 983–990.

Moreira, M., Doucelance, R., Kurz, M.D., Dupré, B., Allègre, C.J., 1999. Helium and lead isotope geochemistry of the Azores Archipelago. Earth Planet. Sci. Lett. 169, 189–205.

Natland, J.H., 1980. The progression of volcanism in the Samoan linear volcanic chain. Am. J. Sci. 280-A, 709–735.

O'Nions, R.K., Hamilton, P.J., Evensen, N.M., 1977. Variations in $^{143}Nd/^{144}Nd$ and $^{87}Sr/^{86}Sr$ ratios in oceanic basalts. Earth Planet. Sci. Lett. 34, 13–22.

Parman, S.W., Kurz, M.D., Hart, S.R., Grove, T.L., 2005. Helium solubility in olivine and implications for high $^3He/^4He$ in ocean island basalts. Nature 437, 1140–1143.

Plank, T., Langmuir, C., 1998. The chemical composition of subducting sediment and its consequences for the crust and mantle. Chem. Geol. 145, 325–394.

Poreda, R.J., Craig, H., 1992. He and Sr isotopes in the Lau Basin mantle: depleted and primitive mantle components. Earth Planet. Sci. Lett. 113, 487–493.

Poreda, R.J., Farley, K.A., 1992. Rare gases in Samoan xenoliths. Earth Planet. Sci. Lett. 113, 129–144.

Ranen, M.C., Jacobsen, S.B., 2006. Barium isotopes in chondritic meteorites: implications for planetary reservoir models. Science 314, 809–812.

Rudnick, R.L., Gao, S., 2003. Composition of the continental crust. In: Rudnick, R.L. (Ed.), Treatise on Geochemistry. The Crust, vol. 3. Permagon, New York, pp. 1–64.

Saal, A.E., Kurz, M.D., Hart, S.R., Blusztajn, J.S., Blichert-Toft, J., Liang, Y., Geist, D.J., 2007. The role of lithospheric gabbros on the com-

Scarsi, P., Craig, H., 1996. Helium isotope ratios in Ethiopian Rift basalts. Earth Planet. Sci. Lett. 144, 505–516.

Staudigel, H., Zindler, A., Hart, S.R., Leslie, T., Chen, C.-Y., Clague, D., 1984. The isotopic systematics of a juvenile intraplate volcano: Pb, Nd and Sr isotope ratios of basalts from Loihi Seamount, Hawaii. Earth Planet. Sci. Lett. 69, 13–29.

Stuart, F.M., Lass-Evans, S., Fitton, J.G., Ellam, R.M., 2003. High $^{3}He/^{4}He$ ratios in picritic basalts from Baffin Island and the role of a mixed reservoir in mantle plumes. Nature 424, 57–59.

Su, Y., in press. Global MORB chemistry compilation at the segment scale. PhD., Columbia University.

Taras, B.D., Hart, S.R., 1987. Geochemical evolution of the New England seamount chain: isotopic and trace element constraints. Chem. Geol. 64, 35–54.

Todt, W., Cliff, R.A., Hanser, A., Hofmann, A.W., 1996. Evaluation of a ^{202}Pb–^{205}Pb double spike for high-precision lead isotope analysis. In: Basu, A., Hart, S.R. (Eds.), Earth Processes: Reading the Isotopic Code. AGU Geophysical Monograph, vol. 95, pp. 429–437.

Turner, S., Hawkesworth, C., Rogers, N., King, P., 1997. U–Th disequilibria and ocean island basalt generation in the Azores. Chem. Geol. 139, 145–164.

Valbracht, P.J., Staudacher, T., Malahoff, A., Allègre, C.J., 1997. Noble gas systematics of deep rift zone glasses from Loihi Seamount, Hawaii. Earth Planet. Sci. Lett. 150, 399–411.

van der Hilst, R.D., de Hoop, M.V., Wang, P., Shim, S.-H., Ma, P., Tenorio, L., 2007. Seismostratigraphy and thermal structure of Earth's core–mantle boundary region. Science 315, 1813–1817.

van Keken, P.E., Hauri, E.H., Ballentine, C.J., 2002. Mantle mixing: the generation, preservation and destruction of chemical heterogeneity. Annu. Rev. Earth Planet. Sci. 30, 493–525.

Wombacher, F., Becker, H., 2007. Barium isotope compositions of chondrites revisited. 17th Annual V.M. Goldschmidt Conference, Cologne, Germany, p. A1125.

White, W.M., 2005. Helium not in store. Nature 436, 1095–1096.

White, W.M., Hofmann, A.W., 1982. Sr and Nd isotope geochemistry of oceanic basalts and mantle evolution. Nature 296, 821–825.

Wright, E., White, W.M., 1987. The origin of Samoa: new evidence from Sr, Nd and Pb isotopes. Earth Planet. Sci. Lett. 82, 151–162.

Woodhead, J.D., 1996. Extreme HIMU in an oceanic setting: the geochemistry of Mangaia Island (Polynesia), and temporal evolution of the Cook-Austral hotspot. J. Volcanol. Geotherm. Res. 72, 1–19.

Workman, R.K., Hart, S.R., 2005. Major and trace element composition of the depleted MORB mantle (DMM). Earth Planet. Sci. Lett. 231, 53–72.

Workman, R.K., Hart, S.R., Jackson, M.G., Regelous, M., Farley, K.A., Blusztajn, J., Kurz, J., Staudigel, H., 2004. Recycled metasomatized lithosphere as the origin of the Enriched Mantle II (EM2) end-member: evidence from the Samoan Volcanic Chain. Geochem., Geophys., Geosystem 5, Q04008. doi:10.1029/2003GC000623.

Zindler, A., Hart, S.R., 1986. Chemical geodynamics. Annu. Rev. Earth Planet. Sci. 14, 493–571.

Please cite this article as: Jackson, M.G., et al., New Samoan lavas from Ofu Island reveal a hemispherically heterogeneous high $^{3}He/^{4}He$ mantle, Earth Planet. Sci. Lett. (2007), doi:10.1016/j.epsl.2007.09.023

Appendix A. Supplementary data (as it appears, published, on the Elsevier website)

Supplementary material for on-line publication only
Click here to download Supplementary material for on-line publication only: Supplement.pdf

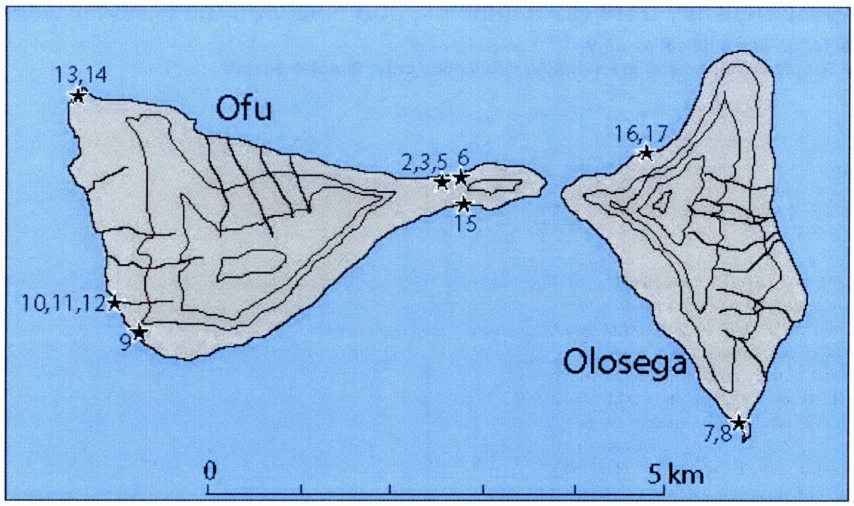

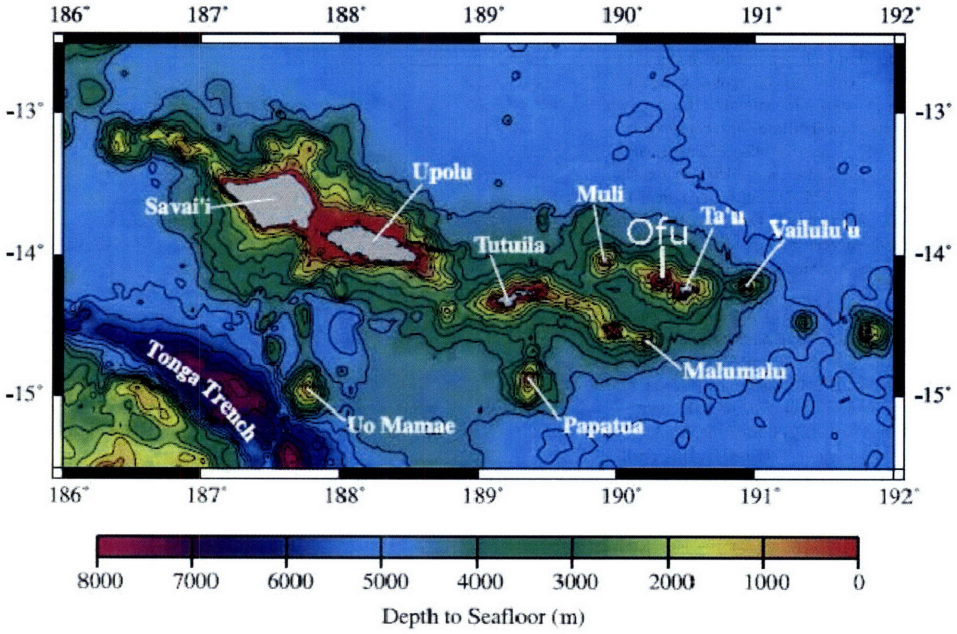

Supplementary Material Fig. 1. Upper panel: Location map for samples taken from Ofu and Olosega islands that are reported in this study. Samples were taken from the major geologic formations recorded by Stice and McCoy (1968). Lower Panel: Ofu Island relative to the subaerial islands (Savai`i, Upolu, Tutuila and Ta`u) and submarine volcanoes (Muli, Malumalu and Vailulu`u) of the Eastern volcanic province (map from Workman et al. (2004)). Papatua and Uo Mamae are isolated, "off-axis" seamounts. Note Samoa's proximity to the northern termination of the Tonga arc/trench system.

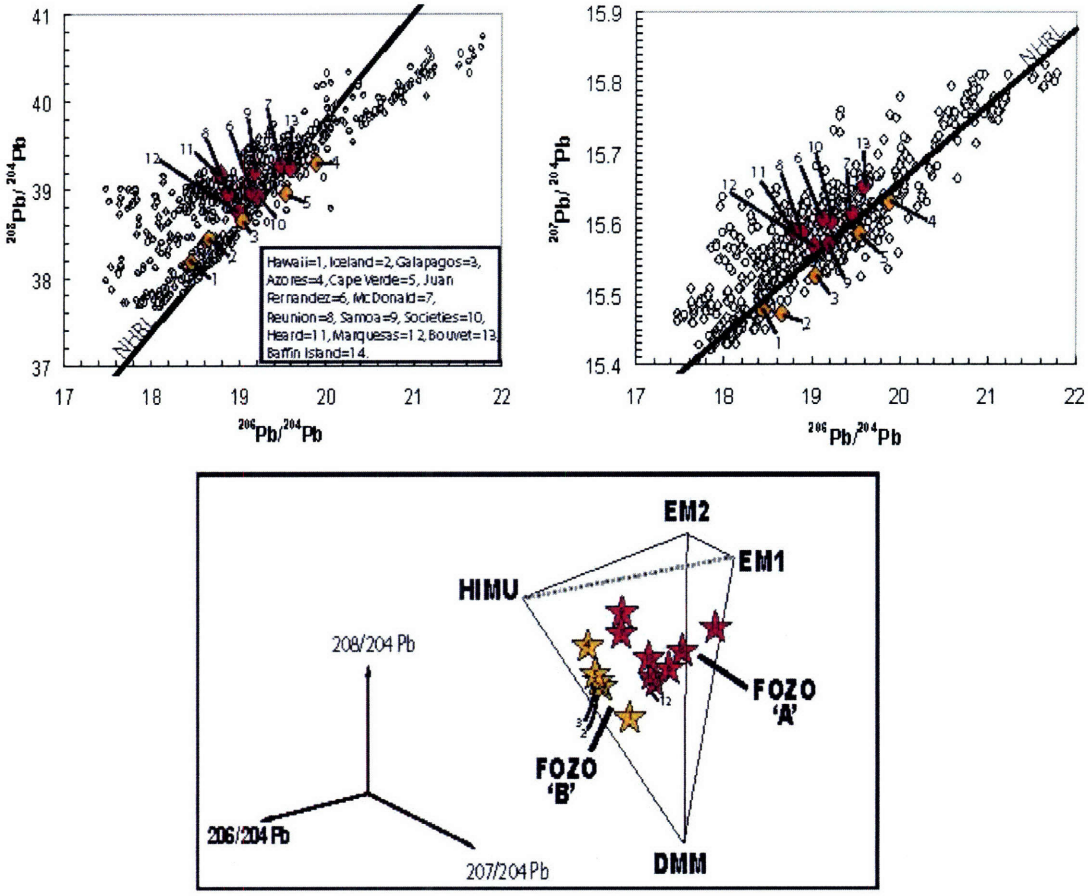

Supplementary Material Fig. 2. The separation of FOZO-A and FOZO-B in Pb-isotope space. Top panels: In two dimensional Pb-isotope space ($^{208}Pb/^{204}Pb$ vs. $^{206}Pb/^{204}Pb$ and $^{207}Pb/^{204}Pb$ vs $^{206}Pb/^{204}Pb$ isotope spaces), the two FOZOs can be separated by a line. However, the Northern Hemisphere Reference Line (NHRL) from Hart (1984) does not appear to divide the two FOZO's in $^{208}Pb/^{204}Pb - ^{206}Pb/^{204}Pb$ space, but does divide them in $^{207}Pb/^{204}Pb - ^{206}Pb/^{204}Pb$ space. Open black diamonds are global OIB data. Lower panel: FOZO-A and FOZO-B separate in 3D Pb-isotope space, indicating that Pb-isotopes are consistent with the hemispheric separation of the two high $^{3}He/^{4}He$ reservoirs. Pb-isotope data used to define FOZO-A and FOZO-B are found in Table 2.

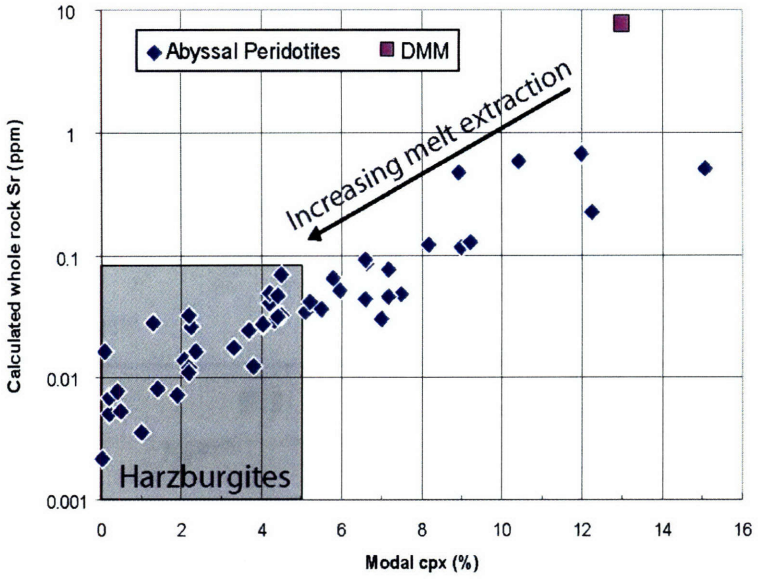

Supplementary Material Fig. 3. Modal abundance of cpx compared to reconstructed whole-rock Sr concentrations in abyssal peridoties, a proxy for recycled, depleted, oceanic upper mantle lithosphere. Sr concentrations in abyssal peridotites diminish rapidly with small reductions in cpx modal abundance, a result of melt extraction from DMM in a fractional melting regime. Harzburgites and other cpx-poor lithologies that are produced in the mantle lithosphere at mid-ocean ridges are extremely trace element depleted. These peridotites may not be good candidates for a source that generates the enriched trace-element budgets observed in Ofu lavas. The abyssal peridotite compilation accompanies Workman and Hart (2005), and the estimate for the Sr concentration in DMM concentrations is from the same source. Samples with modal plagioclase have been excluded.

References

Hart, S.R., 1984. A large-scale isotope anomaly in the Southern Hemisphere mantle. Nature 309, 753-757.

Stice, G.D., McCoy, F.W., 1968. The geology of the Manu'u Islands, Samoa. Pacific. Science 22, 427-457.

Workman, R.K., Hart, S.R., 2005. Major and trace element composition of the depleted MORB mantle (DMM). Earth Planet. Sci. Lett. 231, 53-72.

Chapter 4

High $^{3}He/^{4}He$ hotspot lavas expose the Earth's "missing" titanium, tantalum and niobium (TITAN): The missing link between continental crust and depleted mantle found?

Abstract

A shortage of the elements titanium, tantalum and niobium (TITAN) exists in the Earth's shallow geochemical reservoirs—the depleted MORB (mid-ocean ridge basalt) mantle and continental crust—and the location of these missing elements is unknown. Here we report evidence for a global, TITAN-enriched reservoir sampled by OIBs (ocean island basalts) with high $^{3}He/^{4}He$ ratios, an isotopic signature associated with the deep mantle. Excesses of Ti (and to a lesser degree Nb and Ta) correlate remarkably well with $^{3}He/^{4}He$ in a dataset of global OIBs. The observation of TITAN enrichment in high $^{3}He/^{4}He$ OIB lavas suggests that the mantle domain hosting the Earth's "missing" TITAN is sampled by deep, high $^{3}He/^{4}He$ mantle plumes. The TITAN enrichment in the high $^{3}He/^{4}He$ reservoir has profound implications for the origin of the high $^{3}He/^{4}He$ mantle component, and suggests that, far from being a primitive reservoir, or simply a depleted peridotite reservoir, the high $^{3}He/^{4}He$ mantle sampled by OIBs appears to host a component of recycled, refractory, rutile-bearing oceanic crust that was processed in subduction zones.

*Submitted to Geochemistry, Geophysics, Geosystems (G3) as: M. G. Jackson, S. R. Hart, A. E. Saal, N. Shimizu, M. D. Kurz, J. S. Blusztajn, A. C. Skovgaard, High $^{3}He/^{4}He$ hotspot lavas expose the Earth's "missing" Titanium, Tantalum and Niobium (TITAN): The missing link between continental crust and depleted mantle found? Submitted October, 2007.

1. Introduction

The standard model for the evolution of the silicate earth maintains that the depleted MORB (mid-ocean ridge basalt) mantle (DMM) is the residue of continental crust (CC) extraction from an early primitive mantle (Jacobsen and Wasserburg, 1979; O'Nions et al., 1979; Allegre et al., 1980; Hofmann, 1988, 1997). If the earth has chondritic abundances of the refractory elements, DMM and CC must be geochemically complementary reservoirs within the earth. However, the TITAN trio of elements are prominently depleted in the continents (Rudnick and Gao, 2003), and their absence is not balanced by a corresponding enrichment in DMM (Workman and Hart, 2005). Thus, another deeper reservoir hosting the missing TITAN elements has been proposed to exist in the earth (McDonough, 1991; Rudnick et al., 2000; Kamber and Collerson, 2000).

Oceanic plates are formed by melting and depletion of the upper mantle at mid-ocean ridges. The resulting oceanic lithosphere, composed of mafic oceanic crust and the uppermost region of the depleted peridotite mantle, is subducted back into the mantle at trenches, thereby contributing to its compositional heterogeneity (Hofmann and White, 1980, 1982; Chase, 1981; Zindler and Hart, 1986; van Keken et al., 2002). During subduction, the mafic portion of the plate is dehydrated and may be partially melted, and the resulting lavas erupted at subduction zone volcanoes are depleted in the TITAN elements. Incompatible elements are largely lost to the overlying mantle during dehydration and melting of the eclogite portion of slabs. By contrast, titanium-rich phases, such as rutile, may preferentially sequester the TITAN elements in the mafic portion of the downgoing slab, balancing the depletion observed in subduction zone lavas (Green and Pearson, 1986; Ryerson and Watson, 1987; Brennan et al., 1994; Foley et al., 2000; Schmidt et al., 2004; Kessel et al., 2005). Refractory, rutile-bearing eclogites have been subducted in large quantities over geologic time, and may form a reservoir in the mantle that hosts the Earth's missing TITAN (McDounough, 1991; Rudnick et al., 2000).

TITAN enrichment in hotspot lavas also has enormous potential as a geochemical tracer for recycled oceanic plates (Rudnick et al., 2000). If TITAN-enriched refractory eclogites are returned to the surface in mantle plumes, their presence would be evident as TITAN enrichment in hotspot lavas. A common mantle dynamics paradigm maintains

that mantle plumes complete the process of recycling by transporting plate remnants from the core-mantle boundary back to the surface, where they melt and erupt as ocean island basalts (OIBs) (Hofmann and White, 1980, 1982; Chase, 1981). However, the reservoir hosting the Earth's missing TITAN has been difficult to detect in hotspot lavas (McDonough, 1991; Rudnick et al., 2000).

Rare, high $^3He/^4He$ (>30 Ra, ratio to atmosphere) ratios in lavas erupted at some hotspots, including Hawaii, Iceland, Galapagos and Samoa, are thought to be tracers of buoyantly upwelling mantle plumes that sample an ancient reservoir residing in the mantle (e.g., Kurz et al., 1982; Hart et al., 1992). Variously called FOZO (Focus Zone; Hart et al., 1992; Jackson et al., 2007a), PHEM (Primitive Helium Mantle; Farley et al., 1992) or C (Common; Hanan and Graham, 1996), the precise location (shallow or deep mantle) of the high $^3He/^4He$ reservoir is a source of intense debate (e.g., Anderson, 1998). Nonetheless, there is a growing consensus that this reservoir hosts a significant component of depleted mantle peridotite (e.g., Hart et al., 1992; Anderson, 1998; Parman et al., 2005; Heber et al., 2007). Recent work suggests that the high $^3He/^4He$ mantle may also host a component of recycled eclogite (Dixon et al., 2001; Brandon et al., 2007). In this paper, we argue that the high $^3He/^4He$ mantle sampled by OIBs hosts a component of recycled, refractory eclogite, and that this component balances Earth's budget for the elements titanium, tantalum and niobium (TITAN).

2. New Data and Observations

We report new trace element data by ICP-MS (inductively coupled plasma mass spectrometer) on the highest $^3He/^4He$ lavas from Hawaii (32.3 Ra; Kurz et al., 1982), Iceland (37.7 Ra; Hilton et al., 1999) and Samoa (33.8 Ra; Jackson et al., 2007a) (see Table 1). In Fig. 1, these new data are presented together with previously published ICP-MS trace element data for the highest $^3He/^4He$ Galapagos lava (30.2 Ra; Kurz and Geist, 1999; Saal et al., 2007). These high $^3He/^4He$ lavas exhibit Ti, Ta, and Nb excesses, or positive anomalies, relative to elements of similar compatitiblity in peridotite (on a primitive mantle normalized basis, see Fig. 1). While the association of positive TITAN anomalies and high $^3He/^4He$ (or plume) signatures were previously observed regionally in

Hawaii (Dixon et al., 2001), Iceland (Fitton, 1997) and the Galapagos (Kurz and Geist, 1999; Saal et al., 2007), we suggest that the large, positive TITAN anomalies are a global phenomenon in high $^{3}He/^{4}He$ OIBs. The primitive-mantle normalized trace element patterns (spidergrams) of the highest $^{3}He/^{4}He$ lavas from Hawaii, Iceland, Galapagos and Samoa all share prominent, anomalous enrichment in the TITAN elements compared to elements of similar compatibility in peridotite (Fig. 1). In fact, the Nb/U ratios in the high $^{3}He/^{4}He$ OIB lavas are all higher than the average Nb/U value of 47 previously proposed for OIBs and MORBs (Hofmann et al., 1986).

By contrast, the mantle endmembers (Zindler and Hart, 1986) with low $^{3}He/^{4}He$, including HIMU (high 'μ', or $^{238}U/^{204}Pb$; Graham et al., 1992; Hanyu and Kaneoka, 1997), EM1 (enriched mantle 1; Honda and Woodhead, 2005), EM2 (enriched mantle 2; Workman et al., 2004; Jackson et al., 2007b) and DMM exhibit spidergrams (Hart and Gaetani, 2006) that lack such pronounced TITAN anomalies (Fig. 1). While HIMU basalts can have positive Nb and Ta anomalies (Weaver et al., 1987; Weaver et al., 1991; Chauvel et al., 1992), they generally have lower anomalies than high $^{3}He/^{4}He$ lavas, and can even have negative Nb anomalies (Sun and McDonough, 1989). Importantly, HIMU lavas exhibit flat or negative Ti-anomalies (McDonough, 1991), and thus lack the positive Ti-anomalies observed in high $^{3}He/^{4}He$ lavas.

Available data (see Appendix A) also indicate that the TITAN enrichment is enhanced with increasing $^{3}He/^{4}He$ in OIB lavas (Fig. 2): Large, positive Ti (high Ti/Ti*), Nb (elevated Nb/Nb*) and Ta (Ta/Ta*, not shown) anomalies are observed in the highest $^{3}He/^{4}He$ basalts. While all high $^{3}He/^{4}He$ lavas (>30 Ra) have large, positive TITAN anomalies, not all lavas with positive TITAN anomalies have high $^{3}He/^{4}He$. In the plots of TITAN anomalies vs. $^{3}He/^{4}He$, the OIB data outline a "wedge-shaped" pattern. For example, Cape Verde lavas have large, positive Nb/Nb* values, but have low $^{3}He/^{4}He$ (Fig. 2). However, high $^{3}He/^{4}He$ lavas with negative TITAN anomalies are absent in the available dataset.

High $^{3}He/^{4}He$ lavas exhibit moderately radiogenic Os-isotopes ($^{187}Os/^{188}Os>0.135$), an observation that is contrary to previous suggestions that this reservoir hosts unradiogenic $^{187}Os/^{188}Os$ ratios (Hauri et al., 1996) similar to DMM

(Standish et al., 2002) (Fig. 2). Radiogenic $^{187}Os/^{188}Os$ in the high $^{3}He/^{4}He$ reservoir is consistent with the positive correlation observed between $^{3}He/^{4}He$ and $^{187}Os/^{188}Os$ in Icelandic hotspot lavas (Brandon et al., 2007). However, radiogenic $^{187}Os/^{188}Os$ is not unique to the high $^{3}He/^{4}He$ mantle: the low $^{3}He/^{4}He$ mantle endmembers EM1 and HIMU also have radiogenic $^{187}Os/^{188}Os$. Importantly, unradiogenic $^{187}Os/^{188}Os$ is not observed in high $^{3}He/^{4}He$ OIB lavas.

3. The case for a refractory, rutile-bearing eclogite component in the high $^{3}He/^{4}He$ mantle sampled by OIBs

3.1. TITAN enrichment and high $^{187}Os/^{188}Os$: Evidence for refractory eclogite.

The lack of large TITAN anomalies in DMM (Fig. 1) demonstrates that phases contained in upper mantle peridotites do not preferentially sequester the TITAN elements relative to other incompatible lithophile elements. By contrast, subduction zone lavas are TITAN-depleted, indicating that processes operating in their mantle source can fractionate TITAN from the other lithophile trace elements. It was suggested that eclogite melting in subduction zones may generate rutile-bearing residues that are residually-enriched in TITAN elements (e.g., McDonough, 1991). Experimental studies indicate that the TITAN elements are strongly partitioned into rutile during eclogite melting (Green and Pearson, 1986; Ryerson and Watson, 1987; Ayers, 1998; Stalder et al., 1998; Foley et al., 2000; Schmidt et al., 2004; Kessel et al., 2005), thereby generating positive TITAN anomalies in refractory, rutile-bearing slab residues that balance the depletion observed in subduction zone lavas.

Like TITAN-enrichment, radiogenic $^{187}Os/^{188}Os$ is not a geochemical signature typically associated with a peridotite reservoir. While peridotites tend to have low Re/Os and $^{187}Os/^{188}Os$, mafic igneous rocks generally exhibit elevated Re/Os and $^{187}Os/^{188}Os$ ratios, (Walker et al., 1989; Reisberg et al., 1991; Hauri and Hart, 1993; Reisberg et al., 1993; Snow and Reisberg, 1995; Becker, 2000). Oceanic crust enters subduction zones with initially high Re/Os, and owing to moderate compatibility of Re in garnet, oceanic crust may retain high Re/Os (and with time, radiogenic $^{187}Os/^{188}Os$) ratios during

subduction zone processing in the garnet stability field (Righter and Hauri, 1998). While it has been suggested that Os and Re are extracted from the slab in the subduction zone (e.g., Brandon et al., 1996; McInnes et al., 1999; Becker et al., 2000), we note that the Re/Os ratios of altered oceanic crust ($^{187}Re/^{188}Os$ averages of 349 and 353 in composites of two separate drill cores; Peuker-Ehrenbrink et al., 2003) and oceanic crust gabbros ($^{187}Re/^{188}Os$ average of 472, Hart et al., [1999]) are similar to the ratios found in metabasalts metamorphosed in paleosubduction zones (median $^{187}Re/^{188}Os = 326$, including eclogites, blueschists and mafic granulites; Becker, 2000). Thus, there is ample evidence supporting the contention that high Re/Os ratios can be preserved in the slab during subduction zone metamorphism. Like TITAN enrichment, the observation of moderately radiogenic $^{187}Os/^{188}Os$ in high $^{3}He/^{4}He$ lavas is consistent with a refractory eclogite component in their mantle sources, and not consistent with the high $^{3}He/^{4}He$ reservoir being primitive mantle.

3.2. Depletion in the ^{4}He-producing elements (U and Th) and TITAN enrichment.

While recycled oceanic crust has been suggested to be ubiquitous in the mantle sources beneath hotspots (Sobolev et al., 2007), the close association of a refractory, TITAN-enriched mafic component with the high $^{3}He/^{4}He$ mantle may appear contradictory since eclogites are quantitatively degassed in subduction zones (Staudacher and Allegre, 1988; Moreira and Kurz, 2001; Moreira et al., 2003). Far from hosting the high $^{3}He/^{4}He$ signature in the mantle source of high $^{3}He/^{4}He$ OIB lavas, the eclogite will instead contribute ^{4}He (via alpha decay of U and Th) and generate low time-integrated $^{3}He/^{4}He$ ratios. However, the long-term ^{4}He production of an eclogite can be greatly reduced by melt (or fluid) extraction of highly incompatible elements like U and Th from the slab during subduction processing. By contrast, the TITAN elements will be conserved if melt (or fluid) extraction occurs in the presence of rutile (e.g., McDonough, 1991). In this scenario, a positive TITAN anomaly indicates U and Th (including other incompatible trace elements, like La, Tb and Sm) depletion in a slab. The positive TITAN anomaly is formed by relative enrichment of TITAN due to conservation of Ti,

Ta and Nb and concomitant loss of U and Th. Therefore, the refractory eclogite model of McDonough (1991) is potentially consistent with the preservation of a high $^3He/^4He$ in the mantle. A U- and Th-depleted, TITAN-enriched eclogite will not produce significant post-subduction radiogenic ^4He ingrowth (see below), and may explain why TITAN enrichment is associated with high $^3He/^4He$ signatures.

By contrast, subducted oceanic crust that conserves much of its original U and Th budget through the subduction zone will not possess positive TITAN anomalies and will produce more ^4He over time than a U and Th-depleted slab. Consequently, the abundant ^4He produced by an undepleted slab would infect the surrounding mantle with radiogenic ^4He due to rapid diffusion of helium in the mantle (Hart, 1984; Trull and Kurz, 1993; Hart et al., 2007), and is not compatible with the preservation of a high $^3He/^4He$ signature in the mantle. This hypothesis is consistent with the observation that high $^3He/^4He$ lavas never have negative (or flat) TITAN anomalies.

3.3. Refractory eclogite and high $^3He/^4He$ peridotite: the raw materials for the high $^3He/^4He$ OIB mantle.

While refractory, rutile-bearing eclogite possesses positive TITAN anomalies, it does not have intrinsically high $^3He/^4He$ ratios: high $^3He/^4He$ signatures in the TITAN-enriched, high $^3He/^4He$ OIB source must be derived from another lithology. Ancient mantle peridotites can potentially preserve elevated $^3He/^4He$ ratios over time (Hart et al., 1992; Anderson, 1998; Parman et al., 2005; Heber et al., 2007; Jackson et al., 2007a) if they were isolated from the convecting mantle early in Earth's history. However, mantle peridotites do not generally exhibit positive TITAN anomalies (McDonough, 1991). Alone, neither eclogite nor peridotite can contribute both TITAN-enrichment and high $^3He/^4He$ to the mantle source sampled by high $^3He/^4He$ OIB lavas. Both refractory eclogite and the high $^3He/^4He$ peridotite are required to generate such a mantle source. Thus, an important question is how the TITAN-enriched eclogites came to be associated (i.e., mixed) with high $^3He/^4He$ peridotites in the high $^3He/^4He$ mantle sampled by OIBs.

3.4. Peridotite and eclogite portions of ancient subducted slabs: A high $^{3}He/^{4}He$, TITAN-enriched "package".

One possible explanation for the generation of a hybrid lithology in the high $^{3}He/^{4}He$ OIB mantle is that the crust and mantle components of ancient, subducted oceanic lithosphere contain the raw materials required for the generation of a mantle source sampled by high $^{3}He/^{4}He$ basalts. TITAN-enriched refractory eclogite exists at the top of the slab, and ancient high $^{3}He/^{4}He$ asthenospheric peridotite (with the same composition as contemporary DMM) is coupled to the underside of the downgoing plate. After processing in subduction zones, the crustal portion of the subducted plate hosts TITAN enrichment, and the asthenospheric DMM coupled to the bottom of the downgoing plate remains unscathed by subduction zone processes. The two components, TITAN-enriched eclogite and high $^{3}He/^{4}He$ asthenospheric peridotite, should be intimately associated as a "package" in space and time within a subducted plate, a geometry that is conducive to later mixing in the mantle.

We present a simple model for the generation of the high $^{3}He/^{4}He$ mantle sampled by OIBs, whereby the eclogitic and peridotitic components of the oceanic plate are subducted and isolated from the convecting mantle at 3 Ga and mixed during storage in the lower mantle (Fig 3). We assume that the upper mantle began with a primitive composition (McDonough and Sun, 1995) at 4.4 Ga, and evolved by continuous depletion to the present-day DMM composition of Workman and Hart (2005). Oceanic plates were continuously injected into the mantle over this time period, and the eclogitic and peridotitic portions of these subducted plates were thoroughly mixed in the lower mantle and were later sampled by upwelling mantle plumes and erupted at hotspots.

In order to develop a quantitative geochemical model for the $^{3}He/^{4}He$, $^{187}Os/^{188}Os$, and TITAN of the two lithologies (peridotite and eclogite) in a subducted plate, we make the following assumptions about their compositions over time:

i. $^{3}He/^{4}He$ of ancient asthenospheric DMM peridotite and refractory eclogite: The $^{3}He/^{4}He$ of DMM is thought to have decreased significantly over time (Fig. 3). However, portions of asthenospheric DMM peridotite that are isolated with the downgoing plate

(i.e., removed from the upper mantle) are not subject to further depletion. In the model, the subducted asthenospheric DMM peridotite "locked in" the high $^{3}He/^{4}He$ and $^{3}He/^{238}U$ ratios of ancient, less-depleted DMM, and evolved by closed-system decay of U and Th. By contrast, if the subducted portion of ancient asthenospheric DMM had remained as part of the convecting asthenosphere, it would have evolved by continuous melt extraction to become modern DMM with low $^{3}He/^{4}He$ and $^{3}He/^{238}U$ (see Fig. 3 and Appendix B for details of $^{3}He/^{4}He$ evolution in the mantle). Consequently, following subduction and isolation, the $^{3}He/^{4}He$ of the isolated, ancient DMM rapidly diverged from (and preserved higher $^{3}He/^{4}He$ than) its upper mantle counterpart, which continued to be depleted (in He relative to U and Th, see Appendix B) by continental and oceanic crust extraction (Fig. 3).

By comparison, we model the $^{3}He/^{4}He$ evolution of the subducted eclogite using the trace element composition of a hypothetical refractory eclogite calculated by McDonough (1991) (see Fig. 4 for a spidergram of the refractory eclogite). The eclogite is assumed to start with a $^{3}He/^{4}He$ ratio equal to DMM at its time of isolation, and following over 99% degassing in the subduction zone, the U and Th of the eclogite generates ^{4}He by decay, thus rapidly diminishing the $^{3}He/^{4}He$ of the eclogite over time (Fig. 3, Table 2). Degassing of the eclogite portion of the subducted slab is simulated by increasing the $^{238}U/^{3}He$ of the eclogite by a factor of 1,000 relative to contemporary DMM.

ii. $^{187}Os/^{188}Os$ of ancient asthenospheric DMM peridotite and refractory eclogite:
The $^{187}Os/^{188}Os$ of DMM and Primitive Mantle are not very different (0.12-0.13; Standish et al., 2002; Meisel et al., 2001), and thus the isolated, ancient asthenospheric peridotite portions of the subducted plates are assumed to have an intermediate present-day composition (0.125). DMM is also assumed to have had an Os concentration of 3000 ppt over geologic time. In contrast to the asthenospheric DMM peridotite, the eclogitic portion of the subducted plate likely evolved extremely radiogenic $^{187}Os/^{188}Os$ over time (Fig. 3). The $^{187}Os/^{188}Os$ evolution of the refractory eclogite is modeled using the median $^{187}Re/^{188}Os$ (325) and Os (6 ppt) from eclogites metamorphosed in paleosubduction zones

reported by Becker (2000): earlier subduction injection of eclogites with this composition yielded higher $^{187}Os/^{188}Os$ in the present day. The high calculated present-day $^{187}Os/^{188}Os$ ratios in the recycled eclogites are similar to the most radiogenic eclogites presented by Becker (2000).

iii. TITAN anomalies of ancient asthenospheric DMM peridotite and refractory eclogite: The trace element content of the present-day asthenospheric DMM peridotite is assumed to be the same as the DMM compositions calculated by Workman and Hart (2005). However, DMM has likely become increasingly depleted throughout geologic time. We assume that DMM began with a primitive mantle composition (McDonough and Sun, 1995) and evolved by continuous depletion until the present day. Using the continuous transport equations in Appendix B, the trace element budget of DMM is calculated at various times, and "snapshots" of DMM compositions through time are plotted as spidergrams in Fig. 4 (see Table 2 for compositions). By contrast, the subducted eclogites are assumed to have the same present-day trace element composition as the hypothetical refractory eclogite from McDonough (1991), regardless of the isolation time (see Table 2). This hypothetical eclogite has a trace element composition similar to the eclogites with the largest positive TITAN anomalies presented in Becker et al. (1999) (see Table 2).

3.5. Mixing asthenospheric DMM peridotite with refractory eclogite.

The high $^{3}He/^{4}He$, moderately radiogenic $^{187}Os/^{188}Os$, and positive TITAN anomalies observed in the highest $^{3}He/^{4}He$ OIB lavas can be generated by mixing refractory eclogite and the asthenospheric DMM peridotite that were subducted together (in the same plate) at 3 Ga. When the proportion of refractory eclogite in the mixture is between 20 and 25%, the model generates $^{3}He/^{4}He$, $^{187}Os/^{188}Os$ and positive TITAN anomalies that are similar to the highest $^{3}He/^{4}He$ OIB lavas (Fig. 2). If the proportion of refractory eclogite is increased, the present-day $^{3}He/^{4}He$ in the resulting mixture is diminished and the positive TITAN anomalies and $^{187}Os/^{188}Os$ ratios are both increased to values above those observed in high $^{3}He/^{4}He$ OIB lavas.

Fig. 4 shows that the addition of 20% eclogite to a 3 Ga DMM composition generates a hybrid eclogite-peridotite spidergram that is similar in shape to the spidergram of the highest $^3He/^4He$ lava from Iceland. (Sr is a poor fit, however, due to the positive Sr anomalies in the Icelandic lava, a possible result of interaction with shallow lithospheric gabbros [Gurenko and Sobolev, 2006]). This hybrid spidergram may thus serve as a plausible melt source for the high $^3He/^4He$ lava. It is important to note that the TITAN elements are "bracketed" by elements of similar compatibility (as long as rutile is absent) in the spidergram, and these bracketing elements are used to calculate the TITAN anomalies. Thus, the magnitude of TITAN anomalies are little affected by partial melting beneath a hotspot, and the positive TITAN anomalies in the mantle source of high $^3He/^4He$ lavas are reflected in the erupted hotspot lavas. Clearly, this assumes that the rutile present in the downgoing slab is no longer present in the high $^3He/^4He$ mantle that melts beneath hotspots. One way to destabilize rutile is to completely mix the (smaller proportion of) eclogite and the (larger proportion of) peridotite in the ancient recycled slab. Alternatively, if eclogite is still present in the source of the high $^3He/^4He$ OIB mantle source, it must be melted to a sufficiently high degree to eliminate rutile as a phase in the residue of melting (Gaetani et al., 2007).

This model for the generation of high $^3He/^4He$, TITAN-enriched mantle can also generate a low $^3He/^4He$ that has positive TITAN anomalies. Subduction is a continuous process that has operated for much of geologic time, and the $^3He/^4He$ ratio of the upper mantle has likely decreased significantly (Fig. 3). Thus, the peridotite portion of more recently subducted oceanic plates will trap and preserve a lower $^3He/^4He$ upper mantle signature than ancient subducted plates, and the refractory eclogite portion of recently subducted plates will also host positive TITAN anomalies. For example, the lower $^3He/^4He$, TITAN-enriched mantle source sampled by Cape Verde lavas can be generated by mixing refractory eclogite (10-30% by mass) and asthenospheric DMM components of a plate subducted between 1-2 Ga (Fig. 2).

The "wedge-shaped" outline of the OIB data in Fig. 2 highlights a striking absence of high $^3He/^4He$ lavas with negative (or even small positive) TITAN anomalies. Why do all high $^3He/^4He$ lavas exhibit TITAN-enrichment, or rather, why have high

$^{3}He/^{4}He$-TITAN depleted (or only mildly TITAN enriched) lavas not been found? Continental crust and arc lavas (and associated sediments) compose the only known reservoir to exhibit TITAN depletion. Due to its extremely high U and Th contents, admixture of CC with high $^{3}He/^{4}He$ peridotite may not be conducive to the preservation of high $^{3}He/^{4}He$ (Jackson et al., 2007b), and could explain why TITAN-depleted lavas always exhibit low $^{3}He/^{4}He$ (Fig. 2). OIB lavas lacking TITAN anomalies may host an eclogite component that was not U and Th-depleted (and thus did not acquire positive TITAN anomalies) in a subduction zone, and may also produce significant ^{4}He.

On the other hand, the absence of high $^{3}He/^{4}He$ lavas with flat (or even slightly positive) TITAN anomalies may be explained by the intimate spatial and temporal association between the TITAN-enriched eclogites and high $^{3}He/^{4}He$ peridotites suggested by this model: The peridotite and refractory eclogite components—the raw materials for the formation of the high $^{3}He/^{4}He$, TITAN-enriched mantle—are always together in subducting plates, and it may not be possible to melt pure high $^{3}He/^{4}He$ peridotite without also melting some eclogite. This will be true particularly if subducted slabs are stretched, thinned and folded in the dynamic mantle (Allegre and Turcotte, 1986), such that the diminished thickness of the (eclogite and peridotite) slab is less than the width of melting zones beneath hotspots. Such a process might explain why an eclogite signature (positive TITAN anomalies and radiogenic $^{187}Os/^{188}Os$) is invariably present in high $^{3}He/^{4}He$ lavas.

3.6. Two alternative models for a hybrid high $^{3}He/^{4}He$ mantle: "Eclogite Injection" and diffusion of "Ghost" primordial helium.

An alternative process for generating the hybrid eclogite-peridotite high $^{3}He/^{4}He$ mantle assumes that subducted slab peridotite contributes little to the helium budget of the high $^{3}He/^{4}He$ mantle sampled by OIBs. In this model, the refractory slab eclogite penetrates into the lower mantle and mixes with a hypothetical lower mantle high $^{3}He/^{4}He$ peridotite reservoir (i.e., not associated with the peridotite portion of slabs). The hybrid mixture then rises in a plume where it is melted beneath a hotspot. By comparison to the slab peridotite-eclogite "package" model describe in section 3.4 and 3.5 above, this

alternative "eclogite injection" model does not guarantee an intimate spatial and temporal association of the high $^3He/^4He$ peridotite and TITAN-enriched eclogite components. For example, deep mantle high $^3He/^4He$ peridotite could upwell in a plume without first being inoculated with refractory eclogite, in which case the erupted high $^3He/^4He$ lavas would lack positive TITAN anomalies. Such lavas have not been observed. While this model is not explored further here, one possible solution could be that, due to mixing by stretching and thinning of slabs in a convecting mantle over geologic time (Allegre and Turcotte, 1986), recycled eclogite has become pervasive in the mantle and is distributed at lengthscales smaller than the melting zones beneath hotspot volcanoes. In this way, volcanoes fed by upwelling high $^3He/^4He$ mantle plumes will inevitably sample subducted eclogite.

Instead of mechanically mixing the high $^3He/^4He$ peridotite and TITAN-enriched eclogite, as suggested in the "slab package" and "eclogite injection" models above, it may be possible to diffusively mix helium from a high $^3He/^4He$ peridotite into a degassed, U and Th-poor pyroxenite (i.e., refractory eclogite) (Albarede and Kaneoka, 2007). Due to the higher diffusivity of helium compared to non-volatile major and trace elements, helium isotopes may become decoupled from other lithophile isotope tracers (Hart et al., 2007), and primordial helium may become associated with recycled materials like refractory eclogites (Albarede and Kaneoka, 2007). Albarede and Kaneoka (2007) propose that helium from deep (high $^3He/^4He$) mantle peridotites can diffuse into embedded, tightly folded layers of stretched and thinned refractory eclogite. They suggest that changing the duration of the diffusion process, as well as the U and Th contents of the refractory eclogite layers, can generate mantle sources for both high and low $^3He/^4He$ hotspots. U and Th-poor refractory eclogite that was processed in subduction zones will have positive TITAN anomalies (McDonough, 1991), and because such eclogites will produce little ^4He over time, they are perfect "containers" for preserving diffusively acquired high $^3He/^4He$ signatures. If these eclogites become sufficiently thinned (to <1-2 km thickness, by mantle mixing), they could acquire high $^3He/^4He$ signatures by diffusion from the ambient deep mantle peridotite (Hart et al., 2007). Thus, the "ghost" helium model of Albarede and Kaneoka (2007) may offer a

resolution to the paradoxical association of high $^{3}He/^{4}He$ signatures in lavas with strong eclogite signatures.

Nonetheless, the "ghost helium" model suffers from the same spatial and temporal issues as the "eclogite injection" model: There is no obvious mechanism preventing ambient lower mantle (eclogite-free) peridotite from upwelling and melting beneath a hotspot, thus generating a high $^{3}He/^{4}He$ lava that lacks positive TITAN anomalies. However, one possible resolution is that plume-entrained, high $^{3}He/^{4}He$ lower mantle peridotites are too refractory to contribute significantly to melting beneath OIBs (i.e., Albarede and Kaneoka [2007] invoke dunites and harzburgites), so that pure peridotites are never melted. Alternatively, if eclogite layers are pervasive in the mantle at lengthscales smaller than those sampled by melting zones (<100 km), it may be inescapable that eclogites always contribute to mantle melts. An additional problem with the "ghost helium" model is that rutile may still be stable in a pure eclogite mantle component that is upwelling beneath a hotspot; the residual rutile will hold back TITAN in the source, and as a result, positive TITAN anomalies will not be observed in the erupted lavas. However, if the eclogite is melted to sufficiently high degrees beneath a hotspot, the rutile will be completely consumed and not present in the residue (Gaetani et al., 2007).

3.7. High $^{3}He/^{4}He$ lavas without positive TITAN anomalies?

If a high $^{3}He/^{4}He$ peridotite could be melted in pure (no eclogite) form, there would be no positive TITAN-anomalies in the erupted lavas. There would also be no contribution of ^{4}He ingrowth from the eclogite, and an even higher $^{3}He/^{4}He$ might be expected in the melts of such a mantle source. Such lavas have not been identified. However, with the highest magmatic $^{3}He/^{4}He$ values on record, Baffin Island lavas (Stuart et al., 2003) may provide an important test case for this hypothesis.

3.8. TITAN anomalies due to partitioning between lower mantle phases?

It is difficult to rule out the possibility of TITAN fractionation in lower mantle materials. Experimental studies of high pressure partitioning and mineralogy are in the

early phases. However,Ca-perovskite in peridotitic and basaltic systems shows negative Ti and Nb partitioning patterns compared to Th, U and the rare earth elements (REEs) (Hirose et al., 2004). This means that a Ca-perovskite bearing solid assemblage would have negative anomalies, but melt equilibrated with Ca-perovskite could have positive anomalies. It if it possible to generate Ca-perovskite melts at the appropriate pressures and temperatures (for example, D''), and extract them from the lower mantle (the inferred home of the high $^3He/^4He$ domain), then Ca-perovskite melting in the lower mantle may offer a potential explanation for the origin of TITAN-enriched, high $^3He/^4He$ lavas.

4. The high $^3He/^4He$, TITAN-enriched mantle: A reservoir for the "missing" TITAN elements in the earth?

In addition to offering insights into the composition and generation of the high $^3He/^4He$ mantle reservoir, TITAN-enrichment in high $^3He/^4He$ OIBs may provide information about the location and composition of the reservoir hosting the earth's missing TITAN elements. If the refractory lithophile trace elements have chondritic abundances in BSE (bulk silicate earth), mass balance constraints require that the TITAN elements missing in the shallow earth reservoirs—DMM and CC—must exist in the deeper earth (McDonough, 1991; Rudnick et al., 2000), perhaps in a deep reservoir composed of subducted oceanic plates (Christensen and Hofmann, 1994). In this section, we calculate the trace element budget of a hypothetical missing TITAN-rich reservoir that, when added together with DMM and CC, generates a BSE (McDonough and Sun, 1995) spidergram. We show that, like high $^3He/^4He$ OIB lavas, the spidergram of the TITAN-rich reservoir has positive TITAN anomalies.

In order to estimate the trace element composition of this deep, TITAN-enriched reservoir, we assume that the composition of BSE can be approximated with just three reservoirs: CC, DMM and subducted plates (here called PLATE, which is composed of oceanic crust, mantle lithosphere, and everything else--like sediment--subducted along with downgoing plates). The trace element budget of the PLATE reservoir is calculated using the following mass balance relationship:

$$[x]_{CC} \times M_{CC} + [x]_{DMM} \times M_{DMM} + [x]_{PLATE} \times M_{PLATE} = [x]_{BSE} \times M_{BSE} \quad \text{(eq. 1)}$$

where [x] represents the concentration of the element x in the four reservoirs, and M is the mass of the reservoirs. Assuming the mass of CC is fixed at 0.6% of BSE, and given that the mass proportions of the DMM and PLATE reservoirs are unknown, the following relationships are used to calculate possible trace element budgets for the PLATE reservoir:

$$M_{CC} = 0.006 \times M_{BSE} \quad \text{(eq. 2)}$$

$$M_{PLATE} = \beta \quad \text{(eq. 3)}$$

$$M_{DMM} = 0.994 - \beta \quad \text{(eq. 4)}$$

where the mass of the three reservoirs, PLATE, CC, and DMM sum to the mass of the total silicate mantle. Employing the trace element budgets previously derived for CC (Rudnick and Gao, 2003), DMM (Workman and Hart, 2005) and BSE (McDonough and Sun, 1995), the trace element budget of the subducted PLATE reservoir is calculated for different values of M_{PLATE} (β). The results of the mass balance model are plotted in Fig. 5 (assuming that $\beta \geq 0.4$). The calculated PLATE spidergram changes as a function of its mass proportion (β) of BSE. For large values of β, the PLATE reservoir is more trace element depleted, and for smaller values of β, the PLATE reservoir is increasingly trace element enriched. The most important observation is that, regardless of the value of β, the PLATE reservoir exhibits positive TITAN anomalies.

It is possible to place constraints on the minimum size of the subducted PLATE reservoir and show that its mass proportion of BSE is unlikely to be small. Following Rudnick et al. (2000), we assume that the present mass of the oceanic crust (5.3×10^{21} kg) has been subducted every 100 Ma for the past 2.5 Ga, and the total mass of the reservoir comprised of subducted oceanic crust is 1.3×10^{23} kg. Assuming that the portion of the subducted oceanic plate that is oceanic mantle lithosphere is 10 times thicker and 10% denser than the oceanic crustal lithosphere, then the total mass of oceanic plates

subducted over the past 2.5 Ga is ~1.4×10^{24} kg (~8% of which is oceanic crust), which is ~40% of the mass of BSE. We consider this a minimum estimate for the size of the subducted PLATE reservoir, as subduction probably operated before 2.5 Ga, and the Archaen mantle was hotter, thereby leading to higher rates of plate formation and subduction (Rudnick et al., 2000). Thus, the PLATE reservoir composes ≥40% of BSE, and all possible spidergrams for the plate reservoir are more depleted than the PLATE spidergram shown in Fig. 5.

Therefore, mass balance considerations (equations 1-4) and estimates of plate recycling budgets suggest that a large mantle reservoir host for the missing TITAN elements. The spidergram of the calculated PLATE reservoir exhibits hints of the positive TITAN-anomalies observed in high $^{3}He/^{4}He$ OIBs. Thus, it is not implausible that high $^{3}He/^{4}He$ lavas are sampling the "missing" TITAN hosted in the PLATE reservoir.

While there are many similarities, there is some disagreement between the shape of the spidergrams of the calculated PLATE reservoir and the high $^{3}He/^{4}He$ OIB lavas. Most significantly, the positive TITAN anomalies in the PLATE reservoir are not as large as those observed in the high $^{3}He/^{4}He$ lavas from Hawaii, Iceland, Galapagos and Samoa. One solution to this discrepancy is the following: The PLATE reservoir is likely to be heterogeneous, as it includes everything in BSE that is not DMM or CC. These other components in the PLATE reservoir will dilute the large, positive TITAN-anomalies contributed from recycled, rutile-bearing eclogites. While the PLATE reservoir is not purely a high $^{3}He/^{4}He$ reservoir, its spidergram balances the Earth's budget of TITAN, and recycled, refractory, rutile-bearing eclogite likely contributes the positive TITAN anomalies to the PLATE reservoir (McDonough, 1991). It is this TITAN-enriched domain of the PLATE reservoir that may be associated with the source for high $^{3}He/^{4}He$ lavas.

In section 3.5 it was shown that, if mixed with high $^{3}He/^{4}He$ peridotite, approximately 20 to 25% refractory, rutile-bearing eclogite can generate the $^{3}He/^{4}He$, $^{187}Os/^{188}Os$ and TITAN anomalies in high $^{3}He/^{4}He$ OIBs. However, this percentage of eclogite greatly exceeds the percentage of eclogite in the PLATE reservoir (~8%).

Perhaps this inconsistency can be explained by the fact that eclogites have lower solidus temperatures than pure, unadulterated peridotites. Thus, when melting the high $^{3}He/^{4}He$ portion of the PLATE reservoir beneath a hotspot, the eclogite's (be it pure eclogite or eclogite completely mixed into a peridotite) contribution to the melt will exceed its mass proportion in the mantle source.

5. Implications for $^{142}Nd/^{144}Nd$ measurements on terrestrial mantle rocks

A recent discovery demonstrated that the $^{142}Nd/^{144}Nd$ ratios in all measured terrestrial mantle rocks are 20 ppm higher than chondrite (Boyet and Carlson, 2005, 2006), indicating that these rocks were derived from a reservoir that had superchronditic Sm/Nd during the lifetime of ^{146}Sm (the first few hundred million years following accretion). If the BSE has chondritic abundances of the refractory elements, then the superchondritic $^{142}Nd/^{144}Nd$ ratios observed in the accessible terrestrial rocks suggest that they sample the depleted residue (early depleted reservoir, or EDR) of an early differentiation event. In this model, a complementary hidden "early enriched reservoir" (EER) with subchondritic $^{142}Nd/^{144}Nd$ must exist in the deep earth (Boyet and Carlson, 2005, 2006; Andreasen and Sharma, 2006; Carlson et al., 2007). Alternatively, if BSE accreted from non-chondritic materials, an early differentiation of the silicate earth is not required (Caro et al., 2007).

If the earth accreted from non-chondritic materials, the superchondritic $^{142}Nd/^{144}Nd$ ratios in the terrestrial mantle could be a result of superchondritic $^{147}Sm/^{144}Nd$ (≥ 0.209) ratios in BSE (Boyet and Carlson, 2006). However, a non-chondritic earth does not necessarily obviate the need for a deep, TITAN-enriched SLAB reservoir, because we see evidence for its presence in high $^{3}He/^{4}He$ OIBs.

Alternatively, if BSE does have chondritic abundances of the refractory elements, neither of the two early formed reservoirs—EDR and EER—have the appropriate isotopic and trace element characteristics to be the mantle source of high $^{3}He/^{4}He$ lavas. The EDR was suggested to be the high $^{3}He/^{4}He$ reservoir variously called FOZO, PHEM

or C (Boyet and Carlson, 2006). While the EDR does have higher $^{143}Nd/^{144}Nd$ than chondrite, consistent with globally high (superchondritic) $^{143}Nd/^{144}Nd$ ratios in high $^{3}He/^{4}He$ lavas (Jackson et al., 2007a), the EDR is calculated to have negative TITAN anomalies (Boyet and Carlson, 2005) and is not consistent with being the mantle source of TITAN-enriched, high $^{3}He/^{4}He$ OIB lavas. By contrast, the EER does have positive TITAN anomalies like those observed in high $^{3}He/^{4}He$ OIB lavas. An early crust isolated at the bottom of the mantle has been suggested to host high $^{3}He/^{4}He$ ratios (Tolstikhin and Hofmann, 2005). However, the EER cannot be the mantle source of the high $^{3}He/^{4}He$ as it has Sm/Nd ratios lower (more enriched) than chondrite, and will generate lower $^{143}Nd/^{144}Nd$ ratios than observed in high $^{3}He/^{4}He$ OIBs. Thus, neither of the two initial reservoirs suggested by Boyet and Carlson (2005) describe both the isotopic and trace element characteristic of the high $^{3}He/^{4}He$ OIB mantle. The depleted peridotite and refractory, rutile-bearing eclogite in ancient plates that were subducted and stored in the mantle are ideally suited to be a mantle source for high $^{3}He/^{4}He$ OIB lavas.

6. The fate of slabs and the high $^{3}He/^{4}He$ reservoir

The presence of recycled eclogites in the mantle source of high $^{3}He/^{4}He$ lavas has important implications for the helium isotope evolution of the mantle, since subduction zone processing likely plays an important role in determining the composition of recycled eclogites. Specifically, the uniqueness of the thermal regimes of different subduction zones may affect the composition of eclogites in dramatically different ways. Slab melting and dehydration in ancient, hot subduction zones may residually enrich the slab in TITAN elements while depleting it in U and Th, a process that is conducive to the formation and preservation of a high $^{3}He/^{4}He$, TITAN-enriched mantle reservoir. Alternatively, cooler subduction zones may not generate TITAN anomalies (or deplete the ^{4}He -producing elements, U and Th) in the slab, a scenario that may produce mantle reservoirs with small positive TITAN anomalies and low $^{3}He/^{4}He$. Thus, the fate of the $^{3}He/^{4}He$ evolution of the various mantle reservoirs may hinge on the processes operating in subduction zones.

Appendix A: $^{3}He/^{4}He$, $^{187}Os/^{188}Os$ and trace element data compilation.

$^{3}He/^{4}He$, $^{187}Os/^{188}Os$ and trace element data for representative OIB samples (plotted in fig. 2) are from the GEOROC database (http://georoc.mpch-mainz.gwdg.de/), from the helium database of Abedini et al. (2006), and from the literature. Some of the $^{3}He/^{4}He$ and $^{187}Os/^{188}Os$ data from Iceland are unpublished, as are $^{187}Os/^{188}Os$ data for Samoan samples with $^{3}He/^{4}He$ >20 Ra (the protocol's for measuring $^{187}Os/^{188}Os$ are the same as Skovgaard et al. [2001] for the unpublished Icelandic data and Workman et al. [2004] for the unpublished Samoan data). The $^{3}He/^{4}He$ data from OIBs (plotted in Fig. 2) were obtained by both crushing and fusion of olivine, clinopyroxene and glass, and are not filtered based on helium concentrations. However, samples suggested to have suffered shallow contamination by crust (e.g., several samples in Macpherson et al., 2005) were not included. Additionally, very evolved rocks (MgO<5.3 wt.%) were excluded, so as to preclude the effects of extensive fractional crystallization on the various trace element ratios (e.g., Ti/Ti* and Nb/Nb*). Using Ba/Rb as a filter for alteration, samples with high ratios (Ba/Rb > 25) were not considered. Only trace element (Th, La, Sm, Tb) data measured by ICP-MS and neutron activation are included, thereby eliminating samples with low-precision trace element measurements.

Appendix B: Helium isotope model.

The precise timing of the genesis of the high $^{3}He/^{4}He$ reservoirs cannot be calculated using helium isotopes because the degassing history of the DMM reservoir, the initial $^{4}He/^{3}He$ and ^{3}He abundance of a (hypothetical) undegassed mantle (and DMM), and the present-day ^{3}He abundance in DMM are not well known. Thus, the age of the reservoir (3 Ga), as sampled by the high $^{3}He/^{4}He$ lava from Iceland (sample SEL 97, see Table 1), is poorly constrained. For example, in the model presented in Section 3.5 above, a present-day undegassed mantle $^{238}U/^{3}He$ ratio of 70 was assumed (Table 2). However, if the initial $^{238}U/^{3}He$ ratio of the mantle is increased to a value of ~250, then our model can generate the TITAN anomalies, $^{187}Os/^{188}Os$ and $^{3}He/^{4}He$ of the mantle sampled by the Icelandic lava by subducting and isolating a plate at 4 Ga (in this case, the amount of eclogite required to generate the high $^{3}He/^{4}He$, $^{187}Os/^{188}Os$ and positive

TITAN anomalies in this older, high $^3He/^4He$ mantle reservoir increases slightly). In order to generate a TITAN-enriched, high $^3He/^4He$ mantle at 2 Ga, unrealistically low $^{238}U/^3He$ ratios ($^{238}U/^3He < 10$) are required.

Our preferred model for the time evolution of $^3He/^4He$ in DMM and primitive mantle are as follows. If an initial $^{238}U/^3He$ and $^3He/^4He$ of the undegassed mantle are assumed (see Table 2 for assumed values), and if DMM was formed by continuous depletion by extraction of oceanic and continental crust from a chondritic primitive mantle over Earth's history, the known $^3He/^4He$ of present day DMM (8 Ra) can be used to calculate the present-day $^{238}U/^3He$ of DMM. Thus, assuming that the continuous transport equations (Allegre, 1969; Hart and Brooks, 1970; Workman and Hart, 2005) accurately model the continuously depleting upper mantle (DMM), the $^{238}U/^3He$ and $^3He/^4He$ of DMM can then be calculated at any time from 4.4 Ga to the present day (see Table 2 for list of these values for DMM at different times in earth's history). The helium isotope evolution of the continuously depleting DMM reservoir (shown in Fig. 3) is modeled using the following continuous transport equations:

$$^4He/^3He_t = {}^4He/^3He_T +$$
$$8\lambda_{238}/(\lambda_{238}+k_{238})(^{238}U/^3He)_T(1-\exp(-1(T-t)(\lambda_{238}+ k_{238}))) +$$
$$7\lambda_{235}/(\lambda_{235}+k_{235})(^{235}U/^3He)_T(1-\exp(-1(T-t)(\lambda_{235}+ k_{235}))) +$$
$$6\lambda_{232}/(\lambda_{232}+k_{232})(^{232}Th/^3He)_T(1-\exp(-1(T-t)(\lambda_{232}+ k_{232}))) \quad \text{(eq. 5)}$$

where

$$k_{238} = -1\ln((^{238}U/^3He)_0/(^{238}U/^3He)_T)/(T-t) - \lambda_{238}; \quad \text{(eq. 6)}$$
$$k_{235} = -1\ln((^{235}U/^3He)_0/(^{235}U/^3He)_T)/(T-t) - \lambda_{235}; \quad \text{(eq. 7)}$$
$$k_{232} = -1\ln((^{232}Th/^3He)_0/(^{232}Th/^3He)_T)/(T-t) - \lambda_{232} \quad \text{(eq. 8)}$$

where λ_{238} (1.55×10^{-10} y^{-1}), λ_{235} (9.85×10^{-10} y^{-1}) and λ_{232} (4.95×10^{-11} y^{-1}) are the decay constants for ^{238}U, ^{235}U, and ^{232}Th, respectively, and k_{238}, k_{235} and k_{232} are the continuous transport coefficients for the U-Th-He system in DMM. The k-value is the difference in transport coefficients for U (or Th) and He, and is related to the difference in bulk

partition coefficients between U (or Th) and He; negative k-values in the model indicate that He is transported from the mantle more efficiently than U and Th.

When $k_{238,235,232}$ equals zero, equations 5-8 describe closed-system $^3He/^4He$ evolution. It is assumed that the undegassed mantle has been closed to degassing since 4.4 Ga. Thus, the closed-system model starts at time T=4.4 Ga, where "t" is the time before present day (and T-t equals elapsed time). The $^4He/^3He_T$ (initial ratio) of primitive mantle is unconstrained, but is assumed to be 5,995 (or 120 Ra) and is assumed to increase to 7,224 (or ~100 Ra) today. The $^{232}Th/^{238}U_0$ (present-day) ratio of primitive mantle is assumed to be 4.05 (McDonough and Sun, 1995). The primitive mantle $^{238}U/^3He_0$ (present-day) ratio is then 70. From the $^{238}U/^3He_0$ ratio, the ^3He can be calculated by employing a present-day primitive mantle U concentration of 0.0203 ppm (McDonough and Sun, 1995), and is 7.3×10^{11} atoms/g.

The model for the $^3He/^4He$ and $^{238}U/^3He$ of DMM starts at time T=4.4 Ga. It is assumed that DMM and primitive mantle had the same composition ($^4He/^3He_T$, $^{238}U/^3He_T$ and $^{232}Th/^{238}U_T$) at 4.4 Ga, and that DMM began forming immediately by melt extraction from primitive mantle starting at 4.4 Ga. It is further assumed that DMM has evolved to exhibit present-day $^{232}Th/^{238}U_0$ and $^4He/^3He_0$ values of 2.55 (similar to the value for average DMM in Workman and Hart [2005]) and ~89,900 (8 Ra), respectively. Equations 5 through 8 are then solved for $^{238}U/^3He_0$, which is calculated to be ~54,000. For this solution, k_{238} and k_{235} are both $-1.51\times10^{-9}\ y^{-1}$ and k_{232} is $-1.41\times10^{-9}\ y^{-1}$. If a DMM U concentration of 0.0032 ppm is assumed (Workman and Hart, 2005), the ^3He of present-day DMM is calculated to be 1.5×10^8 atoms/g.

The ^3He abundance in DMM calculated with the continuous depletion model is within a factor of 3 to 20 of the ^3He abundances inferred from MORB samples and ^3He flux from ridges (see Ballentine et al. [2002] for summary). Assuming 10% melting of the mantle source, ^3He concentrations for DMM were derived from CO_2 concentrations and canonical mantle $CO_2/^3He$ ratios in MORB melt inclusions ($4.52\times10^8 \pm 1.93$ atoms $^3He/g$ (Saal et al., 2002), "popping" rock ($>2.69\times10^9$ atoms ^3He /g [Moreira et al., 1998]), and flux of ^3He out of mid-ocean ridges (1.18×10^9 atoms ^3He /g [Farley et al., 1995; Ballentine et al., 2002]).

The increase in $^{238}U/^{3}He$ in DMM over the age of the earth (Table 2) requires that He is less compatible than U and Th during melting of this mantle reservoir. However, the assumption of increased $^{238}U/^{3}He$ in DMM over time is realistic given the lherzolitic lithology of DMM, a mantle reservoir that hosts an estimated cpx modal abundance of ~13% (Workman et al., 2005). Results from a recent helium partitioning study (Heber et al., 2007) are consistent with helium being less compatible than U and Th (assuming U and Th partition coefficients from a recent compilation [Kelemen et al., 2003]) during mantle melting of a lherzolite lithology. However, helium partitioning during mantle melting is a controversial subject. Parman et al. (2005) reported olivine-melt partition coefficients for helium suggesting that helium may be more compatible than U and Th during melting of a cpx-poor lherzolite or harzburgite. However, Heber et al. (2007) report values that are over an order of magnitude smaller (less compatible), suggesting the helium may be more compatible than U and Th only when melting cpx-poor harzburgites or dunites. The discrepancy in olivine-melt helium partition coefficients between these two studies is not yet resolved.

Finally, the continuous transport equations can be written to calculate the concentrations of any element in DMM at any time in earth's history, assuming that DMM formed by continuous depletion of BSE starting at 4.4 Ga:

$$X_{DMM,t} = X_{BSE,0}(\exp(-1(\alpha_X)[T-t])) \quad \text{(eq. 9)}$$

where

$$\alpha_X = -1\ln(X_{DMM,0}/X_{BSE,0})/(T) \quad \text{(eq. 10)}$$

where α_X is proportional to the transport of element X out of DMM over time; $X_{BSE,0}$ and $X_{DMM,0}$ are the present-day concentrations of element X in BSE and DMM, respectively; "t" is time before the present day and T = 4.4 Ga, and $X_{DMM,t}$ is the concentration of element X in DMM at any time "t" before the present day. Using equations 9 and 10, concentrations of trace elements that are known in BSE and present-day DMM can be used to calculate their time-dependent concentrations in DMM. For example, the present-day Ti concentrations in DMM (716 ppm) and BSE (1205 ppm) yield an α_{Ti} value

of 1.18×10^{-10} y^{-1} in equation 10. Thus, using this α_{Ti} value and solving for $Ti_{DMM,t}$ in equation 10, the concentration of Ti in DMM can be calculated at any time in earth's history. More incompatible elements have larger values for α. For example, $\alpha_{Th}=5.25\times10^{-10}$ y^{-1} and $\alpha_{U}=4.20\times10^{-10}$ y^{-1}, where Th is more incompatible than U. In Table 2, the abundances of several trace elements in DMM are provided at various times in earth's history.

References Cited

Abedini, A. A., S. Hurwitz, and W. C. Evans, USGS-NoGaDat — A global dataset of noble gas concentrations and their isotopic ratios in volcanic systems, US Geological Survey Digital Data Series, 202, 2006. Available on the web at: http://pubs.usgs.gov/ds/2006/202

Albarede, F., and I. Kaneoka, Ghost primordial He and Ne, Goldschmidt Conference Abstracts and Programs, 17, p. A9, 2007.

Allègre, C. J., Comportement des systemes U–Th–Pb dans le manteau superieur et modele d'evolution de ce dernier au cours des temps geologiques, Earth Planet. Sci. Lett., 5, 261– 269, 1969.

Allègre, C. J., O. Brévart, B. Dupré, and J. F. Minster, Isotopic and chemical effects produced in a continuously differentiating convecting earth mantle, Phil. Trans. R. Soc. London, A297, 447-477, 1980.

Allègre, C. J., and D. L. Turcotte, Implications of a two-component marble-cake mantle, Nature, 323, 123-127, 1986.

Anderson, D. L., A model to explain the various paradoxes associated with mantle noble gas geochemistry, Proc. Natl. Acad. Sci. U.S.A., 95, 9,087-9,092, 1998.

Andreasen, R., and M. Sharma, M., Solar nebula heterogeneity in p-process samarium and neodymium isotopes, Science, 314, 806–809, 2006.

Ayers, J., Trace element modeling of aqueous fluid – peridotite interaction in the mantle wedge of subduction zones, Contrib. Min. Pet. 132, 390-404, 1998

Ballentine, C.J., P.E. van Keken, D. Porcelli, E.H. Hauri, Numerical models, geochemistry and the zero-paradox noble-gas mantle, Phil. Trans. R. Soc. Lond., A 360, 2611-2631, 2002.

Becker, H., Re-Os fractionation in eclogites and blueschists and the implications for recycling of oceanic crust into the mantle. Earth Planet. Sci. Lett., 177, 287-300 2000.

Becker, H, K. P. Jochum, R. W. Carlson, Trace element fractionation during dehydration of eclogites from high-pressure terranes and the implications for element fluxes in subduction zones, Earth Planet. Sci. Lett., 163, 65-99, 2000.

Boyet, M., and R. W. Carlson, ^{142}Nd evidence for early (>4.53 Ga) global differentiation of the silicate earth, Science, 309, 576–581, 2005.

Boyet, M., and R. W. Carlson, A new geochemical model for the Earth's mantle inferred from ^{146}Sm–^{144}Nd systematics, Earth Planet. Sci. Lett., 250, 254–268, 2006.

Brandon, A. D., R. A. Creaser, S. B. Shirey, and R. W. Carlson, Osmium recycling in subduction zones, Science, 272, 861–864, 1996.

Brandon, A.D., D. W. Graham, T. Waight, and B. Gautason, ^{186}Os and ^{187}Os enrichments and high ^{3}He/^{4}He sources in the Earth's mantle: Evidence from Icelandic picrites, Geochim. Cosmochim. Acta, 71, 4,570-4,591, 2007.

Brenan, J.M., H.F. Shaw, D.L. Phinney, and F.J. Ryerson, Rutile-aqueous fluid partitioning of Nb, Ta, Hf, Zr, U and Th: implications for high field strength element depletions in island-arc basalts, Earth Planet. Sci. Lett., 128, 327-339, 1994.

Carlson, R.W., M. Boyet, M. Horan, Chondrite barium, neodymium, and samarium isotopic heterogeneity and early earth differentiation, Science, 316, 1,175–1,178, 2007.

Caro, G., B. Bourdon, A. N. Halliday, and G. Quitté, Super-chondritic Sm/Nd in Mars, Earth, and the Moon, Eos Trans. AGU, 88, Fall Meet. Suppl., 2007.

Chase, C. G., Oceanic island Pb: two-stage histories and mantle evolution, Earth Planet. Sci. Lett., 52, 277-284, 1981.

Chauvel, C., A. W. Hofmann, and P. Vidal, HIMU-EM: the French–Polynesian connection, Earth Planet. Sci. Lett., 110, 99-119, 1992.

Christiansen, U. R., and A. W. Hofmann, Segregation of subducted oceanic crust in the convecting mantle, J. Geophys. Res., 99, 19,867–19,884, 1994.

Class, C., and S. L. Goldstein, Evolution of helium isotopes in the Earth's mantle, Nature 436, 1,107-1,112, 2005.

Dixon J.E., Leist, L., Langmuir, C. & Schilling, J.G. Recycled dehydrated lithosphere observed in plume-influenced mid-ocean-ridge basalt. Nature **420**, 385-389 (2002).

Farley, K.A., E. Maierreimer, P. Schlosser, and W.S. Broecker, Constraints on mantle He-3 fluxes and deep-sea circulation from an oceanic general circulation model, J. Geophys. Res. Solid Earth, 100, 3829-3839, 1995.

Farley, K. A., J. H. Natland, and H. Craig, Binary mixing of enriched and undegassed (primitive?) mantle components (He, Sr, Nd, Pb) in Samoan lavas, Earth Planet. Sci. Lett., 111, 183-199, 1992.

Fitton, J.G., A.D. Saunders, M.J. Norry, B.S. Hardarson, and R.N. Taylor, Thermal and chemical structure of the Iceland plume, Earth Planet. Sci. Lett. 153, 197-208, 1997.

Foley, S. F., M. G. Barth, and G. A. Jenner, Rutile/melt partition coefficients for trace elements and an assessment of the influence of rutile on the trace element characteristics of subduction zone magmas, Geochim. Cosmochim. Acta, 64, 933-938, 2000.

Frey, F.A., and D. A. Clague, Geochemistry of diverse basalt types from Loihi Seamount, Hawaii: petrogenetic implications, Earth Planet. Sci. Lett., 66, 337-355, 1983.

Gaetani, G. A., P. D. Asimow, E. M. Stolper, Titanium coordination and rutile saturation in eclcogite partial melts at upper mantle conditions, submitted to Earth. Planet, Sci. Lett., 2007.

Graham, D. W., S. E. Humphris, W. J. Jenkins, and M. D. Kurz, Helium isotope geochemistry of some volcanic rocks from Saint Helena, Earth Planet. Sci. Lett., 110, 121–131, 1992.

Green, T. H., and N.J. Pearson, Ti-rich accessory phase saturation in hydrous mafic-felsic compositions at high P,T, Chem. Geol., 54, 185-201, 1986.

Gurenko, A. A., and Sobolev, A. V., Crust–primitive magma interaction beneath neovolcanic rift zone of Iceland recorded in gabbro xenoliths from Midfell, SW Iceland, Contrib. Min. Pet., 151, 495–520, 2006.

Hanan, B. B., and D.W. Graham, Lead and helium isotope evidence from oceanic basalts for a common deep source of mantle plumes, Science, 272, 991-995, 1996.

Hanyu, T., and I. Kaneoka, The uniform and low $^{3}He/^{4}He$ ratios of HIMU basalts as evidence for their origin as recycled materials, Nature, 390, 273-276, 1997.

Hart, S. R., He Diffusion in olivine, Earth Planet. Sci. Lett., 70, 297–302, 1984.

Hart, S. R., J. Blusztajn, H. J. B. Dick, P. S. Meyer, and K. Muehlenbachs, The fingerprint of seawater circulation in a 500-meter section of oceanic crust gabbros, Geochim. Cosmochim. Acta, 63, 4,059-4,080, 1999.

Hart, S.R., and C. Brooks, Rb–Sr mantle evolution models, Year b.-Carnegie Inst., 68 426–429, 1970.

Hart, S.R., and G.A. Gaetani, Mantle Pb paradoxes: the sulfide solution, Contrib. Mineral. Petrol., 152, 295-308, 2006.

Hart, S.R., E. H. Hauri, L. A. Oschmann, and J. A. Whitehead, Mantle plumes and entrainment: Isotopic evidence, Science, 256, 517-520, 1992.

Hart, S. R., M. D. Kurz, and Z. Wang, Scale length of mantle heterogeneities: constraintsfrom He diffusion, submitted Earth Planet. Sci. Lett., 2007.

Hauri, E.H., and S.R. Hart, Re-Os isotope systematics of HIMU and EMII oceanic island basalts from the south Pacific Ocean, Earth Planet. Sci. Lett., 114, 353-371, 1993.

Hauri, E. H., J. C. Lassiter, and D.J. DePaolo, Osmium isotope systematics of drilled lavas from Mauna Loa, Hawaii, J. Geophys. Res., 101, 11,793-11,806, 1996.

Heber, V.S., R.A. Brooker, S.P. Kelley, B.J. Wood, Crystal-melt partitioning of noble gases (helium, neon, argon, krypton, and xenon) for olivine and clinopyroxene, Geochim. Cosmochim. Acta, 71, 1,041-1,061, 2007.

Hilton, D. R., K. Grönvold, C. G. Macpherson, and P. R. Castillo, Extreme $^{3}He/^{4}He$ ratios in northwest Iceland: constraining the common component in mantle plumes, Earth Planet. Sci. Lett., 17, 53-60, 1999.

Hirose, K., N. Shimizu, W. van Westrenen, and Y. Fei, Trace element partitioning in Earth's lower mantle and implications for geochemical consequences of partial melting at the core-mantle boundary, Phys. Earth Planet. Int., 146, 249-260, 2004.

Hofmann, A.W., Chemical differentiation of the Earth: the relationship between mantle, continental crust, and oceanic crust, Earth Planet. Sci. Lett., 90, 297-314, 1988.

Hofmann, A.W., Mantle geochemistry: The message from oceanic volcanism, Nature 385, 219-229, 1997.

Hofmann, A.W., K. P. Jochum, M. Seufert, and W. M. White, Nb and Pb in oceanic basalts: new constraints on mantle evolution, Earth Planet. Sci. Lett., 79, 33-45, 1986.

Hofmann, A. W., and W. M. White, The role of subducted oceanic crust in mantle evolution, Carnegie Inst. Washington Yearbook, 79, 477-483, 1980.

Hofmann, A.W., and W. M. White, Mantle plumes from ancient oceanic crust, Earth Planet. Sci. Lett., 57, 421-436, 1982.

Honda, M., and J. D. Woodhead, A primordial solar-neon enriched component in the source of EM-I-type ocean island basalts from the Pitcairn Seamounts, Polynesia, Earth Planet. Sci. Lett., 236, 597– 612, 2005.

Jackson, M. J., S. R. Hart, A. A. P. Koppers, H. Staudigel, J. Konter,J. Blusztajn, M. D. Kurz, and J. A. Russell, Evidence for the return of subducted continental crust in Samoan lavas, Nature, 448, 684-697, 2007b

Jackson, M.G., M.D. Kurz, S.R. Hart, and R.K. Workman, New Samoan lavas from Ofu Island reveal a hemispherically heterogeneous high $^{3}He/^{4}He$ mantle. Earth Planet. Sci. Lett., 2007a, doi:10.1016/j.epsl.2007.09.023.

Jacobsen, S.B., and G. J. Wasserburg, The mean age of mantle and crustal reservoirs, J. Geophys. Res., 84, 7411-7427, 1979.

Kamber, B.S., and K.D. Collerson, Role of "hidden" deeply subducted slabs in mantle depletion, Chem. Geol., 166, 241-254, 2000.

Kelemen, P.B., G.M. Yogodzinski, D.W. Scholl, Alongstrike variation in lavas of the Aleutian island arc: implications for the genesis of high Mg# andesite and the continental crust, Inside the Subduction Factory, AGU Monograph 139, John Eiler, editor, American Geophysical Union, Washington, DC, 223– 276, 2003.

Kessel, R., M. W. Schmidt, P. Ulmber, and T. Pettke, Trace element signature of subduction-zone fluids, melts and supercritical liquids at 120-180 km depth, Nature, 437, 724-727, 2005.

Kurz, M. D., and D. J. Geist, Dynamics of the Galapagos hotspot from helium isotope geochemistry, Geochim. Cosmochim. Acta, 63, 4,139-4,156, 1999.

Kurz, M. D., W. J. Jenkins, and S.R. Hart, Helium isotopic systematics of oceanic islands and mantle heterogeneity, Nature, 297, 43-47, 1982.

Kurz, M. D., W. J. Jenkins, S. R. Hart, and D. Clague, Helium isotopic variations in volcanic rocks from Loihi Seamount and the Island of Hawaii, Earth Planet. Sci. Lett., 66, 388-406, 1983.

Macpherson, C. G., D. R. Hilton, J. M. D. Day, D. Lowry, and K. Grönvold, High-$^{3}He/^{4}He$, depleted mantle and low $\delta^{18}O$, recycled oceanic lithosphere in the source of central Iceland magmatism, Earth Planet. Sci. Lett., 233, 411-427, 2005.

McDonough, W.F., Partial melting of subducted oceanic crust and isolation of its residual eclogitic lithology, Philos. Trans. R. Soc. London, Ser. A, 335, 407-418, 1991.

McDonough, W. F., and S. S. Sun, The composition of the Earth, Chem. Geol., 120, 223-253, 1995.

McInnes, B. I., J. S. McBride, N. J. Evans, D. D. Lambert, and A. S. Andrew, Osmium isotope constraints on ore metal recycling in subduction zones, Science, 286, 512-516, 1999.

Meisel, T., R. J. Walker, A. J. Irving, and J. P. Lorand, Osmium isotopic compositions of mantle xenoliths: A global perspective, Geochim. Cosmochim. Acta, 65, 1311–1323, 2001.

Moreira, M., J. Blusztajn, J. Curtice, S. Hart, H. Dick, and M. D. Kurz, He and Ne isotopes in oceanic crust: implications for noble gas recycling in the mantle, Earth Planet. Sci. Lett., 216, 635-643, 2003.

Moreira, M., J. Kunz, and C.J. Allègre, Rare gas systematics in popping rock: Isotopic and elemental compositions in the upper mantle, Science, 279, 1178-1181, 1998.

Moreira, M., and M. D. Kurz, Subducted oceanic lithosphere and the origin of the 'high μ' basalt helium isotopic signature, Earth Planet. Sci. Lett., 189, 49-57, 2001.

Niemann, H.B., S.K. Atreya, G.R. Carignan, T.M. Donahue, J.A. Haberman, D.N. Harpold, R.E. Hartle, D.M. Hunten, W.T. Kasprzak, P.R. Mahaffy, T.C. Owen, N.W. Spencer, and S.H. Way, The Galileo probe mass spectrometer: Composition of Jupiter's atmosphere, Science, 272, 846-849, 1996.

O'Nions R. K., N. M. Evensen, and P. J. Hamilton P. J., Geochemical modeling of mantle differentiation and crustal growth. J. Geophys. Res., 84, 6091-6101, 1979.

Parman, S. W., M. D. Kurz, S. R. Hart, and T. L. Grove, Helium solubility in olivine and implications for high $^{3}He/^{4}He$ in ocean island basalts, Nature, 437, 1,140-1,143 2005.

Peucker-Ehrenbrink, B., W. Bach, S. R. Hart, J. S. Blusztajn, and T. Abbruzzese, Rhenium-osmium isotope systematics and platinum group element concentrations in oceanic crust from DSDP/ODP Sites 504 and 417/418, Geochemisty, Geophysics, Geosystems, 4, doi:10.1029/2002GC000414, 2003

Reisberg, L. C., C. J. Allègre, and J. M. Luck. The Re-Os systematics of the Ronda Ultramafic Complex of southern Spain, Earth Planet. Sci. Lett., 105, 196-213, 1991.

Reisberg, L., A. Zindler, F. Marcantonio, W. White, D. Wyman, and B. Weaver, Os isotope systematics in ocean island basalts, Earth Planet. Sci. Lett, 120, 149-167, 1993.

Righter, K., and E. H. Hauri, Compatibility of Rhenium in garnet during mantle melting and magma genesis, Science, 280, 1,737-1,741, 1998,

Rudnick, R.L., M. Barth, I. Horn, and W. F. McDonough, Rutile-bearing refractory eclogites: the missing link between continents and depeted mantle. Science, 287, 278-281, 2000.

Rudnick, R.L., and S. Gao, Composition of the continental crust, in The Crust, Treatise on Geochemistry, 3, R. L. Rudnick, editor, Permagon, New York, 1-64, 2003.

Ryerson, F.J., and E. B. Watson, Rutile saturation in magmas: implications for Ti-Nb-Ta depletion in island-arc basalts, Earth Planet. Sci. Lett., 86, 225-239, 1987.

Saal, A.E., E.H. Hauri, C.H. Langmuir, and M.R. Perfit, Vapour undersaturation in primitive mid-ocean-ridge basalt and the volatile content of Earth's upper mantle, Nature, 419 451-455, 2002.

Saal, A. E., M. D. Kurz, S. R. Hart, J. S. Blusztajn, J. Blichert-Toft, Y. Liang, and D. J. Geist, The role of lithospheric gabbros on the composition of Galapagos lavas, Earth Planet. Sci. Lett., 257, 391-406, 2007.

Schmidt, M.W., A. Dardon, G. Chazot, and R. Vannucci, The dependence of Nb and Ta rutile-melt partitioning on melt composition and Nb/Ta fractionation during subduction processes, Earth Planet. Sci. Lett., 226, 415-432, 2004.

Skovgaard, A.C., M. Storey, J. Baker, J. Blusztajn, and S.R. Hart, Osmium-oxygen isotopic evidence for a recycled and strongly depleted component in the Icelandic mantle plume, Earth Planet Sci. Lett., 194, 259-275, 2001.

Snow, J.E., and L. Reisberg, Os isotopic systematics of the MORB mantle: results from altered abyssal peridotites. Earth Planet. Sci. Lett., 133, 411-421, 1995.

Sobolev, A.V., A. W. Hofmann, D. V. Kuzmin, G. M. Yaxley, N. T. Arndt, S.-L. Chung, L. V. Danyushevsky, T. Elliott, F. A. Frey, M. O. Garcia, A. A. Gurenko, V. S. Kamenetsky, A. C. Kerr, N. A. Krivolutskaya, V. V. Matvienkov, I. K. Nikogosian, A. Rocholl, I. A. Sigurdsson, N. M. Sushchevskaya, and M. Teklay, The amount of recycled crust in sources of mantle-derived melts, Science, 316, 412-417, 2007.

Stalder, R., S. F. Foley, G. P. Brey, and I. Horn, Mineral-aqueous fluid partitioning of trace elements at 900-1200°C and 3.0-5.7 GPa: New experimental data for garnet, clinopyroxene, and rutile and implications for mantle metasomatism, Geochim. Cosmochim. Acta, 62, 1781-1801, 1998.

Standish, J.J., S. R. Hart, J. Blusztajn, H. J. B. Dick, and K. L. Lee, Abyssal peridotite osmium isotopic compositions from Cr-spinel, Geochemistry, Geophysics, Geosystems, 3, 2001GC000161, 2002.

Staudacher, T. and C. J. Allegre, Recycling of oceanic crust and sediments: the noble gas subduction barrier, Earth Planet. Sci. Lett., 89, 173-183, 1988.

Staudigel, H., A. Zindler, A. R. Hart, T. Leslie, C.-Y. Chen, D. Clague, The isotopic systematics of a juvenile intraplate volcano: Pb, Nd and Sr isotope ratios of basalts from Loihi Seamount, Hawaii, Earth Planet. Sci. Lett., 69, 13-29, 1984.

Stuart, F., S. Lass-Evans, J. G. Fitton, and R. M. Ellam, High $^{3}He/^{4}He$ ratios in picritic basalts from Baffin Island and the role of a mixed reservoir in mantle plumes, Nature, 424, 57-59, 2003

Sun, S.-S., and W. F. McDonough, Chemical and isotopic systematics of oceanic basalts: implications for mantle composition and processes, in Magmatism in the ocean basins, Geol. Soc. Lond. Spec. Publ., 42, A. D. Saunders and M. J. Norry, editors, 313-345, 1989.

Tolstikhin, I., and A.W. Hofmann, Early crust on top of the Earth's core, Phys. Earth Planet. Interiors, 148, 109-130, 2004.

Trull, T. W., and M. D. Kurz, Experimental measurements of ^{3}He and ^{4}He mobility in olivine and clinopyroxene at magmatic temperatures, Geochim. Cosmochim. Acta, 57, 1,313-1,324, 1999.

van Keken, P. E., E. H. Hauri, and C. J. Ballentine, Mantle mixing: the generation, preservation, and destruction of chemical heterogeneity, A. Rev. Earth Planet. Sci. 30, 493-525, 2002.

Walker, R. J., R. W. Carlson, S. B. Shirey, and F. R. Boyd, Os, Sr, Nd and Pb isotope systematics of southern African peridotite xenoliths: implications for the chemical evolution of subcontinental mantle, Geochim. Cosmochim. Acta, 53, 1,583-1,595, 1989.

Weaver, B. L, The origin of ocean island basalt end-member compositions: Trace element and isotopic constraints, Earth Planet. Sci. Lett., 204, 381–397, 1991.

Weaver, B. L., D. A. Wood, J. Tarney, J. L. Joron, Geochemistry of oceanic island basalts from the South Atlantic: Ascension, Bouvet, St Helena, Gough and Tristan da Cunha, in Alkaline igneous rocks, Geol. Soc. London Spec. Publ. 29, J. G. Fitton and B. G. J. Upton, editors, Geological Society of London, 253-267, 1987.

Workman, R.K., and S. R. Hart, Major and trace element composition of the depleted MORB mantle (DMM), Earth Planet. Sci. Lett. 231, 53-72, 2005.

Workman, R.K., S.R. Hart, M.G. Jackson, M. Regelous, K.A. Farley, J. Blusztajn, M. Kurz, H. Staudigel, Recycled metasomatized lithosphere as the origin of the Enriched Mantle II (EM2) end-member: Evidence form the Samoan Volcanic Chain, Geochem. Geophys. Geosyst., 5, doi:10.1029/2003GC000623, 2004.

Zindler, A., and S.R. Hart, Chemical Geodynamics, Ann. Rev. Earth Planet. Sci., 14, 493–571, 1986.

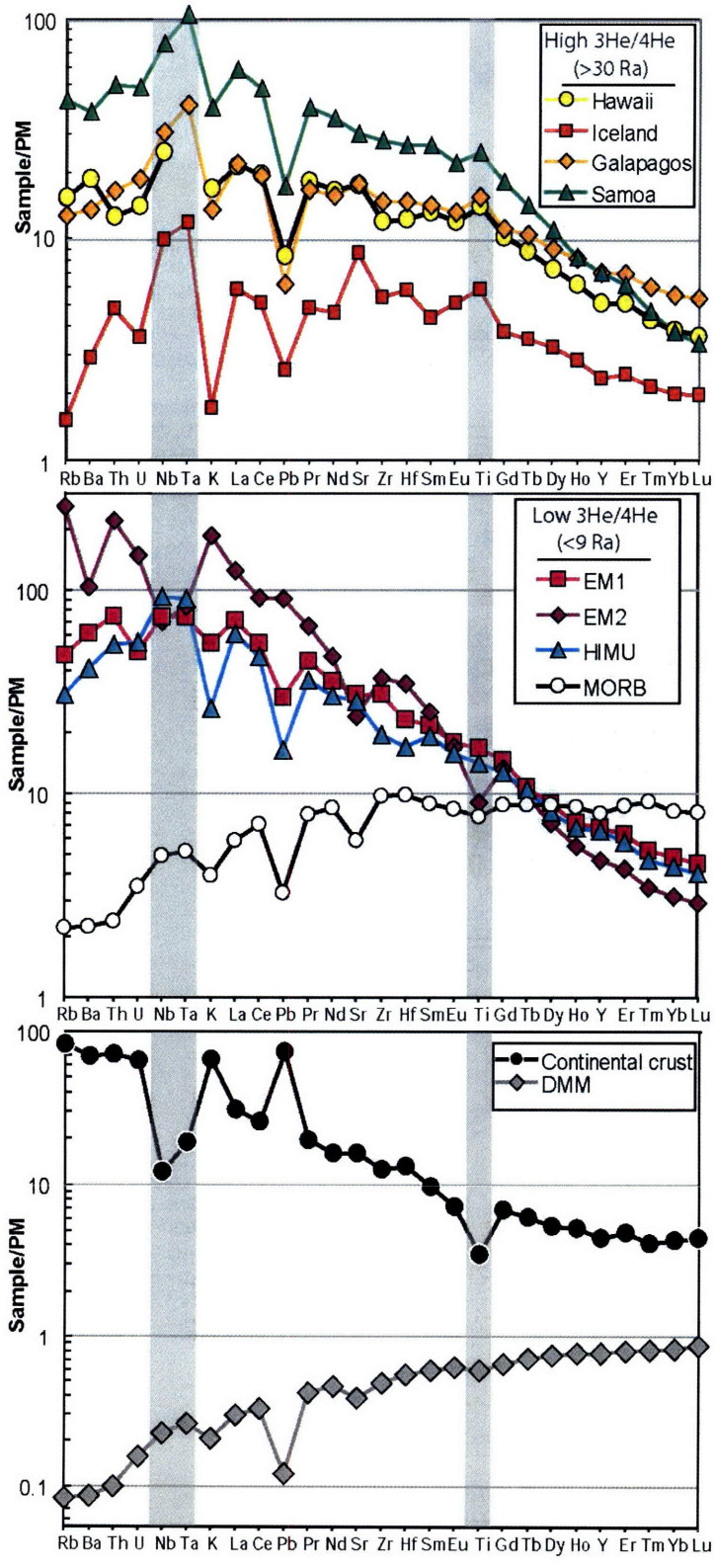

Figure 1. Titanium, tantalum and niobium (TITAN) are highly enriched in ocean island basalts (OIBs) with high $^{3}He/^{4}He$. Top panel: Primitive mantle (PM) normalized trace element data (spidergrams) for basalts with the highest $^{3}He/^{4}He$ (>30 Ra) from 4 different hotspots. All high $^{3}He/^{4}He$ samples exhibit TITAN enrichment relative to neighboring elements on the spidergrams. Middle panel: Spidergrams for the low $^{3}He/^{4}He$ (<9 Ra) mantle endmembers. EM1 lavas are from Pitcairn, EM2 lavas are from Samoa, HIMU lavas are from Mangaia and Tubuaii. Spidergrams for the mantle endmembers and MORB are from Hart and Gaetani (2006) and (for EM2) Jackson et al. (2007b). TITAN enrichment is not as pronounced, or is absent, in the average spidergrams of the low $^{3}He/^{4}He$ mantle endmembers. Bottom panel: Spidergrams for DMM (Workman and Hart, 2005) and continental crust (Rudnick and Gao, 2003) indicate that these two shallow earth reservoirs are not entirely geochemically complementary: TITAN depletion in the continents is not balanced by corresponding enrichment in DMM (see Fig. 5 for mass balance details). However, the TITAN-enrichment in high $^{3}He/^{4}He$ lavas suggests that these lavas sample a (deeper) mantle reservoir that hosts the TITAN that is "missing" in the shallow geochemical reservoirs, DMM and continental crust. Sources of the $^{3}He/^{4}He$ data for the mantle endmembers and the high $^{3}He/^{4}He$ lavas can be found in the text and in Table 1.

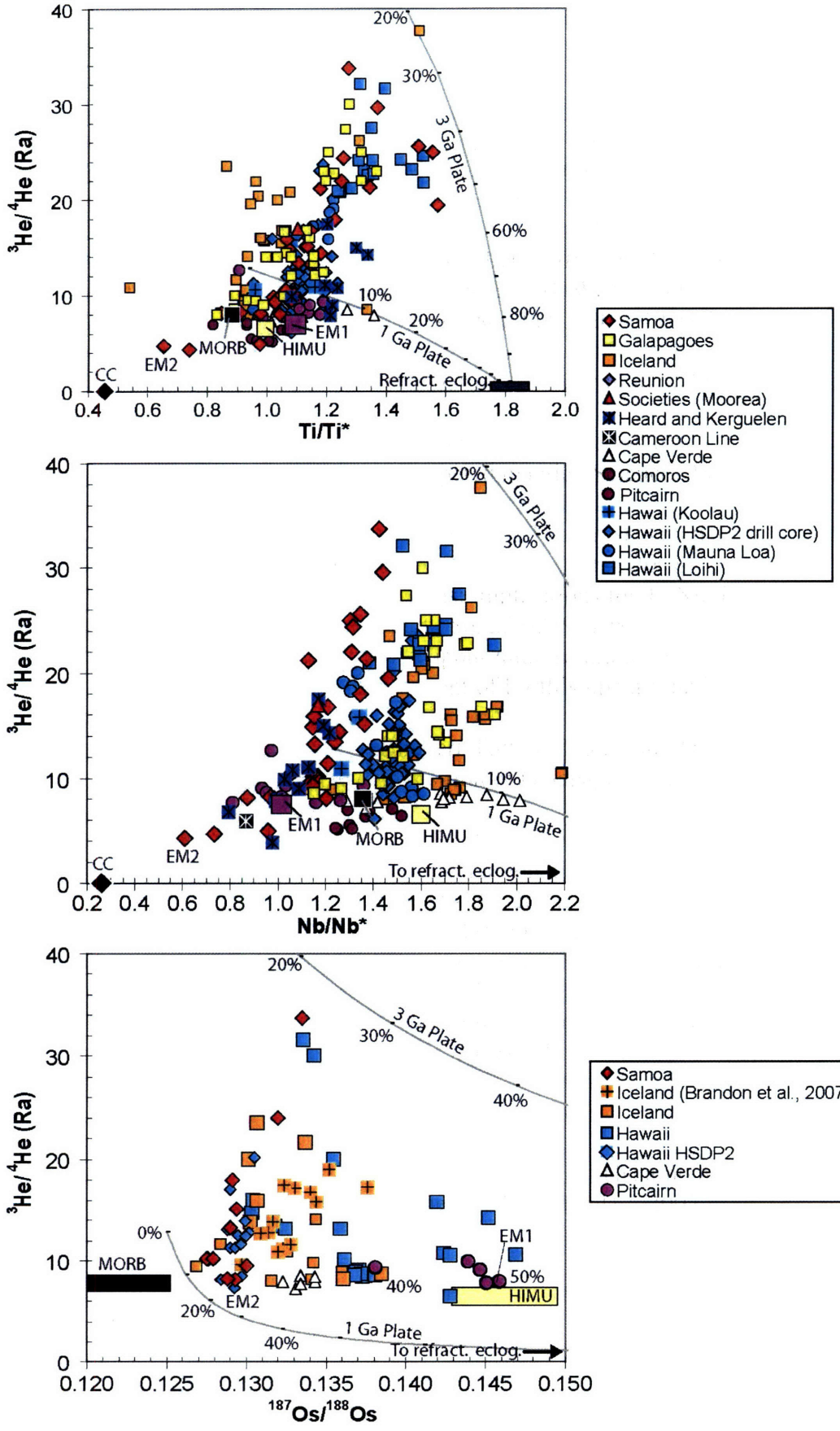
$^3He/^4He$ (Ra)
Ti/Ti*
20%
30%
3 Ga Plate
60%
80%
10%
20%
1 Ga Plate
Refract. eclog.
EM1
MORB
HIMU
EM2
CC
Samoa
Galapagoes
Iceland
Reunion
Societies (Moorea)
Heard and Kerguelen
Cameroon Line
Cape Verde
Comoros
Pitcairn
Hawai (Koolau)
Hawaii (HSDP2 drill core)
Hawaii (Mauna Loa)
Hawaii (Loihi)
Nb/Nb*
To refract. eclog.
Iceland (Brandon et al., 2007)
Hawaii
Hawaii HSDP2
0%
40%
50%
$^{187}Os/^{188}Os$

Figure 2. Relationships between TITAN anomalies, $^{187}Os/^{188}Os$ and $^{3}He/^{4}He$ in representative hotspot lavas. High $^{3}He/^{4}He$ lavas all have elevated Ti/Ti* (top panel), Nb/Nb* (middle panel) and $^{187}Os/^{188}Os$ (bottom panel). With increasing positive TITAN anomalies and $^{187}Os/^{188}Os$ ratios in the OIBs, the maximum observed $^{3}He/^{4}He$ increases. All samples with high $^{3}He/^{4}He$ (>20 Ra) host radiogenic $^{187}Os/^{188}Os$ (> 0.130). The model curves describe mixing between the high $^{3}He/^{4}He$ (low TITAN anomaly) peridotitic and low $^{3}He/^{4}He$ (high TITAN anomaly) refractory eclogite portions of ancient oceanic plates. More recently isolated plates, and/or more contribution from eclogite, both tend to generate lower $^{3}He/^{4}He$ ratios in the peridoite-eclogite mixture over time. The model curves are not meant to describe the global OIB array. Instead, the model curves are only intended to constrain the mixing proportions of eclogite and peridotite in the high $^{3}He/^{4}He$ mantle sampled by the highest $^{3}He/^{4}He$ lavas (>30 Ra). In the model, more recently isolated plates (the 1 Ga plate example is shown) can generate TITAN anomalies, but cannot generate high $^{3}He/^{4}He$. However, the mixing model does match the $^{3}He/^{4}He$ ratios, moderately radiogenic $^{187}Os/^{188}Os$ and large positive TITAN anomalies observed in the highest $^{3}He/^{4}He$ lava (sample SEL 97 from Iceland, see Table 1) when the eclogitic (20-25%) and peridotitic (75-80%) portions of a 3 Ga plate are mixed. Mixing is marked at 10% intervals, with increasing contribution from eclogite. The most extreme lava in the figure (sample SEL 97) is the highest $^{3}He/^{4}He$ lava available that also has a complete suite of trace elements measured by ICP. Unfortunately, $^{187}Os/^{188}Os$ is not available for this sample, and the $^{187}Os/^{188}Os$ of the highest $^{3}He/^{4}He$ mantle is instead approximated using lavas (with $^{3}He/^{4}He$ > 30 Ra) from Hawaii and Samoa. Samoan post-erosional (from Savai'i) data are excluded; all $^{187}Os/^{188}Os$ data in the figure are >50 ppt Os, except Cape Verde (>10 ppt) and Pitcairn (>20 ppt). Data sources for the highest $^{3}He/^{4}He$ mantle endmembers can be found in Table 1 and Appendix A. $Nb/Nb^{*}=Nb_N/(Th_N \times La_N)^{0.5}$ and $Ti/Ti^{*} = Ti_N/(Sm \times Tb)^{0.5}$, where N means normalized to primitive mantle.

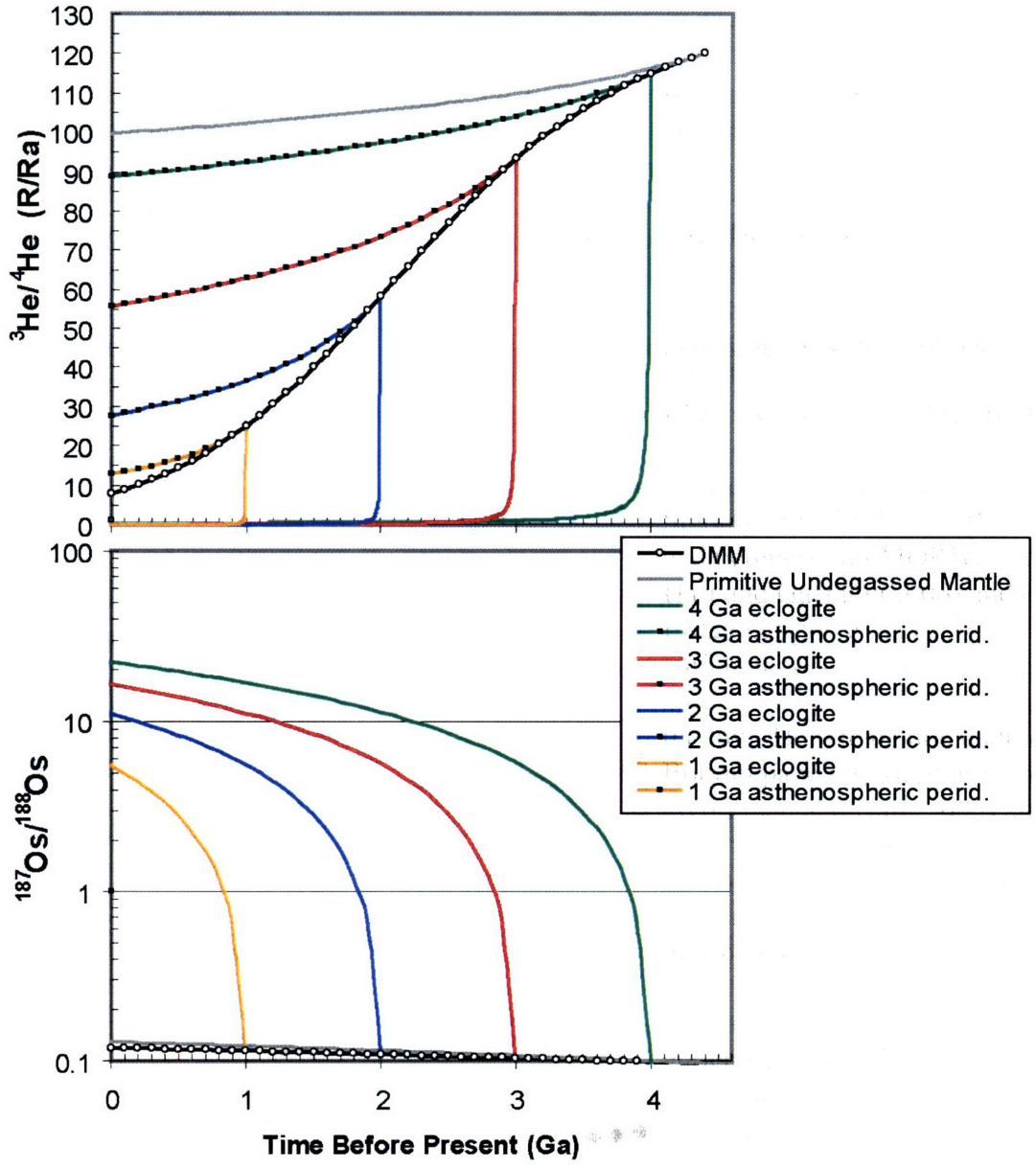
130
120
110
100
90
80
70
60
50
40
30
20
10
0
$^3He/^4He$ (R/Ra)
100
10
1
0.1
$^{187}Os/^{188}Os$
0
1
2
3
4
Time Before Present (Ga)
DMM
Primitive Undegassed Mantle
4 Ga eclogite
4 Ga asthenospheric perid.
3 Ga eclogite
3 Ga asthenospheric perid.
2 Ga eclogite
2 Ga asthenospheric perid.
1 Ga eclogite
1 Ga asthenospheric perid.

Figure 3. Time evolution of $^{3}He/^{4}He$ and $^{187}Os/^{188}Os$ of DMM, ancient subducted (asthenosperic) DMM and eclogite. Top panel: At 4.4 Ga, DMM starts forming by melt extraction from primitive mantle to form continental and oceanic crust, and the $^{3}He/^{4}He$ trajectories of DMM and the (hypothetical) primitive undegassed mantle separate immediately. Due to continuous depletion by melt extraction, DMM evolves low $^{3}He/^{4}He$. Portions of the ancient (asthenospheric) DMM, coupled to the bottomside of downgoing slabs, are sent into the lower mantle throughout geologic time (model curves are shown at 1 Ga intervals, and this is not intended to imply that the isolation of oceanic plates is episodic). These isolated peridotite portions of the downgoing slabs are modeled as having exactly the same U, Th/U, $^{238}U/^{3}He$ and $^{3}He/^{4}He$ as ambient DMM at the time of isolation, and they preserve higher $^{3}He/^{4}He$ than DMM due to their isolation from further melt depletion. Also shown is the concomitant subduction of the eclogitic portions of the same slabs, which begin with the same $^{3}He/^{4}He$ as DMM at the time of subduction; the U and Th of the subducted refractory eclogite are from McDonough (1991) and shown in Table 2. To simulate degassing, the $^{238}U/^{3}He$ of the eclogite is increased by a factor of 1000 (Parman et al., 2005) relative to the contemporary DMM composition, and as a result the $^{3}He/^{4}He$ ratios of the subducted eclogites rapidly decrease. Bottom Panel: The $^{187}Os/^{188}Os$ of Primitive Mantle (0.130; Meisel et al., 2001) and DMM (0.125; Standish et al., 2002) are very similar, thus ancient subducted asthenospheric DMM is well-approximated by the trajectory of DMM in the figure (a continuous depletion model is not used to describe the evolution of $^{187}Os/^{188}Os$ of DMM). The present-day $^{187}Re/^{188}Os$ of the refractory eclogite is from Becker (2000), and this composition generates increasingly radiogenic present-day $^{187}Os/^{188}Os$ for earlier isolation times. Refer to Appendix B and Table 2 for all parameters used in the model. When 20-25% of a refractory eclogite from an oceanic plate subducted at 3 Ga is mixed together with 75-80% of the asthenospheric portion of the same plate, the models generate the $^{3}He/^{4}He$ and $^{187}Os/^{188}Os$ of the mantle sampled by the highest $^{3}He/^{4}He$ (>30 Ra) OIBs (see Fig. 2 for mixing results). Note that the very radiogenic Os of the eclogite is vastly reduced in the mixture due to the very low Os contents of the eclogite (6 ppt) and the high Os contents of the isolated DMM peridotite (3,000 ppt).

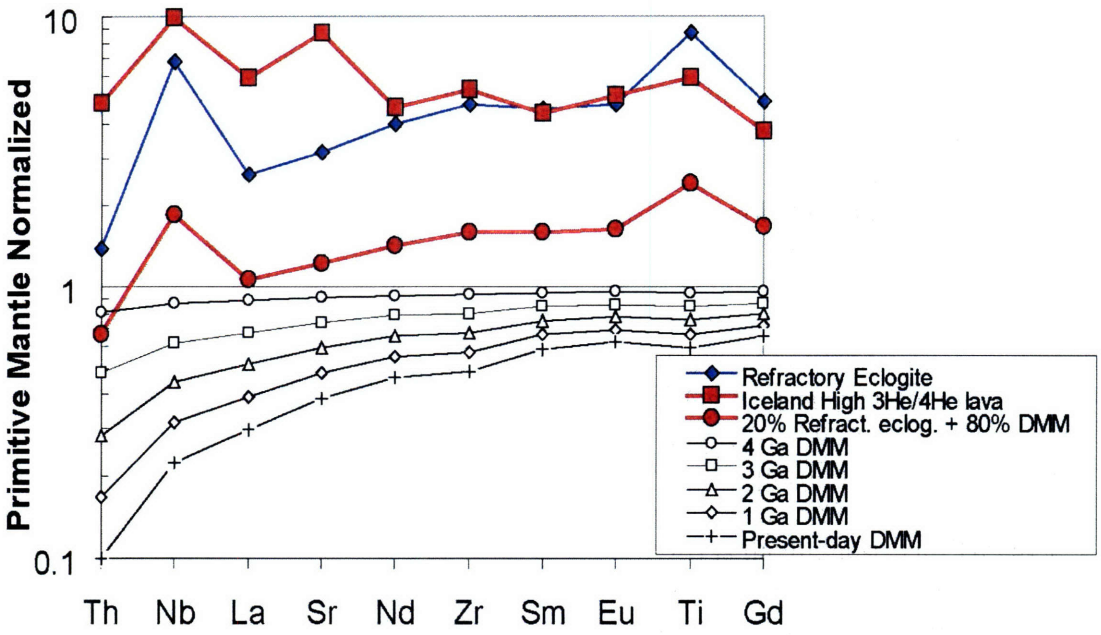

Figure 4. Spidergram of McDonough's (1991) refractory eclogite used in the modeling, including spidergrams demonstraing the time-dependent trace element composition of DMM. In the mixing models shown in Fig. 2, the asthenospheric DMM and refractory eclogitic portions of a 3 Ga subucted plate are mixed together such that the final mixture has 20-25% eclogite. This mixing calculation is shown in the spidergram of this figure, where 20% refractory eclogite has been added to the composition of DMM at 3 Ga (See Table 2 for compositions of the refractory eclogite and the 3 Ga DMM peridotite). Excluding Sr (see text for discussion of shallow lithospheric contamination, and the resulting Sr-anomalies in some Icelandic lavas), the shape of the hybrid peridotite-eclogite spidergram, including the positive Nb and Ti anomalies, is very similar in shape to the spidergram of the high $^{3}He/^{4}He$ Icelandic lava. This similarity is consistent with the hybrid peridotite being the source of the high $^{3}He/^{4}He$ mantle sample by OIBs.

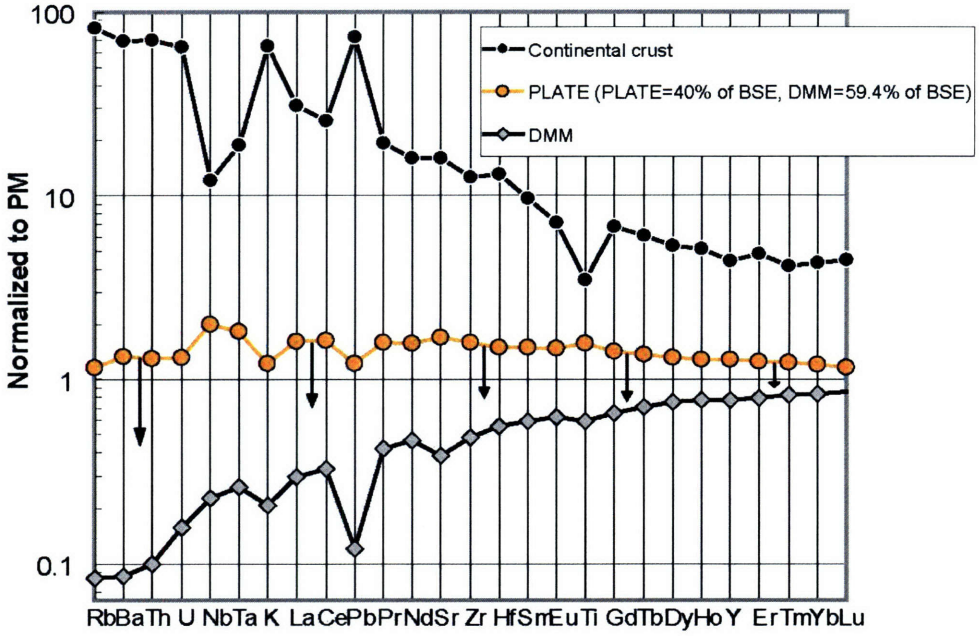

Figure 5. Spidergram of a reservoir composed of recycled oceanic plates (called PLATE) hosting the elements missing in the CC and DMM reservoirs. If BSE (McDonough and Sun, 1995) is chondritic, then CC (continental crust; Rudnick and Gao, 2003) and DMM (depleted MORB mantle; Workman and Hart, 2005) are not wholly complementary reservoirs in the earth. Regardless of the relative proportions of CC and DMM, there is a shortage of the elements Ti, Ta and Nb in the silicate earth. The trace element composition of a PLATE reservoir is calculated to balance the budget of elements missing in CC and DMM (the PLATE spidergram is calculated such that the three reservoirs, PLATE, CC and DMM, sum to the total silicate mantle). The PLATE reservoir is thus composed of everything in the silicate earth that is not in the DMM and CC reservoirs, and is likely composed of mostly subducted plates and (a small portion of) sediment. The plotted spidergram of the PLATE reservoir assumes that it constitutes 40% of the mass of the silicate earth, the minimum mass of oceanic crust and lithosphere subducted over the past 2.5 Ga. If the PLATE reservoir constitutes more than 40% of BSE, its spidergram becomes more depleted (note direction of arrows in figure), but it will still exhibit positive TITAN anomalies. The PLATE spidergram shares the positive TITAN anomalies with the high $^{3}He/^{4}He$ OIB lavas, consistent with the hypothesis that high $^{3}He/^{4}He$ OIBs sample the domain of the PLATE reservoir composed of subducted, refractory, rutile-bearing eclogites.

Supplementary Table 1. Major and trace element and isotopic composition of the highest $^{3}He/^{4}He$ lavas from 4 hotspots.

Hotspot	Iceland	Samoa	Hawaii	Galapagos
Volcano	Selardalur	Ofu	Loihi	Fernandina
Sample No.	SEL 97	OFU-04-06	KK18-8	NSK 97-214
rock type	Tholeiite	Alkali basalt	Tholeiite	Tholeiite
SiO_2	45.94	44.84	48.43	49.44
Al_2O_3	9.72	11.04	12.62	14.77
TiO_2	1.19	4.95	2.88	3.12
FeOT	10.37	12.78	11.90	11.3
MnO	0.15	0.18	0.18	0.19
CaO	10.15	12.42	12.82	11.6
MgO	18.74	9.81	8.06	6.41
K_2O	0.05	1.14	0.50	0.39
Na_2O	1.18	2.24	2.34	2.46
P_2O_5	0.06	0.59	0.50	0.31
$^{87}Sr/^{86}Sr$	0.703465	0.704584	0.703680	0.703290
$^{143}Nd/^{144}Nd$	0.512969	0.512827	0.512945	0.512937
$^{206}Pb/^{204}Pb$	18.653	19.189	18.448	19.080
$^{207}Pb/^{204}Pb$	15.473	15.571	15.447	15.537
$^{208}Pb/^{204}Pb$	38.453	39.202	18.189	38.710
$^{3}He/^{4}He$	37.7	33.8	32.3	30.3
Ni	759	201	80	49
Cr	1728	533	384	155
V	203	364	350	366
Ga		21		26
Cu		80		83
Zn		132		110
Cs	0.02	0.33	0.09	0.07
Rb	0.915	25.64	9.12	7.60
Ba	19.03	248.9	123.1	89.0
Th	0.382	3.956	0.994	1.310
U	0.072	0.991	0.285	0.380
Nb	6.50	50.56	16.35	20.00
Ta	0.434	3.84		1.50
La	3.85	37.93	13.82	14.1
Ce	8.52	80.5	32.9	32.3
Pb	0.38	2.61	1.25	0.93
Pr	1.23	9.99	4.62	4.23
Nd	5.80	44.08	20.65	19.5
Sr	173	599	349	351
Zr	57	293	125	155
Hf	1.65	7.56	3.48	4.15
Sm	1.78	10.75	5.33	5.77
Eu	0.79	3.39	1.83	2.04
Gd	2.05	9.93	5.50	6.01
Tb	0.35	1.40	0.87	1.03
Dy	2.16	7.34	4.89	6.08
Ho	0.42	1.23	0.92	1.21
Y	10.03	30.29	21.87	30.1
Er	1.06	2.70	2.24	3.04
Tm	0.15	0.32	0.29	0.41
Yb	0.88	1.66	1.69	2.46
Lu	0.13	0.23	0.24	0.36
Sc	33.9	31.2	35.4	44.3

Trace element data (excluding Ni, Cr, V, Ga, Cu, Zn and Sc) are by ICP-MS and are here reported for the first time the on the high $^{3}He/^{4}He$ samples from Hawaii, Iceland and Samoa; the trace element data on the Galapagoes sample are reported elsewhere. (Saal et al., 2007). The isotope data for all four lavas are also reported elsewhere (Hilton et al., 1999; Jackson et al., 2007a; Saal et al., 2007; Kurz et al., 1983; Staudigel et al., 1984). Major element data for the Samoan lava are reported here for the first time; major element data for the Hawaii, Iceland and Galapagoes samples are available elsewhere (Hilton et al., 1999; Saal et al., 2007; Frey and Clague, 1983). Samoan major element (and Ni, Cr, V, Ga, Cu, Zn and Sc) data reported here were measured by XRF. Trace element (for Samoa, Hawaii and Iceland) data reported here were analyzed by ICP-MS. Major and trace element data reported here were analyzed at the Geoanalytical Lab at Washington State University. Internal and (estimated) external precision for major and trace element analyses at the Geoanalytical Lab are given in Jackson et al. (2007b). The Loihi sample was powdered in Tungsten-carbide, and Ta is therefore not reported for this sample.

Table 2. Components used to model He, Os and TITAN anomalies in the high $^{3}He/^{4}He$ mantle sampled by OIBs.

	$^{238}U/^{3}He$ [1]	^{3}He atoms/g [1]	$^{3}He/^{4}He$ (Ra) [5]	^{4}He atoms/g	$^{232}Th/^{238}U$	$^{187}Re/^{188}Os$	Os (ppt)	$^{187}Os/^{188}Os$	Th (ppm)	U (ppm)	Nb (ppm)	La (ppm)	Sr (ppm)	Nd (ppm)	Zr (ppm)	Sm (ppm)	Eu (ppm)	Ti (ppm)	Gd (ppm)	Tb (ppm)
Undegassed Mantle [2]	7.00E+01	7.3E+11	99.6	5.3E+15	4.05	0.396	3400	0.130	0.0795	0.0203	0.658	0.648	19.9	1.25	10.5	0.406	0.154	1205	0.54	0.099
Present-day DMM [3]	5.40E+04	1.5E+08	8.0	1.3E+13	2.55	0.314	3000	0.120	0.0079	0.0032	0.149	0.192	7.664	0.581	5.08	0.239	0.096	716	0.36	0.070
Pure peridotite component [4]																				
DMM peridotite (isolated at 1 Ga)	1.19E+04	1.0E+09	12.8	5.8E+13	2.81	0.314	3000	0.125	0.0134	0.0049	0.207	0.253	9.52	0.692	5.99	0.270	0.107	806	0.39	0.076
DMM peridotite (isolated at 2 Ga)	2.63E+03	7.1E+09	27.7	1.8E+14	3.12	0.314	3000	0.125	0.0226	0.0074	0.291	0.334	11.83	0.823	7.07	0.304	0.119	907	0.43	0.082
DMM peridotite (isolated at 3 Ga)	5.80E+02	4.9E+10	55.6	6.3E+14	3.47	0.314	3000	0.125	0.0381	0.0113	0.409	0.440	14.69	0.980	8.34	0.343	0.132	1021	0.48	0.089
DMM peridotite (isolated at 4 Ga)	1.28E+02	3.4E+11	88.6	2.7E+15	3.85	0.314	3000	0.125	0.0644	0.0172	0.574	0.580	18.25	1.166	9.83	0.387	0.148	1149	0.52	0.096
Pure eclogite component [6,7]																				
Refrac. eclogite (isolated at 1 Ga)	1.19E+07	9.4E+06	0.026	2.6E+14	2.81	325	6	5.5	0.11	0.044	4.5	1.7	63	5.0	50	1.9	0.7	10500	2.7	0.5
Refrac. eclogite (isolated at 2 Ga)	2.63E+06	4.2E+07	0.053	5.8E+14	3.12	325	6	11.0	0.11	0.044	4.5	1.7	63	5.0	50	1.9	0.7	10500	2.7	0.5
Refrac. eclogite (isolated at 3 Ga)	5.80E+05	1.9E+08	0.137	1.0E+15	3.47	325	6	16.6	0.11	0.044	4.5	1.7	63	5.0	50	1.9	0.7	10500	2.7	0.5
Refrac. eclogite (isolated at 4 Ga)	1.28E+05	8.7E+08	0.385	1.6E+15	3.85	325	6	22.3	0.11	0.044	4.5	1.7	63	5.0	50	1.9	0.7	10500	2.7	0.5

All values are calculated for the present-day. The $^{236}U/^{3}He$, U, $^{232}Th/^{236}U$, $^{3}He/^{4}He$ and trace element budgets of DMM at all times (4 Ga to present) are calculated using the continuous transport equations in Appendix B and initial values provided in this table.

[1] The undegassed mantle has been a closed system to all elements, volatile and non-volatile, since 4.4 Ga. The $^{238}U/^{3}He$ of undegassed mantle is based on a primitive mantle U concentration (McDonough and Sun, 1995) and a ^{3}He concentration of $7.3x10^{11}$ atoms/g, a ^{3}He value that is well within the range suggested for the undegasased mantle in the literature ($1.1x10^{11}$ atoms/g in Class and Goldstein [2005] and ~$1x10^{12}$ atoms/g in the D'' layer in Tostikhin and Hofmann [2006]). To simulate >99% degassing of the slab in the subduction zone, the $^{238}U/^{3}He$ value of the refrac. (refractory) eclogite is taken to be a factor of 1,000 times greater than the $^{238}U/^{3}He$ of the contemporary DMM peridotite (Parman et al., 2005).

[2] The trace element concentrations for undegassed mantle (excluding Os and He) are from McDonough and Sun (1995). The $^{187}Os/^{188}Os$ is from Meisel et al. (2001), and the Os and $^{187}Re/^{186}Os$ are from McDonough and Sun (1995).

[3] The trace element concentrations (excluding He and Os) for present-day DMM are from Workman and Hart (2005). The $^{187}Os/^{188}Os$ of DMM is from Standish et al. (2002).

[4] Using the continuous transport equations in Appendix B, the U and Th contents of the DMM peridotite are calculated to be the same as ambient upper mantle during the time of subduction and isolation; all other trace elements concentrations (except Os) are calculated the same way. Helium concentrations are derived from the calculated $^{236}U/^{3}He$ and U concentrations.

[5] At 4.4 Ga, the mantle is assumed to have had a $^{3}He/^{4}He$ ratio of 120 Ra, a ratio that is similar to the present-day atmosphere of Jupiter (Niemann et al., 1996); given the assumed $^{238}U/^{3}He$ and $^{232}Th/^{238}U$ primitive mantle ratios, closed system evolution yields a present-day $^{3}He/^{4}He$ ratio of 99.6 Ra (see Appendix B). Using the continuous transport equations in Appendix B, the $^{3}He/^{4}He$ ratios of isolated DMM peridotite (asthenosphere) throughout time are the same as ambient upper mantle DMM at the time of subduction and isolation.

[6] The $^{187}Re/^{188}Os$ and Os concentrations for refractory eclogite are the median values reported for metamorphosed metabasalts in Becker (2000). The various $^{187}Os/^{188}Os$ values shown for the recycled eclogites are then calculated assuming different isolation times of the same eclogite.

[7] Four of the trace elements for the refractory eclogite (Nb, La, Zr and Ti) were provided explicitly in McDonough (1991). Th, Sr, Nd, Sm, Eu and Gd were estimated from Fig. 5 in the same source. U concentrations for the refractory eclogite are not provided by McDonough (1991). U concentrations are estimated assuming a Th/U ratio of 2.5 and using the Th concentration provided; Tb (used to calculate Ti/Ti*) is not provided by McDonough (1991), and its concentration in the refractory eclogite is set by a linear (on a Primitive Mantle normalized basis) extrapolation from Gd and Sm, which are provided. The trace element composition of McDonough's (1991) hypothetical eclogite is quite similar to the eclogites with the highest Nb/Th and Ti/Sm (proxies for Nb and Ti anomalies) in the eclogite dataset of Becker et al. (2000). Considering only the eclogites with Ti/Sm > 3000 and Nb/Th>24, and excluding all samples that lack data for all the elements of interest (Nb, Th, Ti, Sm, U, etc.), the average trace element composition of the TITAN-enriched eclogites in Becker et al. (2000) is: Th = 0.159 ppm; U = 0.165 ppm; Nb = 10 ppm; Nd = 7.58 ppm; Sr = 88.7 ppm, Zr = 152 ppm, Sm = 2.16 ppm, Ti = 10,080 ppm.